STRUCTURAL BEHAVIOR OF UNREINFORCED HYBRID SLAB ELEMENTS CAST WITH ULTRA-HIGH PERFORMANCE CONCRETE (UHPC)

BY

IBRAHIM YAHYA AHMED HAKEEM

A Dissertation Presented to the

DEANSHIP OF GRADUATE STUDIES

KING FAHD UNIVERSITY OF PETROLEUM & MINERALS

DHAHRAN, SAUDI ARABIA

In Partial Fulfillment of the
Requirements for the Degree of

DOCTOR OF PHILOSOPHY

In

CIVIL ENGINEERING

MAY 2014

KING FAHD UNIVERSITY OF PETROLEUM & MINERALS

DHAHRAN- 31261, SAUDI ARABIA

DEANSHIP OF GRADUATE STUDIES

This thesis, written by **IBRAHIM YAHYA AHMED HAKEEM** under the direction of his thesis advisor and approved by his thesis committee, has been presented and accepted by the Dean of Graduate Studies, in partial fulfillment of the requirements for the degree of **DOCTOR OF PHILOSOPHY IN CIVIL ENGINEERING.**

Dr. Abul Kalam Azad
(Advisor)

Dr. Nedal T. Ratrout
Department Chairman

Dr. Mohammed H. Baluch
(Member)

Dr. Salam A. Zummo
Dean of Graduate Studies

Dr. Mohammad Maslehuddin
(Member)

23/6/14
Date

Dr. Omar S. B. Al-Amoudi
(Member)

Dr. Shamshad Ahmad
(Member)

This thesis is dedicated to my late parents,

for their inspiration

in my pursuit of excellence,

which still lingers.

And to my wife,

children, brothers and sisters

for their support and encouragement.

ACKNOWLEDGMENTS

All praise and thanks are due to my Lord, ALLAH SUBHAN WA TAALA, for giving me the health, knowledge and patience to complete this work. I acknowledge all the support provided by KFUPM's Civil Engineering Department and Aden University during my graduate studies.

My sincerest gratitude goes to my advisor, Prof. Abul Kalam Azad, who guided me with his dedicated attention, expertise and knowledge throughout this research. Further, I deeply indebted and grateful to my Committee Members, Prof. Mohammed Baluch, and Prof. Mohammad Maslehuddin, Prof. Omar S. Baghabra Al-Amoudi and Dr. Shamsad Ahmad, for their extensive guidance, continuous support, and personal involvement in all phases of this research. Thanks are also due to the Department's Chairman, Prof. Nedal Ratrout, and his secretary for providing aid, and to other faculty members and staff.

I also acknowledge the sincere and untiring efforts of Engr. Omer Hussein, Engr. Syed Imran Ali, Engr. Syed Khaja Najamuddin and Mr. M. Mukarram Khan who assisted me during all stages of my experiments. I would like to offer my acknowledgement to Dr. Nazih Fadel from Aden University, who helped me during all my study. Thanks and acknowledgments are due to Dr. Hussain Jebran Al-Qahtani, Dr. M. Essa and Dr. M. Al-Osta for their help and support.

Special thanks are due to my colleagues in the Civil and Environmental Engineering Department, for their aid and support. Thanks are also due to all my friends for their support and encouragement.

My heartfelt gratitude is given to my beloved father, mother, my wife and my children, who always supported me with their love, patience, encouragement and constant prayers. I would like to thank my brothers, sisters, and all the members of my family in Yemen for their emotional and moral support throughout my study.

TABLE OF CONTENTS

LIST OF TABLES

LIST OF FIGURES

ABSTRACT

Full Name : IBRAHIM YAHYA AHMED HAKEEM

Thesis Title : STRUCTURAL BEHAVIOR OF UNREINFORCED HYBRID SLAB ELEMENTS CAST WITH ULTRA-HIGH PERFORMANCE CONCRETE (UHPC)

Major Field : CIVIL ENGINEERING

Date of Degree : MAY 2014

The advent of ultra-high performance concrete (UHPC), a new generation of advanced concrete, has created enormous possibilities of new construction utilizing the excellent material properties of UHPC. As steel-fiber reinforced UHPC has tensile strength exceeding 30 MPa, this research was undertaken to develop hybrid concrete floor slabs utilizing the tensile strength of steel fiber-reinforced UHPC instead of steel reinforcement. Three concepts for one-way simply supported precast floor units were explored: (i) units with a layer of UHPC at the bottom tension face, (ii) units reinforced with precast UHPC deformed bars, and (iii) hybrid hollow-core units with top and bottom faces cast with UHPC layers. Types (i) and (iii) do not require the use of any steel reinforcement. For smaller widths, type (ii) also may not require any steel reinforcement. Test results using small size specimens have shown adequate flexural strength, and a structural behavior which is characterized by almost linear response up to the peak load followed by a post-cracking softening with increased deflection under declining load. Tests have revealed the size effect on the tensile strength caused by random dispersion

and orientation of steel fibers, signaling a possible reduction in tensile strength for larger size specimens.

The results of this study confirmed that each of the three alternative forms of construction is structurally promising and can be utilized in designing simply supported precast floor slab units for residential and commercial buildings without the use of steel reinforcement. Further research is needed to uphold this viewpoint. In corrosive environment, this may prove to have significant advantage worthy of consideration.

DOCTOR OF PHILOSOPHY
KING FAHD UNIVERSITY OF PETROLEUM AND MINERALS
DHAHRAN, SAUDI ARABIA

ملخص الرسالة

الاسم الكامل: ابراهيم يحي احمد حكيم

عنوان الرسالة: السلوك الانشائي لعناصر السقوف المهجنه الغير مسلحه و المصبوبه باستخدام الخرسانة العاليه و الفائقة الأداء

التخصص : الهندسة المدنية

تاريخ الدرجة العلمية: مايو 2014م

ان ظهور الخرسانة فائقة الأداء (UHPC) ، الجيل الجديد من الخرسانة المتقدمة، قد خلق إمكانيات هائلة من البناء الجديد بالاستفادة من الخصائص الممتازة لل UHPC . كما ان ال UHPC المعززه بالياف الفولاذ لديها قوة شد تزيد عن 30 ميجا باسكال ، فقد تم أجراء محاولة لتطويرمنشاءه مهجنه من بلاطات السقوف بالاستفادة من قوة الشد لخرسانه الUHPC و المعززه بالياف الفولاذ بدلا من حديد التسليح .وقد تم استكشاف ثلاثة مفاهيم للبلاطات المسبقه الصب ذات الاتجاه الواحد والمستنده استادا بسيطا: (أ) وحدات بطبقة من UHPC في منطقه الشد في الاسفل ، (ب) وحدات معززة بقضبان مبرومه و سابقه الصب من UHPC و (ج) وحدات البلاطات المجوفه والمصبوبه بطبقه علويه وسفليه من UHPC. ألانواع (أ) و (ج) لا تتطلب استخدام أي حديد التسليح . و بعرض أصغر ، فان النوع (ب) أيضا قد لا يتطلب أي حديد التسليح . وقد أظهرت نتائج الاختبارات باستخدام عينات صغيرة الحجم قوة انبعاج كافية، وان السلوك الانشائي والذي يتميز باستجابة خطية تقريبا وصولا إلى الذروة يعقبه تشقق متقدم لدن مع زيادة الانحراف تحت تناقص الحمل . وقد كشفت الاختبارات بشكل صارخ تأثير الحجم على قوة الشد الناجمة عن التشتت العشوائي و التوجيه لالياف الحديد ، مما يشير إلى احتمال خفض قوة الشد لعينات أكبر حجما . وقد أكدت هذه الدراسة الاستطلاعية أن كلا من الأشكال البديلة الثلاثة من البناء كانت واعدة انشائيا ويمكن استخدامها في تصميم وحدات بلاطات السقوف المستنده استنادا بسيطا للمباني السكنية والتجارية من دون استخدام حديد التسليح . كما ان هناك حاجة إلى مزيد من البحث و العمل لدعم وجهة النظر هذه . وفي بيئة تآكل ، قد تثبت هذه الدراسه ان لديها ميزة كبيرة تستحق النظر .

CHAPTER 1

INTRODUCTION

1.1. General

Ultra-High Performance Concrete (UHPC) is a special concrete with excellent characteristics compared to normal concrete, which was developed by better understanding of the concrete material in the micro level. A technological breakthrough took place in the 90's with the development of the Reactive Powder Concrete (RPC) offering compressive strength exceeding 200 MPa and flexural tensile strength of over 30 MPa. The attractive features of this new concrete are that it has both high compressive and tensile strengths, and has excellent material properties with significant ductility.

UHPC is optimized at the micro-scales to provide superior mechanical and durability properties compared to conventional and high performance concretes. Improvements in UHPC are achieved through limiting the water-to-cementitious materials ratio up to less than 0.2, optimizing particle packing, eliminating coarse aggregate, using specialized materials, and implementing hot curing, typically at 90 0C for several days to improve the microstructure of the cementitious matrix. In addition, randomly dispersed short fibers are usually used to enhance the tensile and flexural strength, ductility, and toughness.

The absence of coarse aggregate was considered as a key-aspect for the microstructure

and the performance of the UHPC in order to reduce heterogeneity between the cement matrix and the aggregate. However, due to the use of very fine sand instead of ordinary aggregate, the cement content of UHPC is as high as 900 to 1000 kg/m3. One of the primary benefits of this class of concrete is that it can exhibit significant tensile strength and toughness. Much of such properties enhancement is imparted to concrete by the addition of short, discontinuous fibers during the mixing procedure.

Because of the outstanding properties of UHPC, such as compressive strength of 150 to 200 MPa, tensile strength of 8 to 15 MPa, flexural strength of 30 to 50 MPa with significant remaining post-cracking bearing capacity, and remarkable fracture energy of 20 to 30 kJ/m2, UHPC offers new and sometimes exiting possibilities: lighter structures, larger structures, hybrid structures, new design and new products with a potential for a better economy and resource consumption than with traditional concrete, steel and other building materials.

In recent years, the development of steel-fiber reinforced ultra-high performance concrete (UHPC) with tensile strength exceeding 30 MPa has created possibilities for exploring hybrid concrete construction to utilize the excellent tensile strength of UHPC in order to replace the use of traditional passive steel reinforcement. Such constructions have significant advantage for adoption in corrosive environment, where corrosion of steel is a major concern for concrete durability. Use of corrosion-free construction in aggressive environment is highly desired by all concerned. Furthermore, possibilities exist that such a hybrid construction may have economic advantage. Despite its superior material properties, fiber-reinforced UHPC has not yet made a big push in its application, which has thus far been sporadic. Researchers have continued their efforts in seeking possible

new applications of this material in construction. This study is an attempt in this direction, as it explores the possibility of developing new hybrid concrete construction for floor slabs.

Because of the profound impact on concrete construction, it is highly desirable to explore alternative form of construction that may not require the use of steel reinforcement. Three alternative forms of construction conceived at this stage are suitable for one-way floor slabs, cast-in-place or as precast units. In one option, the bottom tension part of a conventional beam is replaced with a layer of UHPC, which provides the needed tensile strength. Thus, the beam consists of two layers, a bottom layer of UHPC and the upper part of ordinary concrete. In the second option, the tensile strength in a beam is provided by embedded 'UHPC bars', a new concept for utilization of UHPC. The UHPC bars, used as replacement of steel bars, can provide the required tensile strength much in the same fashion as the steel bars. In the third option, a hybrid hollow- core slab section with top and bottom thin UHPC layers and a middle layer of ordinary concrete sandwiched in between was explored.

The primary aim of this study was to explore the three new concepts of concrete construction by undertaking an experimental work to examine the structural behavior and performance. This dissertation covers the details of all the work that was carried out. The study indicated that all the options of construction are possible, as members can be proportioned or designed as one-way floor slab element.

1.2. Significance of this Study

The proposed three forms of hybrid construction of floor slabs using ordinary concrete and steel fiber-reinforced UHPC, the latter providing the tensile strength, are all new conceptual ideas which if found structurally feasible and sound, will have significant impact on new construction, particularly in precast construction industry. Each of the three options that are explored does not require the use of steel reinforcement. This study explores, for the first time, the concept of UHPC bars as tension reinforcement and a hollow-core sandwich type construction for floor slabs. The most notable and appealing product under consideration is the proposed hybrid hollow core slab for floors. In Saudi Arabia, a large number of buildings use hollow core slabs, mostly pre-stressed. The proposed form may offer a competitive solution as the section is highly efficient. The elimination of reinforcing steel also makes this type of construction highly attractive for application in aggressive environment. All products under consideration can be made locally, using local resources (except steel fibers).

The proposed alternative forms of construction address the needs of construction industry and may provide a valued contribution to the field. As local precast companies are playing key roles in construction industry, some of the products, notably the hollow-core slab construction, may draw the attention of the companies for commercialization.

1.3. Research Objectives and Scope

The main objective of the proposed work was to develop three new forms of floor slab

construction avoiding reinforcing steel bars and utilizing instead the excellent properties of steel fiber reinforced UHPC and to study, both experimentally and theoretically, their behavior and performance. The specific objectives are the following:

1. Perform a thorough literature review on the application and use of UHPC and report the findings;
2. Develop hybrid floor slab elements using locally developed UHPC and undertake experimental investigation to determine their behavior and strength;
3. Conduct analytical studies to determine the strength of hybrid members and develop simple mechanistic approach for design; and
4. Propose design approach for the suggested form of construction.

1.4. Approach

The approach to achieve the objectives of this dissertation consists of three major steps: (a) review of literature concerning utilization and application of UHPC that can be documented as supplementary information and that may assist to better plan the experimental work; (b) undertaking an exploratory experimental work to evaluate the feasibility of the proposed forms of hybrid concrete construction, and (c) interpretation of the test results and evaluation.

The dissertation work has three distinct phases: Phase 1 is essentially the preparatory work phase, Phase 2 is the execution phase in which all experimental work will be

completed, and Phase 3 is the ending phase in which the findings will be presented and discussed.

The approach to achieve the major objectives of this work mentioned earlier is presented in **Table 1**.

Table 1.1: Approach Utilized for Achieving Objectives of the Study

Objective	Approach of achieving the objective
1	This objective will be achieved through a broad search of available literature and information using library and internet sources. The useful information will be gathered, reviewed and then documented in the report.
2	A well-planned experimental work with a good execution plan will lead to the achievement of this objective. The experimental work is covered by describing the tasks. This is the heart of the project and its proper planning and execution are a required prerequisite to the attainment of the objective.
3	This objective is expected to be achieved through an evaluation of the test results and findings. The test results and findings will be compared with theoretical predictions and will be discussed to form the basis of conclusions and recommendations.

1.5. Organization of the Dissertation

This dissertation was subdivided into ten different chapters and five appendixes. Each of these chapters addressed a particular topic of the work.

- Chapter 1 contains the research objectives, scope, uniqueness and organization of the dissertation.
- Chapter 2 presents the literature review.
- Chapter 3 describes the experimental program.
- Chapter 4 discusses the test results for the material properties used.
- Chapter 5 presents the test results and discussion for hybrid layered specimens.
- Chapter 6 presents the test results and discussion for UHPC reinforced beams.
- Chapter 7 presents the test results and discussion for hybrid hollow core slab specimens.
- Chapter 8 presents the finite element modeling of two forms of construction.
- Chapter 9 covers the design consideration and approach for the design of the proposed hybrid elements.
- Chapter 10 includes conclusions and recommendations.

CHAPTER 2

LITERATURE REVIEW

A brief summary of previous research conducted on UHPC material properties is presented in this chapter. For UHPC, a significant amount of research has been done in recent years on material behavior for structural application and, therefore, many research publications are available for reference. However, for hybrid construction related to the study under consideration, limited research has been conducted with different concepts.

The literature review is presented under the following subheadings:

- Background on UHPC
- General properties
- Hybrid construction with UHPC

2.1. Background on UHPC

Ultra-High Performance Concrete (UHPC), also referred to as Ultra-High Performance Fiber Reinforced Concrete (UHPFRC), is a new generation of cement-based materials that was developed in France in the 1990s [1]. UHPC is relatively a new generation of concrete optimized at the nano-and micro-scale to provide superior mechanical and durability properties compared to conventional and high performance concretes. Improvements in UHPC are achieved through: limiting the water-to-cementitious materials ratio (i.e., w/cm < 0.20), optimizing particle packing, eliminating coarse

aggregate, using specialized materials, and implementing high temperature and high pressure curing regimes. In addition, randomly dispersed and short fibers are typically added to enhance the material's tensile and flexural strength, ductility, and toughness [2].

The range of performances and characteristics that are today covered by concrete have been expanded in various directions from ordinary concrete up to ultra-high performance concrete to self-compacting concrete. The type of high-strength concrete developed thus far is basically a brittle material requiring the use of passive reinforcement. A technological breakthrough took place in the 1990's with the development of the said Reactive Powder Concrete (RPC) [3], offering compressive strength exceeding 200 MPa and flexural tensile strength of over 25 MPa, showing significant ductility. Based on the RPC initial research, the Ductal technology was then developed by the combined efforts of three companies in France, LAFARGE, the construction materials manufacturer, BOUYGUES, contractor in civil and structural engineering, and RHODIA, chemical materials manufacturer. With this joint effort through intensive research and development, the material was patented, industrialized and commercialized. The attractive features of this new concrete are that it has both high compressive and tensile strengths requiring no passive reinforcement and has excellent material properties with some ductility.

Thanks to its exceptional durability, very high strength, and enhanced formability, UHPC presents exciting opportunities to re-think the construction, reconstruction, and maintenance of roads and bridges.

UHPC opens opportunities to new solutions which were not possible. Significant efforts have been focused on developing these types of new solutions which can lead to dramatically better performance of engineered structures over the long term.

As new concrete construction materials, UHPC can be used in the fabrication of precast elements for civil engineering, structural and architectural applications.

Several researchers have defined some of the principles used in UHPC, which can be summarized as follows:

- Enhancement of homogeneity by elimination of coarse aggregate,
- Enhancement of compacted density by optimization of the granular mixture, i.e. the reason for the high silica fume content and use of fine quartz sand as the only aggregate,
- Optional enhancement of the microstructure by heat-treatment., and
- Enhancement of ductility by incorporating small-sized steel fibers.

The application of the first three principles produces a matrix with very high compressive strength, without any improvement in ductility. The addition of the steel fibers noted in the last principle helps to improve both tensile strength and ductility [4].

UHPC can be used for any applications, either structural or architectural, for which normal concrete would normally be specified. UHPC may be best suited for use in prestressed bridge superstructures in the transportation field. Because of its very high mechanical properties, UHPC technology gives access to very thin slender and elegant

structures like footbridges. Such properties provide architects with very high potential of innovative design in all elements that build up new architecture.

UHPC concrete has been used in a number of applications worldwide. Mention can be made of 1997 Sherbrooke footbridge in Canada (**Figure 2.1**), the 2003 Seonyu footbridge in Korea (**Figure 2.2**), and 2003 LRT Train Station, Shawnessy, Canada (**Figure 2.3**).

Generally, the applications of UHPC can be summarized into the following classifications:

- Infra-structural application: such as ultra-light and slender sections for pedestrian and highway bridges.
- Impact-resistant structures: such as security panels against impact, seismic and blast loads, crash safety barriers.
- Prestressed elements: such as piles, culverts, retaining walls, pipes, safety vaults etc.
- Building applications: such as ultra-slender beam, slab and column systems, long span floors and roofs.
- Other applications: such as architectural features, acoustic barrier, structural walls, marine/sea walls and decks, anchorage plates, leave in-place forms/moulds, containers, and storage tanks [5].

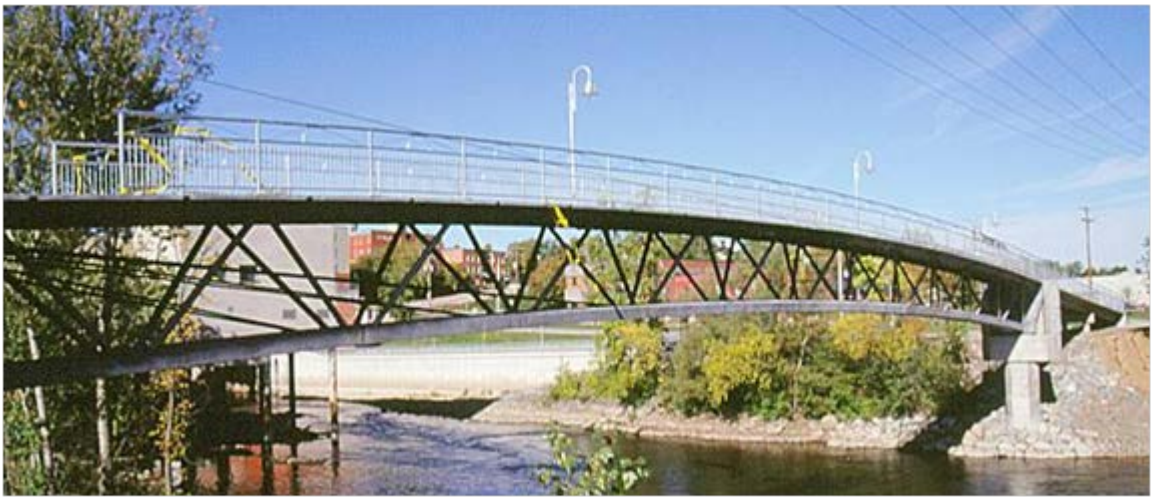

Figure 2.1: Sherbrooke footbridge, Canada, 1997.

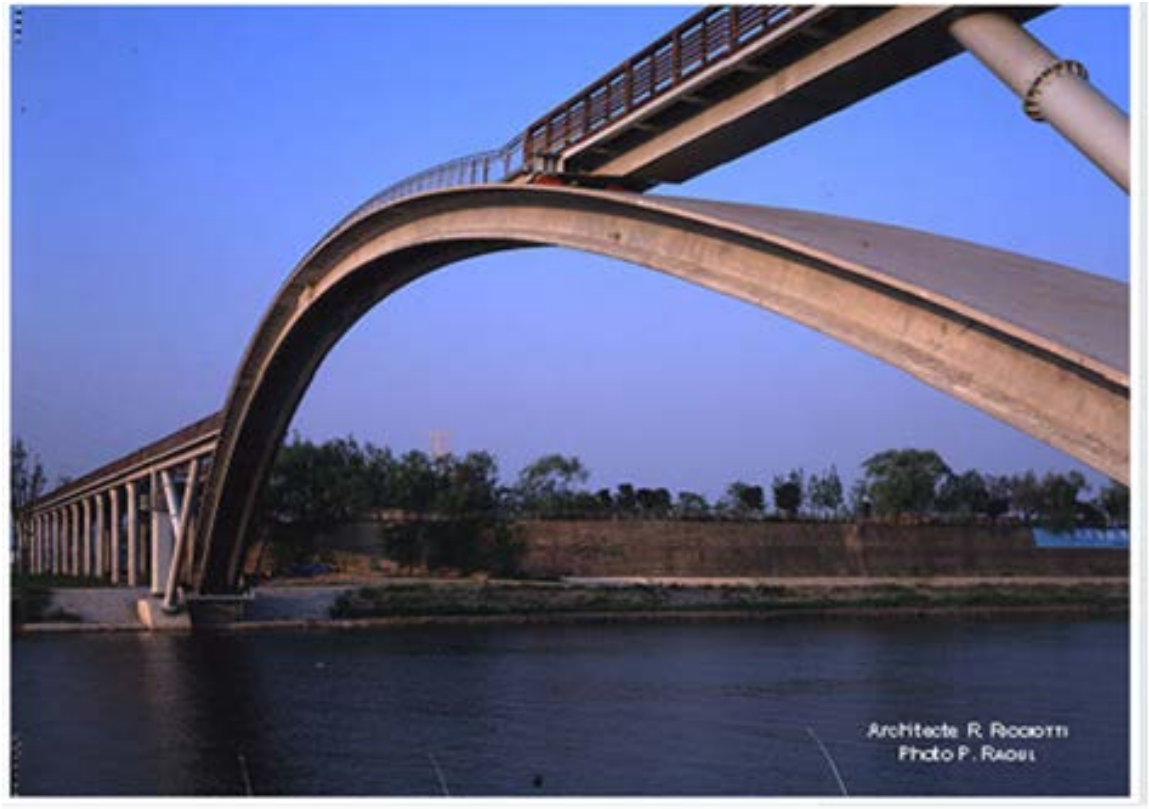

Figure 2.2: Seonyu footbridge, Korea, 2003, arch span 120m deck thickness 3cm [6].

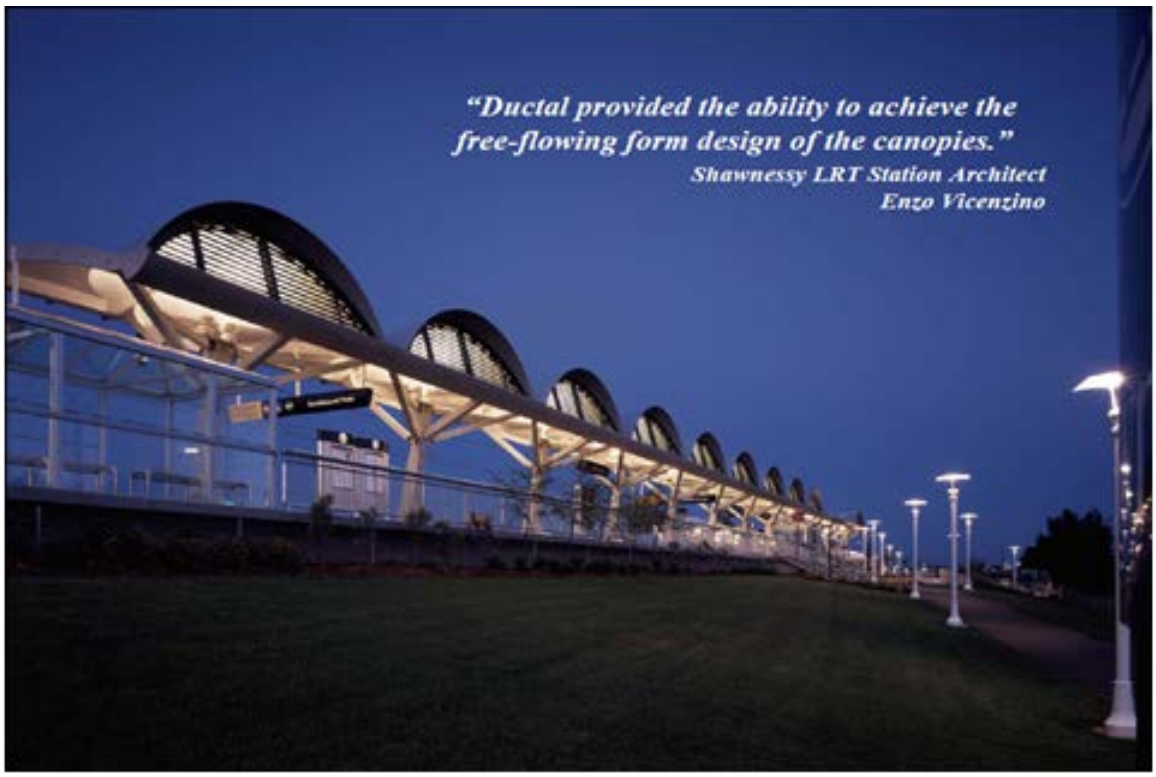

Figure 2.3: LRT Train Station, Shawnessy, Canada, 2003 (Images from Lafarge) Canopies 5x6 m, 2 cm thick, supported on single columns.

The first known use of UHPC in building construction dates to 2001, in Joppa, Illinois, USA, whereby a clinker silo was built with the roof from Ductal® (UHPC) concrete with compressive strength up to 220 MPa and flexural strength 50 MPa. The ultra-light, thin precast panels of UHPC were designed without any conventional reinforcement, as shown in **Figure 2.4**.

Figure 2.4: Overall shot showing all 3 clinker silos and connecting feeder conveyors. The Ductal silo is on the far right [7].

Murthy [8] summarized some of the common benefits and drawbacks of using UHPC compared to the normal concrete.

The benefits of using UHPC are as follows:

1. High compressive strength of up to 180 MPa can be achieved.
2. High shear and tensile strength whereby a tensile strength up to 7 MPa can be achieved, thereby eliminating shear and tensile reinforcement.
3. Low creep and shrinkage, low in creep compared to normal concrete and negligible shrinkage can be achieved by heat treatment.

4. High impermeability, with improved microstructure and reduction of pores makes the concrete highly impermeable.
5. High durability, require less maintenance cost.
6. Self-placing capability, the fluidity nature of the concrete mix makes it suitable for self-placing and no vibration is necessary.
7. Elimination of mild steel reinforcement, due to its high compressive and shear strength compared to normal concrete; mild steel and the labor cost for placing the reinforcement is eliminated.

UHPC with all the above mentioned benefits and the requirements for heat treatment is very well suited for precast construction. The UHPC also provides the following constructability benefits:

A. Because of the high compressive strength and dependable tensile strength, UHPC usage will result in reduction in sizes of many required members and thus producing a lighter section. The light weight members can be transported and erected easily compared to normal concrete members with large sections.
B. Rapid strength development and high early strength capability allow post-tensioning to be applied at an early stage and thus decreasing the time of construction. The high compressive strength of UHPC also allows the structural member to be prestressed to a higher value than a traditional concrete section.

The drawbacks of using UHPC:

1. UHPC is more expensive than conventional concrete.

2. Mixing time, time required to batch a mix is longer.
3. The high energy mixing required could damage the mixer.
4. Cleaning, time required for cleaning is longer due to use of large amount of sand and fibers.
5. Heat treatment, adds as additional cost.

Lee et al., [9], summarized the typical compositions of concrete materials at different levels of performance, as shown in **Figure 2.5**. UHPC is made up of cement, fine aggregates, admixtures, steel fibers, and nano-fillers, while ordinary and high performance concrete consist of cement, fine and coarse aggregates, and admixtures. The coarse aggregate was replaced in UPHC with steel fibers and nano-fillers that enhance the mechanical strength of UHPC.

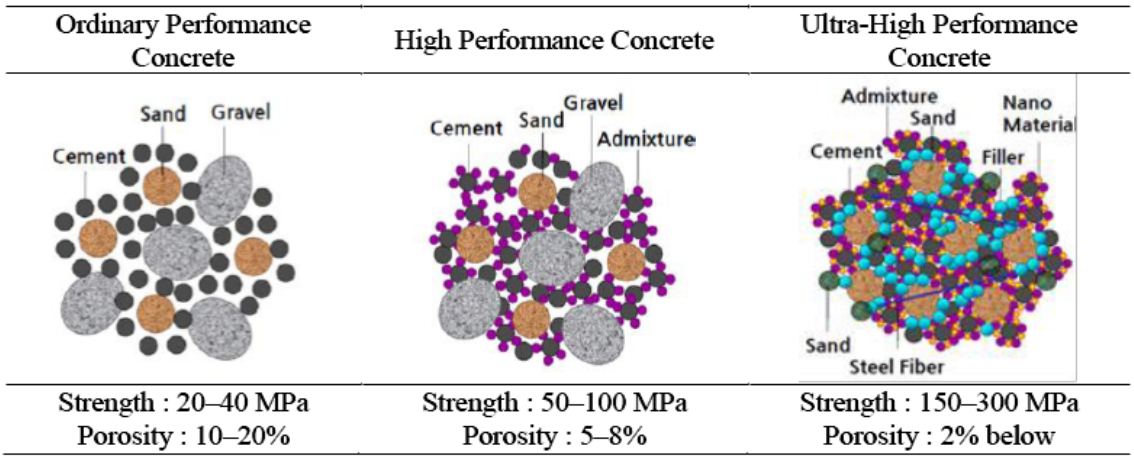

Figure 2.5: Compositions of concrete materials at different levels of performance [9]

A relative comparison between properties of UHPC and high strength concrete (HPC) is shown in **Table 2.1**.

Table 2.1: Properties of UHPC compared with high strength concrete [10]

Material Characteristic	UHPC Compared with HPC
Compressive Strength	2–3 times greater
Flexural Strength	2–6 times greater
Elastic Modulus	1.5 times greater
Total Porosity	4–6 times lower
Micro-porosity	10–50 times lower
Permeability	50 times lower
Water Absorption	7 times lower
Chlorine Ion Diffusion	25 times lower
Abrasive Wear	2.5 times lower
Corrosion Velocity	8 times lower

2.2. General Properties of UHPC

2.2.1 Durability Characteristics

Several research studies were also conducted on various issues related to durability of UHPC [11-27]. Studies have shown that UHPC has excellent durability against chloride

penetration, chemical attack and ingress of moisture due to its low permeability. The durability characteristics of Ductal UHPC using cyclic exposures to repeated heat-cool and wet-dry cycles in addition to other tests have also examined [11-15], and reaffirmed the excellent durability and low permeability of UHPC.

2.2.2 Mechanical Properties

A number of past researches dealt with mechanical and durability characteristics of UHPC different treatment regimes. These studies have firmly established the superior material properties of UHPC.

2.2.2.1 Compressive Behavior

One of the most significant properties of UHPC is its high compressive strength. The increase in compressive strength, over normal concrete or high performance concrete, can be attributed to the particle packing and selection of specific constituents, and thermal curing of UHPC. Compressive strength of UHPC is significantly affected by the type, shape, and content ratio of fiber reinforcement.

Lubbers [10] stated that UHPC could have a compressive strength 2 to 3 times greater than high performance concrete (HPC) and a flexural strength 2 to 6 times greater, and such mechanical properties of UHPC make it ideal for prestressing applications. It was also stated that before UHPC could be used in a prestressing application, bond performance between the UHPC and the prestressing strands had to be seriously investigated.

Graybeal and Hartmann [28] conducted a series of tests and found that the curing method yielded significant variations in compressive strength, up to 65% difference between steam curing and ambient air curing. Although various curing methods can be used, the quality control on curing methods makes UHPC more suitable for precast operations.

Perry and Zakariasen [29], found the compressive strength of thermally treated UHPC ranges between 158 and 228 MPa. The results reported for both heat treated and untreated UHPC in several references [30-32] have shown that the compressive strength of UHPC generally appears to increase with increasing heat treatment temperature. The compressive strength of UHPC, when heat treated at 90°C, increases by about 33 percent of the strengths obtained for untreated specimens [28].

Hakeem [12] studied the compressive behavior of UHPC specimens for different ages (i.e. 6 months) and curing methods with different percentage of steel fibers and also for different exposure conditions. The results indicated that: (i) water-curing is better than exposure in air in improving the strength but not by a big margin, particularly at a higher fiber content; (ii) increase in the fiber content can improve the strength and modulus of elasticity up to a certain extent and beyond that the increase in the fiber content is not proportionally beneficial; and (iii) the effect of six month exposure to wet-dry and heat-cool cycles on strength and modulus of elasticity is negligible, instead the heat-cool cycled specimens have strength and modulus of elasticity higher than the specimens not subjected to the cyclic exposures.

Magureanu et al. [33] reported that the UHPC specimens attained a compressive strength of approximately 150 N/mm^2 and a modulus of elasticity greater than 50,000 N/mm^2. In

addition, they concluded that the compressive strength and the splitting tensile strength were size dependent.

Hassan et al. [34] investigated the effects of steel fibers on the tensile and compressive strength, modulus of elasticity and post-cracking behavior of UHPC at different ages. Their results indicated that for the compressive behavior, the addition of steel fiber appears to have a relatively small effect on the pre-cracking compressive strength and elastic modulus. However, its influence on the post cracking behavior and failure mechanism is significant. Moreover, they found that UHPC specimens behaved elastically up to approximately 90–95% of their compressive strength, followed by strain hardening behavior (compression hardening) up to peak strength, although in some tests this behavior did not occur. Following the peak strength, a progressive strain softening occurred in which the presence of fibers governed the softening stage, similar to its tensile behavior.

2.2.2.2 Flexural Behavior

Several researchers have attempted to characterize the flexural strength of UHPC with single or two-point bending tests on small prisms. Ductal North America claimed that the flexural strength of UHPC after heat treatment ranges from 27–50 MPa. Research by Cheyrezy et al. [4] showed that UHPC was capable of reaching a flexural strength of up to 48 MPa and a toughness of 250 times that of normal strength concrete.

Dugat et al. [35] also reported an ultimate flexural strength of 32 MPa. UHPC with steel fibers exhibited ductility because, as the specimen began to microcrack, the small-scale

fibers reinforced the matrix, causing smaller and less damaging cracks to form [28]. Normal concrete and high-performance concrete exhibited virtually no post-cracking flexural strength but, because of fiber, UHPC exhibited significant post-cracking strength and ductility.

The increase in the flexural behavior of UHPC was attributed to the particle packing and the addition of fibers which held the cement matrix together after cracking has occurred. UHPC with steel fibers exhibits ductility because as the specimen begins to micro crack, the small scale fibers reinforce the matrix causing smaller, less damaging cracks to form [28].

Perry and Zakariasen [29] showed that UHPC exhibited flexural strengths ranging from 34 to 48 MPa, which confirmed Cheyrezy's findings. The typical flexural strength test curves for Ductal UHPC and another three types of concrete shown in **Figure 2.6** indicates that the equivalent stress of Ductal is more than 47 MPa, compared to about 13 MPa for FRC 80 [23].

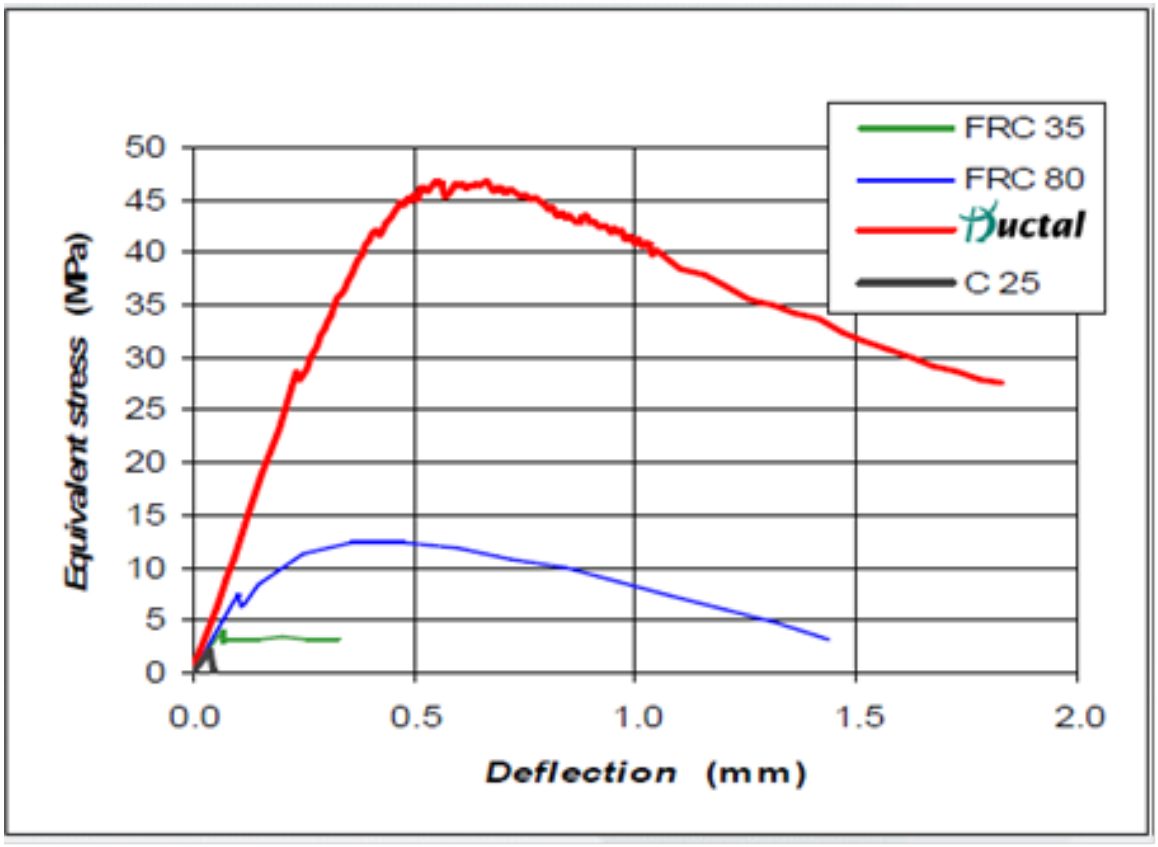

Figure 2.6: Typical flexural strength test curves of four types of concrete [23].

Reineck and Greiner [36] reported the average values of flexural strength for a wider range of prism sizes, showing the size effect. The recorded higher strengths for smaller beams are largely due to local alignment of fibers in small prisms. The local alignment leads to relatively more fibers oriented parallel to the long direction of the prism, making a greater proportion of the fibers effective to bridge flexural cracks [37].

Graybeal [31] conducted flexural testing of 71 specimens utilizing the procedure outlined in ASTM C 1018, which controls the rate of deflection of the prism. The flexural testing results appear to show that the flexural tensile strength of Ductal depends heavily on the size of the prisms used in the test. The results of flexural strength of steam curing

specimens were 35.4 MPa and that of untreated specimens of the same size was 29.9 MPa.

Hakeem [12] has recently reported the flexural tensile strength of UHPC determined from four-point bend tests shows a value of about 31 MPa after 28 days water curing. In his study, he also investigated the effect of different exposure conditions for 6 months on the flexural performance of UHPC. The test results indicated that the wet-dry and heat-cool conditions have virtually no negative impact on the flexural properties of UHPC. Contrarily, heat-cool cycles have shown to improve all the properties. He reported the significance of fiber content in the enhancement of flexural tensile strength at the peak-load increases from 15.2 MPa with no fiber to 24.4 MPa with 3.1% fiber and 31.4 MPa with 6.2% fiber.

Dong et al. [38] investigated the influence of the type of macro fiber on the flexural performance of hybrid ultra-high performance fiber reinforced Concrete (H-UHPFRC). In their study, they estimated the influence of material ductility (strain capacity) of H-UHPFRC on both structural ductility (deflection capacity) and the ratio between flexural strength and tensile strength. For that, they investigated four macro high strength fibers: long smooth steel fiber, two types of hooked steel fibers, and twisted steel fibers with different volume content of micro fibers. They found that H-UHPFRCs show significantly better flexural performance in both deflection capacity and energy absorption capacity compared with UHPFRC with micro fibers only. In addition, H-UHPFRCs produce different equivalent bending stress–deflection curves according to the types of macro fiber and the volume contents of micro fiber.

Azad el al. [14] have reported the results of experimental work conducted to study the effect of wet–dry and heating–cooling cycles and fiber content on tensile properties of a commercially available UHPC (Ductal®). The results of this study showed that there was no degradation in tensile properties under wet–dry cycles and modestly gain strength under thermal cycling, indicating the possibility of the applications of UHPC in aggressive exposure conditions.

Hakeem et al. [13] have investigated the fracture properties of UHPC mixtures reinforced with steel fiber and subjected to thermal cycles to examine the effect of heat–cool cycles of standard prism of 100x100x400 mm with a central notch in a three-point bend test. In their study, two exposure conditions were used: a 6-month thermal cycling and a 6-month laboratory exposure for further self-curing. The thermal cycling comprised heating in an oven at 60 $^{\circ}$C for 2 days and then cooling them at room temperature for the next 2 days over a period of 6 months. Their test results indicated that UHPC reinforced with 6.2% steel fiber exhibited excellent fracture properties with significant ductility. They also observed that both thermal cycling and prolonged self-curing of water-cured UHPC specimens enhanced fracture properties because of more complete hydration of cement in UHPC. This improvement in properties signals an additional advantage of water-cured UHPC for its application in hot climatic conditions.

Nguyen et al. [39] investigated the size effect by testing three different sizes of UHPC specimens using four-point bending in a three-dimensional scale: 50 x 50 x 150 mm (small), 100 x 100 x 300 mm (medium), and 150 x 150 x 450 mm (large). They found that as the size of the specimen increased, the equivalent bending strength decreased, as shown in **Figure 2.7**. Finally, they concluded that UHP-HFRC specimens in flexure

showed clear size effects not only on flexural strength but also on normalized deflection capacity, normalized energy absorption capacity, and average crack spacing. In addition, as the size of the specimen decreased, the flexural strength, normalized deflection, and normalized energy absorption capacity of UHP-HFRC increased significantly, while the average crack spacing on the bottom surface of the specimen was noticeably decreased.

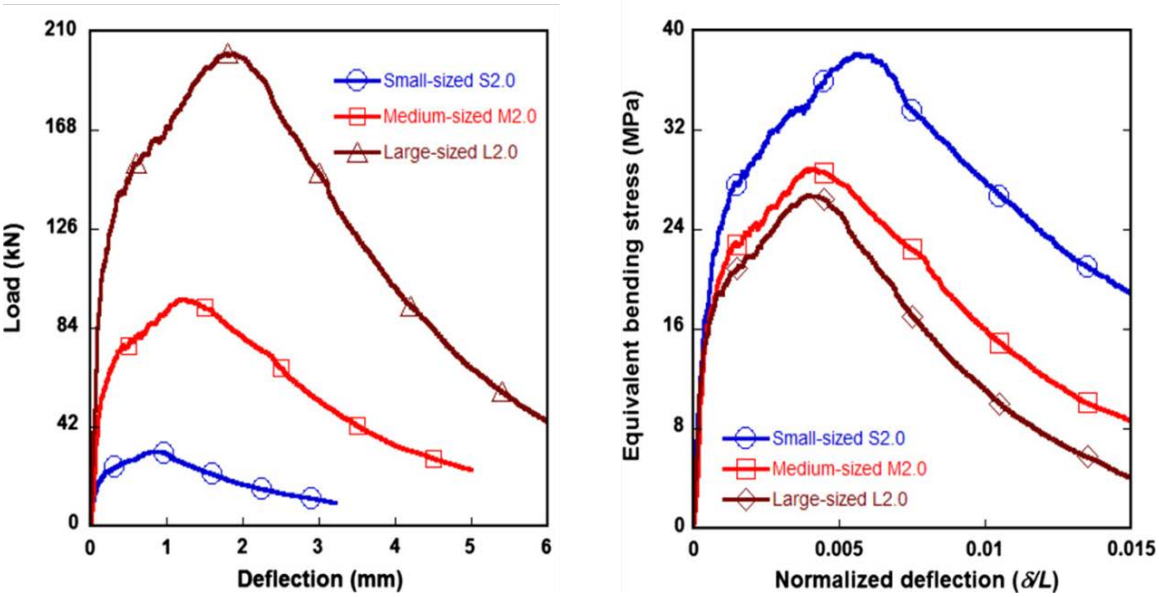

Figure 2.7: Average load versus deflection curve (left) and average equivalent bending stress versus normalized deflection curve (right) of UHP-HFRCs for various specimen sizes [39]

Cornelia et al. [33] reported that the value of the flexural strength obtained on 40 x 40 x 160 mm prisms was approximately 1.47 times higher than 100 x 100 x 300 mm prisms. Also, they observed that the flexural characteristics depended on the fiber addition and the specimen's dimensions. Overall, the flexural tensile strength displayed values between 14 and 34 N/mm^2.

Studies [40-41] reported the effect of the fiber dispersion and orientation on the flexural performance of UHPC; their results showed that the method of placing UHPC was significantly influenced by the fiber dispersion and orientation.

Yang et al. [42] provided a detailed presentation of experimental test results for the flexural behavior of ultra-high performance concrete beams. They concluded that the cracking and failure patterns revealed that many tightly spaced cracks formed perpendicular to flexural tensile forces in the beam. These results indicate the ability of UHPC to redistribute stresses and undergo multiple cracks before fiber pullout. Additionally, the flexural capacity was also affected by the placing method of the UHPC as placing the UHPC at the end of the beam provides better structural performance than placing the UHPC at mid span. This result shows that the arrangement and orientation of the steel fibers are influenced by the UHPC placing method.

Barnett et al. [43] investigated the fiber distribution and orientation in a series of round panel specimens of ultra-high performance fiber reinforced concrete (UHPFRC) by using electrical resistivity measurements and confirmed by X-ray CT imaging. In their study, they tested round panels in flexure and the results are discussed in relation to the observed orientation of fibers in the panels. They found out that the fiber orientation has a very significant effect on the flexural strength of the panels as the fibers tended to align perpendicular to the direction of flow. As a result, panels poured from the center were significantly stronger than panels poured by other methods because the alignment of fibers led to more fibers bridging the radial cracks formed during mechanical testing.

Kang et al. [44] evaluated the fiber distribution characteristics to investigate their effect on the flexural strength of steel fiber-reinforced ultra-high strength concrete in conjunction with the direction of placement. The authors carried out flexural tests to quantify the effect of fiber distribution characteristics on flexural strength. They found that the fiber distribution characteristics were dependent on the direction of placing. They concluded that fiber distribution characteristics revealed strong effect on the ultimate flexural strength, while hardly affecting the first cracking strength.

2.2.2.3 Tensile Behavior

UHPC tensile properties are distinct from those of conventional concrete due to the increased tensile cracking capacity of the cementitious composite matrix and the crack-bridging behavior of the fiber reinforcement. In contrast to fiber-reinforced conventional concretes, UHPC can exhibit significant, sustained post-cracking tensile capacity prior to crack localization, fiber pullout, and loss of tensile capacity [45].

Doo et al. [34] stated that the characteristics of fibers such as fiber content, shape, aspect ratio, orientation, and distribution are considerably affect the tensile performance of fiber-reinforced ultra-high performance concrete [47-52]. Increasing the amount of fiber is the most convincing method to improve the tensile performance including tensile strength and fracture energy capacity. This means that the demanded tensile strength can be achieved by using adequate amount of fiber.

Habel et al. [53] show a schematic of the three distinct tensile behaviors that UHPC can exhibit: I) linear-elastic behavior before cracking; II) post cracking strain hardening

behavior and dispersed discrete cracking; and III) softening behavior during strain localization across specific cracks (**Figure 2.8**).

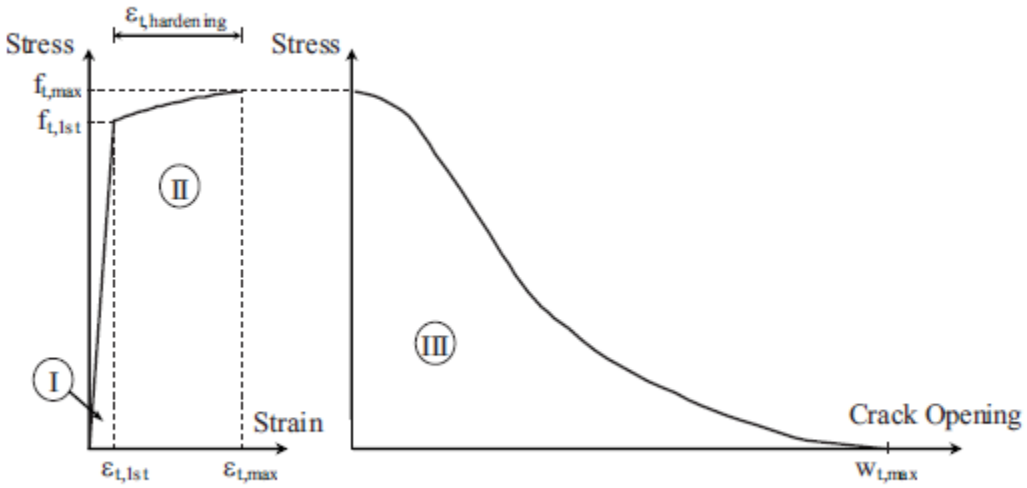

Figure 2.8: Tensile behavior of UHPC [53].

With the growing use of UHPFRC in modern construction, determining its tensile and compressive properties is essential in the study of its structural behavior, numerical modeling and fracture mechanics [34].

It was found that the average tensile strength of commercially available UHPC varies between 10 to 15 MPa. The tensile flexural strength ranges between 24 MPa to 29 MPa.

The addition of steel fibers to UHPC matrices successfully increased the fracture toughness, tensile strength, ductility and energy absorption capacity of UHPCs, although their performance were various according to the types of fiber [54].

Nguyen et al. [54] investigated the direct tensile stress versus strain response of Ultra-

High-Performance Fiber Reinforced Concrete (UHPFRC) with various sizes and geometries. The UHPFRC used in their research contained 1% macro twisted and 1% micro smooth steel fibers by volume. The effects of gauge length, section area, volume and thickness of the specimens on the measured tensile response of the UHPFRC were experimentally discovered. They found out that the different sizes and geometries of specimens did not generate significant influence on the post cracking strength of UHPFRC whereas they produced clear effects on the strain capacity, energy absorption capacity and multiple cracking behavior of UHPFRC. The strain capacity, energy absorption capacity and the number of multiple micro cracks within unit length obviously decreased as the gauge length, section area and volume of UHPFRC specimens increased. In contrast, as the thickness of the specimen increased, different tendency was observed.

Hassan et al. [34] concluded that the steel fiber content in UHPFRC had a significant effect on improving the tensile strength by almost double compared to those of UHPC without fibers. This is a significant benefit for concrete structures where punching shear failure is an important consideration such as with bridge deck designs. Moreover, ductility in both tension and compression were improved substantially. In contrast, their influence on the compressive strength and modulus of elasticity was relatively small. They reported that the Maximum tensile strain attained at peak strength was in range of 1.5–3% compared to the values of 0.15–0.25% for the UHPC (without fibers).

Kay et al. [55] conducted a research work on the optimization of strength and ductility of ultra-high performance fiber reinforced concretes (UHP-FRC) under direct tensile loading. In their research they focused on the development of strain-hardening UHP-FRC characterized by: (1) a relatively high tensile strength (exceeding 13 MPa, (2) a high

ductility, expressed by the strain at peak stress ε_{pc} in tension exceeding 0.3%, and (3) a relatively low fiber content (not exceeding 2.5% by volume). Their results show that, with appropriate high strength steel fibers, and 1% fiber volume fraction it is sufficient to trigger strain hardening behavior accompanied by multiple cracking, this characteristic essential to achieve high ductility. Also, by improving both the matrix and fiber parameters, an UHP-FRC with only 1.5% deformed steel fibers by volume resulted in an average tensile strength of 13 MPa and a maximum post-cracking strain of 0.6%.

The researchers also illustrated a simplified response of strain-hardening FRC comprising Part I (Elastic behavior up to 90–95% of cracking strength, followed by development of micro cracks and activation of fibers; Part II (Strain hardening behavior with multiple cracking, small crack width, and inelastic strain); and Part III (Softening behavior) (**Figure 2.9**).

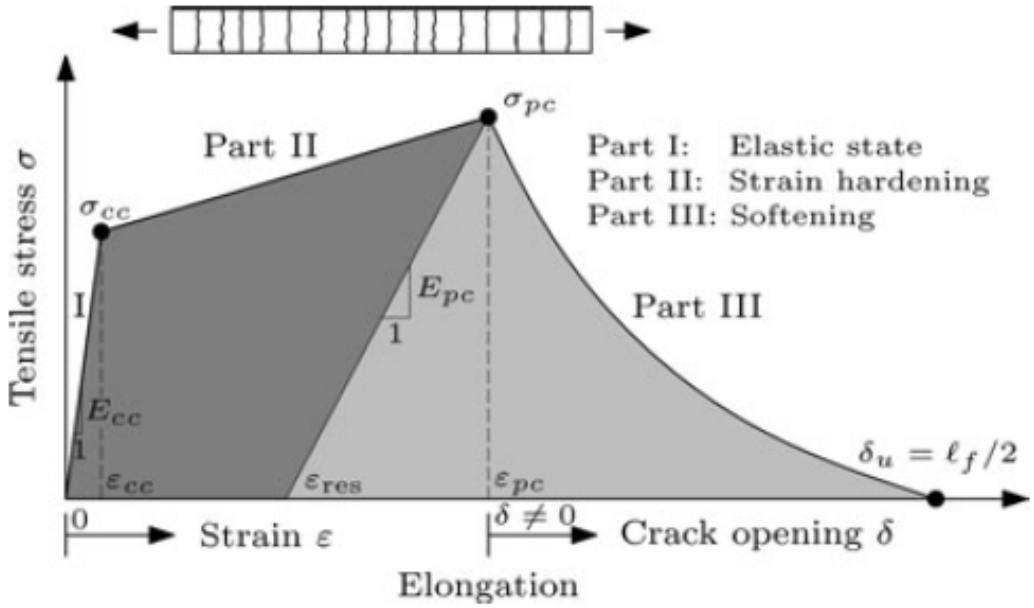

Figure 2.9: Idealized simplified response of strain-hardening FRC composites in tension [55].

They concluded that by improving the fiber bond behavior through: (1) increasing matrix density and strength (up to 200 MPa), (2) increasing fiber strength (up to 3100 MPa), and (3) improving the mechanical bond of the fiber through fiber deformation (end hook or twisted), an UHP-FRC can be designed to achieve a relatively high tensile strength (up to 15 MPa) and ductility (ε_{pc} = 0.6%) with a low fiber volume fraction (about 2%).

2.2.3 Hybrid Construction with UHPC

As UHPC can offer solutions for specific concrete construction which heretofore were not possible, attempts are being made to utilize UHPC for innovative applications.

Azad and Hakeem [56] have completed an exploratory study of hybrid floor slab construction utilizing UHPC at the tension face to provide tensile strength and eliminating the use of steel reinforcement. The findings support the concept of hybrid slab construction. In another study, Azad and Hakeem [57-58] investigated the possibility of utilizing high flexural tensile strength of steel fiber-reinforced UHPC by using a layer of UHPC as the tension face of a hybrid flexure member that would eliminate the need of passive reinforcement to provide the tensile strength.

Azad and Hakeem [59] have studied beam construction using UHPC introducing for the first time the concept of UHPC bars as tension reinforcement. Based on the findings, a patent of the product has been filed [60].

Elmahdy et al. [61] investigated the behavior of hybrid composite hollow-box beams experimentally and analytically to determine the feasibility and effectiveness of the structural section as the main flexural member in bridge construction. This research is

concerned with developing an understanding of the behavior of an innovative beam design. The beam is composed of an Ultra-High Performance Concrete (UHPC) in the compression zone and Steel or Carbon Reinforced Polymer sheets (SRP or CFRP) to resist the tension. The capacity of GFRP box sections was increased significantly by adding UHPC on the compression side and SRP or CFRP sheets on the tension side.

Donna et al. [62] investigated the behavior of composite beams fabricated from fiber reinforced polymers (FRPs) and Ultra-High Performance Concrete (UHPC) under static flexural loading. In this work, the use of high performance materials, such as FRPs and UHPC, in the design of the proposed hybrid cross-section is intended to allow for higher strength to be achieved while reducing section weight and overall size. The cross-section of the hybrid structural member consists of a thin layer of UHPC supported on the top flange of a GFRP hollow box section. Along the base of the GFRP box section, sheets of tensile reinforcement, made from either CFRP or SFRP, are applied. Testing of the hybrid beams have revealed that in addition to the UHPC layer acting to increase the resistance of the GFRP hollow box section beam, it also provides lateral support and prevents compressive flange buckling at higher loads.

Ferrier et al. [63] developed a new hybrid glulam beam that will increase the performance of timber structures and optimize the use of wood in such structures. The hybrid beam is made by combining glulam with ultrahigh-performance short fiber-reinforced concrete (UHPC-SFR) planks with or without internal reinforcement consisting of steel- or fiber-reinforced polymer reinforcement bars. The results show that by combining wood and UHPC-SFR, it is possible to obtain a hybrid beam with greater bending stiffness and increased ultimate load capacity. This experimental investigation confirms the validity of

the concept of a new type of hybrid beam, made of glued-laminated wood and UHPC planks internally reinforced with steel or FRP reinforcement bars.

Hajek et al. [64] studied the timber-concrete composite floor structures benefit from lower weight of UHPC deck while improving acoustic parameters and fire safety of the structure. They reported that one of the key problems is the connection system between timber beam and UHPC deck. The experimental results have showed that this can be solved by gluing. The results show that the high quality of mechanical and environmental performance creates the potential for wider application of UHPC in building construction in the future.

Schäfers et al. [65] investigated the bonded composite constructions from timber and ultra-high performance concrete (UHPC) as a highly innovative structural element. They carried out extensive theoretical and experimental investigations on the bond between timber and UHPC. In most cases they found that the failure of the bond occurs in timber close to the bond-line. From their research, they concluded that the theoretical models were able to describe the behavior of the bond between timber and UHPC and the experimental investigations on the bond behavior depicted that a failure of the bond in timber were close to the bond-line in almost all cases, and that nonlinear effects in the load–relative displacement curve occur with increasing bond length.

Bassam et al. [66] examined experimentally the mechanical properties and permeability characteristics of the interface between normal concrete (NC) substrate which represents old concrete structures and an overlay of ultra-high performance fiber concrete (UHPFC)

as a repair material. Their results show that the newly overlay UHPFC achieves high bond strength and bonds efficiently with the NC substrates.

Youssef et al. [67] investigated the bonded composite constructions using timber and ultra-high performance fiber reinforced concrete (UHPFRC) as highly innovative structural elements technically and economically efficient, and having better environmental performances. Their research described the timber-concrete assembly by adhesive bonding and specially the behavior of bonded joint between Laminated Wood (LW) and UHPFRC.

CHAPTER 3

EXPERIMENTAL PROGRAM

The experimental work involved testing prepared test specimens to observe flexure strength and behavior of hybrid specimens of three types: (i) hybrid layered beam specimens; (ii) UHPC reinforced beam specimens, and (iii) hybrid hollow-core beam specimens with top and bottom UHPC layers and a layer of normal Portland cement concrete (NC) sandwiched in between the UHPC layers. The work proposed was completed in phases. In the first phase, the ingredients for both UHPC and ordinary concrete were procured. In the second phase, the mix design for both concretes was finalized and the test specimens were cast. In the third phase, the specimens were tested to ascertain the flexural performance and behavior of the proposed hybrid floor slab constructions.

3.1. Materials Used in Hybrid Construction

3.1.1 Ultra-High Performance Concrete (UHPC)

A suitable UHPC mixture was developed using locally available materials such as cement, fine sand, micro silica and super plasticizer (Glenium 51®). Only steel fibers were imported.

(i) Cement

Type I ordinary Portland cement conforming to ASTM C 150 with a specific gravity of 3.15 was used in both UHPC and ordinary mixtures. Sufficient amount of cement was procured and stockpiled safely to prevent hardening of cement.

(ii) Micro Silica

Elkem Microsilica was obtained from a local supplier in the Kingdom. It is a byproduct generated from the carbothermic reduction of quartz and quartzite in electric arc furnaces in the production of silicon and ferrosilicon alloys. It is a siliceous material, containing 85–95% SiO_2 with very fine vitreous particles, which improves the strength and durability properties of concrete.

The chemical composition of cement and microsilica (MS) was determined at the Research Institute of the University. The results are shown in **Table 3.1**.

Table 3.1: Chemical Composition of Type I Cement and Microsilica

Composition Weight %	Cement	Microsilica
CaO	64.35	0.48
SiO_2	22	92.5
Al_2O_3	5.64	0.72
Fe_2O_3	3.8	0.96
K_2O	0.36	0.84
MgO	2.11	1.78
Na_2O	0.19	0.5
Equivalent alkalis ($Na_2O + 0.658K_2O$)	0.33	-
SO_3	2.1	-
Loss on ignition	0.7	1.55
C_3S	55	-
C_2S	19	-
C_3A	10	-
C_4AF	7	-

(iii) Fine Sand

Dune sand, a vastly available material in the Kingdom, was used as fine aggregate in this study. The specific gravity of fine aggregate was 2.56, and the absorption was 0.4%. The grading of the dune sand used in the study is shown in **Table 3.2**.

Table 3.2: Grading of the Fine Aggregate used in the Study

ASTM Sieve No.	Size (mm)	Percentage Passing (%)
4	4.75	100
8	2.36	100
16	1.18	100
30	0.6	75
50	0.3	10
100	0.15	5

(iv) Superplasticizer

Glenium 51® as superplasticizer was used in all the mixes of UHPC. It's a new generation polycarboxylic-based ether hyperplasticiser. It was sourced from a local supplier in the Kingdom (BASF). Its technical data is shown in **Table 3.3**, as obtained from the manufacturer.

Table 3.3: Technical Data of Glenium 51®

Property	Brown Liquid
Specific gravity @20^0 C	1.08±0.02 g/cm^3
pH-value @20^0C	7.0±1.0
Alkali content	≤5.0
Chloride content	≤0.1 %

(v) Steel Fibers

Steel fibers are dimensionally the largest constituent in a typical UHPC mixture. The randomly distributed short fibers are generally introduced into the UHPC matrix in order to enhance its mechanical properties such as toughness, impact resistance, ductility (post cracking), tensile and compressive strength.

The imported steel fibers were smooth plain copper coated, having a nominal diameter of 0.2 mm and 13 mm length with aspect ratio (ratio of length to nominal diameter) of 65 (**Figure 3.1**). The manufacturer's specified minimum tensile strength is 2500 MPa.

Figure 3.1: Steel fibers used in UHPC mix

3.1.2 Normal Portland Cement Concrete (NC)

In normal concrete mixture, the same cement type and fine sand used in developing UHPC were used.

The coarse aggregates used in this study were crushed limestone sourced from a local quarry in Abu Hadriah, Eastern Province of Saudi Arabia. It has a maximum aggregate size of 12.5 mm, specific gravity of 2.60 and absorption of 1.4%. Three aggregate sizes, 12.5 mm (½ inch), 4.75 mm (3/16 inch), and 2.36 mm (3/32 inch) were used in all NC mixtures.

3.2. Mix Design

3.2.1 UHPC Mix Design and Preparation

Locally developed and optimized mix for UHPC was used for all test specimens. The mix design was invariant in this work. Mixing of UHPC requires special equipment and procedures to develop consistency in batching, casting, and curing in a timely fashion. A high shear capacity mixer along with vibratory table is required. Casting of UHPC was carried out in Civil and Environmental Engineering Department's laboratory, using horizontal pan mixer. The UHPC mixer and UHPC mix used for casting of UHPC is shown in **Figure 3.2**.

The developed UHPC mix utilized in the hybrid construction had the composition per cubic meter as follows: ASTM Type I Portland cement 900 kg; micro-silica 220 kg, fine sand 980 kg, steel fiber 157 kg (about 6.3% by weight of UHPC), superplasticizer 40.3 kg (Glenium 51®) and water 168 kg (representing water-binder ratio of 0.15). The steel fibers were of 0.15 mm in diameter and 12.7 mm in length with minimum tensile strength of 2500 MPa. The UHPC mix design yielded cube compressive strength over 160 MPa and flexural tensile strength exceeding 25 MPa.

The measured quantities of cement, fine sand, microsilica are mixed at low speed for about 3 minutes. Water and superplasticizer are mixed separately. Then, the mixed liquid of water and superplasticizer added slowly to the dry mix (key point) in a course of 4-6 minutes. The observed turning point can be seen in the first 5-7 minutes by which time the mixture will change completely into thick plastic paste. The addition of water and superplasticizer mixture is continued slowly to complete the addition. At this stage, the

mix will transform into a flowable paste. Finally, steel fibers are added to the mix in very slow rate to ensure uniform dispersion of the steel fibers in the mix. The total mixing time of UHPC mix is about 15-20 minutes.

Based on the trial mixes, the optimum dosage of Glenium 51® plasticizer was found to be 4% by weight of the binder (cement and microsilica), equivalent to about 1.8 % by weight of the mixture. This is the maximum limit allowed to prevent delaying the setting time of the mixture which in turn affects the demolding time. For the mix design used, the minimum demolding time was 24 hours following the specified procedure of mixing.

Figure 3.2: UHPC mixer (left), UHPC mix in the mixer (right).

3.2.2 Normal Portland cement concrete (NC) Mix Design

The mix proportion of normal Portland cement concrete used consisted of cement 350 kg/m^3, coarse aggregates 1092 kg/m^3, fine aggregate 729 kg/m^3 and water 184.4 kg/m^3

(corresponding to water-cement ratio of 0.5) to produce an average cylinder compressive strength of about 40 MPa.

3.3. Test Specimens, Casting and Curing

3.3.1 Evaluation of Material Properties

The material properties of the developed UHPC and normal Portland cement concrete used in the hybrid floor slab constructions were determined through a number of tests, the results of which are presented in Chapter 4. Uniaxial compression, splitting tensile strength, uniaxial direct tensile and flexural tensile strength, under four-point-bending, were conducted on the developed UHPC. For ordinary Portland cement concrete, uniaxial compression tests on 100 mm cubes and 75x150 mm cylinders were carried out.

3.3.1.1 Material Properties of UHPC

All test specimens for material properties of UHPC mentioned below were cured using heat treatment by placing specimens for 48 hours at 90 ^{0}C.

i. Compression strength and modulus of elasticity

The compressive strength of UHPC was determined using 30 50 x 50 x 50 mm cubic specimens. Six cylinders of 75 x 150 mm (**Figure 3.3**) were used to determine the stress-strain behavior of UHPC. They were fitted with strain gages diametrically at two opposite sides of the cylinders at mid height.

ii. Splitting tensile strength

Split cylinder is another means of measuring indirectly the tensile strength of concrete using ASTM C 496. Six UHPC cylinders of 75 mm diameter and 150 mm length (**Figure 3.4**) were used.

Figure 3.3: Test specimens used for compressive strength of UHPC.

Figure 3.4: UHPC cylinder under splitting tensile test.

iii. Direct tensile test

In this test, Six UHPC prisms of dimensions 25x25x285 mm (**Figure 3.5**) were used. Two strain gages were mounted on the opposite sides of the specimen at the center of the prism to measure longitudinal strain. The experiment focused also on bridging effect produced by the fibers during the tensile tests.

Figure 3.5: Prisms used in uniaxial direct tension test of UHPC.

iv. Flexural Tensile Strength and Behavior

The flexural strength was determined by testing 34 UHPC prism specimens of size 40 x 40 x 160 mm (**Figure 3.6**) in four- point loading under a displacement controlled testing machine of 600 kN capacity with load rate of 0.5 mm / min. For the purpose of finding the cracking strength of the matrix, three prisms of UHPC were prepared using the same UHPC mix without addition of steel fibers.

Figure 3.6: Prisms used for flexural strength of UHPC.

3.3.1.2 Normal Portland Cement Concrete (NC) Properties

i. Compressive Strength and Modulus of Elasticity

Cube compressive strength was determined by testing six 100 mm cubes in accordance with ASTM C 39 using a digital compression testing machine (MATEST) after 28 of water curing. Additionally, cylinder compressive strength was determined by testing six 75x150 mm cylinders in accordance with ASTM C 39. Cylinders were tested in compression using two strain gages fixed at diametrically opposite sides and two LVDTs

to record the strain and displacement. The results were analyzed to determine the strength and modulus of elasticity (**Figure 3.7**).

Figure 3.7: Test specimens used for compressive strength of NC.

Table 3.4 summarizes all the specimens tested for evaluation of the material properties of UHPC and normal concrete.

Table 3.4: Specimens Details for Properties of Materials used in Hybrid Construction

Material	Test Type	Specimen Size	No. of Specimens
UHPC	Compressive strength	50x50x50 mm cube	30
	Compressive strength and modulus of elasticity	75x150 mm cylinder	6
	Splitting tensile strength	75x150 mm cylinder	6
	Direct tension	25x25x285 mm prism	6
	Flexural strength	40x40x160 mm prism	34
NC	Compressive strength	100x100x100 mm cube	6
	Compressive strength and modulus of elasticity	75x150 mm cylinder	6

3.3.1.3 Hybrid Specimens

Three alternative forms of construction of slab-type members (flexure-controlled design) were explored in this work for their structural adequacy.

(a) Hybrid Layered Specimens

(b) UHPC Reinforced Specimens

(c) Hollow- Core Specimens

The details of each type of the three hybrid construction are presented.

(a) Hybrid Layered Specimens

(i) Specimens Detail

The test program involved testing of simply supported small-size beam-type specimens that would fail in flexure but not in shear, as the beams were not be provided with shear reinforcement, analogous to one-way simply supported slabs that do not normally have shear reinforcement. The size of the test specimens was kept within acceptable dimensions, neither too large to create handling problems nor too small to have any size effects.

Four beam sizes were chosen (**Table 3.5**): Group A- 150x150x760 mm, Group B- 150x150x1000 mm, Group C- 150x200x900 mm (200 mm depth) and Group D- 150x200x1200 mm (200 mm depth).

All test specimens were cast with a bottom layer of UHPC and then topped with ordinary Portland cement concrete (NC) (**Figure 3.8**). For Group A, (150x150x760 mm size) and Group C (150x200x900 mm), two different curing options for UHPC layer, C1 and C2 as

explained later, were adopted. Two different thicknesses of bottom layer of UHPC were used for each beam size. A total of 12 specimens, six with 20 mm thickness of UHPC (three for each curing option) and six with 40 mm UHPC layer (three for each curing option) were cast in 150x150x760 size. Also, 12 specimens were cast, six with 25mm (three for each curing option) and six for 50 mm thickness of UHPC (three for each curing option) in 150 x 200 x 900 size. For the longer span specimens as in Group B (150x150x1000 mm), six specimens were prepared, three with 20 mm (three for one curing option) and three for 40 mm thickness of UHPC and for Group D beam (150x200x1200 mm), also six specimens were cast, three with 25 mm (three for one curing option) and three for 50 mm thickness of UHPC. Thus, in total 36 specimens were cast. **Table 3.5** lists the details of all test specimens, including the test variables and numbers of specimens used.

Table 3.5: Test Specimen's and Details of Hybrid Layered Specimens

Groups	Beam Size (mm)	UHPC Thickness (mm)	Beam ID	Test Span (mm)	No. of Test specimens
Group A	150x150 x 760 (b x h x L)	20	LS-A-C1[+]	630	6
			LS-A-C2[‡]		
		40	LS-B-C1[+]		6
			LS-B-C2[‡]		
Group B	150x150x1000 (b x h x L)	20	LS-C-C2[‡]	900	3
		40	LS-D-C2[‡]		3
Group C	150x 200x 900 (b x h x L)	25	LS-E-C1[+]	750	6
			LS-E-C2[‡]		
		50	LS-F-C1[+]		6
			LS-F-C2[‡]		
Group D	150x 200x 1200 (b x h x L)	25	LS-G-C2[‡]	1100	3
		50	LS-H-C2[‡]		3
Total number of specimens					36

[+]Curing option C1: Concrete cast immediately over uncured UHPC layer
[‡]Curing option C2: Concrete cast after 2 days of curing of UHPC layer

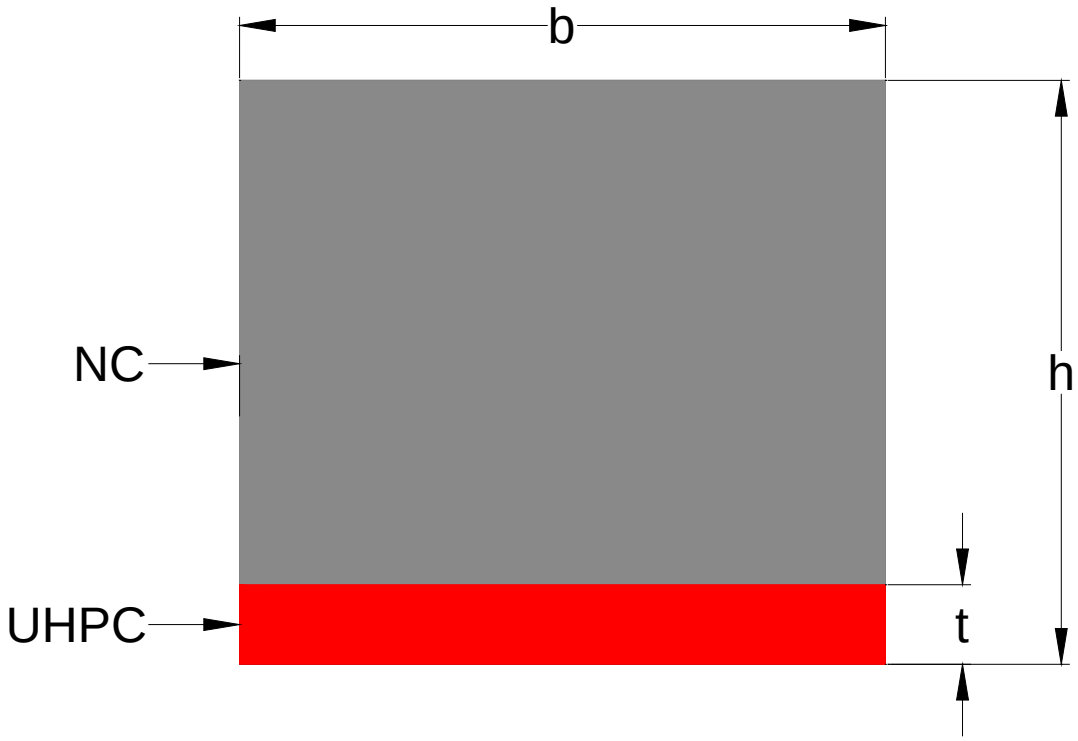

Figure 3.8: Hybrid layered beam specimens.

Test specimens were designed taking into consideration the effect of thickness of UHPC, which was treated as a main variable, on the strength and behavior.

i. Casting and Curing

All specimens were prepared using same UHPC mix and casting procedure. In other words, mix design and casting procedure were invariant.

Two curing conditions were used for groups A and C: in curing option C1, the top normal Portland cement concrete layer was placed immediately over the bottom UHPC layer without allowing any time for curing of UHPC; in curing option C2, the bottom UHPC

layer was first cast in a mold and then left for 2 days for self-curing (**Figure 3.9**). The top surface was left unfinished. Normal concrete was then placed over the UHPC layer and vibrated. The top surface of all specimens was trowel-finished. **Figure 3.10** shows the view of beam specimens with UHPC bottom layer. All specimens were moist-cured for 28 days prior to testing.

Figure 3.9: UHPC layers before casting the ordinary concrete on top.

Figure 3.10: Hybrid beams with bottom UHPC layer after casting.

3.3.1.4 UHPC Reinforced Specimens

i. Specimens Details

UHPC bars, rectangular or square in section, were precast using same UHPC mix and mixing procedure as explained in section 3.3.1. They were used as tension reinforcement in beam specimens as shown in **Figure 3.11**.

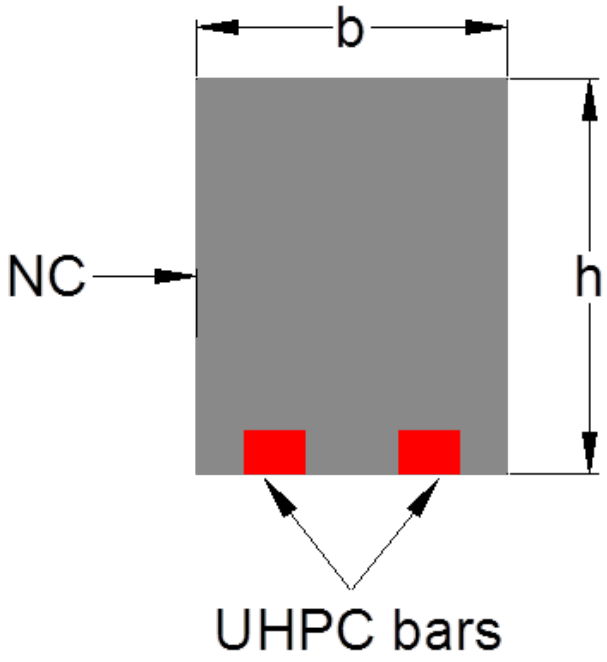

Figure 3.11: Typical UHPC reinforced beam specimens

Six groups of beam sizes were chosen: (i) 150 x 150 x760 mm, (ii) 150 x 200 x 900 mm (200 mm depth), (iii) 150 x 220 x 760 mm (220 mm depth), (iv) 200 x 270 x 1000 mm (270 mm depth)., (v) 200 x 220 x 1000 mm (220 mm depth) and (vi) 200 x 310 x 1000 mm (310 mm depth). The UHPC bars used were square or rectangular cross-section in three sizes: (i) 25 x 25 mm, (ii) 25 x 50 mm, and (iii) 50 x 50 mm and had varying lengths and numbers as shown in **Table 3.6**. The details of all test specimens, including the number of samples used are given in **Table 3.6**.

ii. Casting and Curing

The hybrid specimens with UHPC bars were cast in two steps. First the prepared mix was placed in the molds for casting of UHPC bars according to their sizes. The top surface of the bars was left unfinished to provide good bond with Normal Concrete (NC). To improve further the bond between UHPC bars and NC, the two vertical edges of the bars were cast with grooves as shown in **Figure 3.12**. After casting, the bars were heat-cured at a temperature of 90 ^{0}C for 48 hours to accelerate curing and strength development. In the next step, the precast UHPC bars were transferred to another mold (**Figure 3.13**) and then NC was poured and vibrated for compaction. It should be noted that as the bars were placed directly in the mold, there was no bottom cover to UHPC bars (**Figure 3.14**). The top surface of the hybrid beams was trowel finished. All specimens were moist-cured for 28 days prior to testing.

Table 3.6: Test Specimen's and Details of UHPC Reinforced Beam Specimens

Specimens Group	Beam Size (mm)	Test Span (mm)	UHPC Bar Cross Section (No.-w x d)	Beam ID	No. of Test Specimens
Group (i)	150 x 150 x 760 (b x h x L)	630	2- 25 x 25	UB-1	6
		630	3- 25 x 25	UB-2	3
		630	2- 25 x 50	UB-3	5
		630	2- 50 x 50	UB-4	4
Group (ii)	150 x 200 x 900 (b x h x L)	750	2- 25 x 25	UB-5	3
Group (iii)	150 x 220 x 760 (b x h x L)	680	2- 50 x 50	UB-6	2
Group (iv)	200 x 270 x 1000	900	2- 50 x 50	UB-7	2
Group (v)	200 x 220 x 1000	900	2- 50 x 50	UB-8	2
Group (vi)	200 x 310 x 1000	900	4- 25 x 25	UB-9	2
Total number of specimens					29

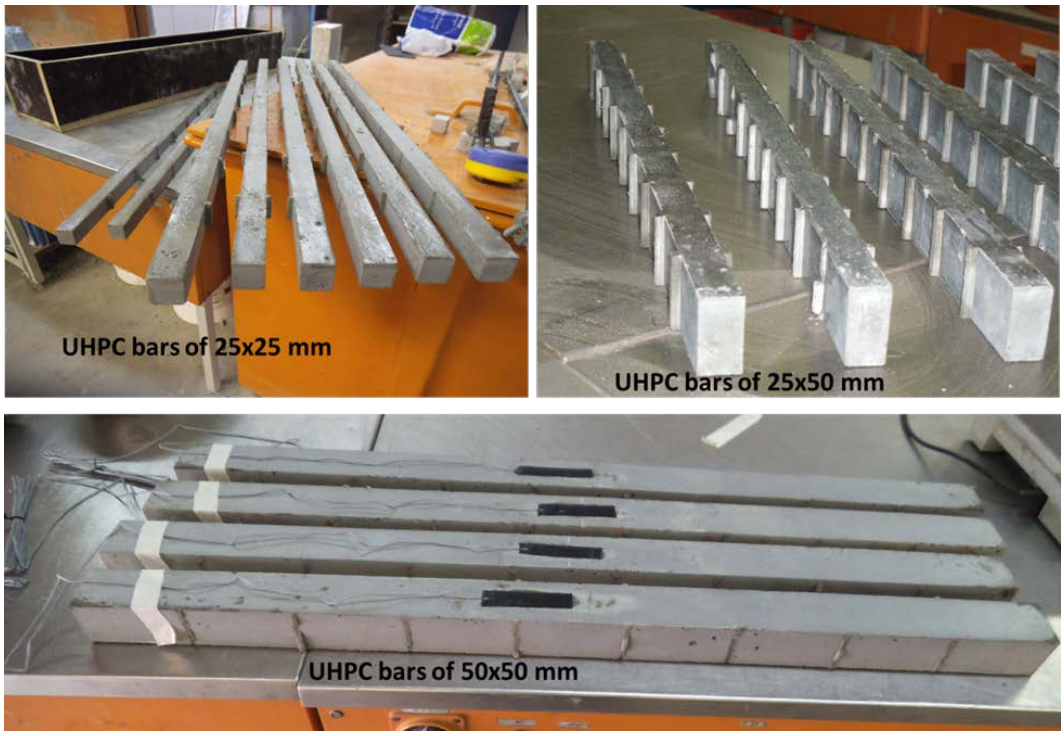

Figure 3.12: UHPC bars of different sizes and cross sections.

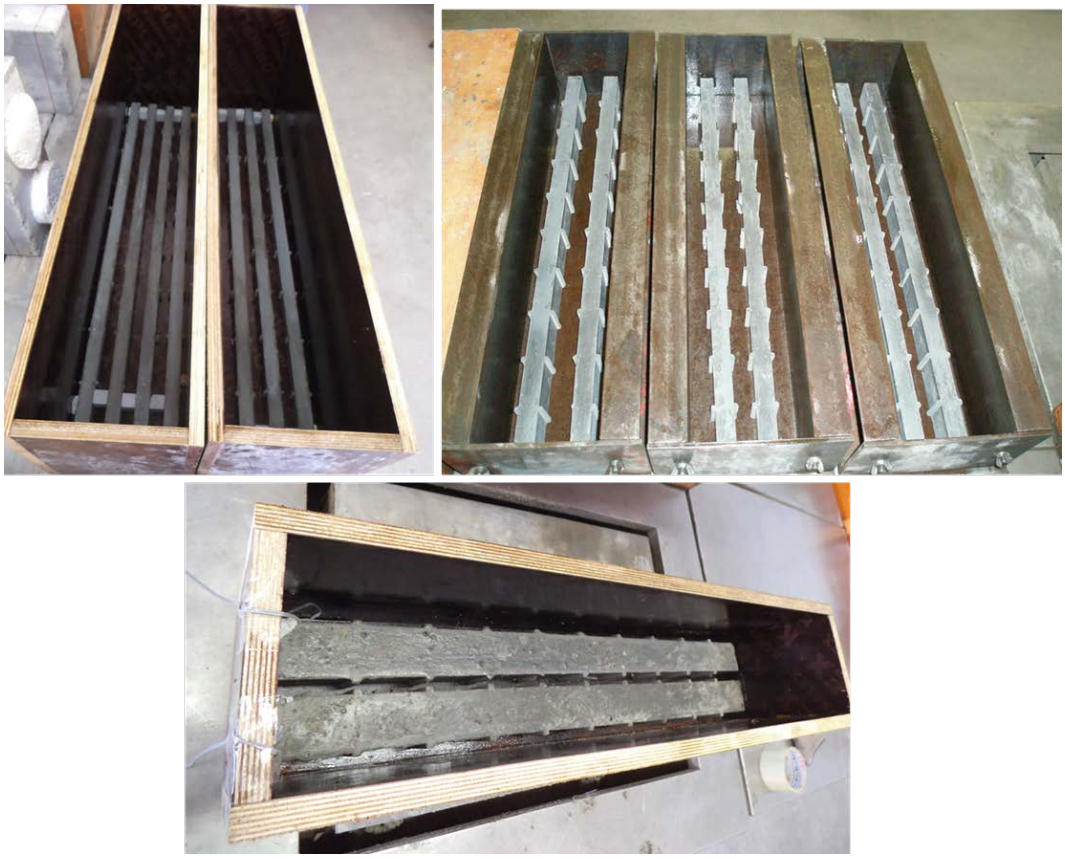

Figure 3.13: UHPC bars in their moulds.

Figure 3.14: Hybrid specimens reinforced with 2 - 50x50 mm UHPC bars.

3.3.1.5 Hybrid Hollow-Core Specimens

i. Specimens Details

The dimensions of the test specimens are chosen to avoid the problem of handling, casting and testing. Five groups of hollow core specimens, as shown in **Figure 3.15**, were chosen: (i) 260x140 mm (140 mm depth) with two circular holes (ii) 330x175 mm (175 mm depth) with two circular holes, (iii) 390x200 mm (200 mm depth) with two circular holes, (iv) 380x140 mm (140 mm depth) with three circular holes, (v) 260x140 mm (140 mm depth) without circular holes (solid section) . For Groups (i) to (iii), two lengths, 1000 mm and 1200 mm, were considered. For Group (iv), the length was 1200 mm and for Group (v) (solid section), the length of the specimens was 1000 mm. All

sections had same thicknesses of UHPC layers: 20 mm thick for the top layer and 30 mm thick for the bottom layer. **Table 3.7** shows the details and number of test specimens.

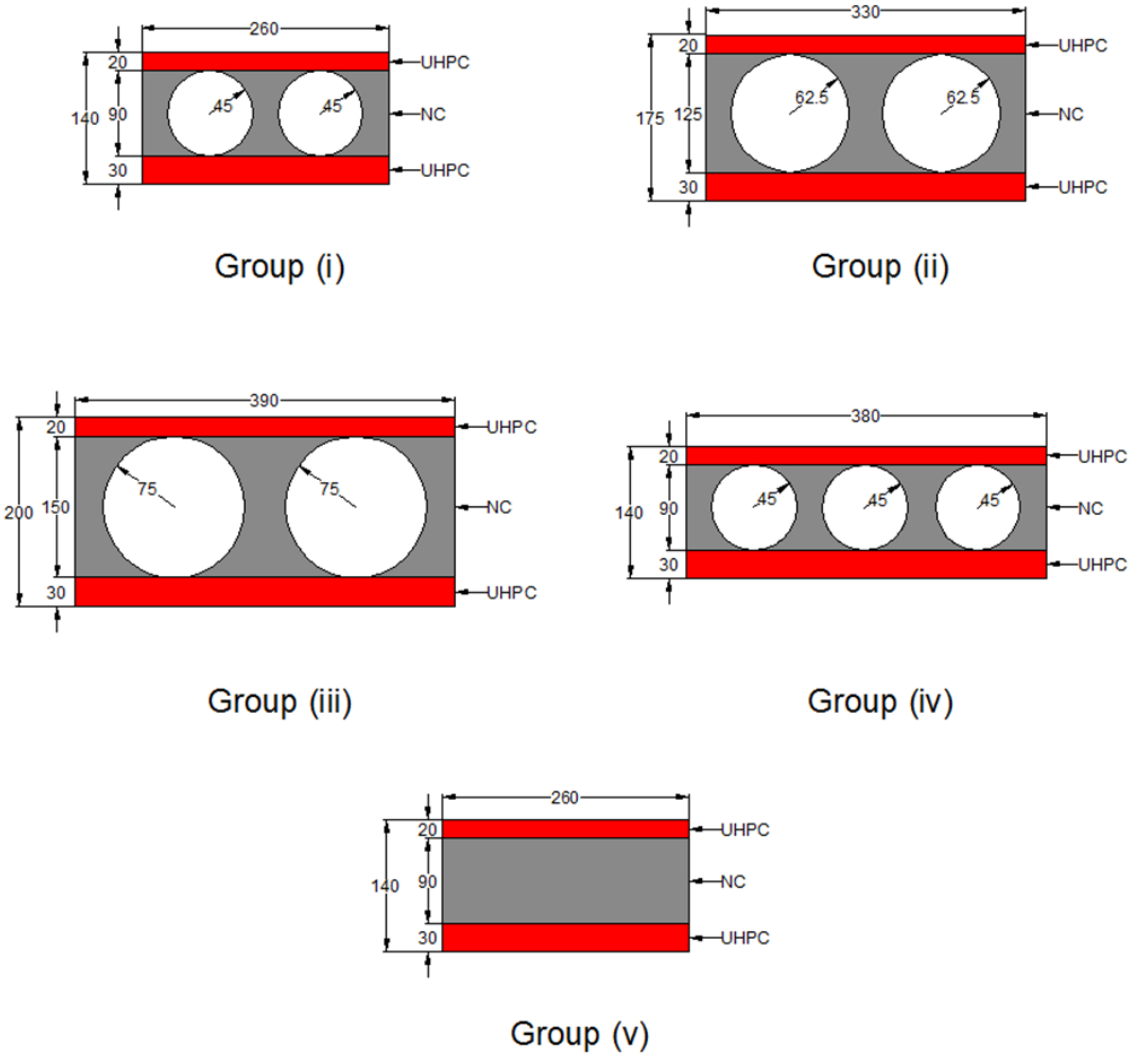

Figure 3.15: Cross-sections of hybrid hollow core specimens.

Table 3.7: Test Specimens and Details

Group	Beam Designation	No. of Holes	Cross Section		Length (mm)	Test Span (mm)	No. of Test Specimens
			Width (mm)	Depth (mm)			
Group (i)	HC-A-S1	2	260	140	1000	900	3
	HC-A-S2						
	HC-A-S3						
	HC-A-L1				1200	1100	3
	HC-A-L2						
	HC-A-L3						
Group (ii)	HC-B-S1	2	330	175	1000	900	3
	HC-B-S2						
	HC-B-S3						
	HC-B-L1				1200	1100	3
	HC-B-L2						
	HC-B-L3						
Group (iii)	HC-C-S1	2	390	200	1000	900	3
	HC-C-S2						
	HC-C-S3						
	HC-C-L1				1200	1100	3
	HC-C-L2						
	HC-C-L3						
Group (iv)	HC-D-L1	3	380	140	1200	1100	3
	HC-D-L2						
	HC-D-L3						
Group (v)	HC-E-S1	No holes	260	140	1000	900	3
	HC-E-S2						
	HC-E-S3						
Total No. of specimens							24

In beam designations shown in **Table 3.7**, the letter ‘S’ indicates shorter length of 1000 mm (e.g. HC-A-S1) and ‘L’ indicates longer length of 1200 mm (e.g. HC-A-L1).

ii. Casting and Curing

All specimens were prepared using same UHPC mix and casting procedure. Each hybrid hollow core specimen was cast in two stages. In the first stage, the top and bottom UHPC faces were cast in separate moulds (**Figure 3.16a**).

Figure 3.16: Steps of fabricating of UHPC layers: (a) Casting of UHPC layers, (b) Surface roughness of UHPC layers, (c) Curing of UHPC layers in oven, (d) Final precast UHPC layers.

The exposed top surface of UHPC layer was roughened provide better bond with in-fill concrete (**Figure 3.16b**). It was demolded after 24 hours and then cured under heat-

treatment at 90 ^{0}C for two days (**Figure 3.16c**). The precast UHPC layers are shown in **Figure 3.16d**.

For casting of the complete section in the second stage, the two UHPC faces were placed in a mould with rough surface facing inside the section. Two or three tubes made of papers or styro-foam were positioned in the mould to construct the holes (**Figure 3.17**) and then the filling was completed by pouring normal concrete mix. After one day, the void forms were removed from the section. Each specimen was water-cured for 28 days.

Figure 3.17: Placement of the void forms in the mould before casting of ordinary concrete

Figure 3.18: Final hybrid hollow core test specimens.

Figure 3.18 shows the view of the hybrid hollow core specimens after demolding.

3.4. Testing of Specimens

3.4.1 Evaluation of Material Properties

A suitable UHPC mixture was developed using locally available materials such as cement, fine sand, micro silica and super plasticizer (Glenium 51®). Only steel fibers were imported.

3.4.1.1 Material Properties of UHPC

i. Compression Test

The compression tests were completed on cubes and cylinders according to the standard test methods of ASTM C109 for cubes (**Figure 28**) and ASTM C 39 for cylinders (**Figure 29**).

The 50 mm cubes were tested under a 3000 kN capacity digital compression testing machine after 48 hours of heat curing at 90 ^{o}C according to the standard test method of ASTM C109 for cubes as shown in **Figure 3.19**.

The compression tests of cylinders were conducted by means of hydraulic press machine with a capacity of 1000 kN and connected to a data acquiring device to record the load-strain diagram as shown in **Figure 3.20**. For all cylinders tested, the standard size had a diameter of 75 mm and a prepared length of about 148 mm by cutting the rough end.

Figure 3.19: Compressive strength of UHPC.

Figure 3.20: Uniaxial compressive testing of UHPC cylinders.

ii. Splitting Tensile Strength

Splitting cylinder tension tests were also conducted to determine the tensile properties of UHPC indirectly using ASTM C496. The tests were performed under a compression testing machine (MATEST) of 3000 kN capacity.

iii. Direct Tensile Test

Experimental tests were carried out by means of an Instron testing machine for tensile test, with a tensile capacity of 250 kN, connected to data logger to acquire data and record the failure tensile load and load–displacement and load-strain diagrams. For small UHPC prisms of 25x25x285 mm size, the tests were displacement controlled, with a rate of 0.5 mm/min (**Figure 3.21**). Some specimen was instrumented with two strain gages prior to testing The aim of the test was the detection of uniaxial tensile strength of the developed UHPC in order to utilize it in the finite element modeling.

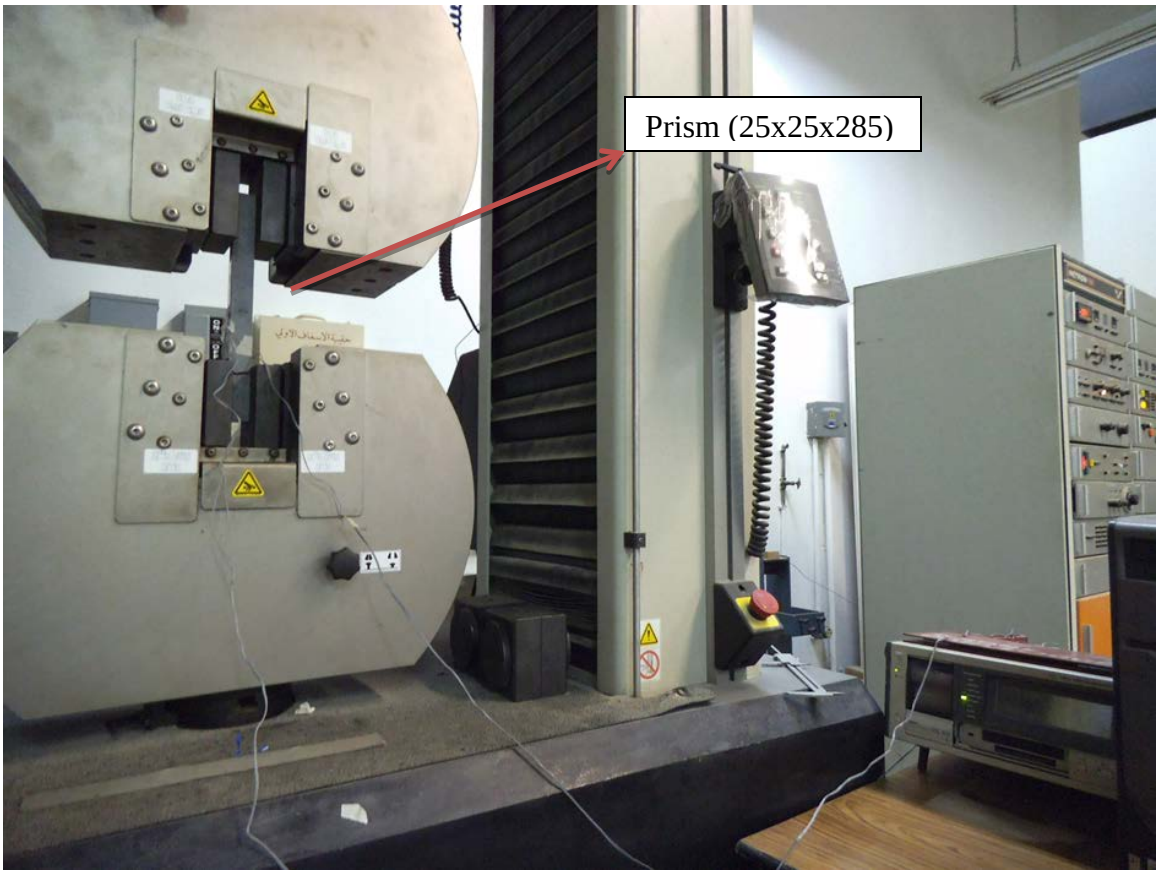

Figure 3.21: Setup for uniaxial direct tension of prisms.

iv. Flexural Tensile Strength and Behavior

The standard four-point flexural test to determine modulus of rupture (MOR) according to ASTM C 78 is one of the most common method for obtaining flexural tensile strength of normal as well as high-performance concretes. To determine the tensile properties of UHPC, the four-point flexural tests were carried out using concrete prisms having dimensions 40×40×160 mm. The load and the cross head deflection of the prisms were recorded. The cast prisms were oriented in the load frame such that the top and bottom of the prism as cast became the back and front of the prism as tested.

31 prisms were tested, after 48 hours of heat curing. Testing of prisms was conducted on a 300 kN LLOYD Instrument Machine with a rate of 0.5 mm/min and the deflection was measured using the cross head deflection of the machine as shown in **Figure 3.22**.

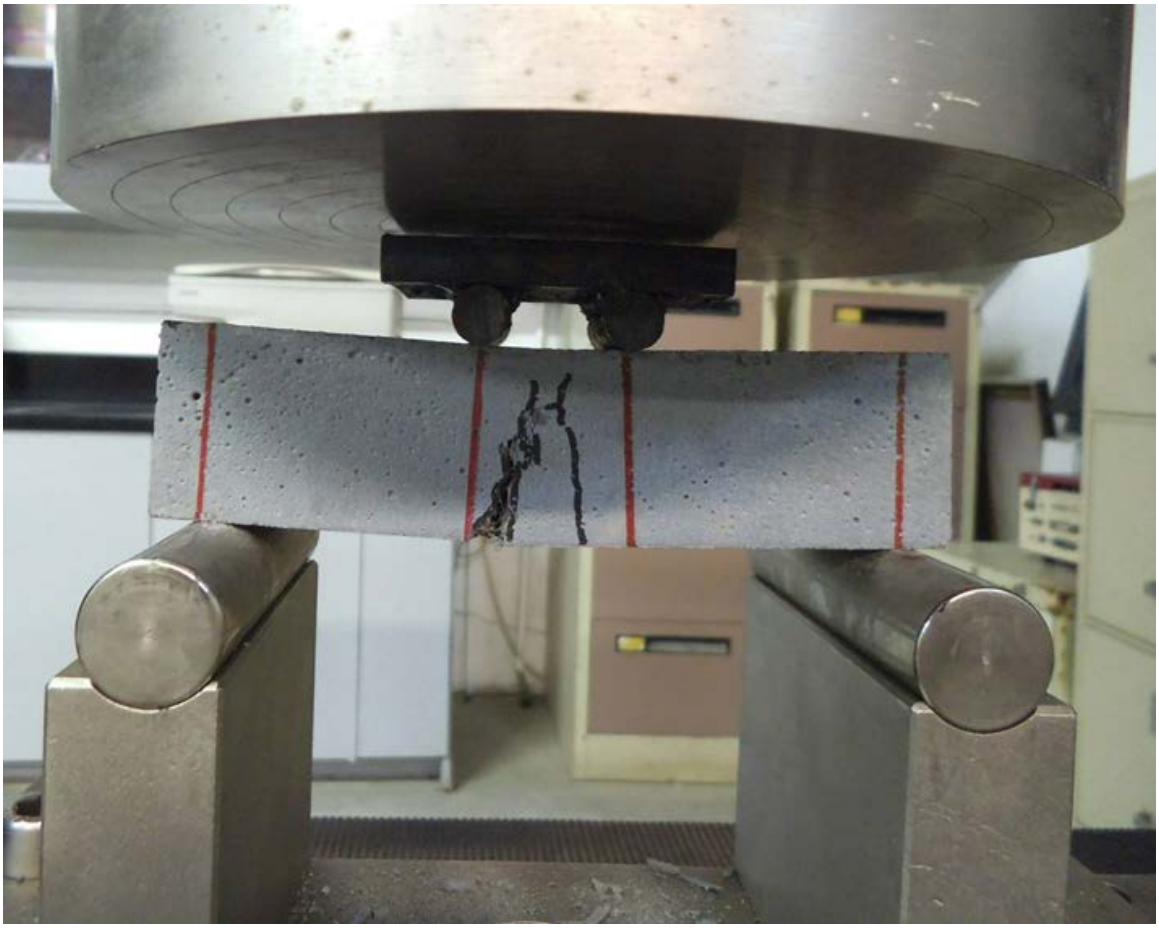

Figure 3.22: Flexural strength setup for UHPC prisms.

3.4.1.2 Normal Portland Cement Concrete (NC) Properties

i. Compressive Strength and Modulus of Elasticity

Compressive strength was determined on 100 mm cube specimens according to ASTM C 39 using a digital compression testing machine (MATEST) after 28 days of water curing. Cylinders were tested in compression using two strain gages on each opposite sides to record the strain and two LVDTs to record the displacement and the results were analyzed to determine the strength, modulus of elasticity (**Figure 3.23**).

Figure 3.23: Setup uniaxial compression test of normal Portland cement concrete.

3.4.2 Hybrid Specimens

3.4.2.1 Material Properties of UHPC

All specimens were tested in a four-point bend test (**Figure 3.24**) under an Instron machine using monotonically increasing load till failure. The maximum load in kN sustained by a beam is denoted by P. The following values of span L and the shear span, a, were used: for Group A, L=630 mm, a= 240 mm, for Group B, L=900 mm, a= 375 mm, for Group C, L=750 mm, a= 300 mm, and for Group D, L=1100 mm, a= 475 mm. In all cases, the span to depth ratio a/h was greater than 1.5. **Figure 3.25** shows a complete test setup.

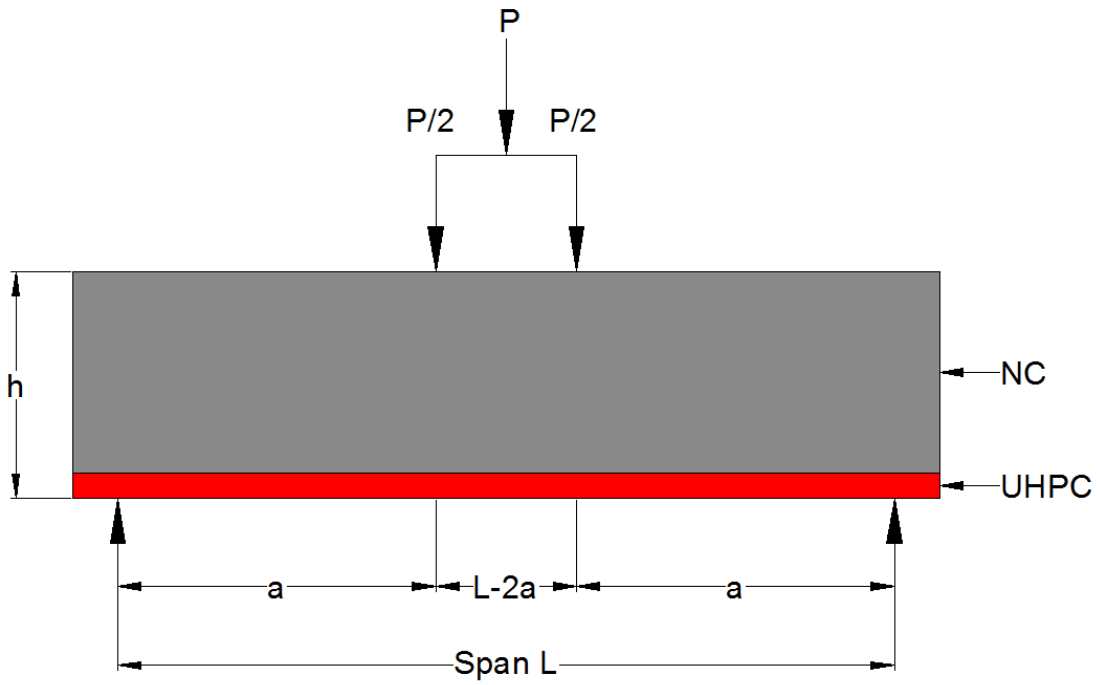

Figure 3.24: Four-point bend test of the hybrid beams.

Figure 3.25: Complete test setup for hybrid layered specimen.

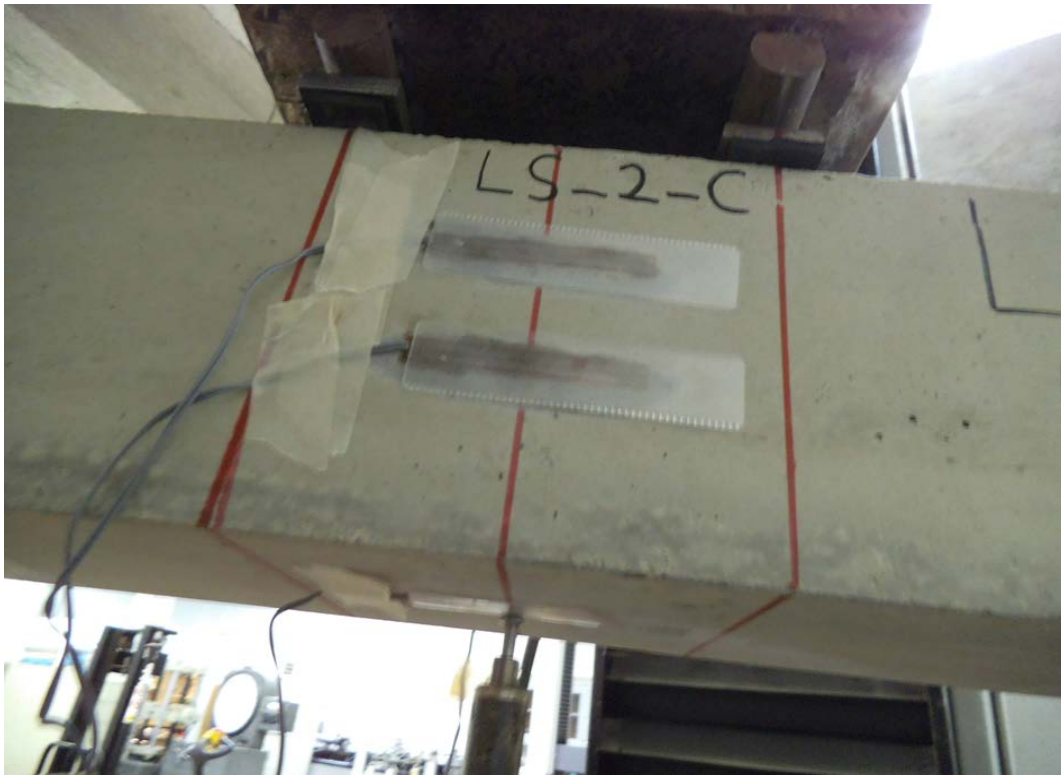

Figure 3.26: Instrumentation for test specimens.

The mid-span deflection was measured by a LVDT attached to the bottom of the beam at mid spa (**Figure 3.26**). The declining post-cracking load path was recorded following the peak load to observe softening. Loading on each specimen was increased at load rate of 0.5 mm / minute till the end recording the strains and deflection at each step of loading. The failure load and the mode of failure were recorded.

Some beams were strain-gauged at top and bottom surfaces and at two locations on the vertical faces (**Figure 3.26**) to record normal strains for comparison with the theoretical values. In addition to measurement of deflection and strains, crack growth was also noted along with the mode of failure for each test specimen. **Figure 3.26** shows the instrumentation for test specimens.

3.4.2.2 UHPC Reinforced Specimens

All beam specimens were tested in a four-point bend test under an Instron machine using monotonically increasing load till failure (**Figure 3.27**). the following values of span L and shear span a were used: For Group (i) of size 150 x150 x 760 mm in size, the span L was 630 mm with a = 240 mm. For Group (ii) of size 150 x 200 x 900 mm beams, L = 750 mm and a = 300 mm. For Group (iii) of size 150 x 220 x 760 mm beams, L = 680 mm and a = 265 mm. For Group (iv) of size 200 x 270 x 1000 mm beams, L = 900 mm and a = 375 mm. For Group (v) of size 200 x 220 x 1000 mm beams, L = 900 mm and a = 375 mm. For Group (vi) of size 200 x 310 x 1000 mm beams, L = 900 mm and a = 375 mm. **Figure 3.28** shows the complete test set up for testing of hybrid slabs with tension UHPC bars.

The shear span to depth ratio a/h varied from 1.2 to 1.7. The maximum load in kN sustained by a beam is denoted by P. The mid-span deflection was measured by a LVDT. The declining post-cracking load path was recorded following the attainment of peak load to observe ductility. In some beams, the UHPC bars were strain-gaged at the bottom with embedded gages before casting of normal concrete in the molds as shown in **Figure 3.29** .Most of the hybrid beams were strain-gauged at top and bottom surfaces and at two locations on the vertical faces to record normal strains for comparison with the theoretical values. In addition, crack growth was also noted along with the mode of failure for each test specimen. **Figure 3.30** shows the instrumentation for test specimens.

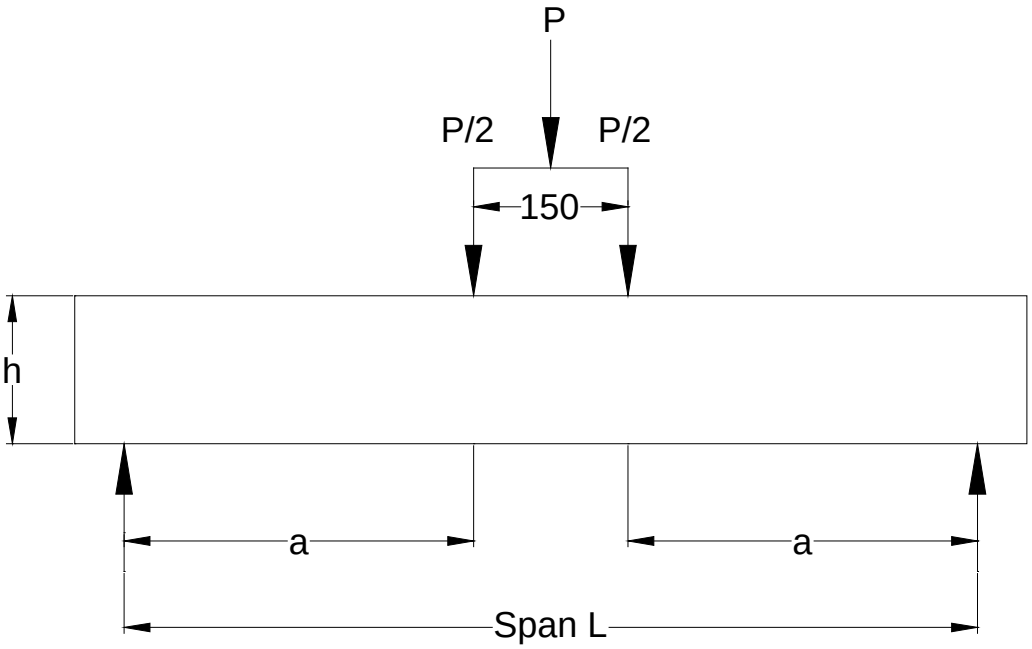

Figure 3.27: Four point bending test of UHPC reinforced bars beam.

Figure 3.28: Complete test set of UHPC reinforced specimen.

Figure 3.29: Embedded Strain gages at the bottom of UHPC bars before casting of NC.

Figure 3.30: Location of strain gages in test specimens.

3.4.2.3 Hybrid Hollow-Core Specimens

All hollow core specimens were tested in a four-point bend test under an Instron machine using monotonically increasing load till failure (**Figure 3.31**). Prior to testing, each specimen was fitted with strain gages at top and bottom face at the midspan to record strains. In each specimen, six strain gages were fixed as follows: three strain gages at the bottom side distributed as: one at the center (SG.2) and one left (SG.1) and one right (SG.3), two strain gages along the depth spaced as one third of the slab depth (SG.4, SG.5) and one at the top (SG.6) along the center line at mid span of the beam as shown in **Figure 3.32**.

In addition, a LVDT was used at midspan to record deflection. Loading on each specimen was increased at a load rate of 0.5 mm / minute under INSTRON testing machine with maximum capacity of 250 kN, recording the strains and deflection at different load levels. The failure load and the mode of failure were recorded.

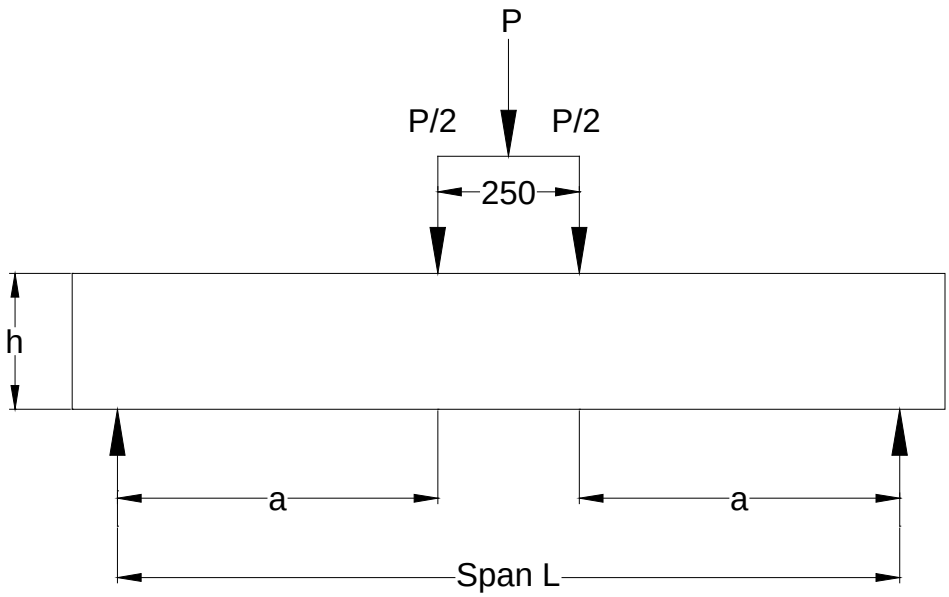

Figure 3.31: Four-point bend test of the hybrid hollow core slab.

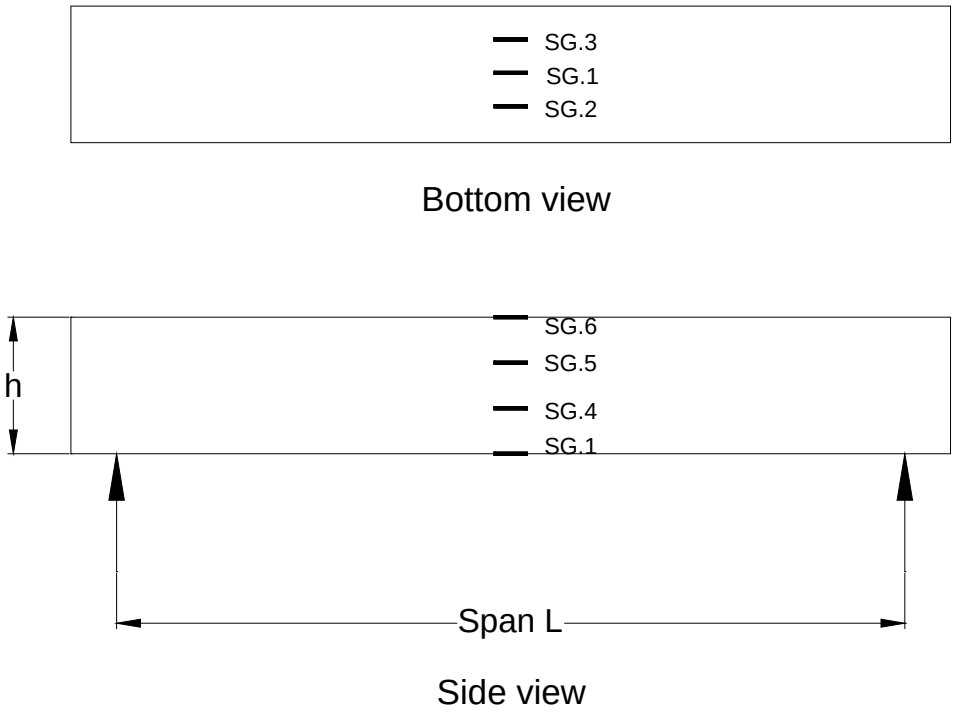

Figure 3.32: Strain gage locations in the hybrid hollow core test specimens.

The shorter span specimens were tested with a shear span to depth ratio of 325, while the longer span specimens were tested with a shear span to depth ratio of 425. **Figure 3.33** shows a complete test setup for four-point bend test.

Figure 3.33: Complete test setup for hybrid hollow core specimens.

The mid-span deflection was measured by a LVDT (**Figure 3.34**). The declining post-cracking load path was recorded following peak load to observe ductility. All hybrid hollow core slabs were strain-gauged at top and bottom surfaces and at two locations on the vertical faces to record normal strains (**Figure 3.34**) for comparison with the theoretical values. In addition to measurement of deflection and strains, crack growth was also noted along with the mode of failure for each test specimen.

Figure 3.34: Instrumentation for test specimens.

CHAPTER 4

TEST RESULTS AND DISCUSSION FOR MATERIAL PROPERTIES

4.1. Ultra High Performance Concrete (UHPC)

The developed UHPC mixture used in the casting of hybrid construction has the following properties:

4.1.1 Uniaxial Compressive Strength

An average value of cylinder compressive strength of six specimens was 160 MPa corresponds to average axial strain of 0.0038 has been attained with a maximum and minimum value of 170 MPa and 150 MPa respectively and standard deviation of 10. The average value of compressive strength of 31 cubes was about 168 MPa with a maximum and minimum value of 180 MPa and 155 MPa respectively and standard deviation of 8. Unlike normal concrete, the compressive failure occurs due to development of multiple vertical cracks due to the presence of fibers as shown in **Figure 4.1**. A typical stress-strain diagram obtained from testing of 75x150 mm cylinders which were strain gaged is shown in **Figure 4.1**. From the measurement of stress and strain, modulus of elasticity of UHPC was found to be varied from 48 GPa to 59 Gpa, with an average value taken as 55 GPa which is consistent with the reported value in the literature. The average value of Poisson's ratio were determined as 0.22.

Figure 4.1: Failure mode under compressive testing of the developed UHPC.

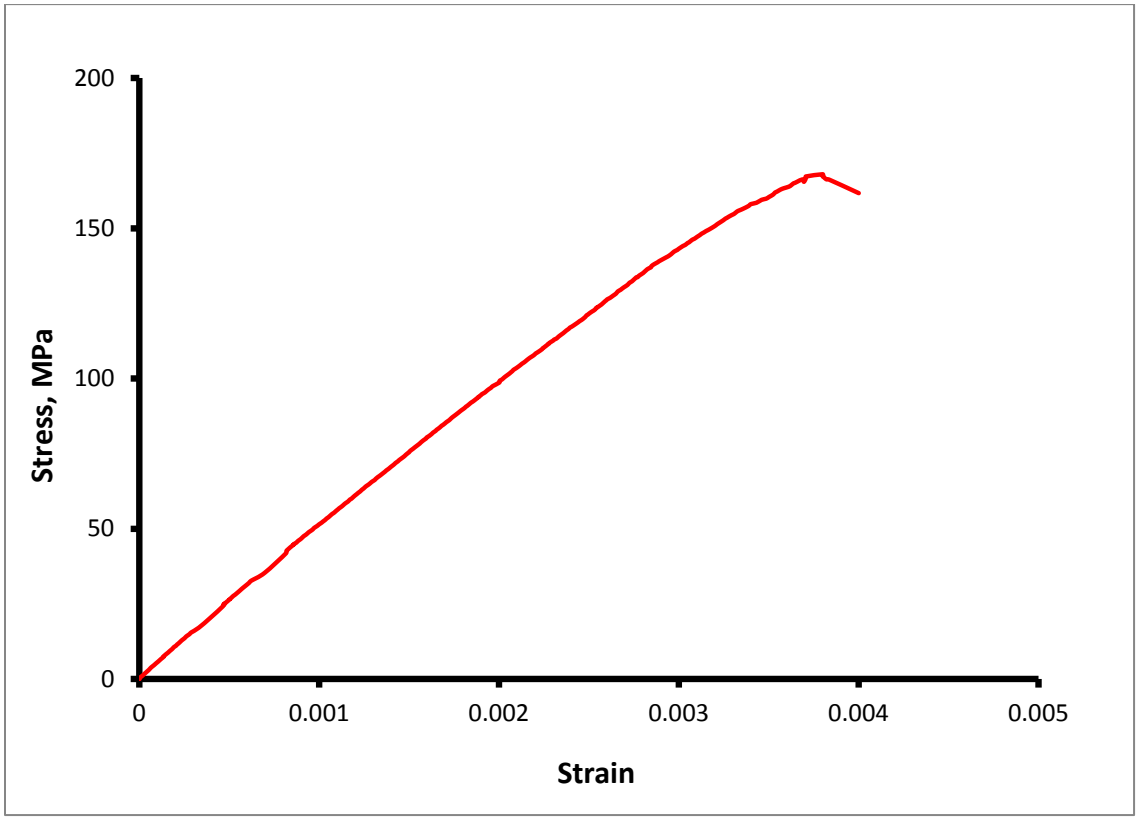

Figure 4.2: Typical compressive stress-strain plot for UHPC cylinder.

4.1.2 Split Tensile Strength

The average value of split tensile strength of six specimens was 26 MPa with a maximum value of 27 MPa and minimum value of 23 MPa respectively and standard deviation of 1.33.

The average split tensile strength of UHPC is about five times more than that for the normal concrete. This value is close to the results of Graybeal et al [28] who have reported a value of 25 MPa for steam cured specimens.

At failure, the cylinders split into two halves as normally seen in NC cylinders. But because of binding effect of steel fibers with the dense microstructure of UHPC cylinders, the cylinders show longitudinal cracks at failure without being split into two halves (**Figure 4.2**) as in the case of NC cylinders.

Figure 4.3: Mode of failure of UHPC cylinders after splitting tensile test.

4.1.3 Uniaxial Direct Tensile Strength

The average value of direct tensile strength of six UHPC prisms was found to be about 10 MPa as shown in **Figure 4.3** with a maximum value of 11.6 MPa and minimum value of 8.8 MPa respectively and standard deviation of 1.0.

The tensile behaviour of UHPC is characterized by almost linear stress rise until the initial cracking strength followed, in some cases, by very limited strain hardening until the ultimate tensile strength, and then a gradual strain softening as shown in **Figure 4.3**.

Figures 4.4 and **4.5** show the crack formation during and after testing of UHPC prisms under uniaxial tensile test respectively.

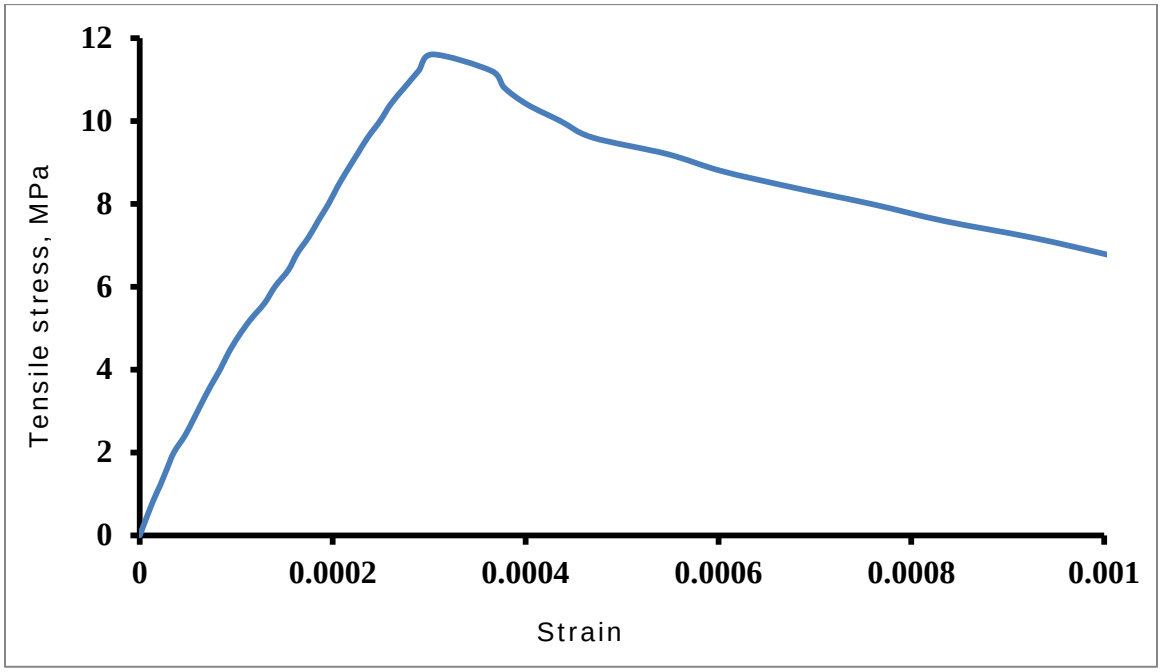

Figure 4.4: Typical uniaxial direct tension response of UHPC.

Figure 4.5: Close-up view of crack formation of UHPC prisms during testing.

Figure 4.6: Close-up view of UHPC prisms showing the cracks after testing.

The uniaxial tensile stress-strain response of UHPC as shown in **Figure 4.3** has also been confirmed by Graybeal and Baby [68], who presented a typical UHPC uniaxial tensile response as illustrated in **Figure 4.6**. The idealized representation includes four distinct phases: I: Elastic; II: Multi-Cracking; III: Crack Straining; and IV: Localized. Phase I, the elastic phase, refers to the global elastic straining of the composite section. This behavior continues through first cracking of the section, which occurs at the tensile strength of the cementitious composite. Phase II, the multiple cracking phase, refers to the portion of the behavior wherein the cementitious matrix repeatedly cracks within the gauge length. The specimen in this phase tends to accumulate elastic strain in both the uncracked sections of the cementitious matrix between cracks and the fiber reinforcement bridging the cracks but does not experience widening of individual cracks. This phase is characterized by a nearly constant stress level, which is attributed to the homogeneity of the cementitious matrix. Phase III, the crack-straining phase, is the portion of the behavior characterized by increasing crack opening as the fiber reinforcement undergoes a combination of elastic straining and interface debonding. The strain-based phases end when the tensile strength of the strain-hardening composite is reached, referred to as the "fiber bridging strength." The final phase, localization, is characterized by the continued widening of an individual crack as the fibers bridging that crack debond and pull out of the matrix. The remainder of the specimen elastically unloads in this phase, meaning that the behaviors in this phase are based on crack opening, not strain.

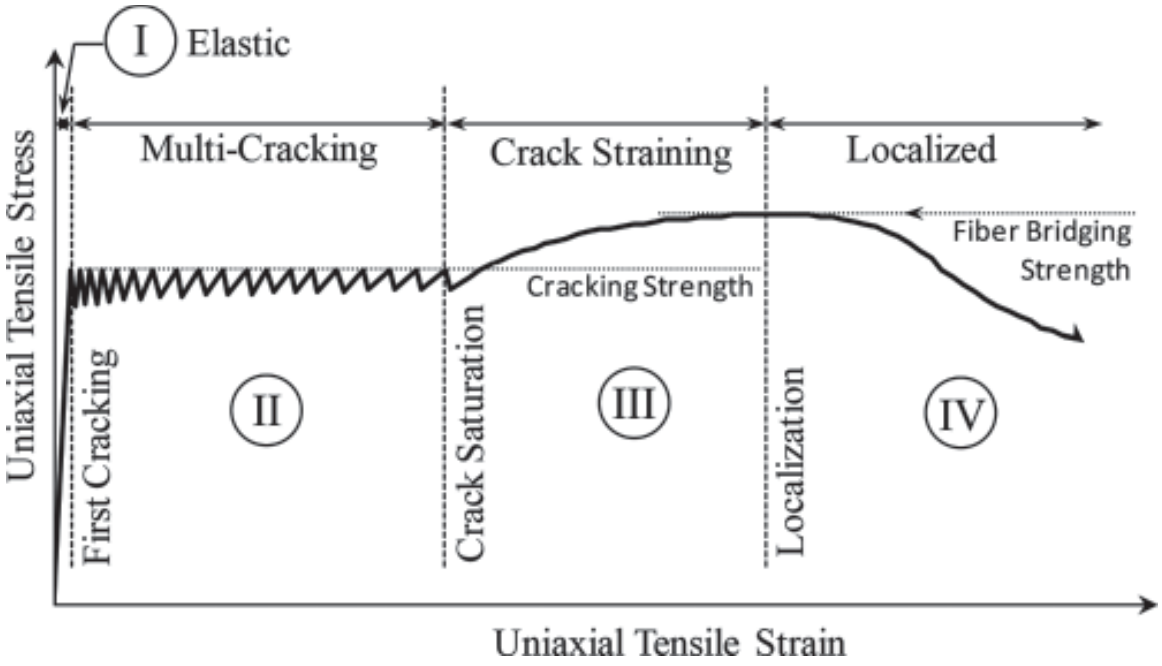

Figure 4.7: Idealized uniaxial tensile mechanical response of UHPFRC [68].

Nezhentseva et al. [69] also divided the uniaxial response into three main groups as shown in **Figure 4.8**: (1) Linear-elastic response: this stage takes place until the point when the stress level in the UHPFRC matrix corresponds to the matrix tensile strength and a first micro crack appears. (2) Pseudo strain hardening: during this stage no real plastic micro structural changes happen, therefore, it is also called “pseudo plastic”. On the contrary, deformations continue to increase intensely as a result of formation of the numerous tiny cracks in the matrix, whereas the uni-axial tensile stress does not change a lot, or increases considerably slower compared to the linear-elastic stage. The process of multiple micro cracking with uniformly distributed openings tied together by fibers in UHPFRC is similar to strain hardening or plastic behavior, thereby, giving the name to this stage. (3) Strain softening: this stage starts when one of the sections of the matrix

(the weakest) fails to transfer the average stress of the same intensity, meaning that the strain hardening capacity of UHPFRC matrix is reached.

Nezhentseva's definition of the third phase as 'strain softening' is at odd with that of Graybeal et al who have referred to this 'fiber bridging strength' (localization) (**Figure 4.7**). As increased deformation is due to crack opening rather than straining, it would be appropriate to call this terminal phase as simply a 'softening phase'.

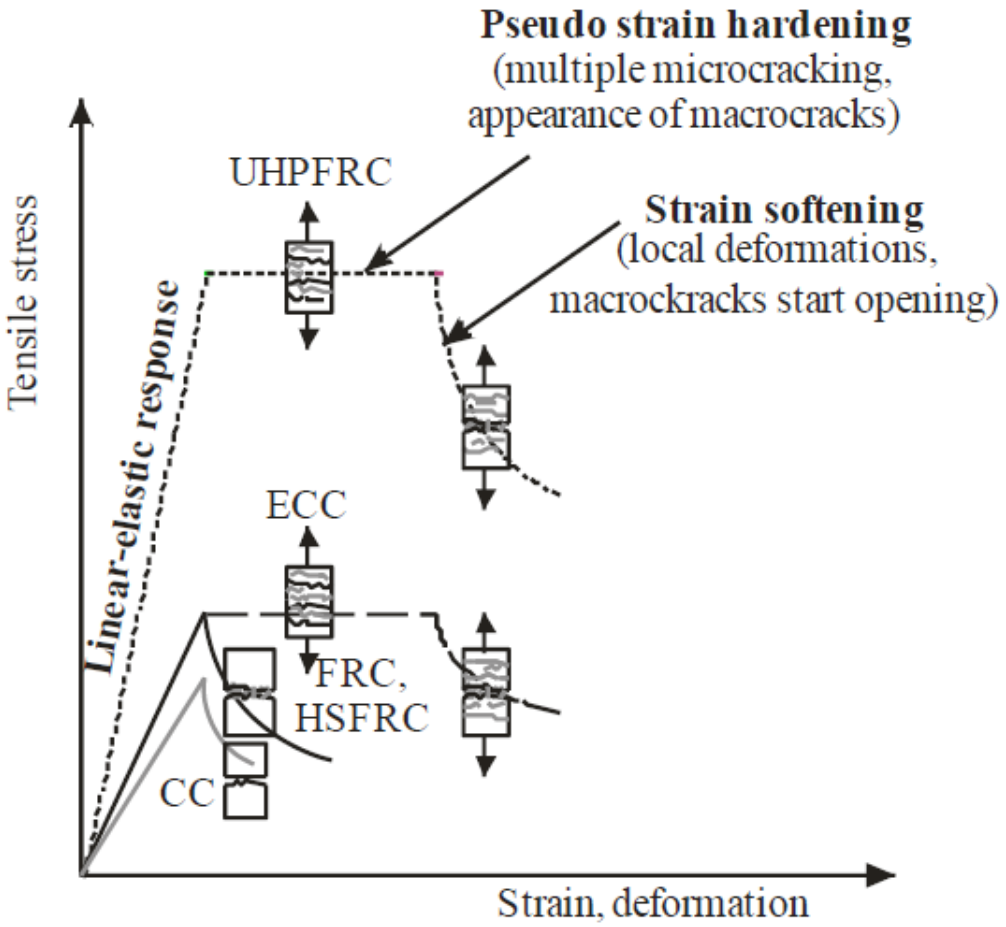

Figure 4.8: Response of UHPFRC in uniaxial tensile stress state [69].

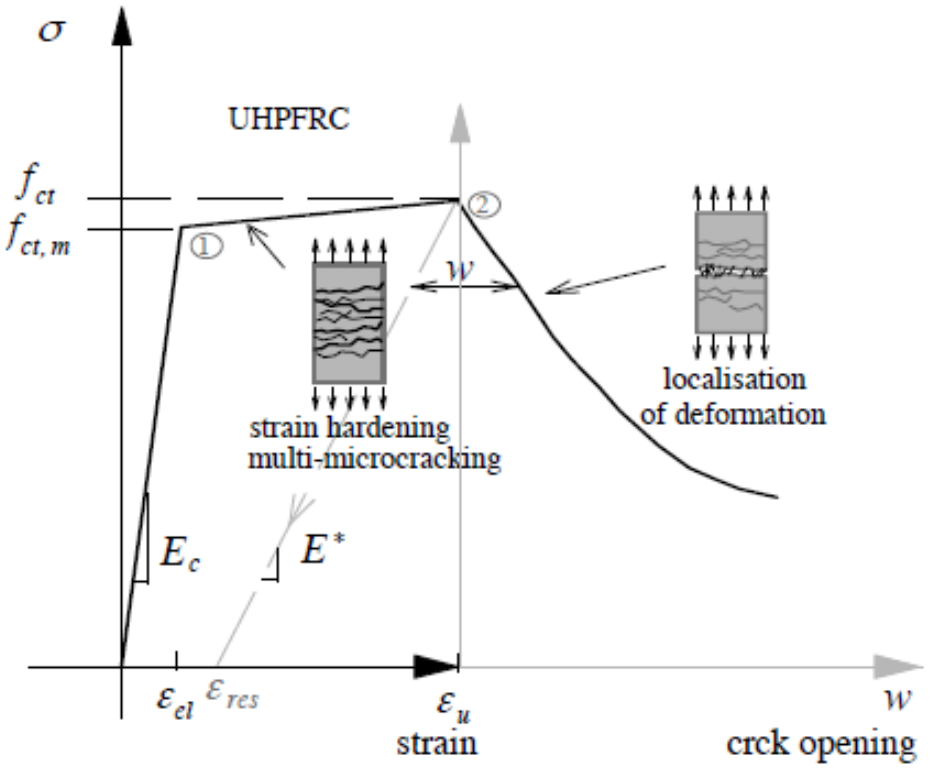

Figure 4.9: Uniaxial tensile response of UHPFRC element and notations for characteristic values [70].

Ana Spasojević, 2008 [70] stated that the addition of fibers to UHPC matrix leads to a tensile behavior that can be schematically presented as in **Figure 4.9**. He divided the behavior into three stages : Linear-elastic behavior up to the stress level corresponding to matrix tensile strength; pseudo strain hardening behavior resulting from multi-micro cracking; and strain softening behavior with localization of deformation.

4.1.4 Flexural Tensile Strength

The average value of flexural tensile strength of 34 UHPC prisms was found to be about 27 MPa with a maximum value of 31 MPa and minimum value of 23 MPa respectively and standard deviation of 2.

Figure 4.10 shows load deflection typical plot for UHPC prisms tested in four points bending after 48 hours heat treatment at 90 ^{o}C. The load-deflection plot shows softening mode of failure with prolonged deformation.

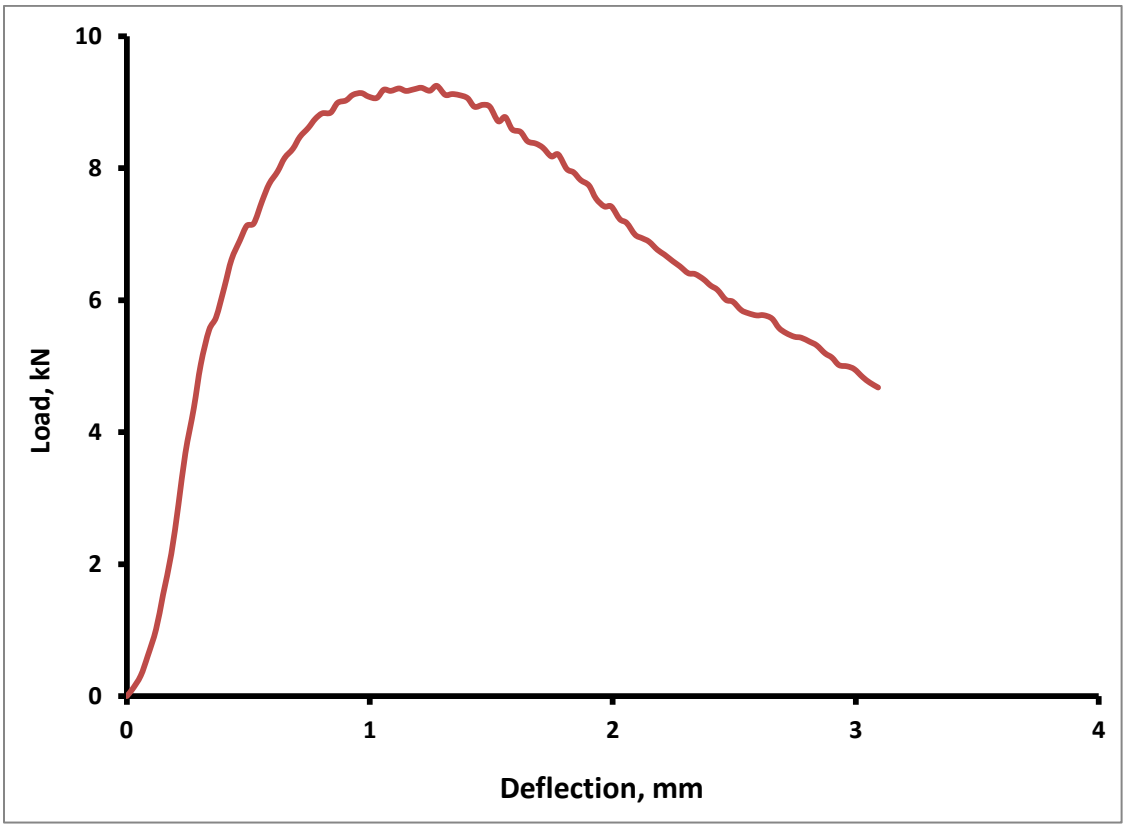

Figure 4.10: Typical load deflection plots for UHPC prisms.

The behavior of the UHPC specimens in flexure was similar to that under uniaxial tensile test in which at first characterized by the appearance of several fine surface cracks followed by very limited hardening phase (its magnitude varied from specimen to specimen) until the ultimate strength was reached and finally gradual softening mode as the last phase (**Figure 4.10**). The softening phase is characterized with the advancement of single crack through the thickness.

As shown recently, the distribution and orientation of the steel fibres in UHPC can have a considerable effect on its mechanical properties. Therefore, these effects must be considered for structural applications where variation of fiber distribution in large sections may result in considerable variability in mechanical properties within the section. The direction of flow of fresh UHPFRC is expected to influence fiber orientation and settlement of fibers may also occur if workability is too high or the concrete is over vibrated [43].

It was found that the fiber orientation have a very significant effect on the flexural strength of the prisms, as the calculated flexural strength varied from 23 to 30 MPa for the type of steel fibers used in this study which was straight fibers with 0.2 mm diameter and 13 mm in length with aspect ratio of about 65. This aspect ratio also plays an important role in the flexural performance as reported by many researchers. **Figure 4.11** shows the typical mode of failure of several specimens tested in flexure under four point bending test.

Figure 4.11: Typical mode of failure of UHPC prisms.

It should be noted the size effect is not reflected in the flexural tensile strength, as all prisms were of the same size and length. It will be shown later that the flexural tensile strength of UHPC varied indeed highly with much lower strength for larger size.

For the purpose of finding the cracking strength of the matrix, three prisms of UHPC were prepares without addition of steel fibers to the mix. Flexure testing under four point bending test was also performed. It was found that the flexural behavior was highly brittle (**Figure 4.12**) as expected with average flexural strength of 13 MPa, which is

much lower than the average strength of 25 MPa for fiber-reinforced specimens. **Figure 4.13** shows the load-deflection response of three UHPC prisms without fibers demonstrating that the failure is abrupt without the inherent softening as witnessed in fiber-reinforced UHPC. The addition of steel fibers significantly enhances the tensile strength of UHPC, and importantly imparts ductility through a softening phase.

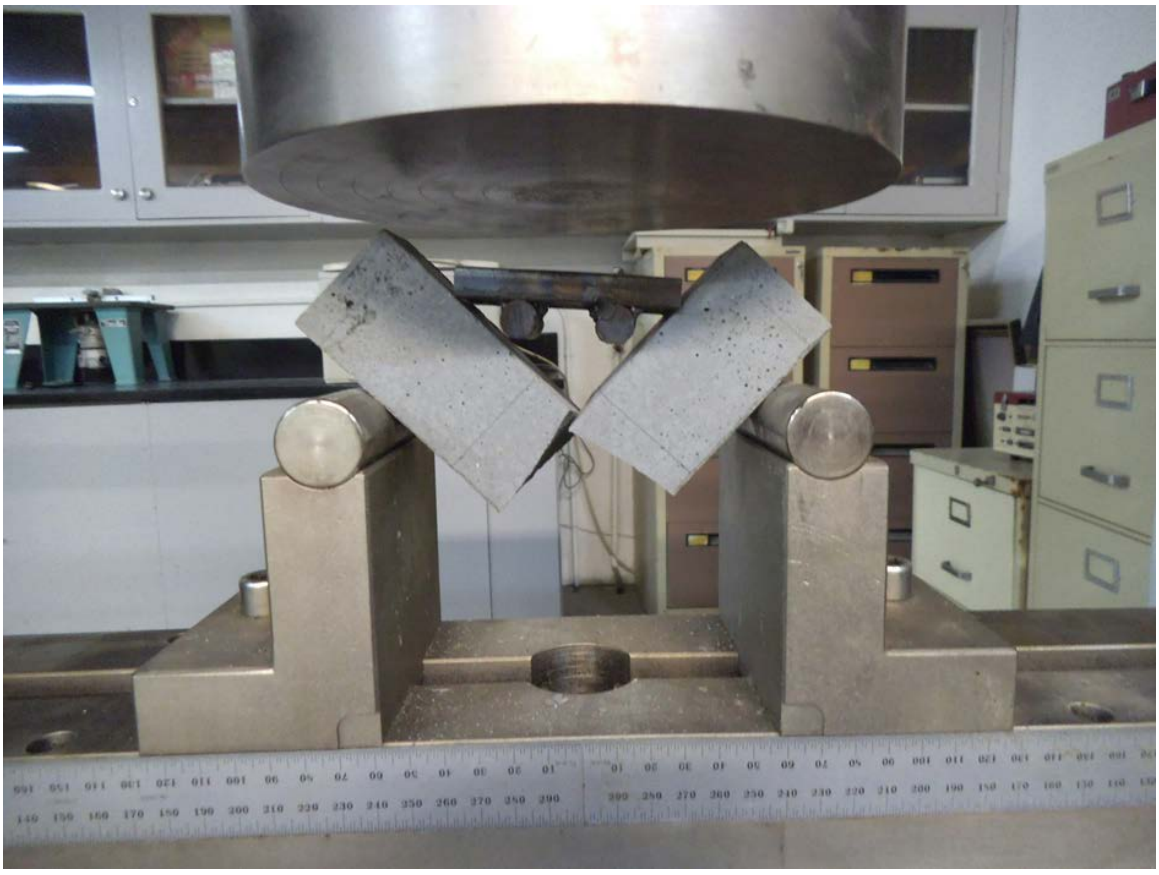

Figure 4.12: Typical mode of failure UHPC prisms without fibers under four point bending.

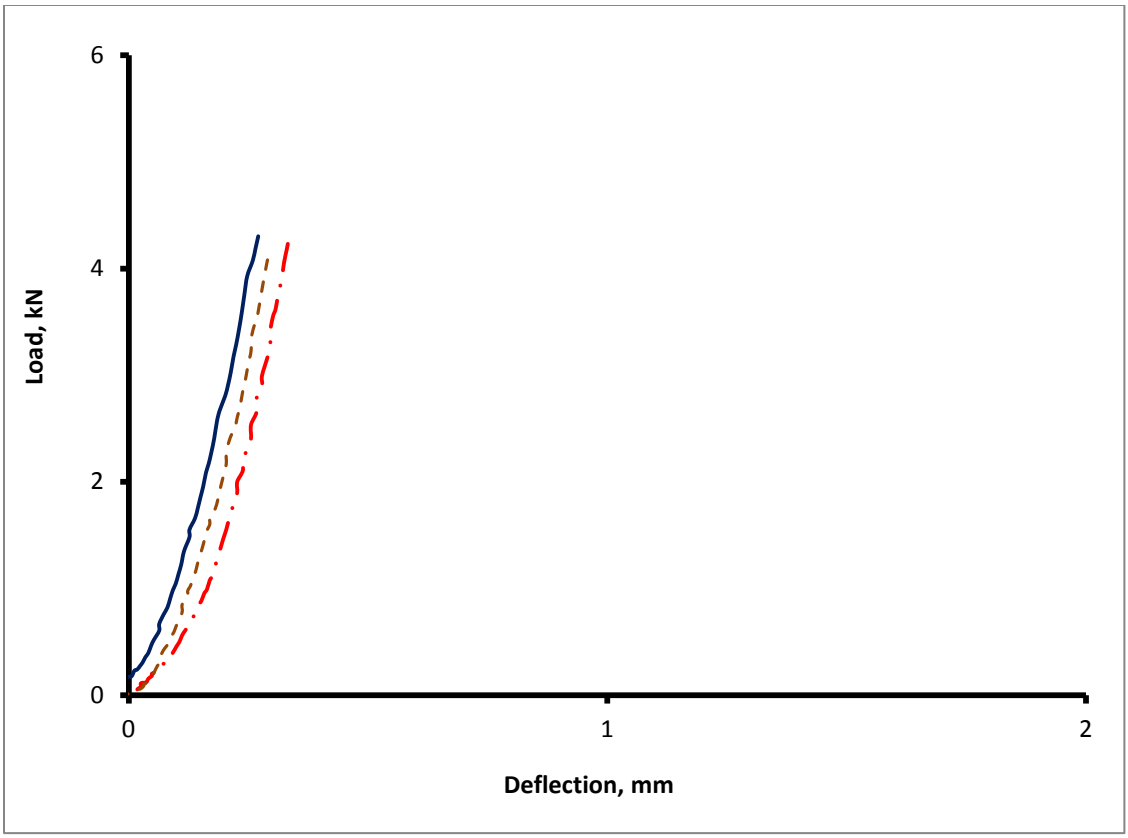

Figure 4.13: Load-deflection response of three UHPC prisms without fibers.

Table 4.1 summarizes the mechanical properties of the developed mix of UHPC which bear testimony to the superior materials of UHPC.

Table 4.1: Mechanical Properties of the Developed UHPC

Property	Specimen's Size	Average Values (MPa)
Compressive strength	50 mm cube	170
	75x150 mm cylinder	160
Modulus of elasticity	75x150 mm cylinder	55000
Direct tensile	25x25x285 mm prism	10
Flexural strength	40x40x160 mm prism	27
Flexural strength (No fibers)	40x40x160 mm prism	13
Splitting tensile	75x150 mm cylinder	15

4.2. Normal Portland Cement Concrete (NC)

4.2.1 Uniaxial Compressive Strength

An average value of cylinder compressive strength of six NC specimens was about 40 MPa has been attained with maximum and minimum value of 43 MPa and 37 MPa respectively and standard deviation of 2. The average value of modulus of elasticity was about 30 GPa. An average value of 100 mm cube compressive strength of six NC specimens was about 50 MPa with maximum and minimum value of 52 MPa and 49 MPa respectively and standard deviation of 1.0. It is well known that for the same concrete, the measured compressive strength of cube specimens (height/width ratio =1) is about 1.25 times that of the standard cylinder strength.

The typical cylinder compressive stress–strain curve for the normal concrete at 28 days water curing is illustrated in **Figure 4.14**.

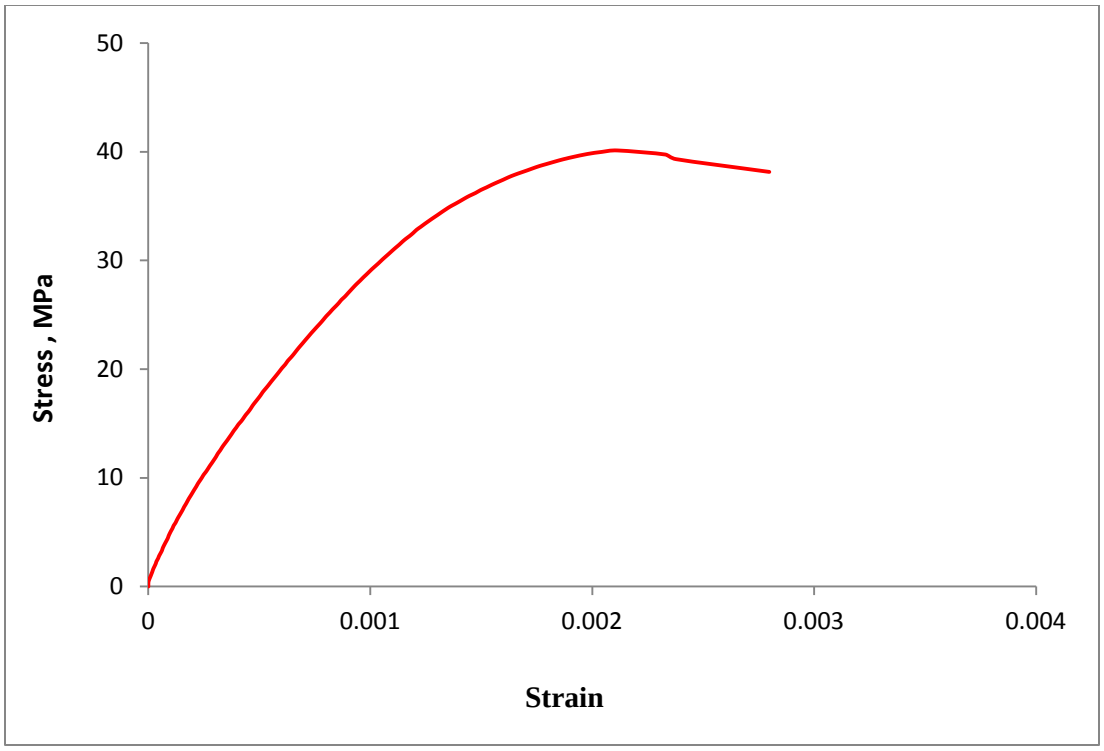

Figure 4.14: Typical uniaxial compressive stress-strain diagram of NC.

CHAPTER 5

RESULTS AND DISCUSSION FOR HYBRID NC-UHPC LAYERED SPECIMENTS

5.1. General

In this chapter, the test results and discussion of hybrid NC-UHPC layered specimens consisting of two layers, a bottom layer of UHPC and the upper part of normal concrete (NC), are presented.

5.2. Transformed Section Properties

As measurement of strains and deflection showed almost linear behavior up to the peak load, the transformed section properties were used to calculate the stress in a section at failure load P_U using the values of modulus of elasticity of concrete Ec = 30 GPa and that of UHPC, E_U = 55 GPa,. For the transformed section (**Figure 5.1**), the cross sectional area of UHPC layer, A_{SU}, is replaced by an equivalent area nA_{SU}, where n, the modular ratio = E_U/E_C = 1.833. The transformed section properties were calculated for cracked and uncracked concrete section on the basis of **Figure 5.1** and are listed in **Tables 5.1** and **5.2**. The properties for cracked concrete section apply at load level greater than the load that would produce cracking of the bottom face of normal concrete due to tensile stress being equal or greater than modulus of rupture of concrete.

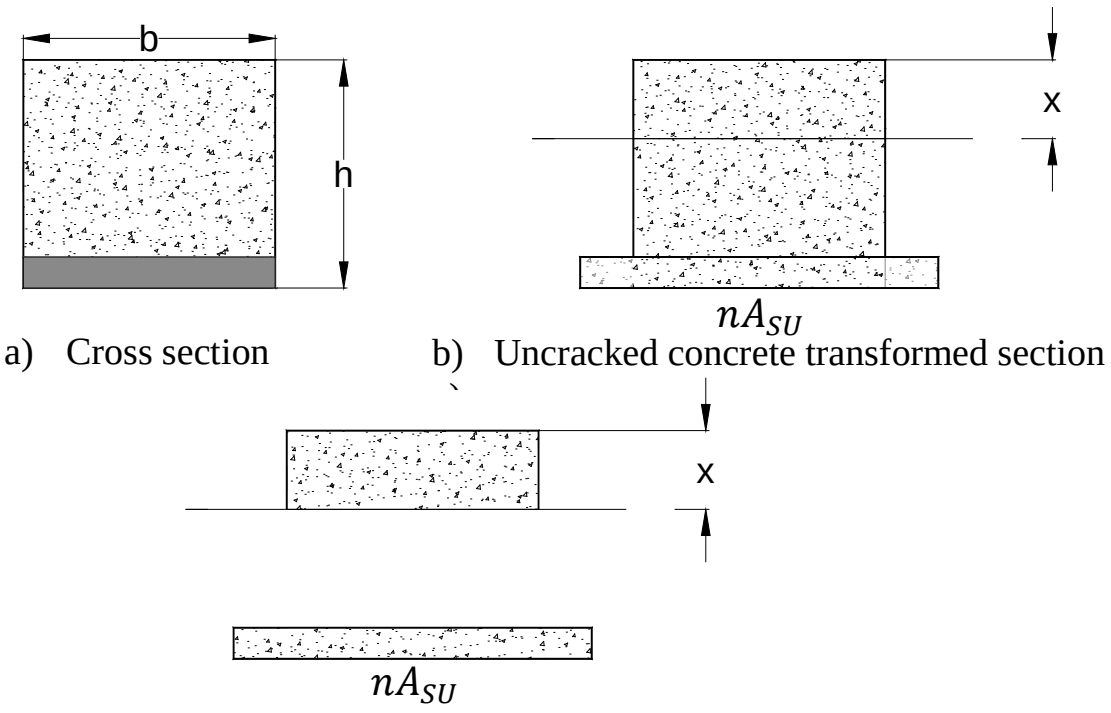

Figure 5.1: Transformed concrete section.

For the designations shown in **Tables 5.1, 5.2** and **5.3**, the symbol 'C1' indicates curing option 1 in which concrete cast immediately over uncured UHPC layer (e.g. LS-A-C1) and 'C2' indicates curing option 2 in which concrete cast after 2 days of curing of UHPC layer (e.g. LS-A-C2).

Table 5.1: Transformed Section Properties of Uncracked Concrete Section

Groups	UHPC Thickness (mm)	Beam Designation	I_{uc} (mm^4) x 10^6	Depth of N.A. from Top (mm)	Section Modulus	
					S_{tuc} (mm^3) x 10^4	S_{buc} (mm^3) x 10^4
Group (A) 150x150 x 760 (b × h × L)	20	LS-A-C1	51.7	81.5	63.4	75.5
		LS-A-C2				
	40	LS-B-C1	54.6	85.0	64.2	84.0
		LS-B-C2				
Group (B) 150x150x1000 (b × h × L)	20	LS-C-C2	51.7	81.5	63.4	75.5
	40	LS-D-C2	54.6	85.0	64.2	84.0
Group (C) 150x 200x 900 (b × h × L)	25	LS-E-C1	121.7	108.2	112.4	132.6
		LS-E-C2				
	50	LS-F-C1	129.1	112.9	114.3	148.2
		LS-F-C2				
Group (D) 150x 200x 1200	25	LS-G-C2	121.7	108.2	112.4	132.6
	50	LS-H-C2	129.1	112.9	114.3	148.2

Curing option C1: Concrete cast immediately over uncured UHPC layer
Curing option C2: Concrete cast after 2 days of curing of UHPC layer

Table 5.2: Transformed Section Properties of Cracked Concrete Section

Groups	UHPC Thickness (mm)	Beam Designation	I_{cr} (mm^4) x 10^6	Depth of N.A. from Top (mm)	Section Modulus	
					S_{tcr} (mm^3) x 10^4	S_{bcr} (mm^3) x 10^4
Group (A) 150x150 x 760 (b × h × L)	20	LS-A-C1	44.1	71.1	62.1	55.9
		LS-A-C2				
	40	LS-B-C1	52.9	83.0	63.7	79.0
		LS-B-C2				
Group (B) 150x150x1000 (b × h × L)	20	LS-C-C2	44.1	71.1	62.1	55.9
	40	LS-D-C2	52.9	83.0	63.7	79.0
Group (C) 150x 200x 900 (b × h × L)	25	LS-E-C1	101.6	93.1	109.2	95.0
		LS-E-C2				
	50	LS-F-C1	124.6	109.5	113.8	137.8
		LS-F-C2				
Group (D) 150x 200x 1200 (b × h × L)	25	LS-G-C2	101.6	93.1	109.2	95.0
	50	LS-H-C2	124.6	109.5	113.8	137.8

5.3. Load Capacity and Tensile Stress at Failure

The average values of the failure load, P_U and the corresponding mid-span deflection for three identical specimens are shown in **Table 5.3**. The variation in the three values of P_U is between 10 to 25% for concrete cast immediately over uncured UHPC layer (curing option C1) and less than 10% for concrete cast after 2 days of curing of UHPC layer (curing option C2). The maximum flexural tensile stresses at the bottom face of UHPC layer and compressive stress at top of normal concrete was calculated at P_U using values of section modulus shown in **Table 5.2** Compressive stresses are shown as negative.

Table 5.3: Failure Loads, Deflection and Tensile Stress for Test Beams with UHPC Layer

Groups	Beam Size (mm)	UHPC Thick., (mm)	Beam Designation	Curing option[+]	Average Failure load, P_U (kN)	Average deflection at failure load, Δ (mm)	Average tensile stress at bottom of UHPC (MPa)	Average compressive stress at top of NC (MPa)
Group (A)	150x150 x 760 (b × h × L)	20	LS-A-C1	C1	41.0	0.68	16.1	-7.9
			LS-A-C2	C2	52.0	0.80	20.5	-13.4
		40	LS-B-C1	C1	58.0	0.70	16.2	-10.9
			LS-B-C2	C2	70.0	0.93	20.0	-13.2
Group (B)	150x150x1000 (b × h × L)	20	LS-C-C2	C2	20.2	1.15	14.0	-6.1
		40	LS-D-C2	C2	34.3	1.28	15.0	-10.1
Group (C)	150x 200x 900 (b × h × L)	25	LS-E-C1	C1	58.0	0.77	16.8	-8.0
			LS-E-C2	C2	70.0	0.98	20.3	-9.6
		50	LS-F-C1	C1	71.0	0.76	14.2	-9.4
			LS-F-C2	C2	90.0	1.21	18.0	-11.9
Group (D)	150x 200x 1200 (b × h × L)	25	LS-G-C2	C2	28.8	1.32	14.0	-6.3
		50	LS-H-C2	C2	46.0	1.64	15.0	-9.6

[+]Curing option C1: Concrete cast immediately over uncured UHPC layer
[+]Curing option C2: Concrete cast after 2 days of curing of UHPC layer

The maximum tensile stress varied from 14 MPa to 20.5 MPa showing a wide range for a UHPC having the same mix design. As flexure failure is initiated by the tensile stress reaching the maximum flexural tensile strength, which for the UHPC mix used was determined from prism tests as 25 MPa (section 4.1), it was expected that the computed

tensile stress at failure load should be somewhat closer to the flexural tensile strength. The significant shortfall can be attributed to two effects: one is the size effect in terms of the length and width of the specimens. As the tensile strength is dependent upon the dispersion and orientation of steel fibers, the uniformity of fiber dispersion is far less secured for larger size specimens. The other one is the unavoidable variation that exists in mixing a large amount of raw materials with fibers and casting UHPC. The size effect on tensile strength variation is one of the challenges of fiber-reinforced UHPC construction.

As reported by Magureanu et al. [33] that the value of the flexural strength obtained on 40 x 40 x 160 mm prisms was approximately 1.47 times higher than 100 x 100 x 300 mm prisms. Nguyen et al. [39] conformed that by investigating the size effect by testing three different sizes of UHPC specimens using four-point bending in a three-dimensional scale: 50 x 50 x 150 mm (small), 100 x 100 x 300 mm (medium), and 150 x 150 x 450 mm (large). They found that as the size of the specimen increase, the equivalent bending strength decreased as shown in **Figure 2.7** and discussed in Chapter 2, section 2.2.2.2.

To further validate this observation of size effect on the flexural tensile strength, four test panels of UHPC, two of 150x30x600 mm (150 mm width) and two of 350x30x600 mm (350 mm width) were cast and then tested in four point bend test over span 500 mm simple span having shear span 175 mm to observe the effect of width on tensile strength. **Figure 5.2** shows the load-deflection plots of two specimens with different widths. The computed flexural tensile strength was 16.3 MPa and 12.1 MPa for panels with 150 mm and 350 mm, respectively as shown in **Figure 5.2**. The findings show the variation in strength due to increase in the width.

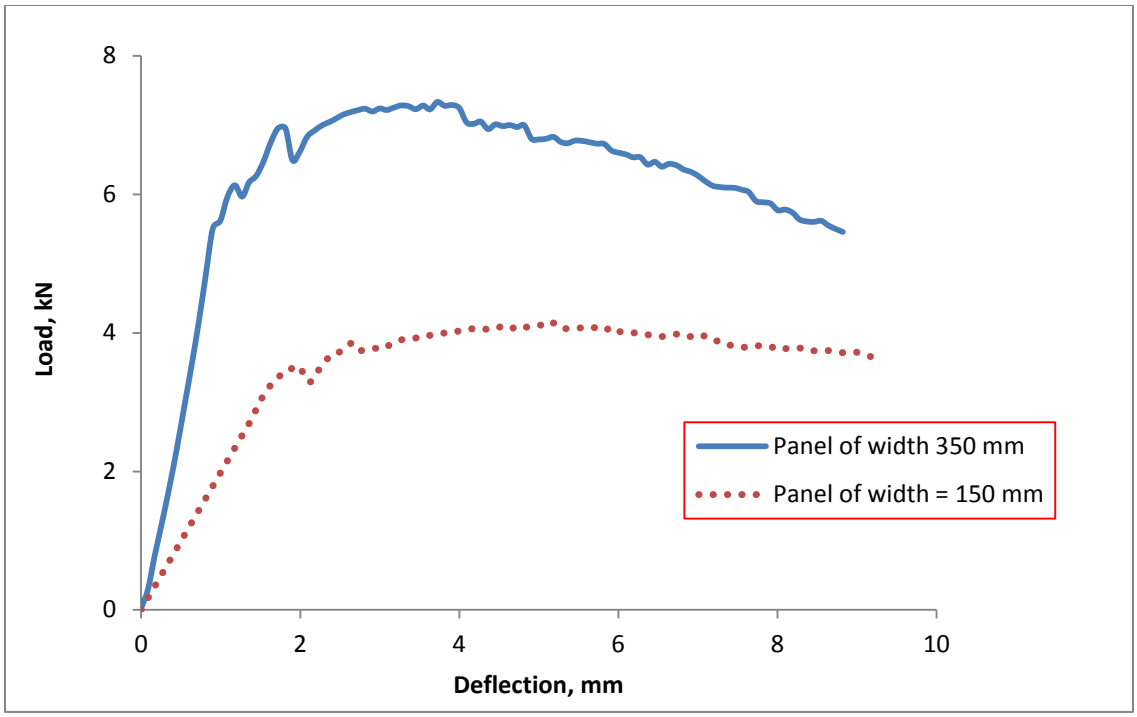

Figure 5.2: Load-deflection plot of UHPC panels.

5.3.1 Effect of Curing of UHPC

It was observed from data in **Table 5.3** that the curing option C1 produces values of failure loads and flexural tensile stress at the bottom consistently lower than those achieved with curing option C2. For Group (A), of 20 mm UHPC thickness, the maximum tensile stress at failure was about 20 MPa for curing option 2, compared to t 16 MPa for curing option 1. Similarly for Group (C), for 25 mm thick of UHPC, the maximum tensile stress at failure about 20 MPa for curing option 2, compared to about 17 MPa for curing option 1. This observation is not unexpected in the sense that UHPC has very low water-binder ratio compared to that of normal concrete and the immediate availability of excess water may impair the strength of uncured UHPC. It seems that initial curing of UHPC, at least for a shorter duration, is essential for higher strength of

the composite beams. It can be stated that at least two-day self-curing of UHPC layer is needed for casting of hybrid beams to take advantage of the enhanced tensile strength of UHPC, and that the effect of longer curing of UHPC layer for further improved properties needs closer examination.

The values of the maximum tensile stress at the bottom fiber for both curing options of UHPC show lack of consistency with some variation. This can be attributed to the possible variation in flexural tensile strength of UHPC caused by the randomness in the dispersion of steel fibers within the UHPC mix that is invariantly present as explained above, as stated earlier. This is an inherent and challenging construction problem with fiber-reinforced UHPC, as uniform dispersion of fibers is difficult to achieve. The problem can only be managed with carefully controlled fiber addition and mixing to ensure reasonably uniform fiber dispersion.

5.3.2 Effect of UHPC Thickness

Of the two thicknesses of the UHPC layers used in four groups (**Table 5.3**), it is clear that higher thickness of UHPC layer results in higher load capacity of the beams for same spans, as expected. But the increase in the failure load is not proportional to the area of the UHPC layer. For Group (A), curing option C2, the failure load for LS-A-C2 which had 20 mm thick UHPC layer was 52 kN compared to 70 kN for LS-B-C2, which had 40 mm thick UHPC layer, an increase in P_U about 34 % only. But the area of UHPC for 40 mm was twice that for 20 mm. For Group (B), for the curing option C2, the failure load for LS-C-C2 which had 20 mm thick UHPC layer was 20.2 kN compared to 34.3 kN for

LS-D-C2, which had 40 mm thick UHPC layer, an increase in P_U about 69 %. But the area of UHPC for 40 mm was twice that for 20 mm. For Group (C), the failure load for LS-E-C2 (25 mm thick UHPC layer) was 70 kN compared to 90 kN for LS-F-C2, which had 50 mm thick UHPC layer, an increase in P about 28 % only with twice UHPC area. For Group (D), the failure load for LS-G-C2 (25 mm thick UHPC layer) was 28.8 kN compared to 46 kN for LS-H-C2, (50 mm thick UHPC layer), an increase in P about 59 % with twice the UHPC area. As the peak load is attained at the formation of well-formed flexural cracks with the incipient of maximum tensile stress at the bottom UHPC face, the full thickness of UHPC is not being subjected to same level of stress. It appears therefore that the gain in the load capacity with increased thickness comes from the increased transformed section properties which yield higher elastic section modulus for the bottom face.

5.4. Strain Distributions along the Depth

The load–strain relationship was evaluated using the strains measured by the strain gauges fixed to the beams with the aim of locating measured neutral axis of a section. Four strain gauges located at mid span (**Figure 5.3**) were used to create a strain profile over the depth of most of beams tested and to identify the location of the neutral axis.

Only the data for two specimens, LS-A-C2 and LS-C-C2 from two groups will be discussed as representative cases here and the data for other specimens are presented in **Appendix B**.

Figure 5.3: Location of strain gages in test specimens.

The measured strains for the two selected specimens are shown in **Table 5.4**. **Figure 5.4** shows the load–strain plot of beam LS-A-C2 below the failure load of P = 48.4 kN (90 % P_U). Positive and negative strains represent tensile and compressive strains, respectively. The plot shows linearity for compressive strains up to close the failure load. However, the tensile strain at the bottom shows some nonlinearity after about 0.6 P_U as the crack moved close to the bottom strain gage as shown in **Figure 5.3**. Overall, it can be said that the beam responded almost linearly, with strain being approximately proportional to the applied load. This linearity of the strain profile confirms that there is no slip at the interfaces between UHPC and normal concrete for a section affirming that adequate bond between NC and UHPC has been achieved in the construction of the hybrid specimens.

The measured values of compressive strain at the load of 48.4 kN (0.9 P_U) were 283 x10^{-6} while the measured tensile strain at the same load level was 350 x10^{-6}. **Figure 5.3** shows the crack propagation under flexure mode of failure.

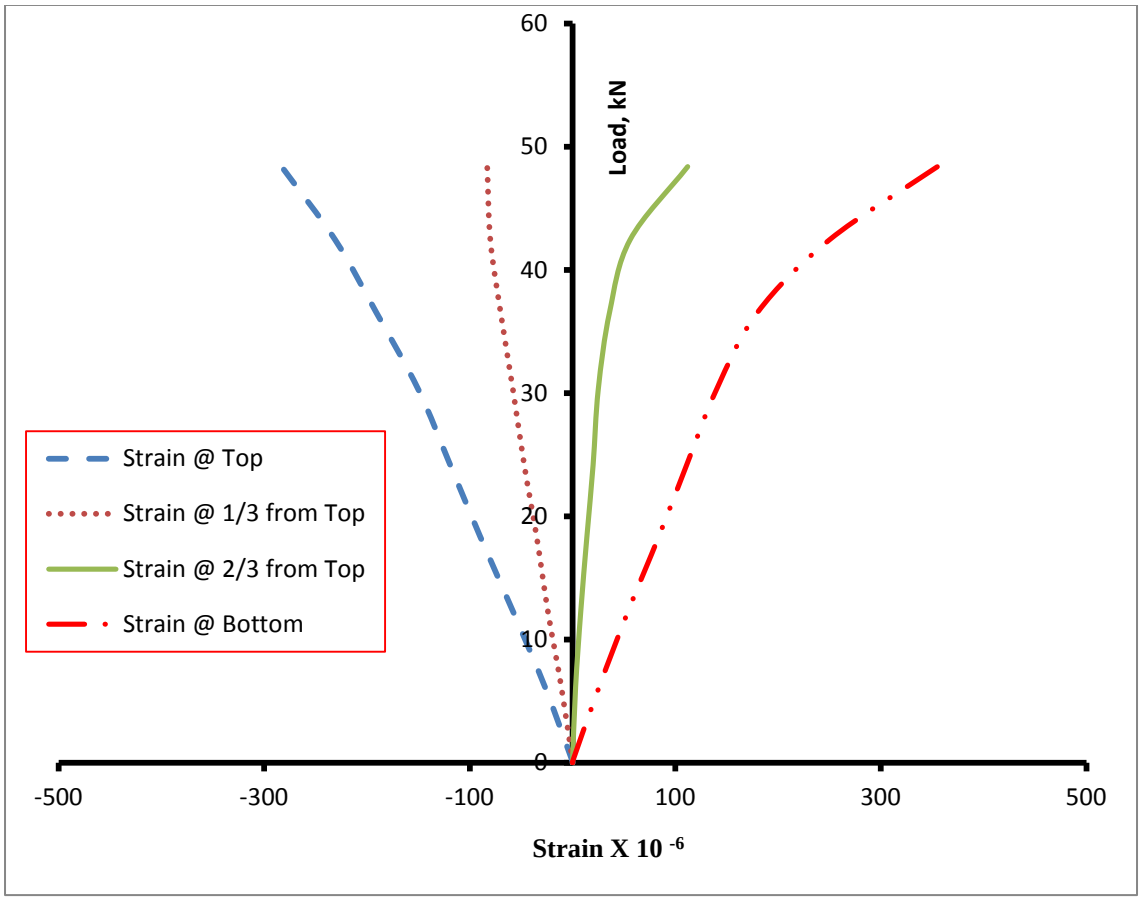

Figure 5.4: Typical load-strain curve for beam LS-A-C2.

Figure 5.5 shows also the load–strain plot of beam LS-C-C2 at 98 % of the failure of P = 19.6 kN. The plot also shows linearity for both tensile and compressive strains almost up to the failure load.

The measured strain for all test specimens clearly show an approximately linear relationship between load and strains, confirming linear response of UHPC hybrid elements. The measured values of compressive strain at load of 19.6 kN were 225 x10^{-6} while the measured tensile strain at the same load level was 255 x10^{-6}.

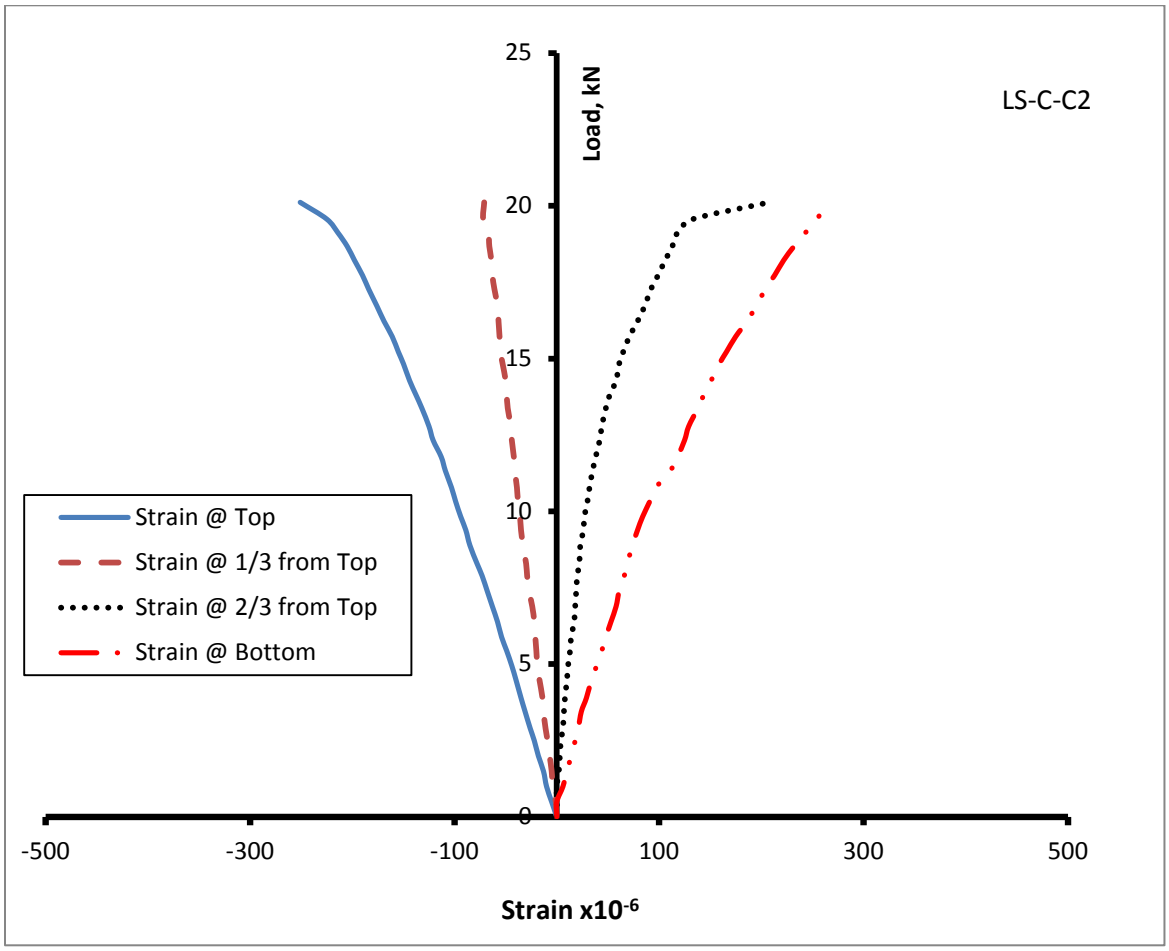

Figure 5.5: Typical load-strain curve for beam LS-C-C2.

The strain profile across the depth of the beam LS-A-C2 is shown in **Figure 5.6** for five load levels, three closer to the early stage and the other two near the failure stage of loading. Also, the strain profile across the depth of the beam LS-C-C2 is shown in **Figure 5.7** for four load levels up to 98 % of the failure load. It is observed from the plots in

Figures 5.5 and **5.7** show that the strain distribution across the depth is almost linear at lower load levels, becoming somewhat skewed at higher load levels. However, from a best linear fit across the four strain readings, as shown by a dotted line for the maximum load, the deviation of strain readings from the best fit profile is small. It is known that the strain measurements in concrete are more often qualitative than quantitative.

The transition of the section from being fully uncracked to cracked concrete may occur if the load P exceeds the load that would cause the tensile stress in NC being greater than the tensile strength of NC. The value of the concrete cracking load P_{conc} can be estimated from the ordinary flexure theory using transform section properties for uncracked section (**Figure 5.1b**). If the flexural tensile strength of NC (modulus of rupture) is f_t, the moment to cause cracking of NC is given as:

$$\mathrm{M_{crc}} = \frac{I_{uncr} f_t}{Y_c} \tag{5.1}$$

when I_{uncr}= moment of inertia of uncracked transformed section and Y_c = distance of the bottom concrete layer from NA. The load corresponding to M_{crc} for the test specimens is given as

$$\mathrm{P_{conc}} = \frac{2M_{crc}}{a} \tag{5.2}$$

when a = shear span for the four-point loading used.

The computed values of P_{conc} for the test specimens with f_t = 4 MPa for normal concrete used are shown in **Tables 5.4** and **5.5**. When P is less or equal to P_{conc}, transformed section properties of uncracked section are applicable for calculation of bending stress. If

P is greater than P_{conc}, the transformed section properties for cracked section (**Figure 5.1c**) are applicable for stress calculation.

For LS-A-C2, P_{conc} =36 kN and P_U=52 kN, indicating there is a transition from uncracked to cracked concrete section. As seen in **Figure 5.6**, there is a clear small upward shift of neutral axis (NA) to reflect this transition. At load P less than 36 kN, the entire section remains uncracked. From the transformed section for an uncracked concrete section (**Table 5.1**), the neutral axis is located at a depth of about 81 mm from the top (**Figure 5.6**), matching to 81 mm observed from the plot of strains at P = 12.3 kN. From the cracked transformed section (**Table 5.2**), the computed depth of neutral axis is found to be about 71 mm from top at load level closer to the failure load while the measured depth from the best-fit strain profile is 68 mm. This shows good agreement between the measured and calculated depth of the compression zone.

For LS-C-C2, P_{conc} =23 kN and P_U=20.2 kN, indicating the section remained uncracked up to P_U. The calculated depth of NA from top is 68 mm compared with the measured depth of 65 mm (**Figure 5.6**), the shift in the observed NA is not as obvious as that seen in **Figure 5.7**.

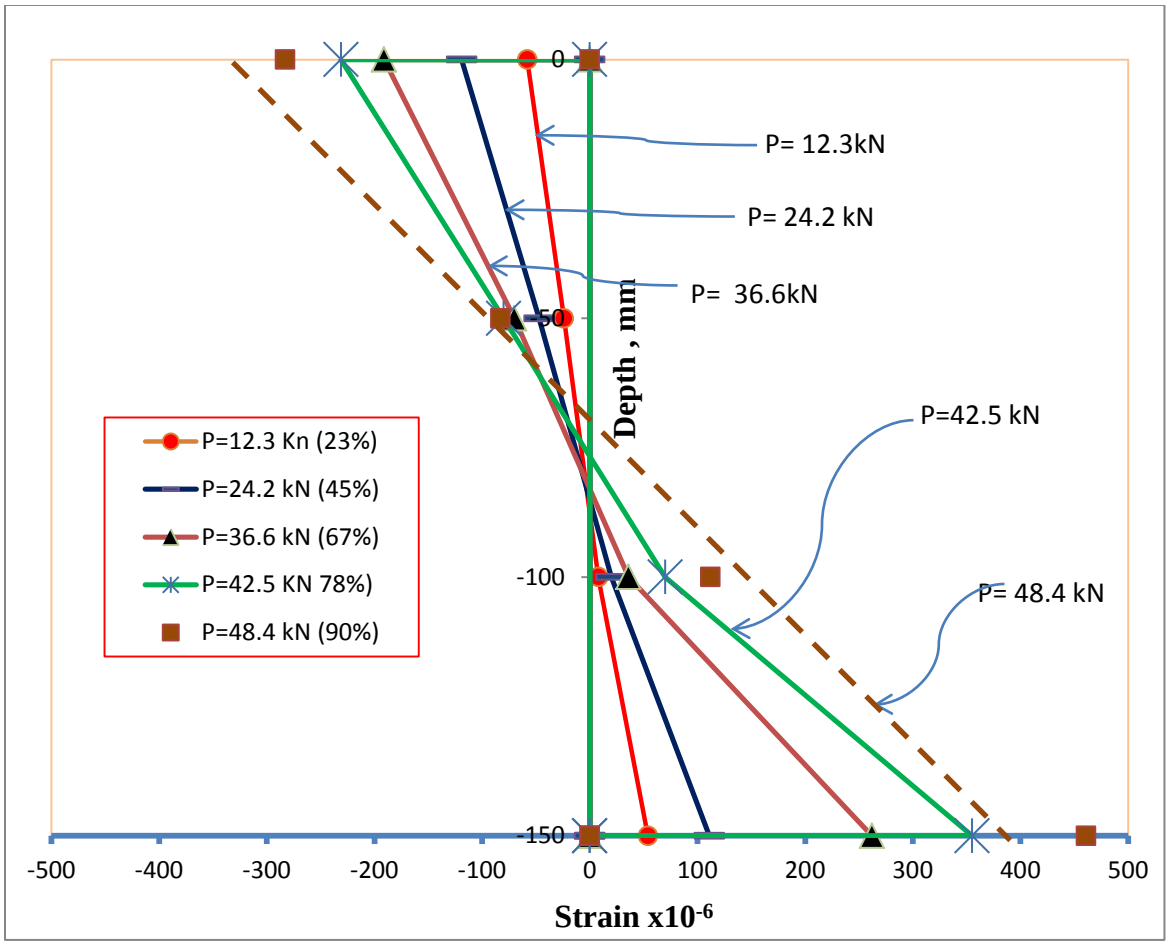

Figure 5.6: Strain profile along the depth of beam LS-A-C2.

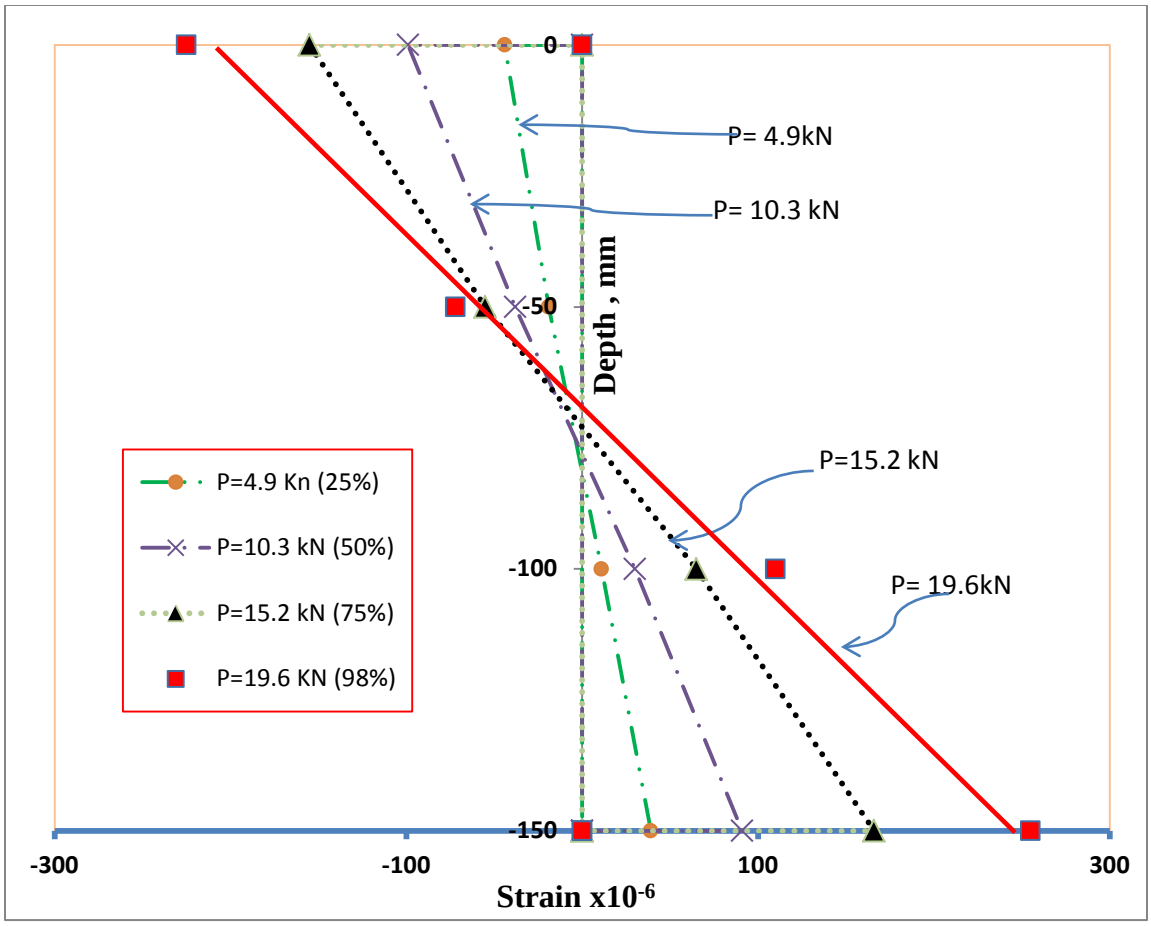

Figure 5.7: Strain profile along the depth for beam LS-C-C2.

The strain profile for other specimens of all other groups is presented in **Appendix B**.

Table 5.4: Load Levels and Strain Values for Beams LS-A-C2 and LS-C-C2

Beam ID	UHPC Thickness (mm)	Beam Size (mm)	Load Level (kN)	% of P_U	Measured Strain $x10^{-6}$				Concrete Cracking Load P_{conc} (kN)
					Top	1/3 from Top	2/3 from Top	Bottom	
LS-A-C2 Span 630 mm	20	150x150x760	12.3	23	-58	-24	8	54	36
			24.2	45	-119	-47	20	111	
			36.6	70	-119	-70	36	262	
			42.5	80	-231	-80	56	300	
			48.4	90	-283	-83	112	350	
LS-C-C2 Span 900 mm	20	150x150x1000	4.9	25	-44	-19	11	39	23
			10.3	50	-99	-38	30	91	
			15.2	75	-155	-55	65	166	
			19.6	98	-225	-72	110	255	

5.5. Measured and Calculated Stress

Generally, the section is considered as cracked concrete section when the tensile strength at the bottom of the normal concrete exceeds the tensile strength of concrete from the transformed section as discussed in Section 5.4.

For a comparison of the measured stresses from strains with theoretical values computed from flexure formula using transformed properties, **Table 5.5** is prepared. The compressive strains at top was converted to stress using E_C= 30 GPa for normal concrete and the tensile stress at the bottom of beams was calculated using E_U= 55GPa. At low

load level, $P < P_{conc}$ the stresses in the beam were calculated using transformed properties of fully uncracked section and at $P > P_{conc}$, the transformed properties of cracked section (**Table 5.2**) were used. The computed stress at all load levels show that the use of transformed section properties yields results that are reasonably close to the measured stresses using the measured strains, except some discrepancies near P_U. This is because of small nonlinearity behavior that exists near P_U (section 5.6).

All the calculated and measured results of all specimens tested are compiled and presented in **Appendix B**.

Table 5.5: Measured and Computed Stresses for Selected Load Levels of Beams LS-A-C2 and LS-C-C2

Beam ID	UHPC thickness mm	Beam Size (mm)	Load Level, KN	% of P_U	Measured Stress (MPa)		Concrete Cracking Load P_{conc} (kN)	Calculated Stress, Mpa			
								Bottom		Top	
					Bottom	Top		Cracked	Un-Cracked	Cracked	Un-Cracked
LS-A-C2	20	150x150x760	12.3	23	3.0	1.8	36	-	3.6	-	2.3
			24.2	45	6.1	3.6		-	7.1	-	4.6
			36.6	70	14.4	5.7		14.4	-	7.1	-
			42.5	80	19.5	7.0		16.7	-	8.2	-
			48.4	90	25.4	8.5		19.1	-	9.4	-
			52.0	100	-	13.8		21.4	-	10.5	-
LS-C-C2	20	150x150x1000	4.9	25	2.2	1.3	23	-	2.3	-	1.5
			10.3	50	5.0	3.0		-	4.8	-	3.1
			15.2	75	9.1	4.7		-	7.1	-	4.5
			19.6	98	14	6.8		-	9.1	-	5.8
			20.2	100	14.4	7.5		-	9.3	-	6.0

5.6. Load Deflection Plots

Typical load-deflection plots of the specimens prepared with curing option C2 are shown in **Figures 5.8** through **5.15**, capturing the ascending and descending load paths. The softening mode of failure in flexure mode implies non-brittle failure with significant post-cracking strength, lesser than the peak load. In those cases, the beams failed with the

formation of multiple fine cracks at NC bottom when $P_{conc} < P_U$ (**Figure 5.16**) and advancement of only one single vertical crack within or near the maximum moment zone and in other cases, the beam failed with advancement of only one single vertical crack within the maximum moment zone (**Figure 5.17**) when $P_{conc} > P_U$.

It should be noted that the lesser values of post-peak strength are attributed to progressive crack growth within the UHPC layer. The uncracked ligament of UHPC and the bridging of steel fibers across the crack that are not pulled out contribute to the residual flexural strength.

The calculated deflections at midspan of the beams using Equation 5.3 for uncracked and cracked transformed section are shown in **Table 5.6** for P_{conc}.

$$\Delta = \frac{wa}{24EI}(3 \quad ^2 - a^2) \tag{5.3}$$

Where Δ= deflection at midspan, w= P/2=half of the applied load, a = shear span, l = test span, E= modulus of elasticity of concrete and I= moment of inertia of transformed concrete section.

Table 5.6: Comparison of Theoretical and Calculated Deflection

Beam Designation	Average Measured Deflection at P_{conc} (mm)	Concrete Cracking Load P_{conc} (kN)	Calculated Δ (mm)
			Based on I_{uncr}
LS-A-C2	0.19	36	0.11
LS-B-C2	0.17	70	0.21
LS-C-C2	0.41	20	0.19
LS-D-C2	0.45	34	0.30
LS-E-C2	0.30	49	0.11
LS-F-C2	0.34	90	0.19
LS-G-C2	0.42	29	0.21
LS-H-C2	0.52	36	0.32

From the load-deflection plots, the following observations can be made:

(1) The deflection can be taken as approximately linear up to the failure load P_U.

(2) The deflection can be calculated using the moment of inertia of the uncracked transformed section, I_{ucr}, as there is marginal difference in moment of inertia in both uncracked and cracked transformed section (**Tables 5.1** and **5.2**).

(3) Depending upon fiber orientation and amount of fiber across the crack, some specimens may show small post-crack stiffening resulting in increased deflection at P_U and while others will not. Thus some specimens showed limited stiffening

(e.g. LS-B-C2, LS-D-C2) others showed softening with increased deflection at reduced load almost immediately after P_U (e.g. LS-A-C2, LS-C-C2).

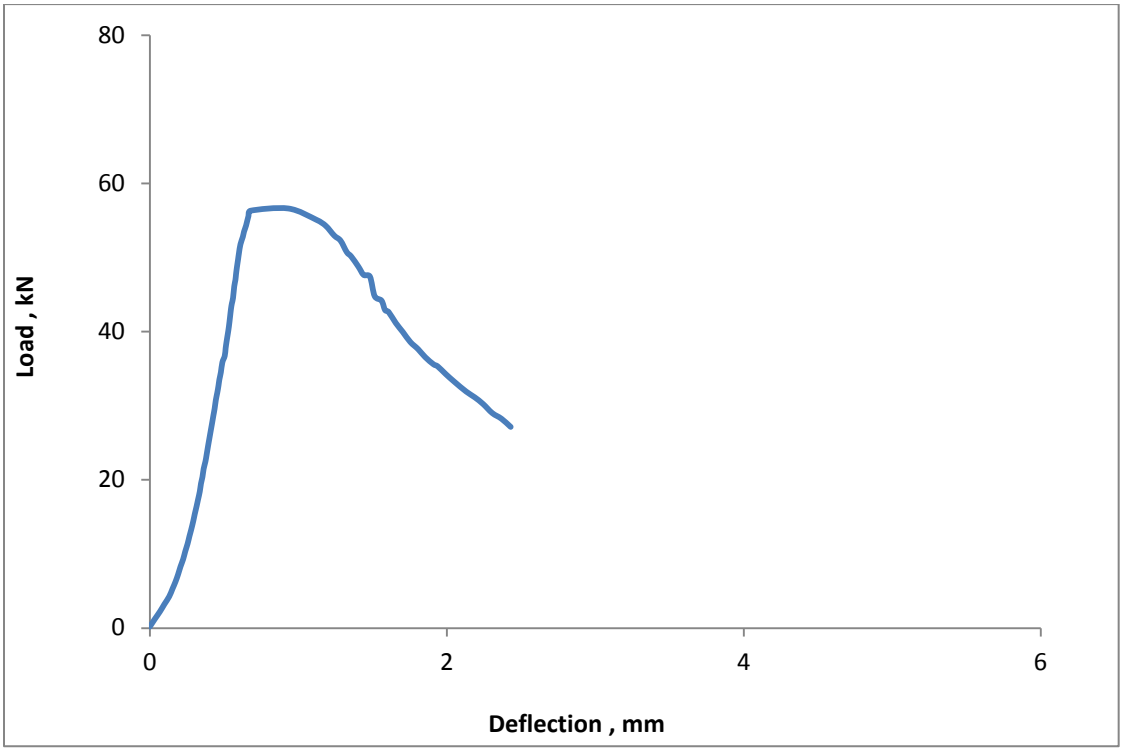

Figure 5.8: Load-deflection curve for beam LS-A-C2 (20 mm thick UHPC).

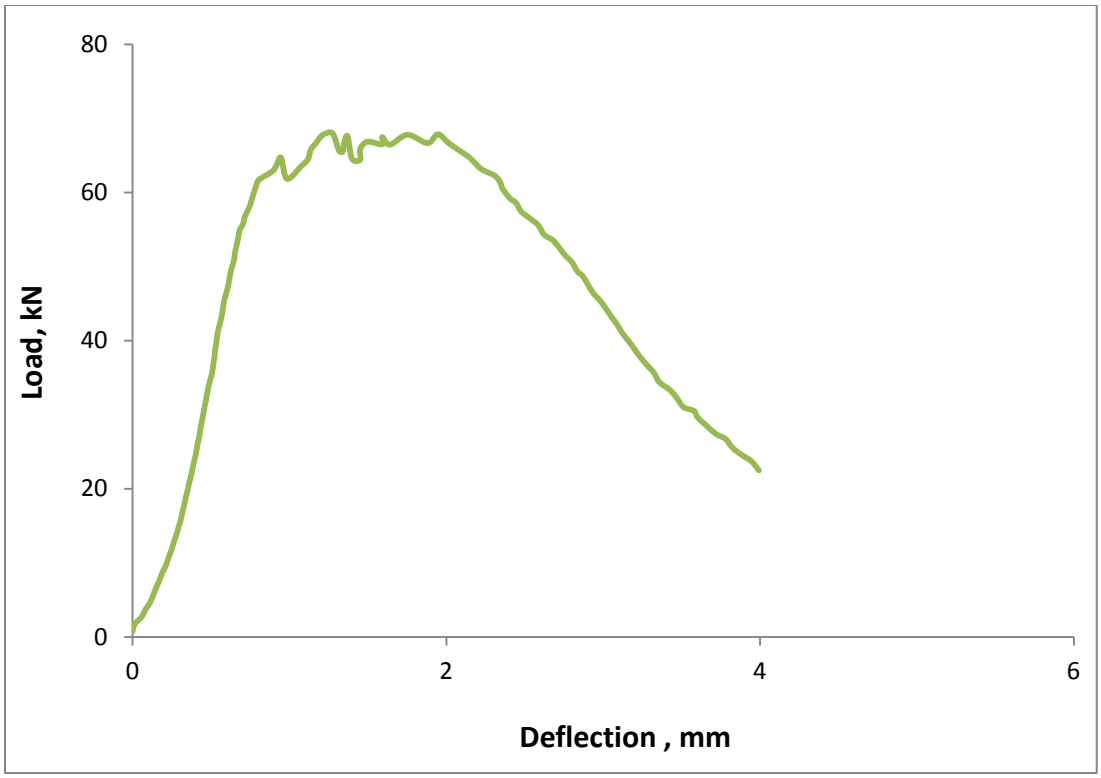

Figure 5.9: Load-deflection curve for beam LS-B-C2 (40 mm thick UHPC).

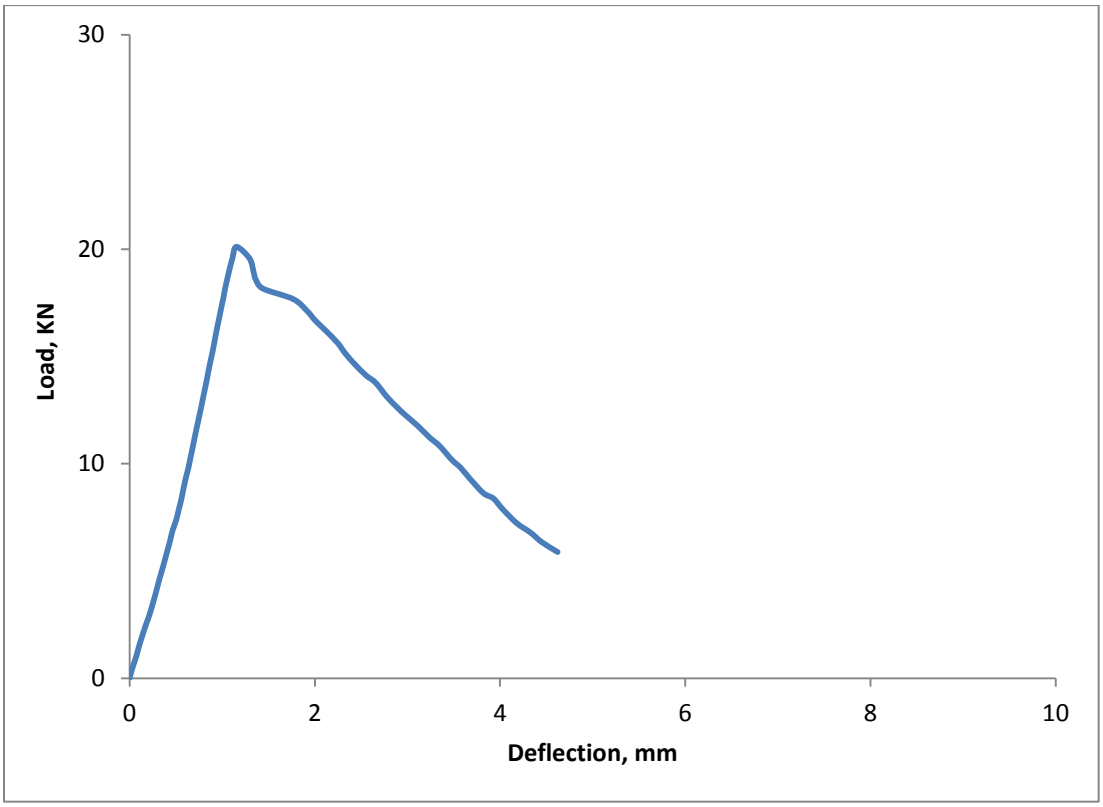

Figure 5.10: Load-deflection curve for beam LS-C-C2 (20 mm thick UHPC).

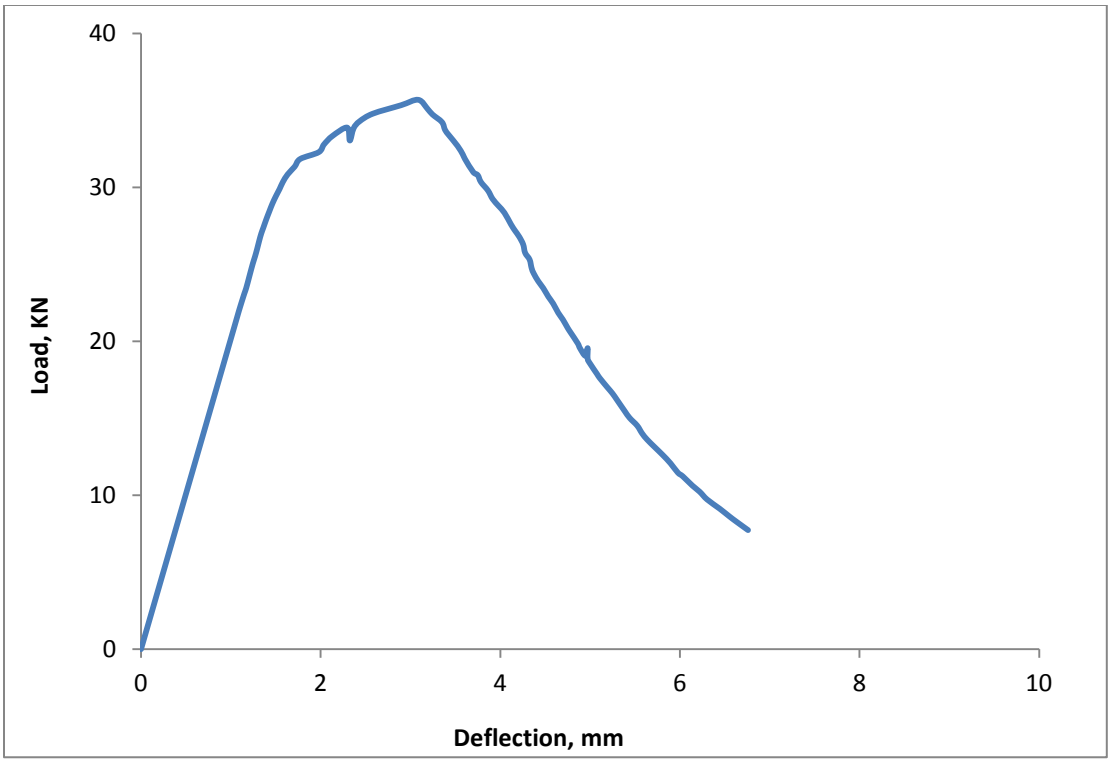

Figure 5.11: Load-deflection curve for beam LS-D-C2 (40 mm thick UHPC)

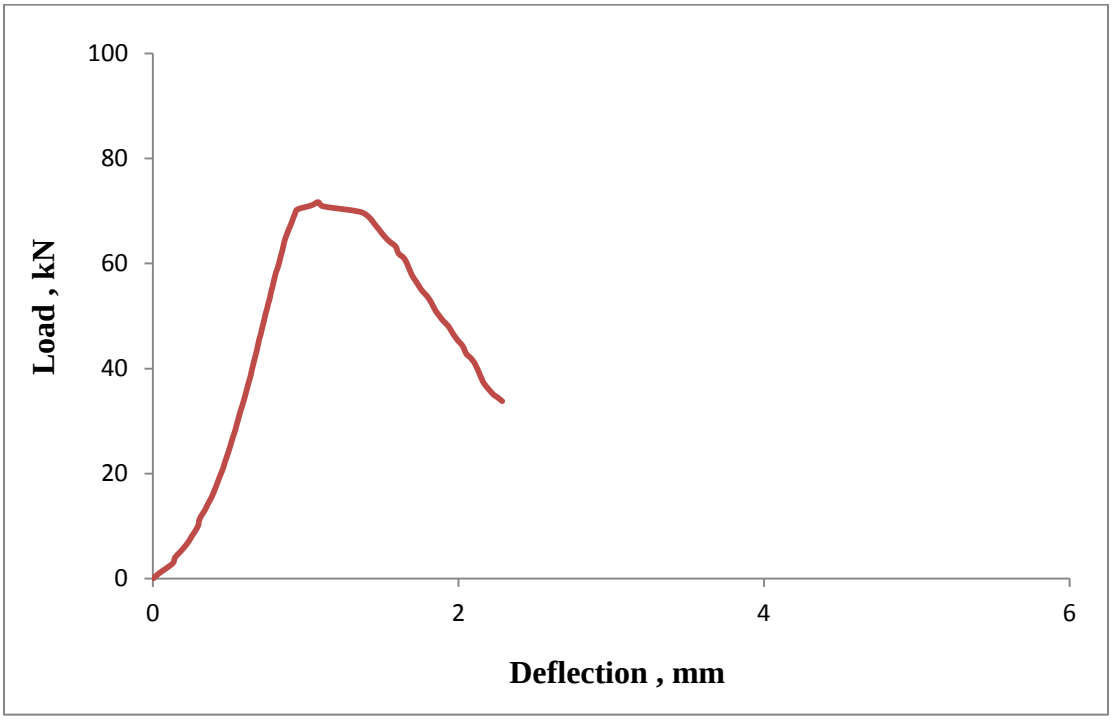

Figure 5.12: Load-deflection curve for beam LS-E-C2 (25 mm thick UHPC)

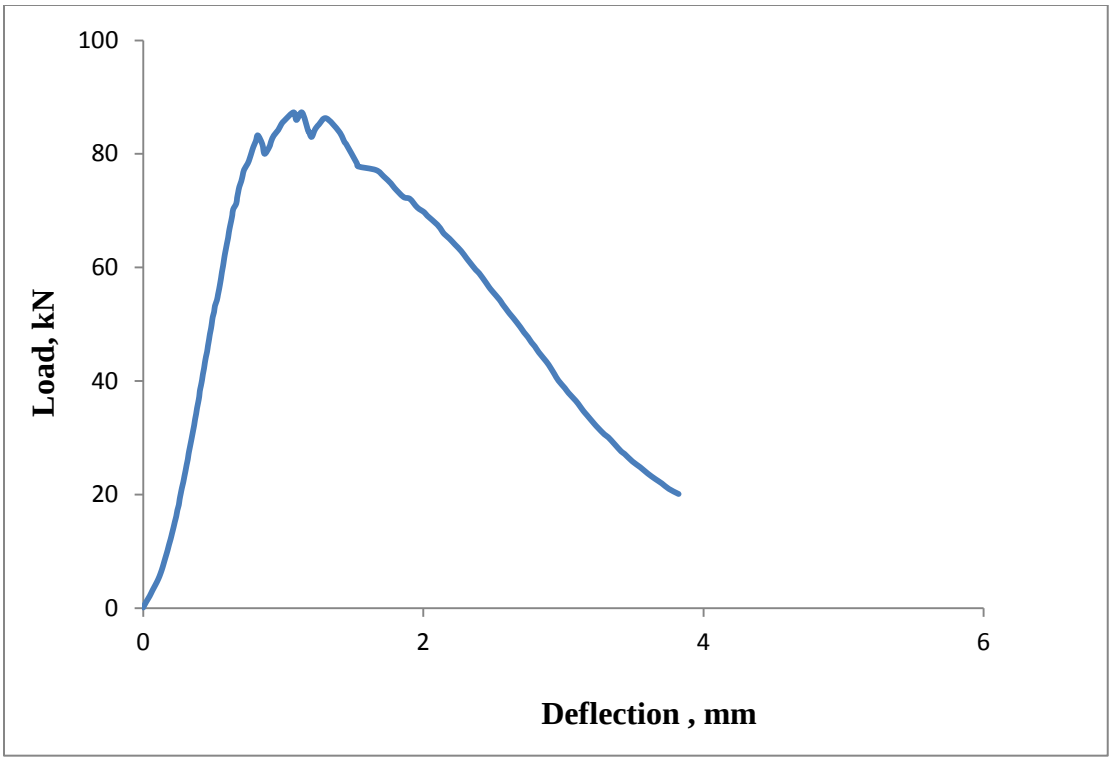

Figure 5.13: Load-deflection curve for beam LS-F-C2 (50 mm thick UHPC)

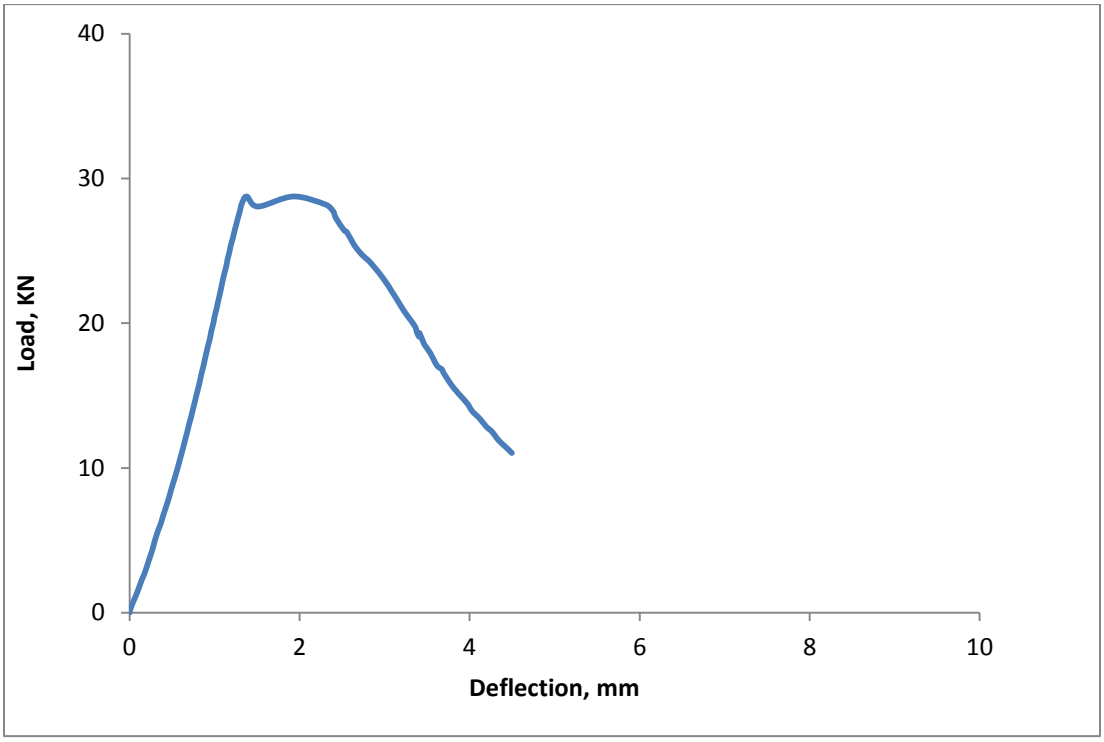

Figure 5.14: Load-deflection curve for beam LS-G-C2 (25 mm thick UHPC)

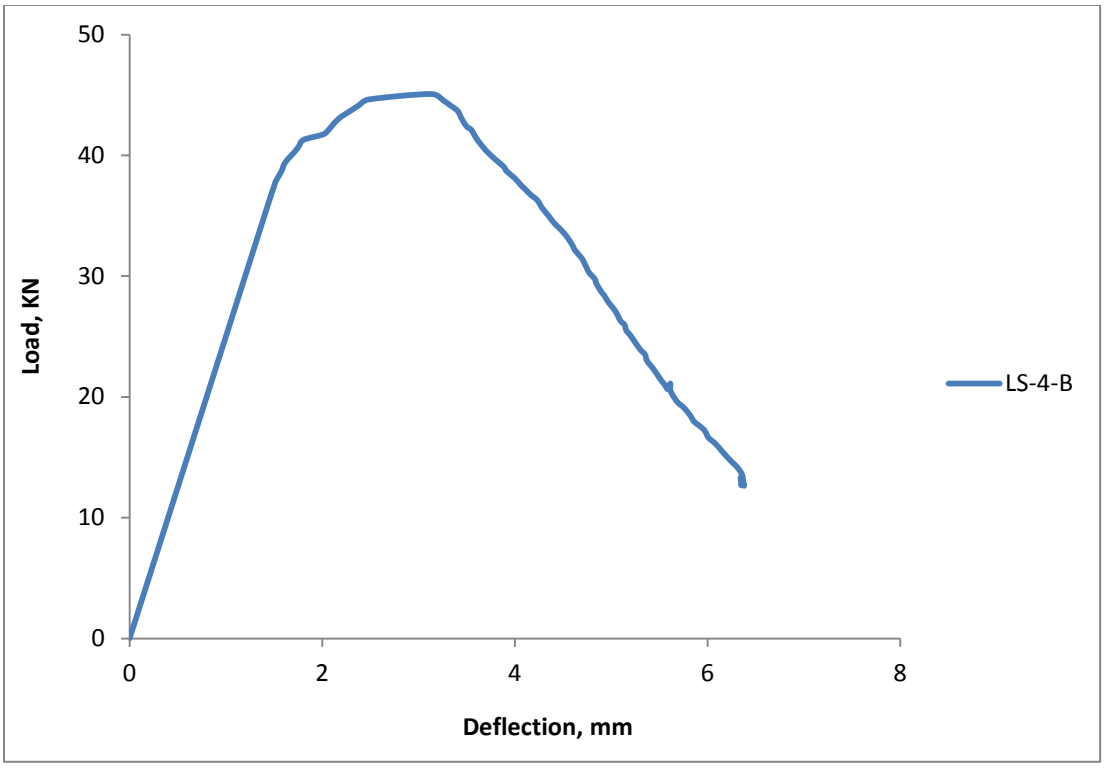

Figure 5.15: Load-deflection curve for beam LS-H-C2 (50 mm thick UHPC)

Figure 5.16: Multiple cracking of hybrid beam LS-H-C2 (50 mm thick UHPC)

Figure 5.17: Crack advancement of beam LS-G-C2 (25 mm thick UHPC)

5.7. Mode of Failure

All test specimens showed linear elastic response almost up to peak load P_U. As the load approaches P_U, multiple fine surface cracks appear in some cases at the bottom UHPC layer within the central part of the specimens between the two loading points. This is followed by very limited hardening and advancement of a single crack through the thickness of UHPC. The peak load P_U occurs at the development of a well-formed single crack in the UHPC layer under the maximum moment.

Following the peak load P_U, the specimens exhibit a gradual softening mode of failure with the advancement of crack almost vertically across the thickness of bottom UHPC layer. In this mode, the cracks always propagate through the UHPC vertically along the

depth and horizontally across the width of the beams as shown in **Figure 5.16**. The bridging of the fibers across the crack and the uncracked ligament of UHPC provides the post cracking residual strength. As the crack advanced, the crack-mouth became wider (**Figure 5.17**).

The softening mode of failure, a characteristic feature of all fiber-reinforced UHPC specimens, is explained by the fact that the fibers bridging the crack have the ability to resist tensile stresses. As the fibers are pulled out due to crack opening, the remaining fibers across the crack tip are able to provide tensile strength to sustain residual load. Once all the fibers are pulled out at the crack, the specimen physically loses its bending strength and fails.

5.8. Prediction of Failure Load

The failure load corresponds to the ultimate moment capacity of the specimens. As the section behaves elastically almost up to the failure load, the stresses in a section can be computed using transformed section properties. The tensile stress at the bottom face of normal concrete (above the bottom UHPC layer) will exceed modulus of rupture for concrete at a moment M_{crc} (or load P_{conc}) (section 7.4), making the section a cracked one. The transformed section properties of cracked section should therefore be used to determine ultimate moment capacity of a section.

If F_{tu} is the maximum flexural tensile strength for UHPC layer used, the moment capacity M_U for a section is given by elementary formula as:

$$M_U = \frac{S_{bcr}\, F_{tu}}{n} \qquad (5.4)$$

Where $n = E_U/E_C$, S_{bcr} = bottom section modulus for transformed cracked concrete section (Table 5.2).

In order to determine M_U and hence P_{uf}, it is necessary to have a fair estimate of F_{tu}. This can only be established through a number of tests of similar size of UHPC specimens.

CHAPTER 6

RESULTS AND DISCUSSION FOR UHPC REINFORCED SPECIMENS

6.1. General

In this chapter, the test results and discussion of hybrid concrete specimens reinforced with precast UHPC deformed bars are presented.

6.2. Transformed Section Properties

As measurement of strains and deflection showed almost linear behavior up to the peak load, the transformed section properties were used to calculate the stress in a section at failure load P_U using the values of modulus of elasticity of concrete Ec = 30 GPa and that of UHPC, E_U = 55 GPa,. For the transformed section (**Figure 6.1**), the cross sectional area of UHPC bars, A_{SU}, is replaced by the equivalent area nA_{SU}, where n, the modular ratio = E_U/E_C = 1.833. The transformed section properties were calculated for cracked section on the basis of **Figure 6.1** and are listed in **Table 6.1**. The properties for cracked concrete section apply when the stress in the bars exceeds the tensile strength of concrete. Unlike specimens with UHPC bottom layer, the bottom face for reinforced specimens is made of UHPC bars and normal concrete. The section becomes cracked when the tensile

stress in concrete exceeds its tensile stress which happens at a lower load level than the failure load P_U. Thus only cracked section is considered.

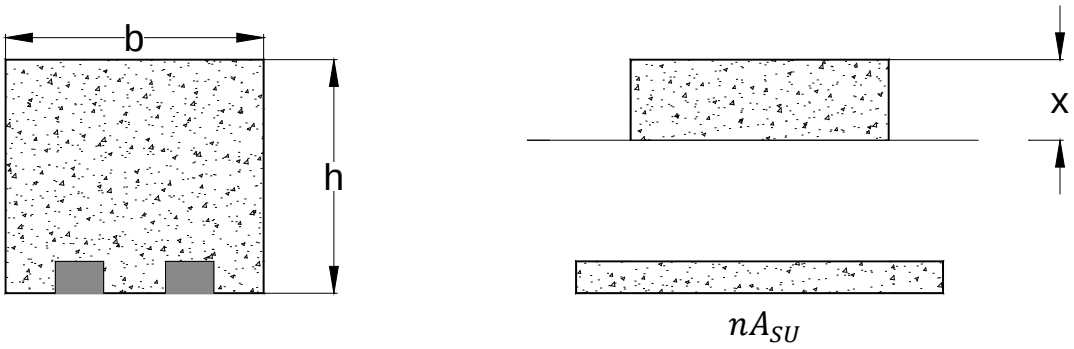

a) Cross section

b) Cracked concrete transformed section

Figure 6.1: Transformed concrete section

Table 6.1: Transformed Cracked Concrete Section Properties

Beam Size (mm)	Beam Designation	UHPC Bar Size (mm)	I_{cr} (mm^4) x 10^6	Depth of N.A. from Top (mm)	Section Modulus	
					S_{tcr} (mm^3) x 10^4	S_{bcr} (mm^3) x 10^4
150 x 150 x 760 (b x h x L)	UB-1	2- 25 x 25	23.8	51.3	46.3	24.1
	UB-2	3- 25 x 25	31.5	59.7	52.7	34.8
	UB-3	2- 25 x 50	30.1	62.0	48.5	34.2
	UB-4	2- 50 x 50	44.0	76.8	57.2	60.0
150 x 200 x 900 (b x h x L)	UB-5	2- 25 x 25	48.0	62.0	77.5	34.8
150 x 220 x 760 (b x h x L)	UB-6	2- 50 x 50	132.1	104.9	125.9	114.8
200 x 270 x 1000 (b x h x L)	UB-7	2- 50 x 50	255.8	110.9	230.7	160.7
200 x 220 x 1000 (b x h x L)	UB-8	2- 50 x 50	148.8	95.5	155.8	119.5
200 x 310 x 1000 (b x h x L)	UB-9	4- 25 x 25	245.1	96.1	255.1	114.6

6.3. Load Capacity and Tensile Stress at Failure

The average values of the failure load, P_U and the corresponding mid-span deflection for three identical specimens are shown in **Table 6.2**. The variation in the three values of P_U is less than 10 % in most cases. The maximum flexural tensile stresses at the bottom face of UHPC bars and compressive stress at top of normal concrete was calculated at P_U using values of section modulus of cracked concrete transformed section properties shown in **Table 6.1**. Compressive stresses are shown as negative.

A comparison of load capacity for UB-1 and UB-2 shows that the increase in the area of UHPC bars, using the same size, increases load capacity almost proportionality, as expected. In order to examine the relative impact of the width and depth of UHPC bars on load capacity, 25x50 mm (width x depth) and 50x50 mm UHPC bars were used in UB-3 and UB-4 respectively with beam size of 150x150x760 mm. The comparison of the load capacities for UB-1 and UB-3 shows that the capacity for UB-3 which had 2-25x50 mm UHPC bars was 38 KN compared to 33 kN for UB-1 with 2-25x25 mm UHPC bars. The area of UHPC bars for UB-3 was twice than that of UB-1. This finding is similar to that observed in layered beams in which increased thickness of UHPC did not produce proportionality higher load capacity. As a beam reaches its maximum load capacity with the attainment of maximum tensile strength at the bottom face, the full utilization of increased area through the increased depth of bars is not realized. The improvement, it seems, is achieved through enhancement of transformed section properties only, an observation that was also made for hybrid layered specimens.

With regard to the increase in width of UHPC bars, the comparison of UB-4 and UB-3 shows that UB-4 with 2-50x 50 mm bars had load capacity of 72 kN compared to 38 kN

for UB-3 with 2-25x50 mm bars. The increase in twice the area of UHPC bars for UB-4 achieved by increasing the width of bars, has resulted in significant increase in load capacity, which was about 90% higher than the capacity of UB-3.

The maximum tensile stress varied from 15.2 MPa to 31.6 MPa showing a wide range similar to layered specimens. However, as the bars showed attainment of higher flexural tensile strength. The variation is mostly attributable to the orientation and dispersion of fibers within the mix.

The test results presented in **Table 6.2** highlight the following:

(i) Load capacity for hybrid beam increases almost proportionality with the increase in number of identical UHPC bars.

(ii) It is structurally superior to use wider bars than thicker bars for same cross sectional areas. The increase in the bar thickness to have identical area does not yield improved load capacity similar to which can be achieved by using wider bars instead.

Table 6.2: Failure Loads and Deflection for Test Beams with UHPC Bars

Beam Designation	UHPC Bar Size (mm)	Average Failure Load P_U (kN)	Deflection at Failure Load Δ (mm)	Average Tensile Stress at Bottom (MPa)	Average compressive Stress at Top (MPa)
UB-1	2- 25 x 25	33	0.49	30.0	-8.5
UB-2	3- 25 x 25	44	0.57	28.0	-10.0
UB-3	2- 25 x 50	38	0.64	24.4	-9.4
UB-4	2- 50 x 50	72	1.3	26.4	-15.1
UB-5	2- 25 x 25	40	0.71	31.6	-7.7
UB-6	2- 50 x 50	72	1.01	15.2	-7.6
UB-7	2- 50 x 50	78	1.90	16.7	-6.3
UB-8	2- 50 x 50	64	1.88	18.5	-7.7
UB-9	4- 25 x 25	82	1.71	24.6	-6.0

6.4. Strain Distributions along the Depth

The load–strain relationship was evaluated using the strains measured by the strain gauges fixed to the beams with the aim of locating measured neutral axis of a section. Four strain gauges located at mid span (**Figure 5.2**) were used to create a strain profile over the depth of most of beams tested and to identify the location of the neutral axis.

The results of two specimens are presented for discussion. The results for the other specimens are presented in **Appendix B**.

Figure 6.2: Location of strain gages in test specimens

Figure 6.3 shows the load–strain plot of beam UB-2 at 0.95 P_U (P_U = 44 kN). Positive strains represent tensile strains while negative strains represent compressive strains. The plot shows linearity for compressive strains up to the failure load. However, the tensile strain at the bottom shows some nonlinearity after about 0.6 P_U. Overall, it can be said that the beam responded linearly with strain being approximately proportional to the applied load. The measured values of tensile and compressive strain at 95% of P_U were 359x 10^{-6} and 234 x10^{-6}, respectively.

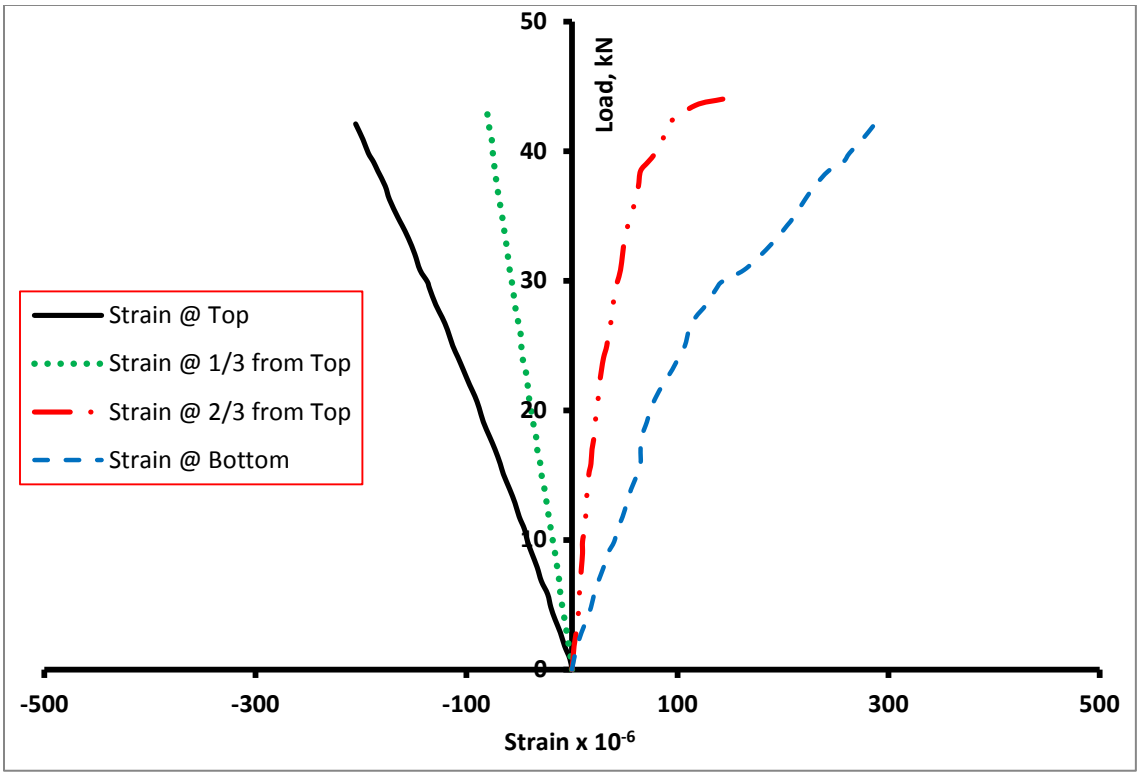

Figure 6.3: Typical load-strain curve for beam UB-2

Figure 6.4 also shows the load–strain plot of beam UB-9 up to the failure of P_U = 82 kN. The plot also shows linearity for both tensile and compressive strains almost up to the failure load.

The measured strain for all test specimens clearly show an approximately linear relationship between load and strains, confirming linear response of UHPC reinforced beams.

This linearity of the strain profile confirms that there is no slip between UHPC bars and normal concrete for a section affirming that adequate bond between NC and UHPC bars has been achieved in the construction of the hybrid specimens. The measured values of

compressive strain at load of failure load were 171 x10^{-6} while the measured tensile strain at the same load level was 314 x10^{-6}.

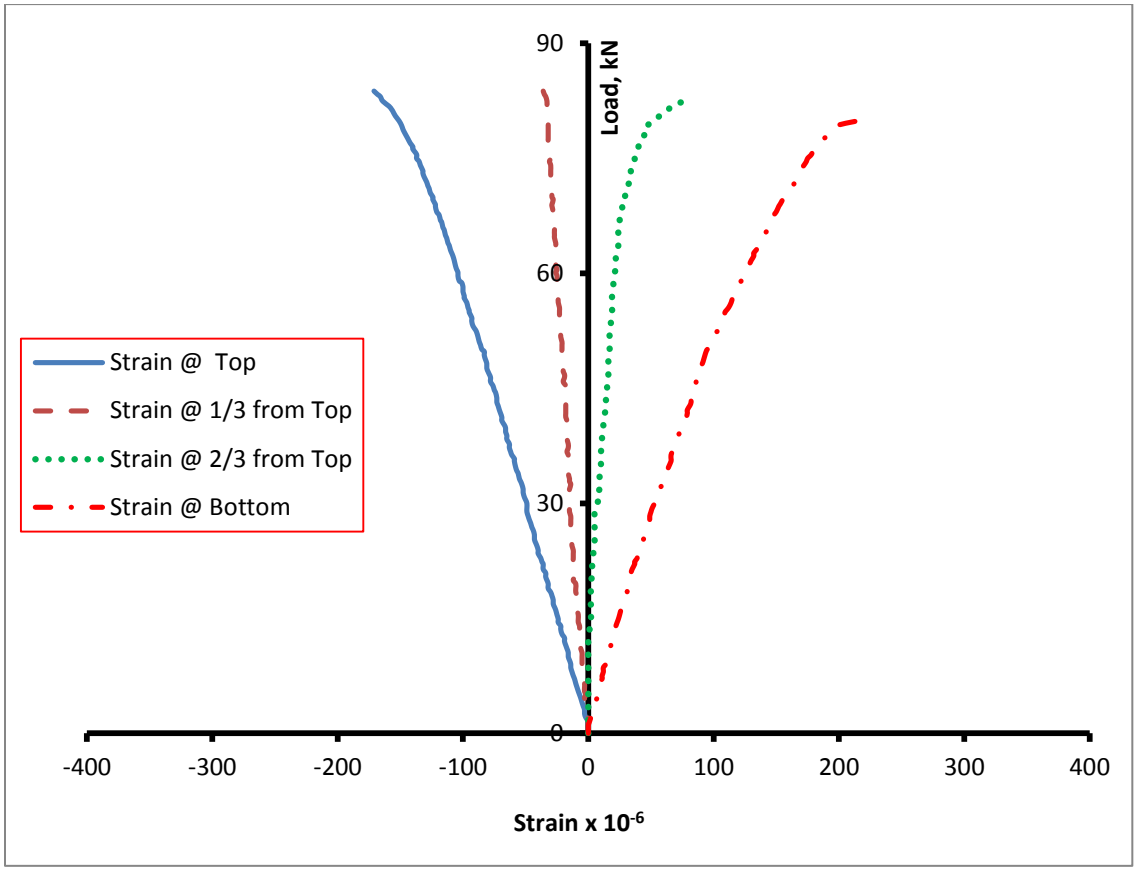

Figure 6.4: Typical load-strain curve for beam UB-9

Using the measured strain data listed in **Table 6.3**, the strain profile across the depth of the beam is plotted in **Figure 6.5** for five load levels of specimen UB-2. Two observations can be made: (i) the distribution across the depth is reasonably linear at all load levels, and (ii) the neutral axis moves upward at higher load. The shift of the neutral axis is caused by the transition of the section from being wholly un-cracked to cracked

section at failure. At load less than failure load, the entire hybrid section remains un-cracked and the neutral axis corresponds to this section unchanged. From the transformed section for an un-cracked section, the neutral axis is calculated at a depth of 79 mm from top. This compares favorably with 80 mm observed neutral axis at P = 12.9 kN. Between the state of fully un-cracked section to the case of cracked section (cracking of UHPC bars), there exist transitional stages due to cracking of normal concrete which cause gradual upward shift of the neutral axis, as noted in strain measurement (**Figure 6.5**). From the cracked transformed section (**Table 6.2**), the computed depth of neutral axis is found to be 60 mm from top at the failure load while the measured depth observed at load close to the failure load PU from strain profile is 63 mm. This shows good agreement between the measured and calculated depth of the compression zone.

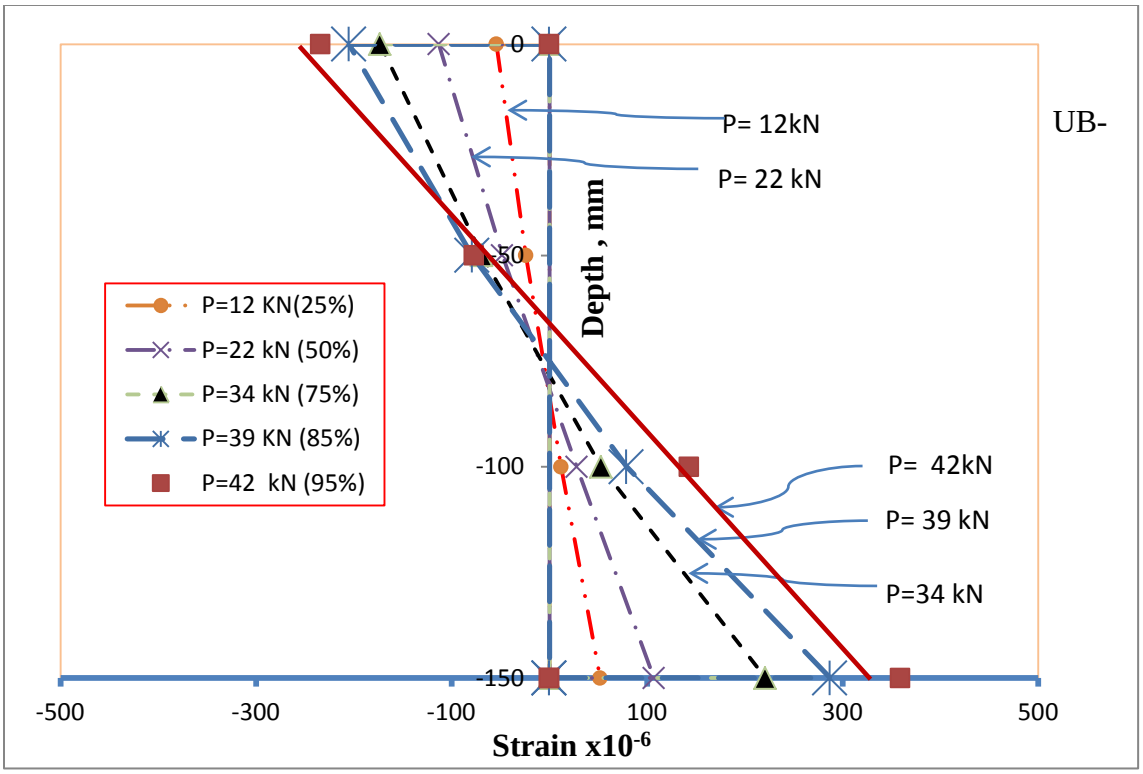

Figure 6.5: Strain profile along the depth for beam UB-2

The strain profile across the depth of the beam UB-9 is also shown in **Figure 6.6** up to the failure load. As seen, the strain distribution across the depth can be assumed to be linear by considering a best-fit linear profile.

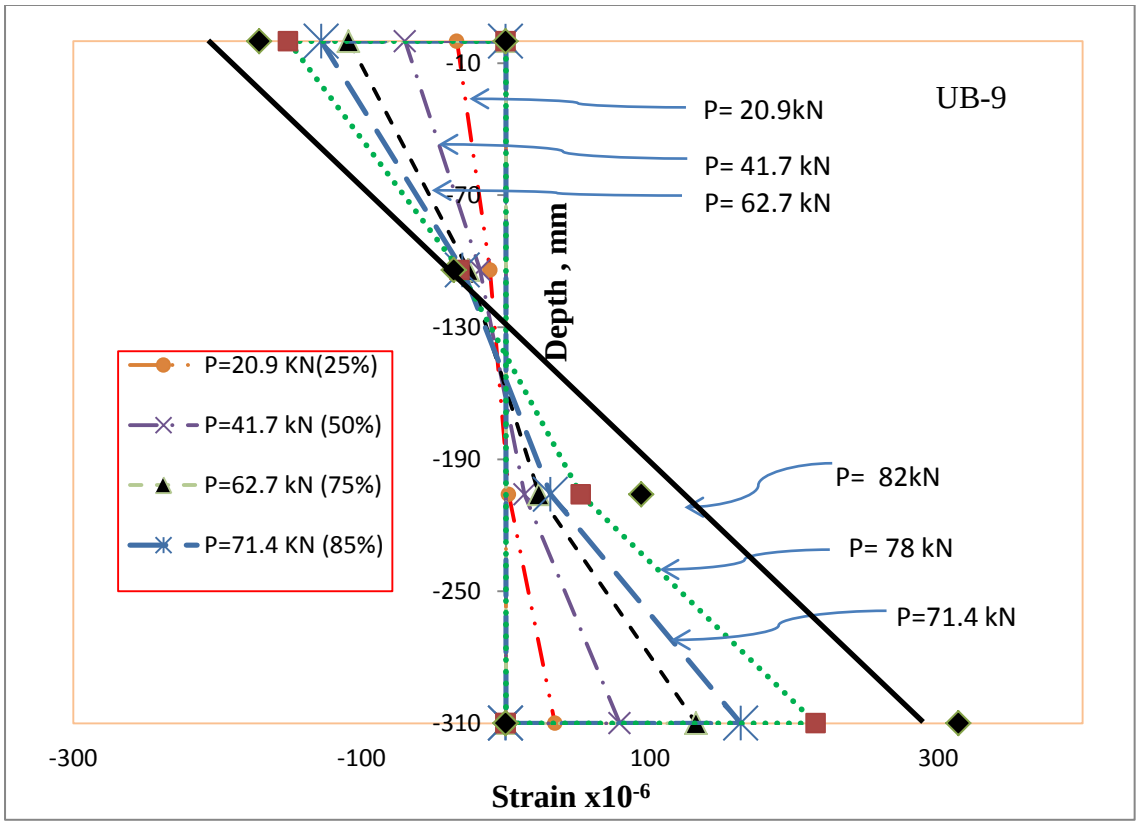

Figure 6.6: Strain profile along the depth for beam UB-9

The measured strains for the two specimens are shown in **Table 6.3**.

Table 6.3: Load Levels and Strain Values for Beams UB-2 and UB-9

Beam Designation	UHPC Bar Size (mm)	Load P (kN)	% of P_U	Measured Strain (x 10^6)			
				Top	1/3 from top	2/3 from top	Bottom
UB-2 (150x150x760) (b x h x L)	3- 25 x 25	12	25	-54	-24	12	52
		22	50	-113	-48	28	107
		34	75	-173	-69	53	221
		39	85	-205	-79	79	287
		42	95	-234	-77	143	359
		44	100	-259	-61	259	498
UB-9 (200x310x1000) (b x h x L)	4- 25 x 25	20	25	-34	-11	2	34
		41	50	-70	-18	13	79
		62	75	-109	-26	23	132
		71	85	-128	-30	31	163
		78	95	-151	-32	52	215
		82	100	-171	-36	94	314

6.5. Measured and Calculated Stresses

For a comparison of the measured stresses from strains with theoretical values computed from flexural formula using transformed properties for hybrid section, **Table 6.4** is prepared using three load levels. The compressive strains at top was converted to stress using E_C = 30 GPa for normal concrete and the tensile stress at the bottom of UHPC bars

was calculated using E_U = 55 GPa. For example, specimen UB-2, for the three load levels at 0.85 P_U, 0.95 P_U and P_U, the transformed properties of cracked section (**Table 6.1**) were used. The computed stress at the three selected load levels show that the use of transformed section properties of cracked section (**Table 6.4**) yields results that are closer to the measured stresses using the measured strains. However, in some cases the calculated stress based on transformed section as mentioned did not show closer agreement with the measured values. This suggests that accurate measurements of strains should be taken for a number of specimens to see the correlation between measured and calculated values. However, for calculation of maximum tensile stress in UHPC bars at failure, the use of transformed cracked section properties appears to be satisfactory.

All the calculated and measured results of all specimens tested are compiled and presented in **Appendix C**.

Table 6.4: Measured and Computed Stresses for Selected Load Levels for Beam UB-2 and UB-9

Beam Designation	UHPC Bar Size (mm)	Load P (kN)	% of P_U	Measured Stress (MPa)		Calculated Stress (MPa)	
				Bottom	Top	Bottom	Top
UB-2 (150x150x760) (b x h x L)	3- 25 x 25	38	85	15.8	6.2	24.1	8.7
		42	95	19.7	7.0	26.5	9.6
		44	100	27.4	7.8	27.8	10.0
UB-9 (200x310x1000) (b x h x L)	3- 25 x 25	70	85	9.0	3.8	21.0	5.2
		78	95	11.8	4.5	23.4	5.7
		82	100	17.3	5.1	24.6	6.0

6.6. Load Deflection Plots

Typical load-deflection plots of hybrid beams reinforced with UHPC bars are shown in **Figures 6.7** through **6.15** (only one typical specimen presented out of three replicate), capturing the ascending and descending load paths. The softening mode of failure in flexure mode implies non-brittle failure with significant post-cracking strength, lesser than the peak load. In all cases, the hybrid beams failed with the formation and advancement of only a single vertical crack within the maximum moment zone (zero shear) (**Figure 6.16**).

It should be noted that the lesser values of post-peak strength are attributed to progressive crack growth within the bottom UHPC bars. The uncracked ligament of UHPC bars and

the bridging of steel fibers across the crack that are not pulled out contribute to the residual flexural strength.

The load-deflection plots show that wider bars have flatter post-peak load deflection (**Figure 6.10**) than those for small bar sizes (**Figure 6.7**). The deformed shape of the bars, along with the rough top face enables the bars to develop full strength without any bond-slip. Load-deflection plots in **Figures 6.7** and **6.8** point to the fact that as the area of UHPC bars increases, immediate post-peak deflection curve becomes flatter. UB-1 had 2 UHPC bars of 25x25 mm size, whereas UB-2 had 3 UHPC bars of the same cross-section.

Likewise, UB-4 which had 2 UHPC bars of 50x50mm cross-section (**Figure 84**) showed flatter post-peak deflection compared to UB-3 which had 2 UHPC bars of 25x50 mm cross-section (**Figure 6.9**). This reconfirm that wider bars have more favorable effect on the beam behavior, both in terms of efficient utilization and post-cracking deformation.

The calculation of deflection at the center of the beams using Equation 5.3 (Chapter 5) for cracked transformed section (**Table 6.1**) is shown in **Table 6.7**. The measured experimental deflection up to the failure load **Table 6.5**. Note that the selected computed and measured deflection values given in **Table 6.5**.

Table 6.5: Comparison of Theoretical and Calculated Deflection

Beam Designation	Measured Deflection (mm)	P_U (kN)	Calculated Deflection, Δ (mm)
			Based on I_{cr}
UB-1	0.33	33	0.22
UB-2	0.35	44	0.25
UB-3	0.44	38	0.21
UB-5	0.35	40	0.22
UB-8	0.20	64	0.21

From the load-deflection plots, the following observations can be made:

(1) The deflection can be taken as approximately linear up to the failure load P_U.

(2) The deflection can be calculated using the moment of inertia of the cracked transformed section, I_{cr}, (**Table 6.1**).

(3) Depending upon fiber orientation and amount of fiber across the crack, some specimens may show small post-crack stiffening resulting in increased deflection at P_U and while others will not. Thus some specimens showed very limited stiffening or constant laod with increased deflection (e.g. UB-4, UB-8) others showed softening with increased deflection at reduced load almost immediately after P_U (e.g. UB-2, UB-3, and UB-5).

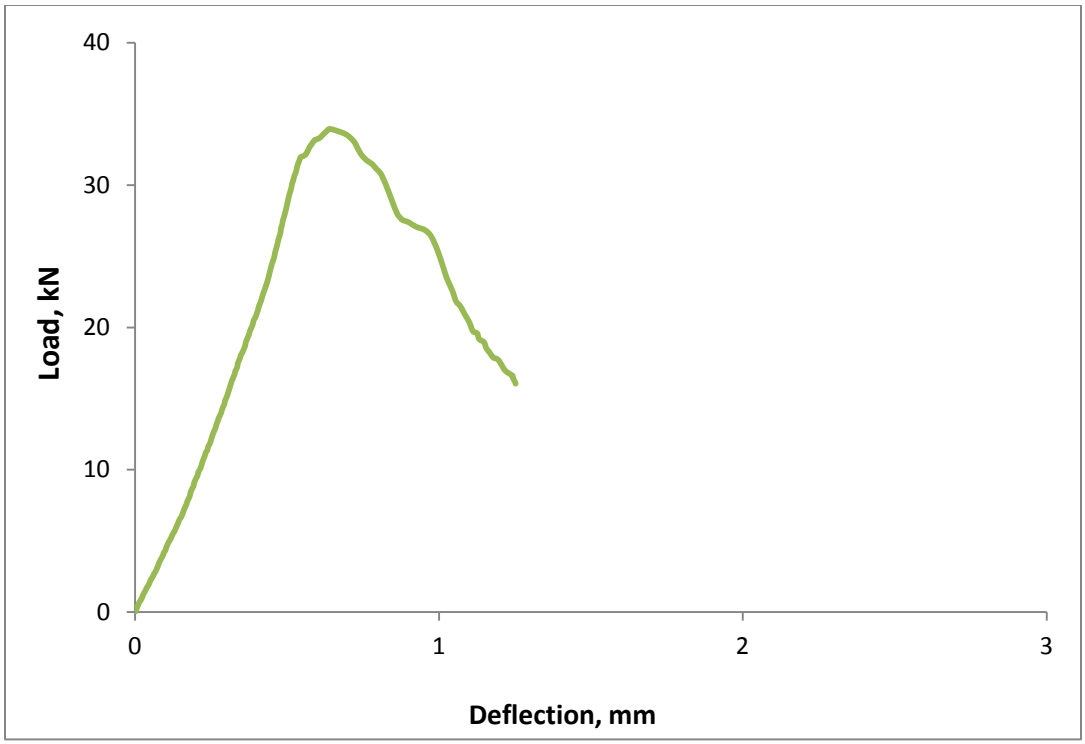

Figure 6.7: Load-deflection curve of beam UB-1 (2 -25x25 mm bars)

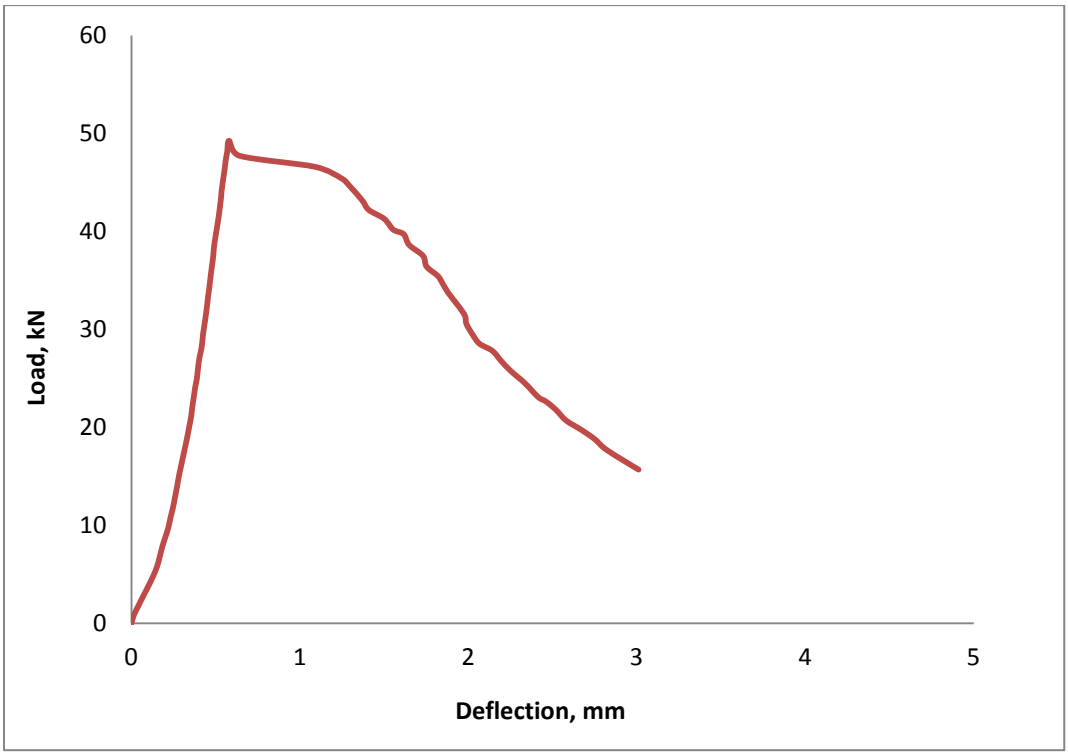

Figure 6.8: Load-deflection curve of beam UB-2 (3-25x25mm bars)

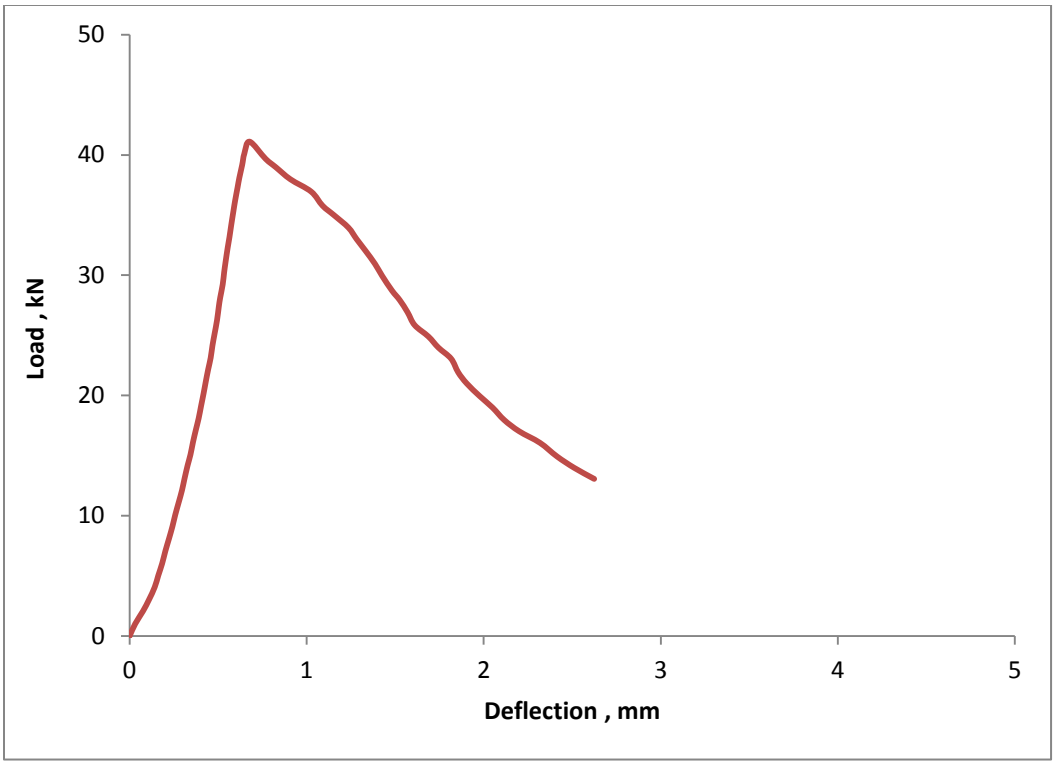

Figure 6.9: Load-deflection curve of beam UB-3 (2 -25x50 mm bars)

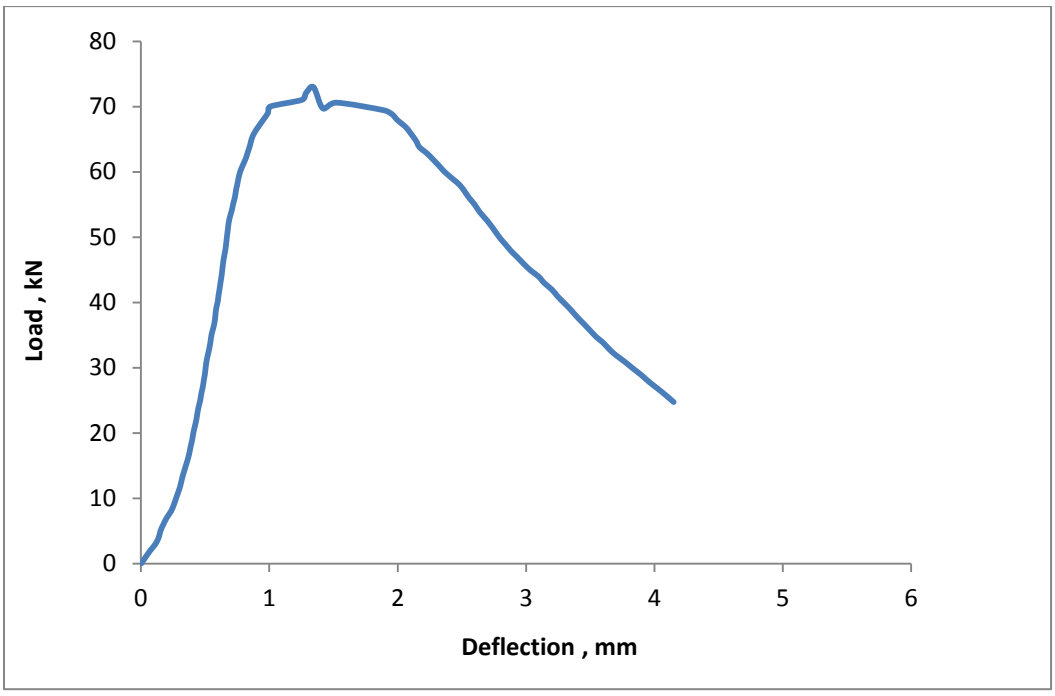

Figure 6.10: Load-deflection curve of beam UB-4 (2 – 50x50 mm bars)

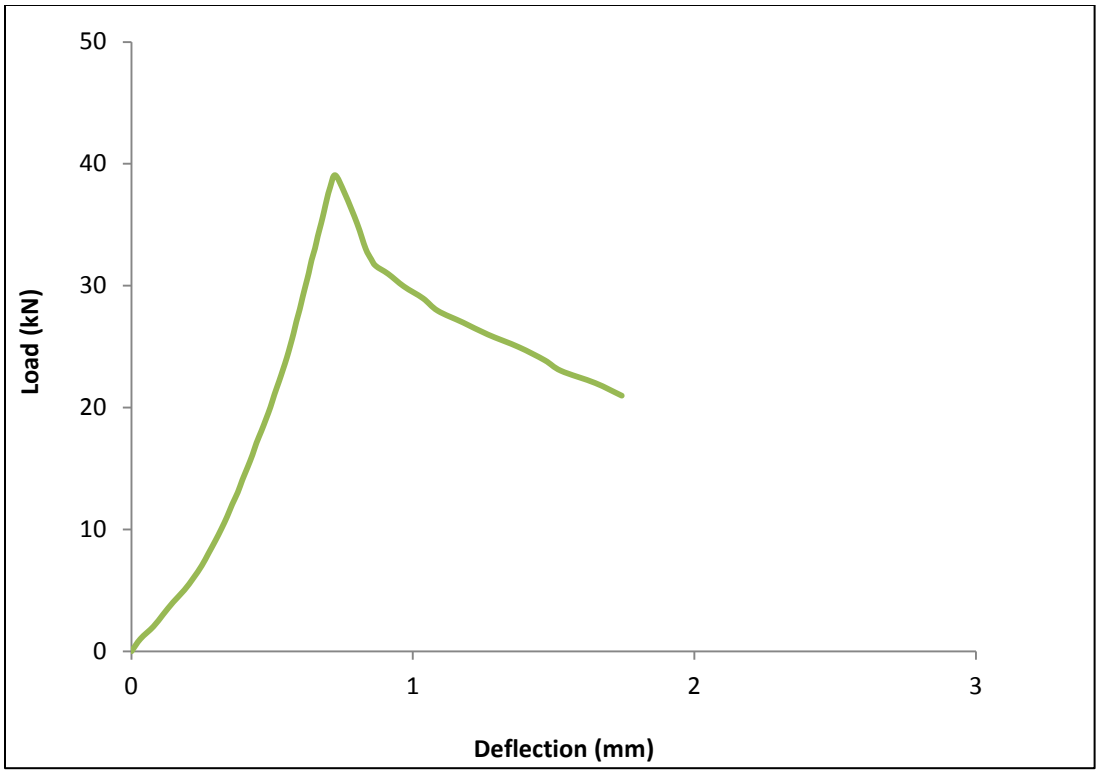

Figure 6.11: Load-deflection curve of beam UB-5 (2 – 25x25 mm bars)

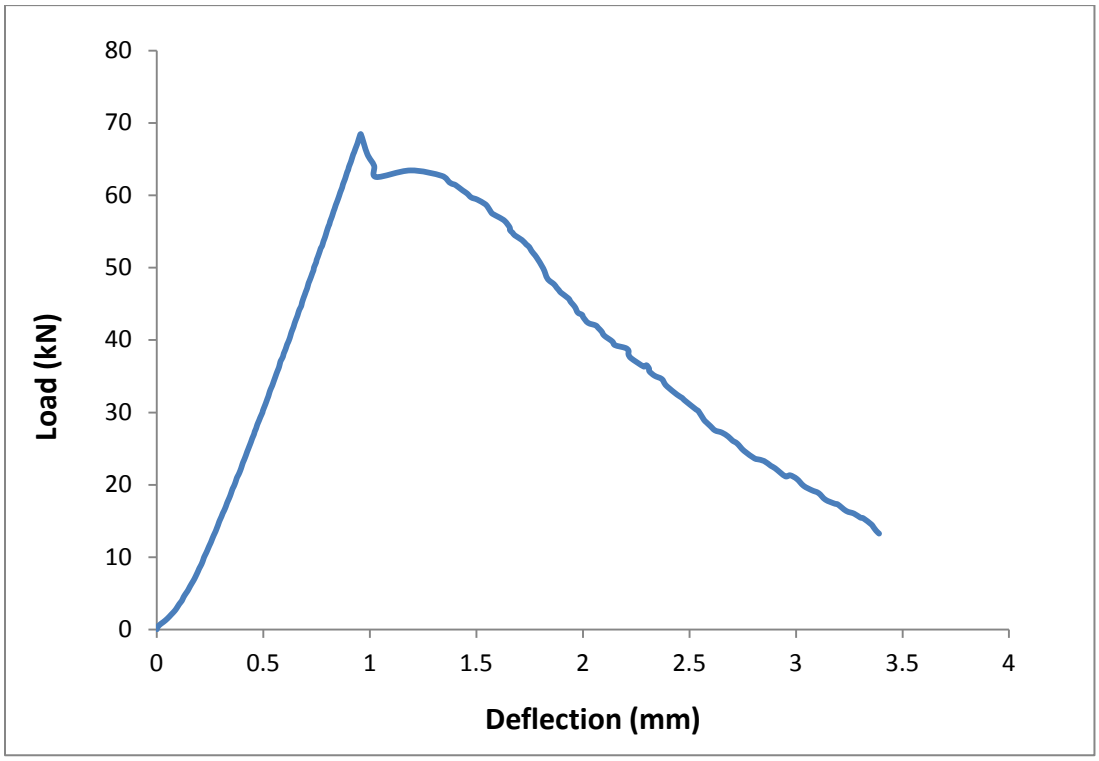

Figure 6.12: Load-deflection curve of beam UB-6 (2 – 50 x 50 mm bars)

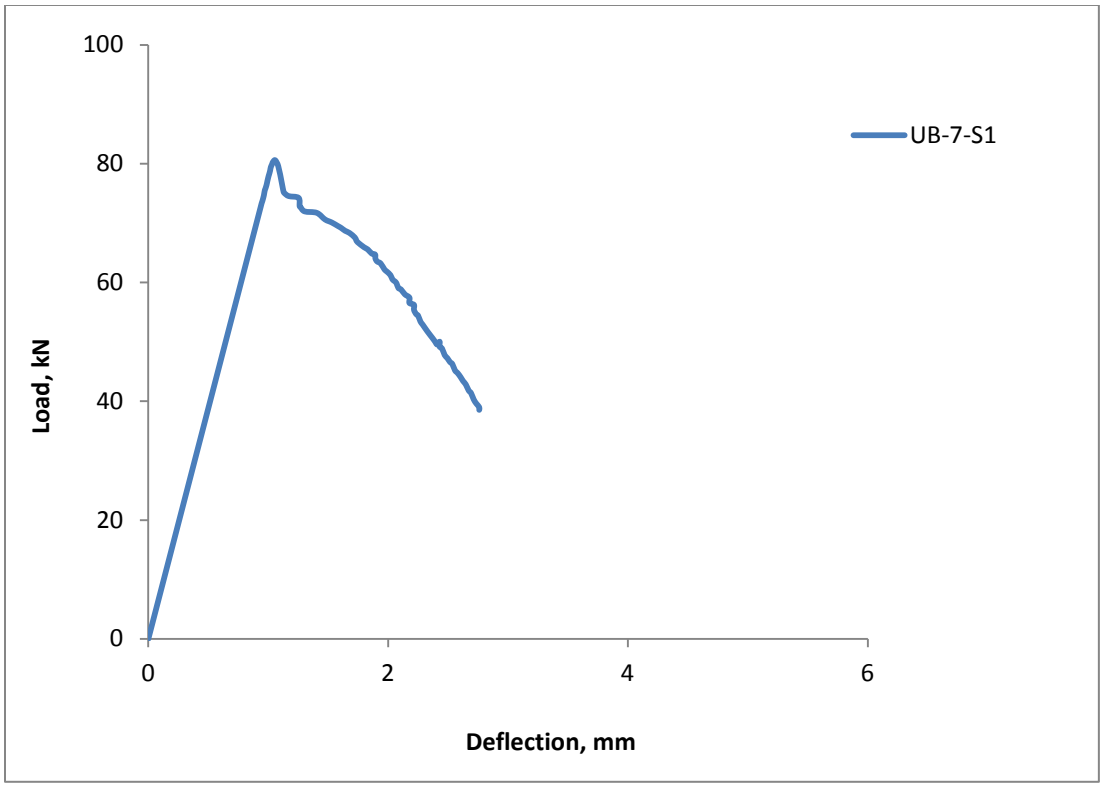

Figure 6.13: Load-deflection curve of beam UB-7 (2 – 50 x 50 mm bars)

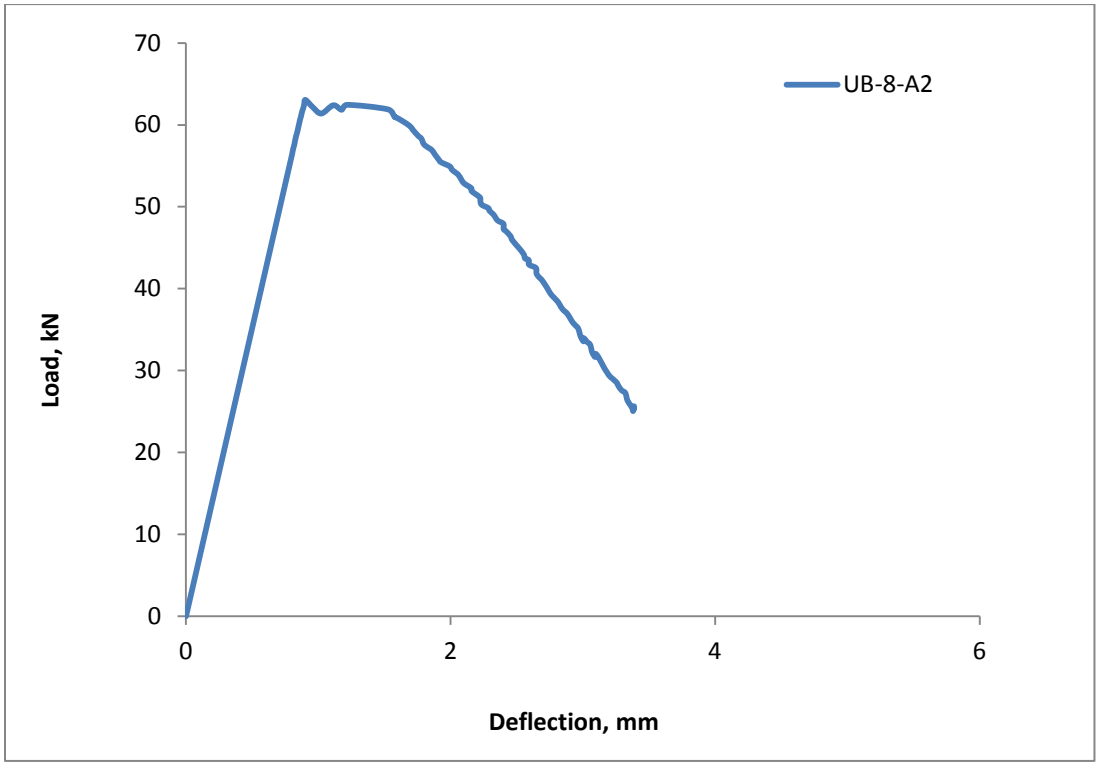

Figure 6.14: Load-deflection curve of beam UB-8 (2 – 50 x 50 mm bars)

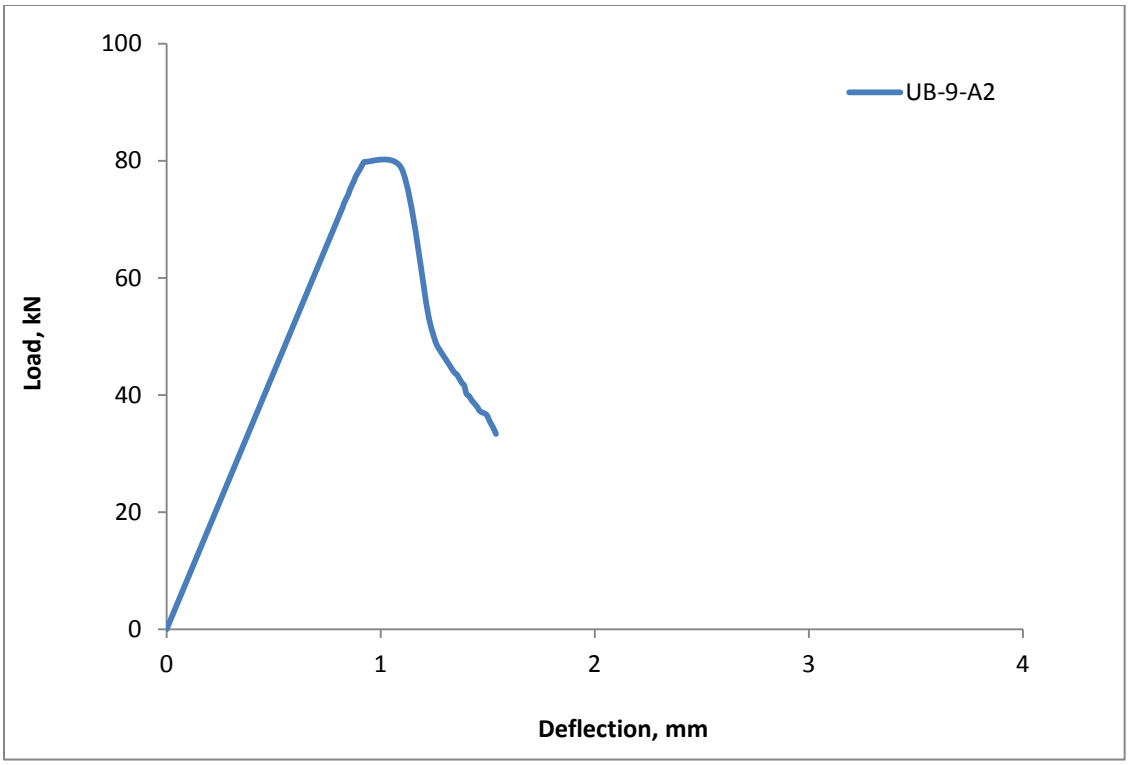

Figure 6.15: Load-deflection curve of beam UB-9 (4 – 25x25 mm bars)

6.7. Mode of Failure

The mode of failure was flexural for all beams, with the occurrence and advancement of a single crack through the UHPC bars. Unlike steel reinforced beam, the development of a single crack in UHPC bars represents the weakest section for the beam and the failure occurs with the advancement of this crack. The beam shows reduced post-peak load capacity with increased deflection. The first micro-cracking occurred at the bottom face of the beam between the loading points where the beam was subjected to pure bending. Tensile failure occurs when the steel fiber begins to pull out of the UHPC matrix. Mechanically, pullout occurs when the load carried by an individual fiber overcomes the ability of the UHPC bars to grip the fiber. Fibers that are pulled out increase the load that

other fibers nearby must carry. At the peak load, the fibers at one specific cross section began to pull out. The crack width becomes significantly wider as shown in **Figure 6.16**. After the peak state, the residual load capacity decreases progressively with the widening of the specific crack. The prolonged post-peak load deflection indicates ductile failure with appreciable amount of softening.

The softening mode of failure, a characteristic feature of all fiber-reinforced UHPC specimens, is explained by the fact that the fibers bridging the crack have the ability to resist tensile stresses. As the fibers are pulled out due to crack opening, the remaining fibers across the crack tip are able to provide tensile strength to sustain residual load. Once all the fibers are pulled out at the crack, the specimen physically loses its bending strength and fails.

Figure 6.16: Typical crack advancement in hybrid beam reinforced with UHPC bars

6.8. Prediction of Failure Load

The failure load corresponds to the ultimate moment capacity of the specimens. As the section behaves elastically almost up to the failure load, the stresses in a section can be computed using transformed section properties. The transformed section properties of cracked section can be used to determine ultimate moment capacity of a section.

If F_{tu} is the maximum flexural tensile strength for UHPC bar used, the moment capacity M_U for a section is given by elementary formula as

$$M_U = \frac{S_{bcr} F_{tu}}{n} \quad (6.1)$$

Where n = E_U/E_C, S_{bcr} = bottom section modulus for transformed cracked concrete section

In order to determine M_U and hence P_{uf}, it is necessary to have a fair estimate of F_{tu}. This can only be established through a number of tests of similar size of UHPC specimens.

CHAPTER 7

RESULTS AND DISCUSSION FOR HYBRID HOLLOW CORE SLAB

7.1. General

In this chapter, the test results and discussion of hybrid hollow core slab using top and bottom layers of UHPC are presented.

7.2. Transformed Section Properties

As measurement of strains and deflection showed almost linear behavior up to the peak load, the transformed section properties were used to calculate the stress in a section at failure load P_U using the values of modulus of elasticity of concrete Ec = 30 GPa and that of UHPC, E_U = 55 GPa,. For the transformed section (**Figure 7.1**), the cross sectional area of UHPC layer, A_{SU}, is replaced by an equivalent area nA_{SU}, where n, the modular ratio = E_U/E_C = 1.833. The transformed section properties were calculated for cracked and uncracked concrete section on the basis of **Figure 7.1** and are listed in **Tables 7.1** and **7.2**. The properties for cracked concrete section apply at load level greater than the load that would produce cracking of the bottom face of normal concrete due to tensile stress being equal or greater than modulus of rupture of concrete.

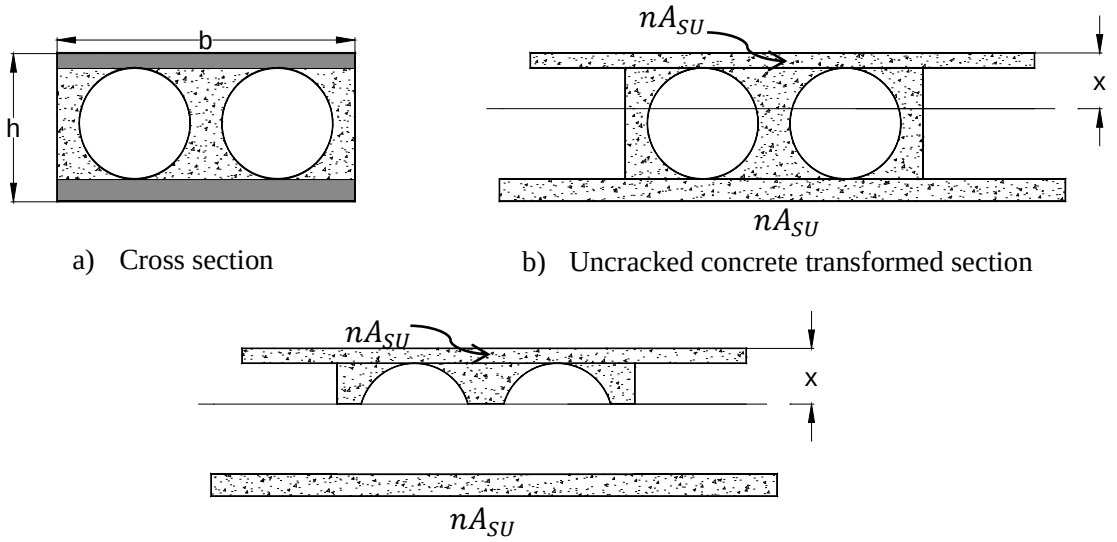

a) Cross section

b) Uncracked concrete transformed section

c) Cracked concrete transformed section

Figure 7.1: Transformed concrete section

Table 7.1: Uncracked Concrete Transformed Section Properties of Hybrid Hollow Core Slab

Group No.	Cross section (mm) width x depth	Moment of inertia I_{uncr} (mm^4) x 10^6	Depth of N.A. from top (mm)	Section Modulus	
				S_{tuc} (mm^3) x 10^6	S_{buc} (mm^3) x 10^6
Group (i)	260 x 140	89.8	74.3	1.21	1.37
Group (ii)	330 x 175	202.0	93.2	2.17	2.47
Group (iii)	390 x 200	339.1	106.5	3.18	3.63
Group (iv)	380 x 140	129.9	74.3	1.75	1.98
Group (v)	260 x 140	95.9	72.1	1.33	1.41

Table 7.2: Cracked Concrete Transformed Section Properties of Hybrid Hollow Core Slab

Group No.	Cross section, (mm) width x depth	Moment of inertia $I_{cr.}$ (mm^4) x 10^6	Depth of N.A. from top (mm)	Section Modulus	
				S_{tcr} (mm^3) x 10^6	S_{bcr} (mm^3) x 10^6
Group (i)	260 x 140	86.6	70.8	1.22	1.25
Group (ii)	330 x 175	190.3	86.9	2.19	2.16
Group (iii)	390 x 200	313.6	97.6	3.20	3.10
Group (iv)	380 x 140	125.3	71.0	1.77	1.82
Group (v)	260 x 140	90.1	67.0	1.35	1.23

7.3. Load Capacity and Tensile Stress at Failure

The average values of the failure load, P_U and the corresponding mid-span deflection for three identical specimens are shown in **Table 7.3**. The variation in the three values of P_U is less than 12 % in most cases. The maximum flexural stress at the top and bottom faces of UHPC layers was calculated at P_U using values of section modulus of cracked concrete transformed section properties shown in **Table 7.2**. Compressive stresses are shown as negative. The maximum tensile stress for specimens failing in flexure varied from 9.5 MPa to 17.6 MPa showing a wide range for a UHPC having the same mix design. As flexure failure is initiated by the tensile stress reaching the maximum flexural tensile strength, which for the UHPC mix used was determined from prism tests as 25 MPa (section 4.1), it was expected that the computed tensile stress at failure load should be somewhat closer to the flexural tensile strength. The significant shortfall can be attributed

to two effects: one is the size effect in terms of the width and span of the specimens. As the tensile strength is dependent upon the dispersion and orientation of steel fibers, the uniformity of fiber dispersion is far less secured for wider and longer sections than for smaller, narrower sections. The other one is the unavoidable variation that exists in mixing a larger amount of row materials with fibers and in casting UHPC lends also to a high degree of variation in tensile strength. The size effect on tensile strength variation is one of the challenges of fiber-reinforced UHPC construction.

For the longer span specimens, the dominant failure mode is the flexure failure and the average computed bottom tensile stress is 16 MPa for Group (i), 11 MPa for Group (ii) , 12 MPa for Groups (iii) and (iv). The maximum variation of computed tensile stress from the average strength for each group is about 10%.

The specimens that failed in web-shear (failure mode discussed in section 7.7) showed a tensile stress at the bottom face ranging from 10.0 to 16.3 MPa. These stresses are not the maximum flexural tensile strength, as the specimens failed prematurely in shear, indicating the load in flexure failure would have been higher. The flexural tensile strength of UHPC for theses specimens were higher than the calculated stresses.

It is clear that higher depth of hollow core slabs results in higher load capacity of the slabs for the same span length, as expected. This is evident from results in **Table 7.3** for all groups of beams. The average failure load for HC-A-L1, HC-A-L2, and HC-A-L3 for Group (i) which had depth of 140 mm and 260 mm wide was 50 kN compared to 62 kN for HC-B-L1, HC-B-L1, HC-B-L1 of Group (ii), which had a depth of 175 mm and 330 mm wide, an increase in P_U about 24%. The comparison of P_U for Group (i) with two

holes and Group (v) without holes for span 900 mm can be used to show the effect of holes. As the presence of holes make the section weaker in shear, two of the specimens in Group (i), HC-A-S1 and HC-A-S2 failed in shear. However, that was not the case in case of Group (v) specimens, all of which failed in flexure as the shear strength of these specimens is considerably higher.

Table 7.3: Test Data and Calculated Stresses at Failure Load

Group No.	Beam Designation	Test Span (mm)	Mode of Failure	Failure Load, P_U (kN)	Deflection at Failure Load, Δ (mm)	Calculated Stress (MPa)	
						Bottom	Top
Group (i) (260 × 140) (Two holes)	HC-A-S1	900	Web-shear	62.9	2.07	15.0	-15.3
	HC-A-S2		Web-shear	68.4	2.38	16.3	-16.7
	HC-A-S3		Flexure	49.0	1.80	11.7	-12.0
	HC-A-L1	1100	Flexure	47.5	2.23	14.8	-15.1
	HC-A-L2		Flexure	47.9	2.20	14.9	-15.3
	HC-A-L3		Flexure	56.4	2.12	17.6	-18.0
Group (ii) (330 × 175) (Two holes)	HC-B-S1	900	Flexure	82.6	2.37	11.4	-11.2
	HC-B-S2		Web-shear	88.7	2.88	12.2	-12.1
	HC-B-S3		Web-shear	95.7	2.71	13.2	-13.0
	HC-B-L1	1100	Flexure	64.1	2.20	11.6	-11.4
	HC-B-L2		Flexure	58.2	2.21	10.5	-10.3
	HC-B-L3		Flexure	65.1	1.95	11.8	-11.6
Group (iii) (390 × 200) (Two holes)	HC-C-S1	900	Flexure	97.6	2.17	9.5	-9.1
	HC-C-S2		Web-shear	111.8	2.53	11.0	-10.4
	HC-C-S3		Web-shear	100.6	2.20	10.0	-9.3
	HC-C-L1	1100	Flexure	93.7	1.02	12.0	-11.4
	HC-C-L2		Flexure	103.1	2.34	13.1	-12.5
	HC-C-L3		Flexure	88.5	2.20	11.3	-10.7
Group (iv) (380 × 140) (Three holes)	HC-D-L1	1100	Flexure	51.5	1.93	11.1	-11.4
	HC-D-L2		Flexure	58.4	2.34	12.5	-12.9
	HC-D-L3		Flexure	57.2	2.40	12.3	-12.6
Group (v) (260 × 140) (Solid section)	HC-E-S1	900	Flexure	60.5	1.80	14.6	-13.4
	HC-E-S2		Flexure	65.4	2.10	15.8	-14.5
	HC-E-S3		Flexure	58.0	2.06	14.0	-13.0

7.4. Strain Distributions along the Depth

The load–strain relationship was evaluated using the strains measured by the strain gauges fixed to the slabs with the aim of locating measured neutral axis of a section. Six strain gauges located at mid-span (**Figure 7.2**) were used to create a strain profile over the depth of all specimens and to identify the location of the neutral axis.

(a) Strain gages before testing

(b) Strain gages during testing

Figure 7.2: Instrumentation for test specimens

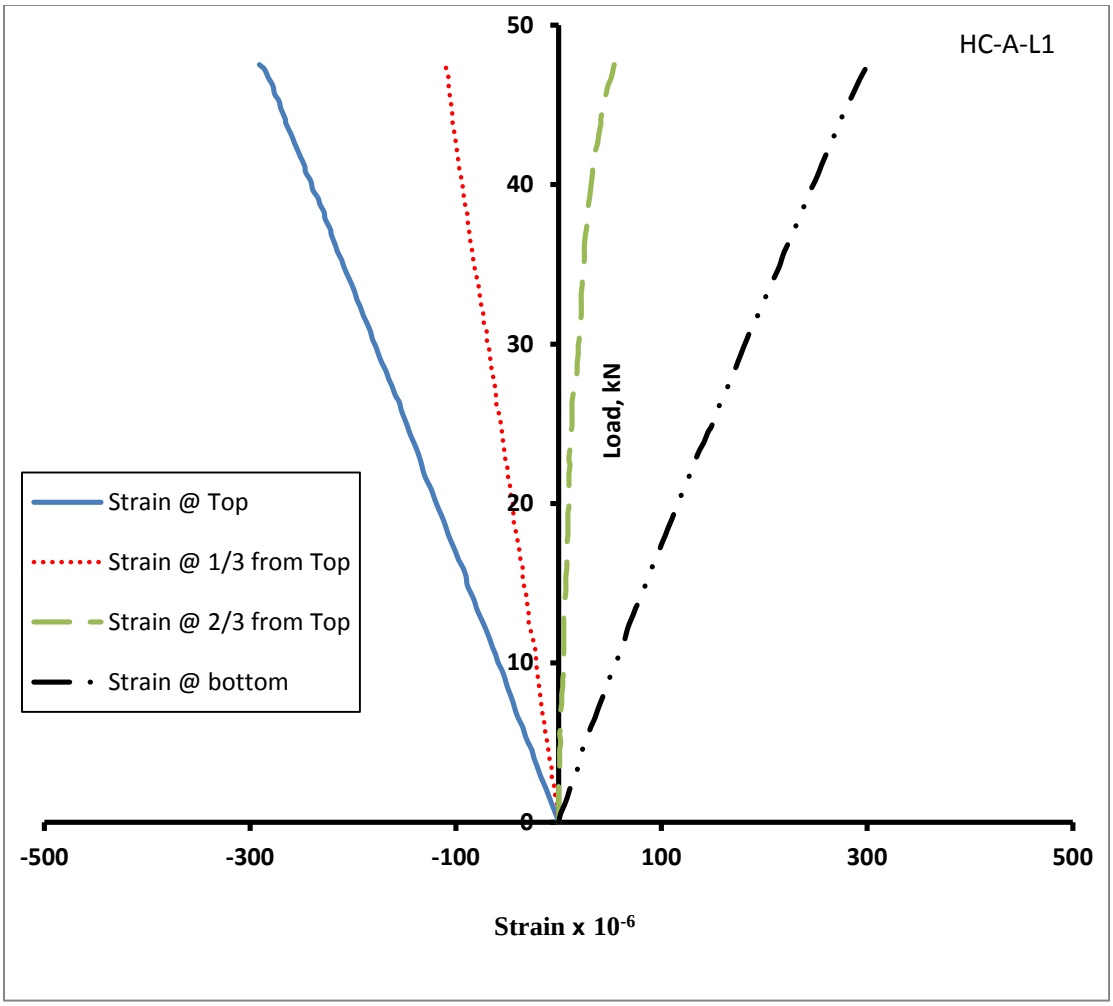

Figure 7.3: Typical load-strain curve for slab HC-A-L1

As a representative plot of strain distribution for longer span specimens that failed in flexure mode, **Figure 7.3** is used to show the load–strain plot of slab HC-A-L1 at 95% of the failure load. Positive and negative strains represent tensile and compressive strains, respectively. The plot shows linearity for tension and compressive strains almost up to the failure load. In other words the beam responded almost linearly, with strain being approximately proportional to the applied load. This linearity of the strain profile confirms that there is no slip at the interfaces between UHPC and normal concrete for a

section affirming that adequate bond between NC and UHPC has been achieved in the construction of the hybrid specimens.

The measured values of compressive strain at the load of 45.3 kN (0.95 P_U) were 272 x 10^{-6} while the measured tensile strain at the same load level was 283 x 10^{-6}. **Figure 7.4** shows the crack propagation under flexure mode of failure of specimen HC-A-L2 at failure.

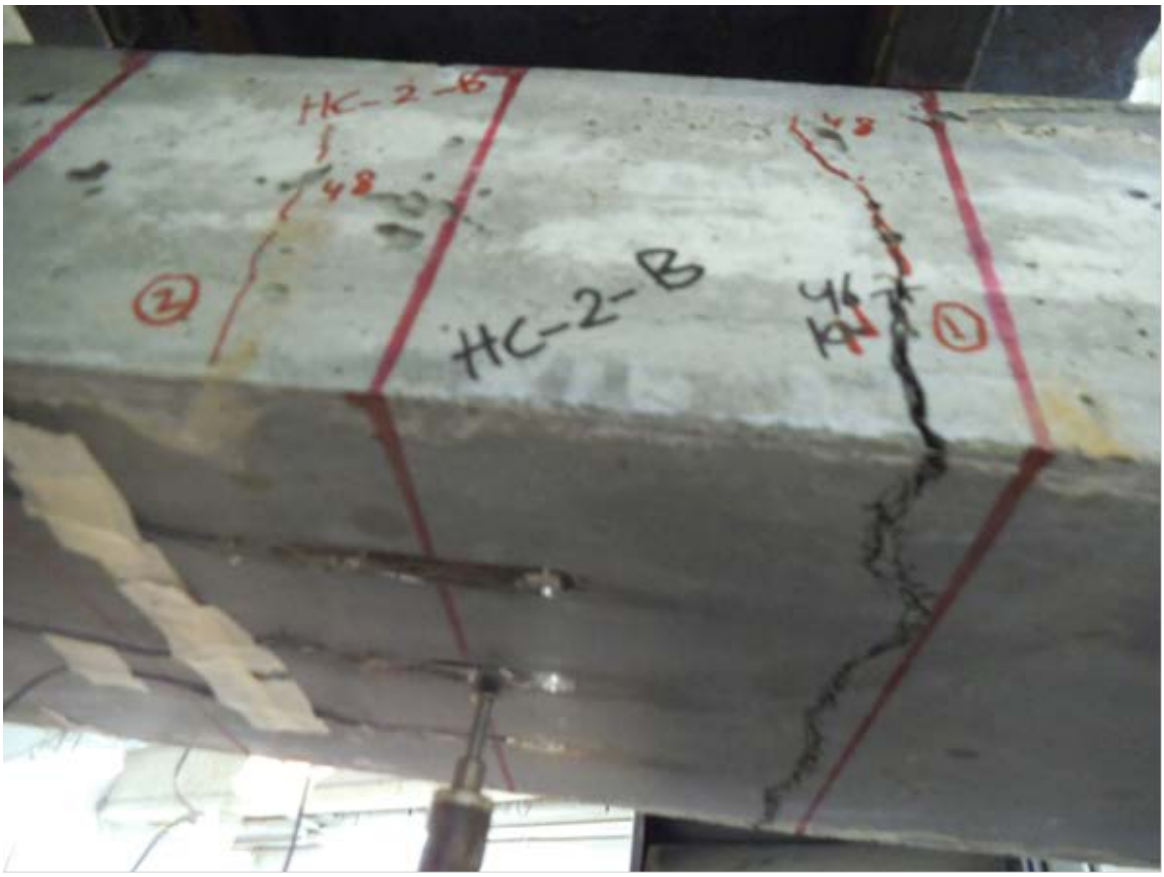

Figure 7.4: Crack advancement of hybrid slab at failure load

Figure 7.5 shows the load–strain plot of slab HC-A-S1 at 99% of the failure load, selected to represent the case of the web-shear mode of failure. The plot shows also

linearity for tensile and compressive strains almost up to the failure load. The measured strain for all test specimens, regardless of the mode of failure, clearly show an approximately linear relationship between load and strains, confirming linear response of UHPC hybrid elements.

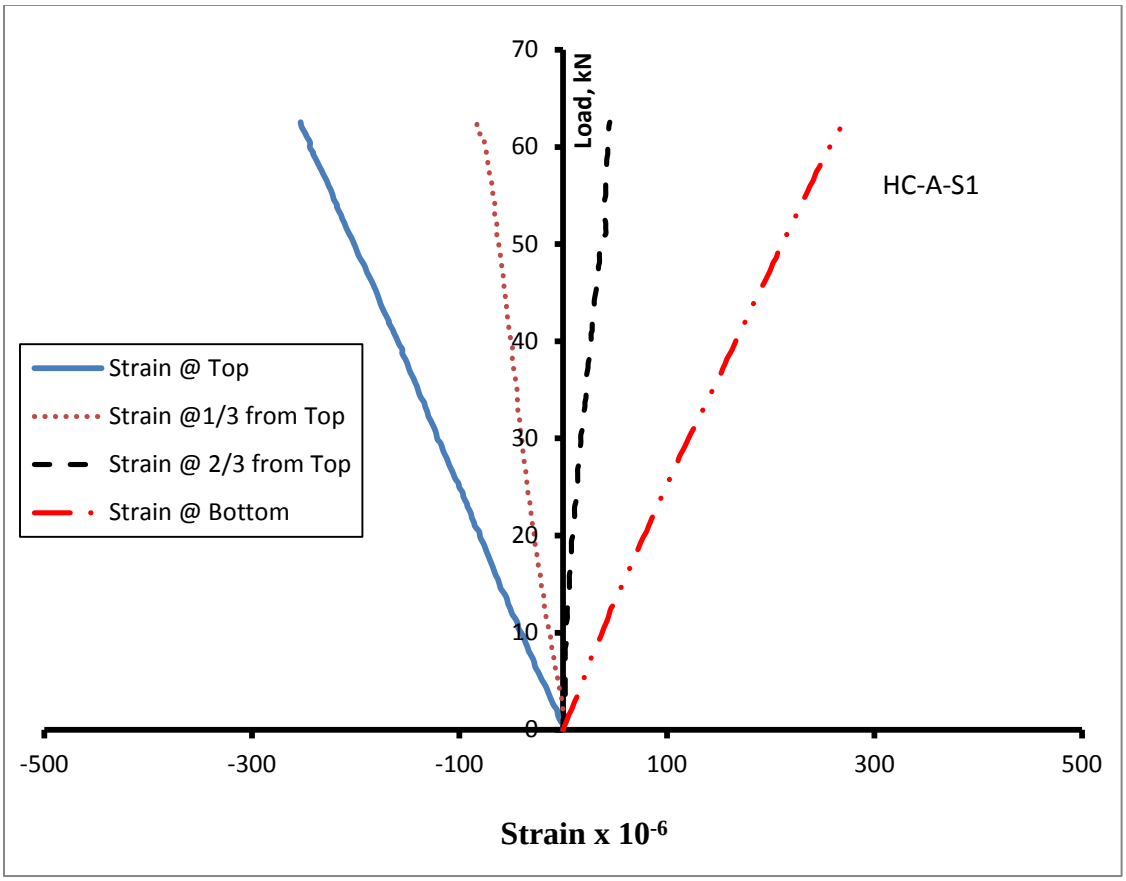

Figure 7.5: Typical load-strain curve for slab HC-A-S1

The strain profile across the depth of the specimen HC-A-L1 is shown in **Figure 7.6** for six load levels at 25%, 50%, 75%, 85%, 95% and 100% of the failure load. Two observations can be made from plots in **Figure 7.6**: (i) the strain distribution across the depth is reasonably linear at all load levels, and (ii) the neutral axis moves upward as the

load approaches P_U. The shift of the neutral axis is caused by the transition of the section from being wholly uncracked to cracked concrete section at failure.

At load less than cracking load for NC, the entire hybrid section remains uncracked and the neutral axis for the section remains unchanged until the occurrence of the crack in NC at the bottom. As NC cracks at load lesser than P_U, the loss of the concrete's strength in tension leads to the upward shift of the neutral axis.

The value of the concrete cracking load P_{conc} can be estimated from the ordinary flexure theory using transform section properties for uncracked section (**Figure 7.1b**). If the flexural tensile strength of NC (modulus of rupture) is f_t, the moment to cause cracking of NC is given as:

$$\mathrm{M_{crc}} = \frac{I_{uncr} f_t}{Y_c} \tag{7.1}$$

where I_{uncr}= moment of inertia of uncracked transformed section and Y_c = distance of the bottom concrete layer from NA (**Table 7.1**).

The load corresponding to M_{crc} for the test specimens is given as

$$\mathrm{P_{conc}} = \frac{2M_{crc}}{a} \tag{7.2}$$

where a = shear span for the four-point loading used.

The computed values of P_{conc} for test specimens are shown in **Tables 7.4** and **7.5**. When P is less or equal to P_{conc}, transformed section properties of uncracked section are applicable for calculation of bending stress. If P is greater than P_{conc}, the transformed section properties for cracked section (**Figure 7.1c**) are applicable for stress calculation.

P_{conc} values for all test specimens are calculated from Equation 7.2 using I_{uncr} values shown in **Table 7.1** with f_t = 4 MPa for normal concrete used.

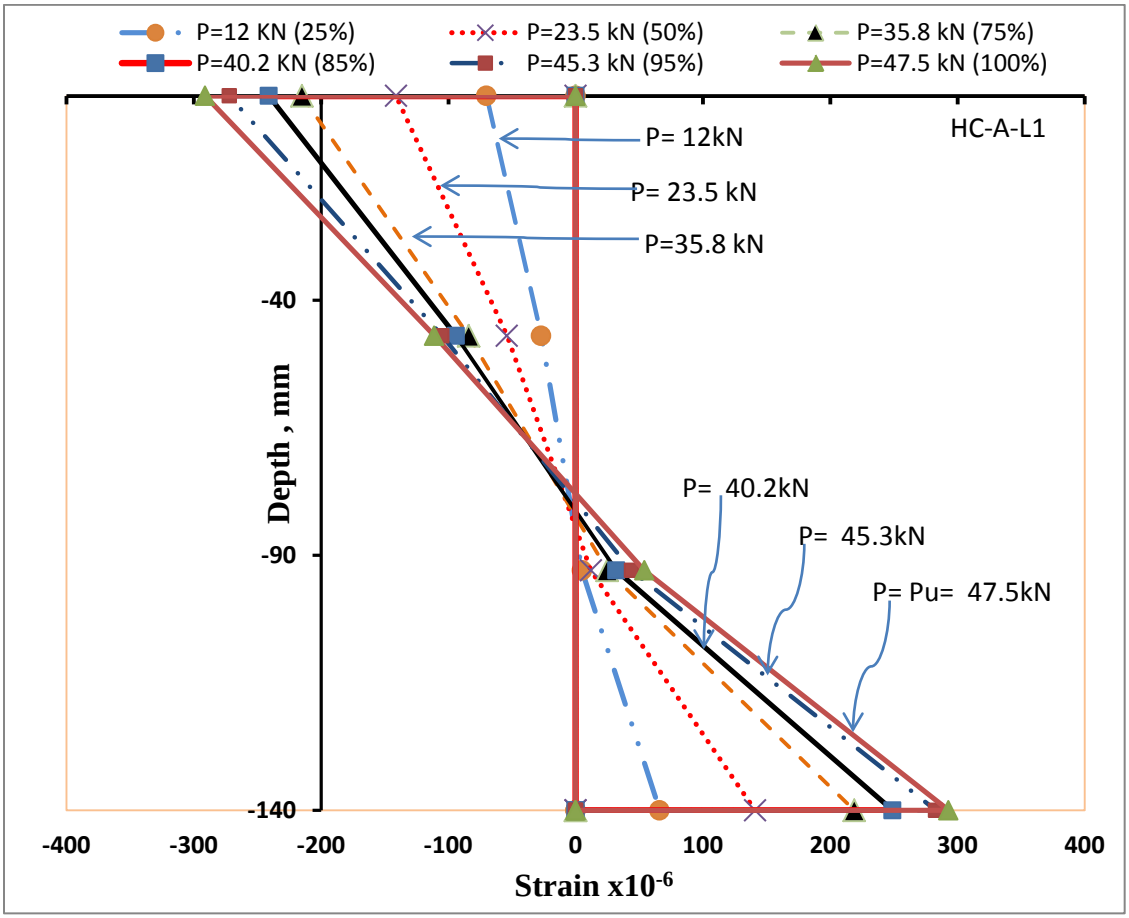

Figure 7.6: Typical Strain profile along the depth for slab HC-A-L1

From the transformed section for an uncracked section (**Table 7.1**), the neutral axis is located at a depth of 74 mm from the top for HC-A-L1 (**Figure 7.6**). This compares to 77 mm observed from the plot of strains at P = 12 kN. Form the cracked transformed section (**Table 7.2**), the computed depth of neutral axis is found to be 71 mm from top at load level close to the failure load while the measured depth observed at the same load

level from strain profile is 73 mm. This shows good agreement between the measured and calculated depth of the compression zone. The measured strains, measured and calculated depth of neutral axis (N.A) for the three identical specimens of Group (i) with longer span are shown in **Table 7.4**. The values of P_{conc} are shown in **Table 7.4** to indicate what type of section, cracked or uncracked to be used at a load level.

The strain profile across the depth of the slab HC-A-S1 is also shown in **Figure 7.7** up to 99 % of the failure load. As seen, the strain distribution across the depth is almost linear at all load levels up to failure load.

The measured strains, measured and calculated depth of neutral axis (N.A) for three selected specimens from Groups (i), (ii) and (iii) of shorter span specimens with diagonal web-shear failure are shown in **Table 7.5**.

The strain profile for other specimens of all other groups is presented in **Appendix C**.

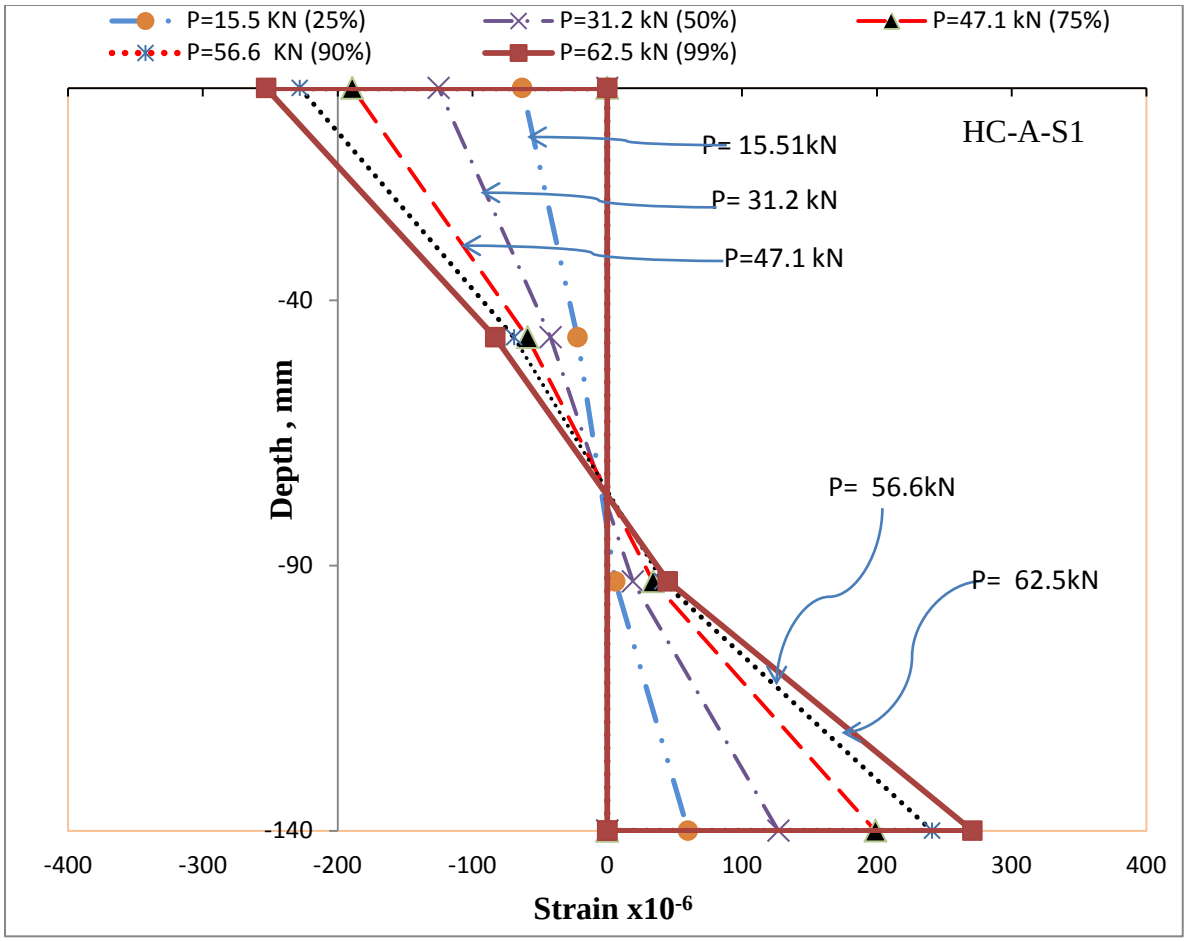

Figure 7.7: Typical Strain profile along the depth for slab HC-A-S1

Table 7.4: Measured Strain and Depth of N.A. Values for Group (i) of Longer Span

Beam Designation	Failure Mode	Load P (kN)	% of P_U	Measured Strain, (x 10^6)				Depth of N.A from top, (mm)		Concrete Cracking Load P_{conc} (kN)
				Top	1/3 from top	2/3 from top	Bottom	Measured	Calculated	
HC-A-L1 (260x140) Span 1100 mm	Flexure	12.0	25	-70	-27	5	66	77	74(Uncrack)	47.5
		23.8	50	-141	-54	12	141	75	74(Uncrack)	
		35.8	75	-215	-84	25	219	74	74(Uncrack)	
		40.2	85	-241	-94	32	249	74	74(Uncrack)	
		45.3	95	-272	-105	44	283	73	74(Uncrack)	
HC-A-L2 (260x140) Span 1100 mm	Flexure	11.9	25	-64	-20	22	67	69	74(Uncrack)	47.5
		23.9	50	-133	-40	45	143	68	74(Uncrack)	
		35.7	75	-201	-62	68	222	68	74(Uncrack)	
		40.8	85	-233	-69	81	258	68	74(Uncrack)	
		46.2	96	-266	-68	115	298	65	74(Uncrack)	
HC-A-L3 (260x140) Span 1100 mm	Flexure	13.8	25	-80	-21	21	71	72	74(Uncrack)	47.5
		27.8	50	-162	-42	48	149	71	74(Uncrack)	
		42.5	75	-253	-66	54	231	72	74(Uncrack)	
		46.5	82	-284	-60	71	258	71	74(Uncrack)	
		47.5	95	-302	-56	66	353	67	71-Crack.	

Table 7.5: Measured Strain and Depth of N.A. Values for Shorter Span Specimens

Beam Designation	Failure mode	Load P (kN)	% of P_U	Measured Strain, ($x\ 10^{-6}$)				Depth of N.A from top, (mm)		Concrete cracking load P_{conc} (kN)
				Top	1/3 from top	2/3 from top	Bottom	Measured	Calculated	
HC-A-S1 (260x140) Span 900 mm	Web-shear	15.5	25	-63	-22	6	60	75	74	62.2
		31.2	50	-125	-42	19	127	73	74	
		47.1	75	-189	-59	34	199	71	74	
		56.6	90	-228	-69	41	241	71	74	
		62.5	99	-253	-83	45	271	71	71	
HC-B-S3 (330x175) Span 900 mm	Web-shear	23.6	25	-52	-26	15	61	88	93	96.0
		47.8	50	-109	-57	33	126	88	93	
		71.6	75	-163	-88	52	193	88	93	
		81.2	85	-182	-100	56	223	87	93	
		90.8	95	-202	-115	79	253	86	87	
HC-C-S2 (390x200) Span 900 mm	Web-shear	27.82	25	-49	-21	10	49	106	106	131.7
		56.2	50	-99	-45	13	110	107	106	
		83.87	75	-145	-71	14	156	107	106	
		95.16	85	-163	-82	18	180	107	106	
		106.6	95	-181	-96	36	208	104	106	
		110.5	99	-188	-106	33	219	105	106	

7.5. Measured and Calculated Stresses

Generally, the section is considered as cracked concrete section when the tensile strength at the bottom of the normal concrete exceeds the tensile strength of concrete from the transformed section as discussed in details later in section 7.8.

For a comparison of the measured stresses from strains with theoretical values computed from flexure formula using transformed properties, **Table 7.6** is prepared. The compressive strains at top and bottom were converted to stresses using E_U= 55 GPa. For example, hollow core slab HC-A-L1, at load level 25% and 50% of the peak load P_U which was 12 kN and 23.8 kN respectively, the stresses in the beam were calculated using transformed properties of fully uncracked section given in **Table 7.1**. For P = 45.3 kN (95% of P_U) and 47.5 kN (100 % of P_U), the transformed properties of cracked section (Table 7.2) were used. The computed stress at all selected load levels show that the use of transformed section properties of uncracked and cracked section (**Table 7.6**) yields results that are closer to the measured stresses using the measured strains. Similarly, **Table 7.7** shows the measured and computed stress values for selected load levels for shorter span specimens which failed in diagonal web-shear.

All the calculated and measured results of all specimens tested are compiled and presented in **Appendix D**.

Table 7.6: Measured and Computed Stresses for Selected Load Levels for Longer Span Specimens in Group (i)

Beam Designation	Failure Mode	Load P (kN)	% of P_U	Measured Stress , (MPa)		Concrete Cracking load P_{conc} (kN)	Calculated Stress, (MPa)			
							Bottom		Top	
				Bottom	Top		Cracked	Uncracked	Cracked	Uncracked
HC-A-L1 (260x140)	Flexure	12	25	3.6	3.9	47.5	-	3.4	-	3.9
		23.8	50	7.8	7.8		-	6.8	-	7.7
		35.8	75	12.1	11.8		-	10.2	-	11.5
		40.2	85	13.7	13.3		12.5	-	12.8	-
		45.3	95	15.6	15.0		14.1	-	14.4	-
		47.5	100	16.1	16.0		14.8	-	15.1	-
HC-A-L2 (260x140)	Flexure	11.9	25	3.7	3.5	47.5	-	3.4	-	3.9
		23.9	50	7.9	7.3		-	6.8	-	7.7
		35.7	75	12.2	11.1		-	10.2	-	11.5
		40.8	85	14.2	12.8		12.7	-	13.0	-
		46.2	96	16.4	14.6		14.4	-	14.7	-
		47.9	100	25.5	21.6		14.9	-	15.3	-
HC-A-L3 (260x140)	Flexure	13.8	25	3.9	4.4	47.5	-	3.9	-	4.5
		27.8	50	8.2	8.9		-	7.9	-	9.0
		42.5	75	12.7	13.9		13.2	-	13.5	-
		46.5	82	14.2	15.6		14.5	-	14.8	-
		47.5	85	19.4	16.6		14.8	-	15.1	-
		56.4	100	-	-		17.6	-	18.0	-

Table 7.7: Measured and Computed Stresses for Selected Load Levels for Shorter Span Specimens

Beam Designation	Failure Mode	Load P (kN)	% of P_U	Measured Stress , (MPa)		Concrete Cracking Load P_{conc}	Calculated Stress, (MPa)			
							Bottom		Top	
				Bottom	Top		Cracked	Uncracked	Cracked	Uncracked
HC-A-S1 (260x140)	Web-shear	15.5	25	3.3	3.5	62.2	-	3.4	-	3.8
		31.2	50	7.0	6.9		-	6.8	-	7.7
		47.1	75	11.0	10.4		-	10.3	-	11.6
		56.6	90	13.3	12.6		13.5	-	13.8	-
		62.5	99	15.0	14.0		14.9	-	15.2	-
		62.9	100	-	-		15.0	-	15.3	-
HC-B-S3 (330x175)	Web-shear	23.6	25	3.4	2.9	96.0	-	2.9	-	3.2
		47.8	50	6.9	6.0		-	5.8	-	6.6
		71.6	75	10.6	9.0		-	8.6	-	9.8
		81.2	85	12.3	10.0		-	9.8	-	11.2
		90.8	95	13.9	11.1		12.5	-	12.3	-
		95.7	100	14.9	11.8		13.2	-	13.0	-
HC-C-S2 (390x200)	Web-shear	27.8	25	2.7	2.7	131.7	-	2.3	-	2.6
		56.2	50	5.6	5.45		-	4.62	-	5.3
		83.9	75	8.6	8.0		-	6.9	-	7.9
		95.2	85	9.9	9.0		-	7.81	-	8.9
		106.6	95	11.44	10.0		-	8.8	-	10
		110.5	99	12.0	10.34		-	9.1	-	10.4
		111.8	100	13.3	11.0		-	9.2	-	10.5

7.6. Load Deflection Plots

Typical load-deflection plots of the hybrid hollow core slabs are shown in **Figures 7.8** through **7.16** (only one typical specimen presented out of three replicate), capturing the ascending and descending load paths. The softening mode of failure in flexure mode implies non-brittle failure with significant post-cracking strength, lesser than the peak load. In some cases, the hollow core slabs failed with the formation of multiple fine surface cracks at the bottom of UHPC and advancement of only one single vertical crack within the maximum moment zone (zero shear) (**Figure 7.17**).

It should be noted that the lesser values of post-peak strength are attributed to progressive crack growth within the UHPC layer. The unracked ligament of UHPC and the bridging of steel fibers across the crack that are not pulled out contribute to the residual flexural strength.

The calculation of deflection at the centre of the slabs using Equation 5.3 for cracked and uncracked section is shown in **Table 7.8**. The measured experimental deflection up to the concrete cracking load P_{conc} is also shown in **Table 7.8**.

Note that the computed and measured deflection values given in **Table 7.8** for all beams failed in flexure mode of as discussed in in section 7.7.

Table 7.8: Comparison of Theoretical and Calculated Deflection

Beam Designation	Average Measured Deflection (mm)	Concrete Cracking Load P_{conc} (kN)	Calculated Deflection, Δ (mm)
			Based on I_{uncr}
HC-A-L1	0.42	32.5	0.31
HC-A-L2			
HC-A-L3			
HC-B-L1	0.23	58.4	0.25
HC-B-L2			
HC-B-L3			
HC-C-L1	0.48	86.1	0.22
HC-C-L2			
HC-C-L3			
HC-D-L1	0.49	46.6	0.31
HC-D-L2			
HC-D-L3			
HC-E-S1	0.25	38.2	0.20
HC-E-S2			
HC-E-S3			

From the load-deflection plots, the following observations can be made:

(1) The deflection can be taken as approximately linear up to the failure load P_U.

(2) The deflection can be calculated using the moment of inertia of the uncracked transformed section, I_{ucr}, as there is marginal difference in moment of inertia in both uncracked and cracked transformed section (**Tables 7.1** and **7.2**).

(3) Depending upon fiber orientation and amount of fiber across the crack, some specimens may show small post-crack stiffening resulting in increased deflection at P_U and while others will not. Thus some specimens showed limited stiffening (e.g. HC-A-L2, HC-C-L2) others showed softening with increased deflection at reduced load almost immediately after P_U (e.g. HC-B-S2, HC-C-S1).

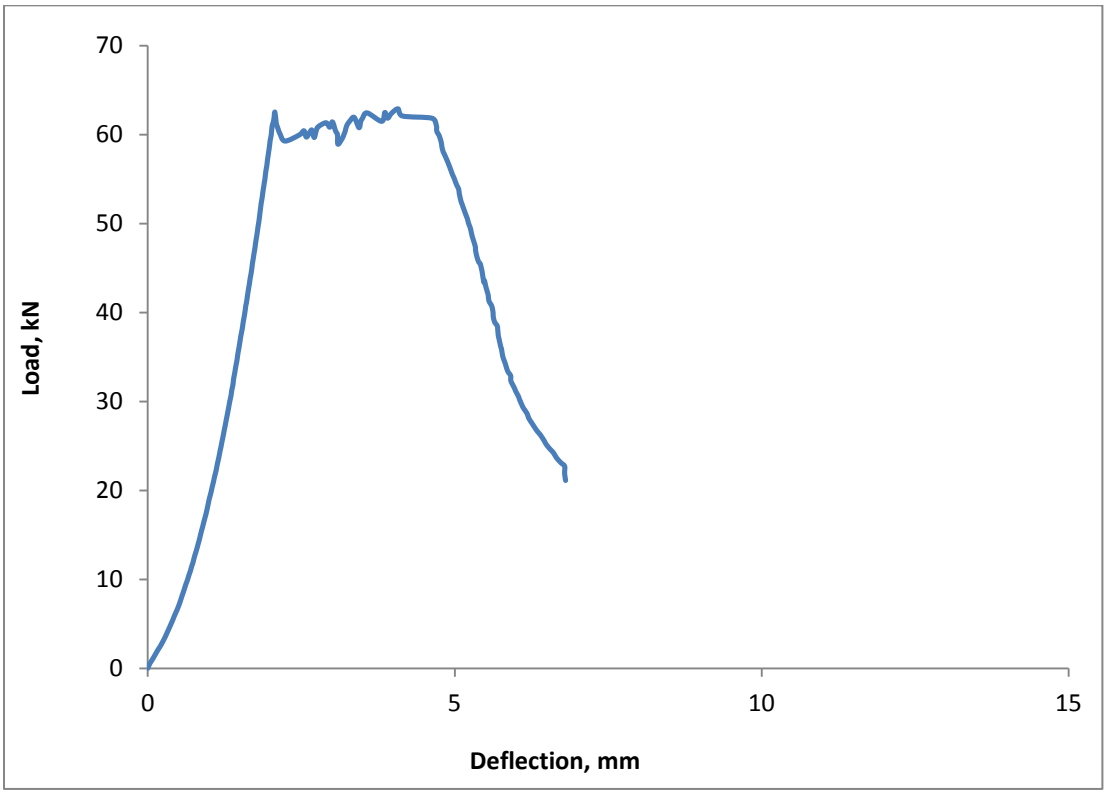

Figure 7.8: Load-deflection curve for hybrid slab HC-A-S1

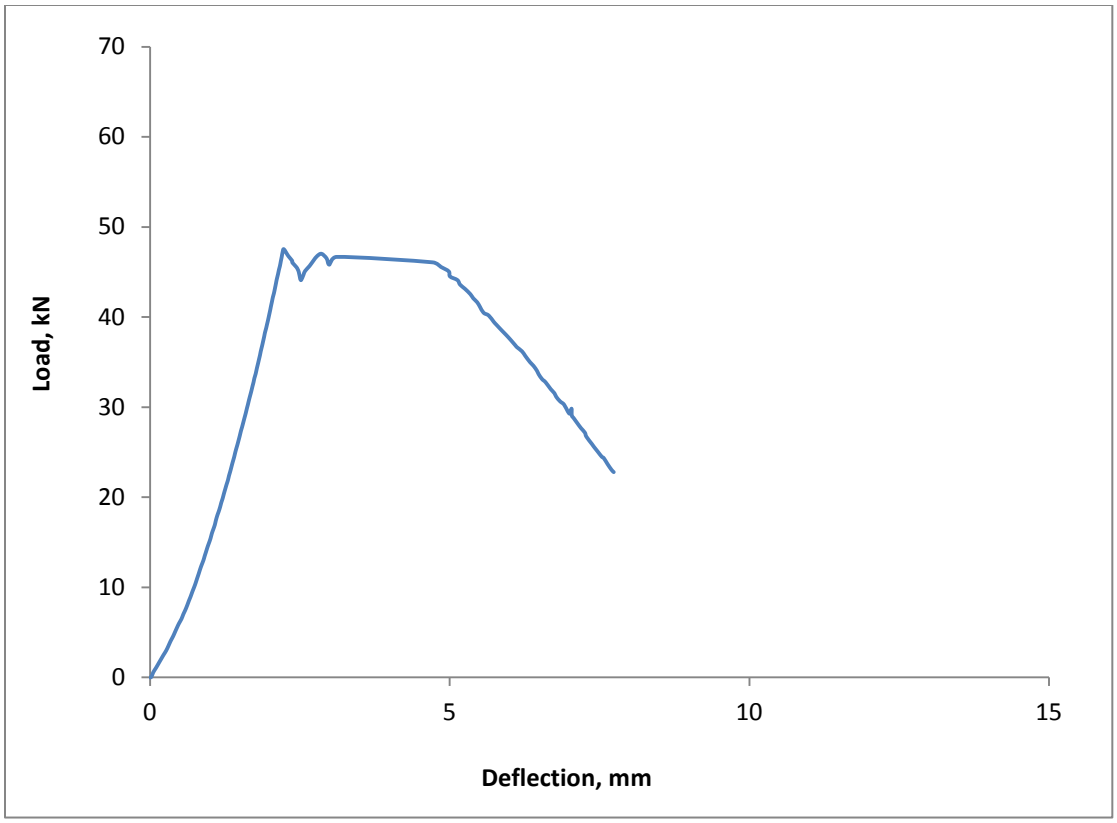

Figure 7.9: Load-deflection curve for hybrid slab HC-A-L1

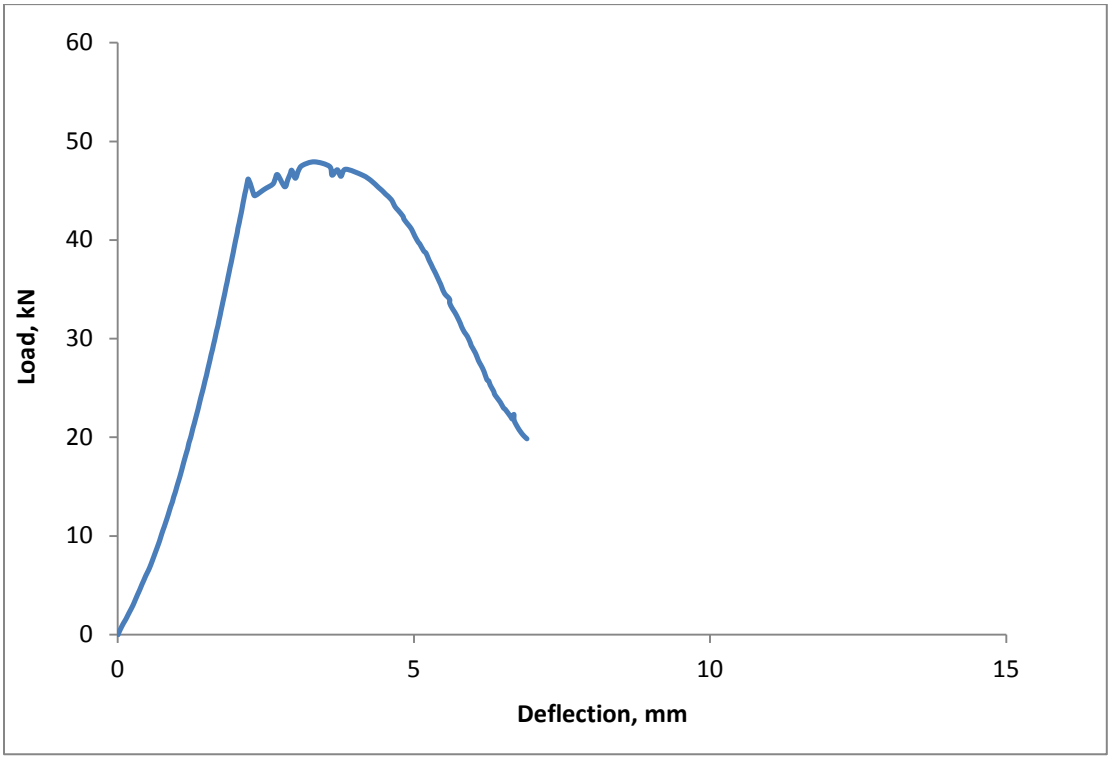

Figure 7.10: Load-deflection curve for hybrid slab HC-A-L2

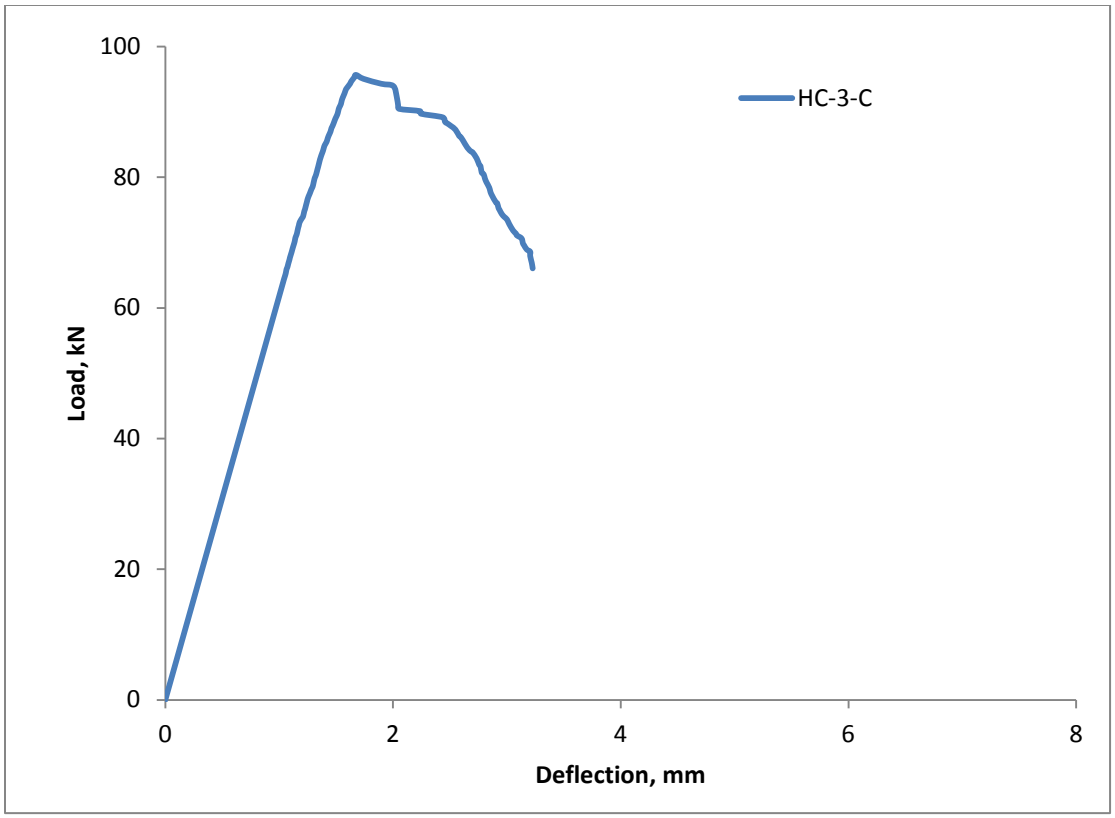

Figure 7.11: Load-deflection curve for hybrid slab HC-B-S3

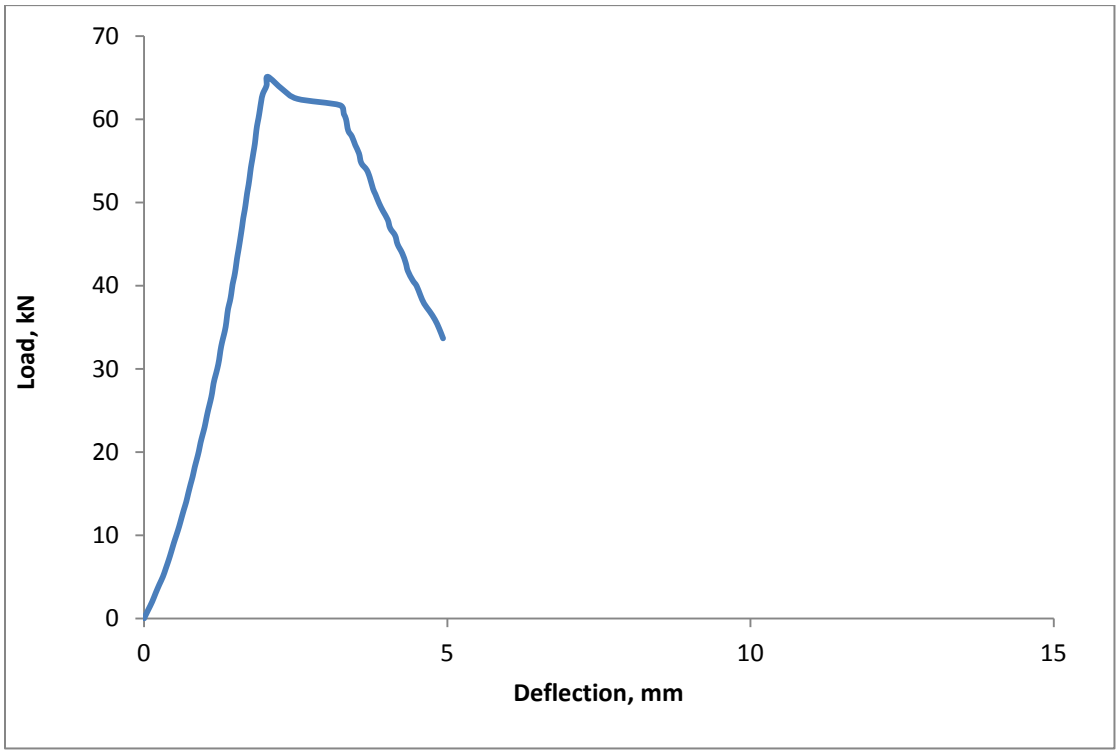

Figure 7.12: Load-deflection curve for hybrid slab HC-B-L2

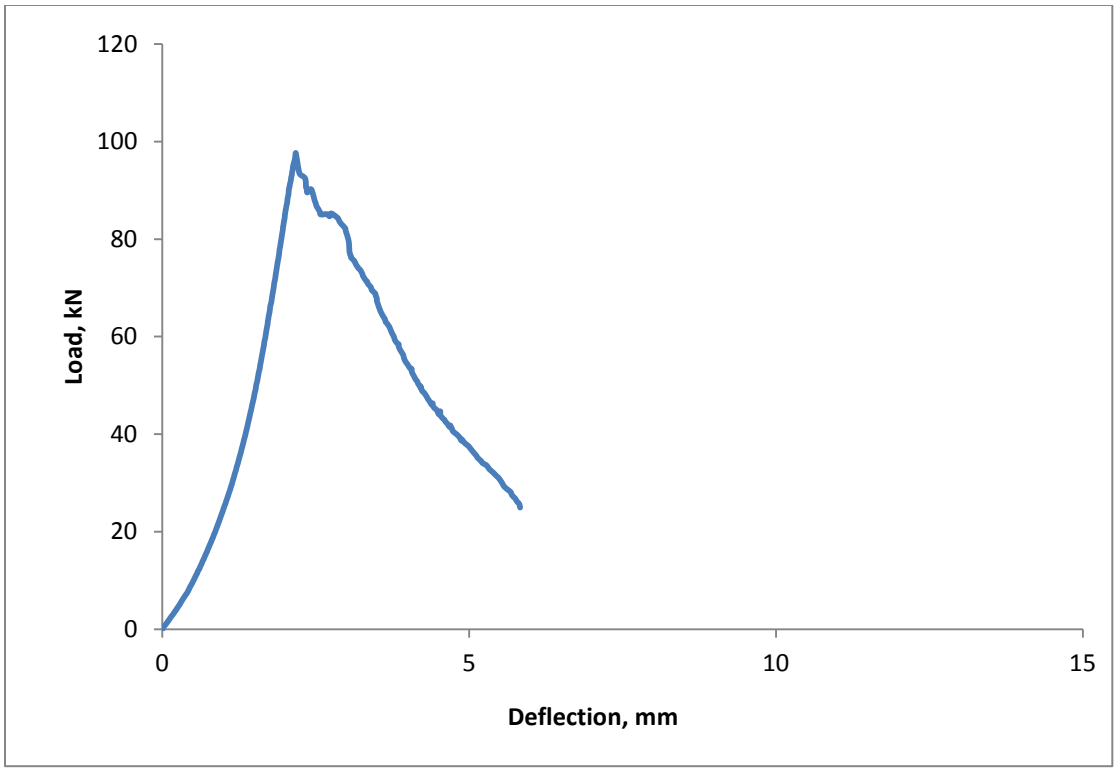

Figure 7.13: Load-deflection curve for hybrid slab HC-C-S1

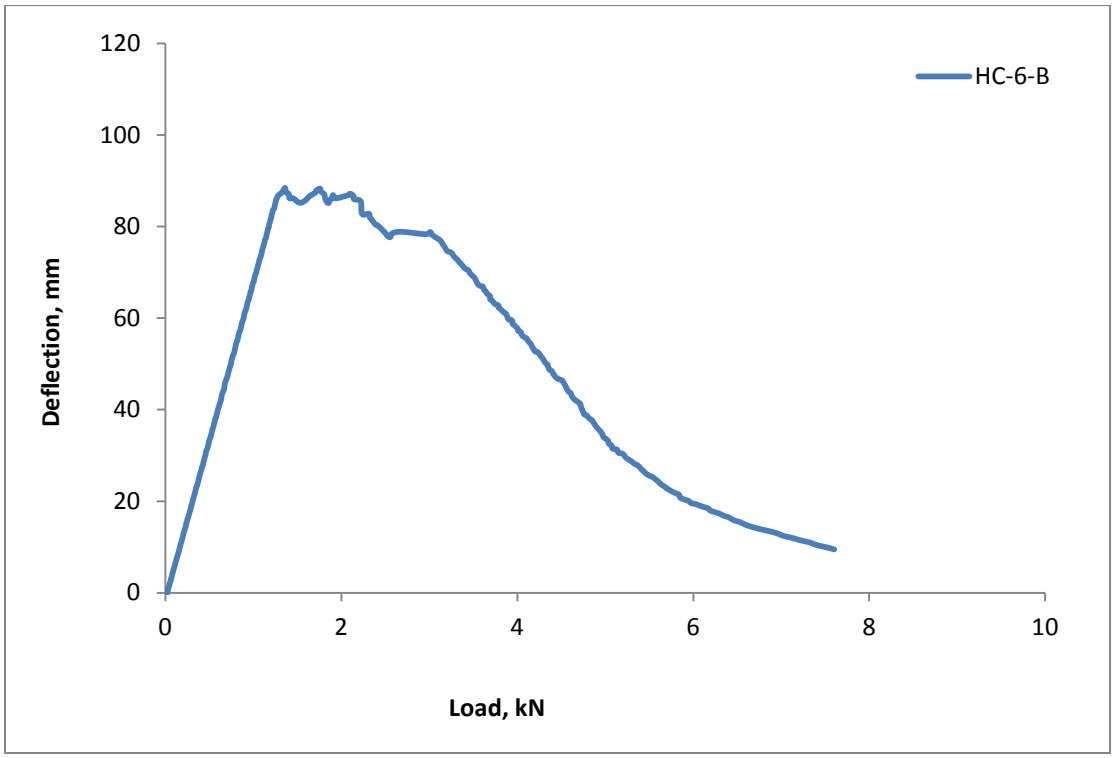

Figure 7.14: Load-deflection curve for hybrid slab HC-C-L2

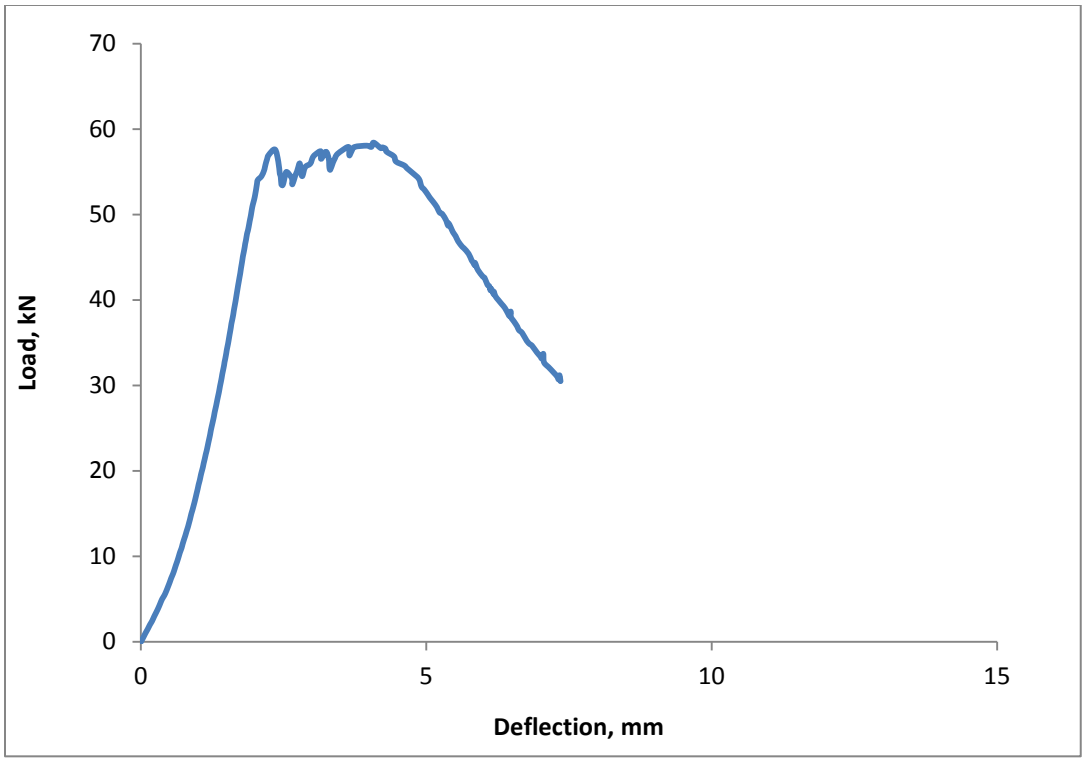

Figure 7.15: Load-deflection curve for hybrid slab HC-D-L2

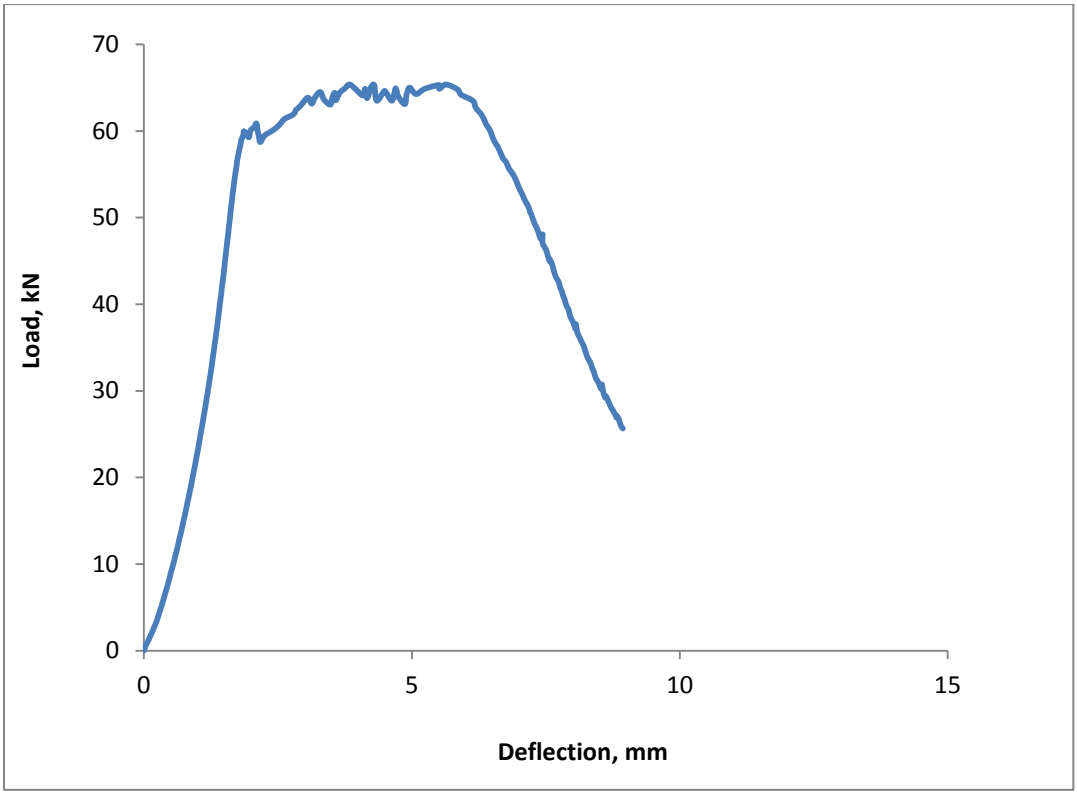

Figure 7.16: Load-deflection curve for hybrid slab HC-E-S2

7.7. Mode of Failure

Two basic modes of failure were witnessed: (i) flexure failure and (ii) diagonal web-shear failure. It is observed from data in **Table 7.3** that for the same cross section, the specimens with longer span (1100 mm) exhibited flexure mode of failure for Groups (i) to (iv) in addition to Group (v) specimens with shorter span (900 mm) (**Figure 7.17**). However, most of the shorter span specimens in Groups (i) to (iii) exhibited diagonal web-shear mode of failure in as shown in **Figure 7.18**.

The flexure failure is encountered with the vertical growth of a flexure crack within the two loading points as shown in **Figure 7.17**. The web-shear failure occurs with the development of a diagonal crack that advances with the combined action of flexure and shear as depicted in **Figure 7.18**.

For shorter span (lower a/h, shorter span to depth ratio), shear force can cause web-shear cracking, as the specimen's shear capacity is impaired by the presence of holes. For longer span (1100 mm), higher a/h ratio produces larger moment resulting in flexure failure.

7.7.1 Flexure Mode of Failure

All test specimens showed linear elastic response almost up to peak load P_U. As the load approaches P_U, multiple fine surface cracks appear at the bottom UHPC layer within the central part of the specimens between the two loading points. This is followed by very limited hardening and advancement of a single crack through the thickness of UHPC. At the peak load P_U, this tension cracking becomes well formed.

Following the peak load P_U, the specimens exhibit a gradual softening mode of failure with the advancement of crack almost vertically across the thickness of bottom UHPC layer. In this mode, the cracks always propagate through the UHPC vertically along the depth and horizontally across the width of the slab as shown in **Figure 7.17**. The bridging of the fibers across the crack and the uncracked ligament of UHPC provides the post cracking residual strength. As the crack advanced, the crack-mouth became wider (**Figure 7.17**).

As an example, in specimen HC-A-L2, the initial first crack which was formed at load of 46.2 kN and deflection of 1.4 mm and maintained this level approximately up to a deflection of 1.8 mm and again the load increased slightly to 47.9 kN at a deflection of 2.5 mm which was the peak failure load. Thereafter, the specimen showed softening ductile mode (**Figure 7.10**).

Figure 7.17: Typical flexure mode of failure for specimens HC-A-L1 and HC-A-L2

The softening mode of failure, a characteristic feature of all fiber-reinforced UHPC specimens, is explained by the fact that the fibers bridging the crack have the ability to resist tensile stresses. As the fibers are pulled out due to crack opening, the remaining fibers across the crack tip are able to provide tensile strength to sustain residual load. Once all the fibers are pulled out at the crack, the specimen physically loses its bending strength and fails.

7.7.2 Diagonal Web-Shear Failure

In this mode, all specimens also showed linear-elastic response up to the initiation of first small diagonal web shear crack in the normal concrete in the vicinity of the neutral axis between the top and bottom UHPC near the support (**Figure 7.18**). As load increased, the diagonal web cracking advanced towards the top and bottom of the specimens. Following the attainment of P_U, the crack propagated towards the support end causing failure (**Figure 7.18**). After the peak load, the crack advancement towards the support occurs at a declining load. Some beams failed with crack advancing towards the support along the interface between the bottom UHPC layer and NC. For web-shear failure, the bottom UHPC layer remained uncracked, implying reserved flexural strength that would have yielded higher P_U.

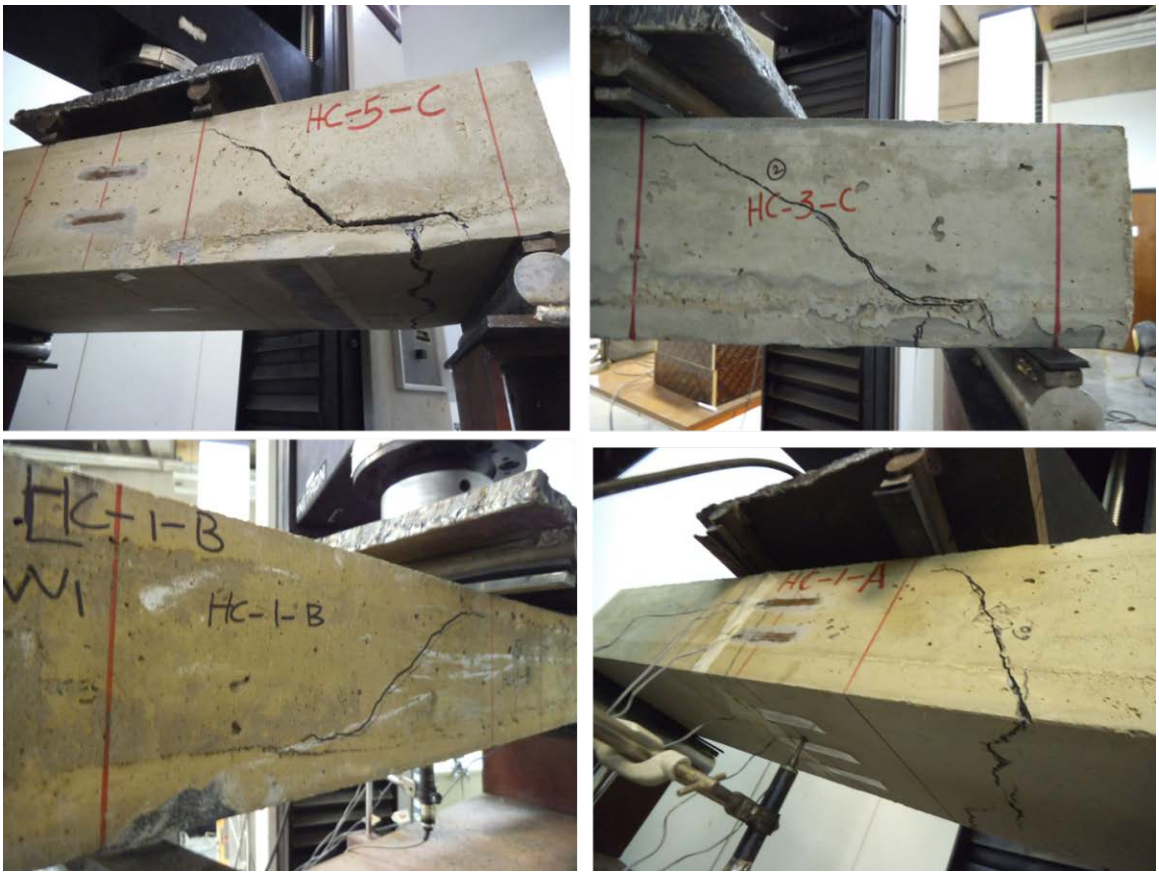

Figure 7.18: Typical web-shear mode of failure of specimens HC-A-S, HC-B-S and HC-C-S

7.8. Prediction of Failure Load and Mode of Failure

7.8.1 Prediction of Failure Load

The failure load corresponds to the lower of the two values of loads; one for the ultimate moment capacity and the other one for the shear capacity of the specimens.

7.8.2 Prediction Load for Flexure Failure

As the section behaves elastically almost up to the failure load, the stresses in a section can be computed using transformed section properties. For hollow core sections, the tensile stress at the bottom face of normal concrete (above the bottom UHPC layer) will exceed modulus of rupture for concrete at a moment M_{crc} (or load P_{conc}) (section 7.4), making the section a cracked one. The transformed section properties of cracked section should therefore be used to determine ultimate moment capacity of a section.

If F_{tu} is the maximum flexural tensile strength for UHPC layer used, the moment capacity M_U for a section is given by elementary formula as

$$M_U = \frac{S_{bcr}\, F_{tu}}{n} \tag{7.4}$$

Where $n = E_U/E_C$, S_{bcr} = bottom section modulus for transformed cracked concrete section (**Table 7.2**). The maximum load P_{uf} to produce flexure failure for the test specimens is

$$P_{uf} = \frac{2\, M_U}{a} \tag{7.5}$$

Where a= shear span for the four-point loading system used.

In order to determine M_U and hence P_{uf}, it is necessary to have a fair estimate of F_{tu}. This, however, can only be established through a number of tests of similar size of UHPC specimens.

7.8.3 Prediction of Load for Diagonal Web-Shear Failure

The shear capacity based on gross concrete web was computed for diagonal web-shear cracking.

As shown in **Table 7.3**, the diagonal web shear failure occurred in the short span (900 mm) in all the three groups (i), (ii) and (iii).

For Group (i), for the shorter span specimens, the average failure load P_U of specimens HC-A-S1 and HC-A-S1 is 65 kN, similarly for Group (ii), the average failure load P_U of specimens HC-B-S2 and HC-A-S3 is 92 kN and finally, for Group (iii), the average failure load P_U of specimens HC-C-S2 and HC-C-S3 is 106 kN. From these three groups, the average shear stress τ can be calculated using:

$$\tau = \frac{V}{b_w h} \tag{7.6}$$

where V = shear force = $P_U/2$, b_w= net width of a section = gross width b – sum of hole diameters and h= depth of the section.

The computed values of τ for Group (i) to (iii) are shown in **Table 7.9** which also contains the values of P_U, b_w, and h used in equation (7.6). It is worth noting that τ values are range-bound. The average value of τ is 2.72 MPa, which is approximately equal to $5\sqrt{f'c}$. Thus, for web-shear failure, the limiting average shear stress for hybrid slabs can

be taken as $5\sqrt{f'c}$. For normal concrete beams, the maximum shear stress for web-shear cracking is typically taken as $3.5\sqrt{f'c}$ and more conservatively as $1.9\sqrt{f'c}$ (Nilson, A. H.). The higher value of shear stress for diagonal web-shear cracking is justified by the presence of two UHPC faces contributing to the overall shear resistance.

The critical shear for web-shear cracking, V_C, is

$$V_C = 5\sqrt{f'c}\, b_w h \quad (7.7)$$

The predicted load P_V to cause failure in web-shear cracking for the test specimens is

$$P_V = 2\, V_C = 10\sqrt{f'c}\, b_w h \quad (7.8)$$

Table 7.9: Computed Average Shear Stress τ

Specimen Group	Average failure load P_U (kN)	Width b (mm)	Depth h (mm)	Net width b_w (mm)	Average shear stress $\tau = \frac{V}{b_w h}$ (MPa)
Group (i)	65	260	140	90	2.58
Group (ii)	92	330	175	88	2.99
Group (iii)	106	390	200	102	2.6

The failure load for a given hollow core beam element can be determined by evaluating the maximum load P_{uf} corresponding to M_U from Equation 7.5 and P_V value corresponding to V_C from Equation 7.8. The lower of the two values, P_{uf} and P_V, represents the failure load or the load capacity of the element and accordingly also the mode of failure.

The common feather of the two modes of failure for hollow-core hybrid specimens is that, after reaching peak load P_U, the specimens exhibit softening mode of failure characterized by increased deflection and crack growth with declining load.

CHAPTER 8

FINITE ELEMENT MODELING OF HYBRID BEAMS

8.1. Introduction

This chapter presents the Finite Element Method (FEM) analysis of both hybrids layered and hollow-core slab elements for the purpose of comparison with the experimental observations and calculated stresses based on the transformed section properties. As the layered and hollow-core construction have the best prospects for practical application and adoption, FE analysis has been made to examine the accuracy of the mechanist approach using transformed section.

A three-dimensional finite element analysis was performed using commercial finite element program (ABAQUS 6.13). The finite element models were built to represent the actual hybrid beams geometry and materials, including the steel plates.

8.2. Mechanical Properties of Materials

Compared with ordinary concrete, UHPC has different stress-strain characteristics. The applicability of available FEM software to UHPC, including the assumptions and mechanical properties of materials, has not yet been proven. In addition, the role of steel

fibers and their contribution to mechanical properties of UHPC after cracking is typically not considered in FEM modeling.

The UHPC parameters is significantly different from conventional concrete and must be carefully calibrated based on available experimental tension and compression data.

On the basis of test data presented and discussed in Chapter 4, the idealized stress-strain relationship for axial tension and compression adopted for FE analysis are shown in **Figures 8.1** and **8.2**. For tension, the stress-strain (σ-ε) is linear upto the ultimate tensile stress σ_u=11.0 MPa corresponding to ε_0 =0.00018. The limited strain-hardening zone is defined by ε_1 =0.00025 and ε_2 =0.0006. The strain-softening is represented by a linear relationship as shown in **Figure 8.1**.

The stress-strain relationship for compression is taken as linear upto the maximum stress of 165 MPa corresponding to strain of 0.00365. The compression failure by crushing is assumed to take place at ε_u =0.0038.

For elastic analysis, unit weight of the UHPC was taken as 2500 kg/m^3 and elastic properties were defined by a Poisson's ratio of 0.22 and a modulus of elasticity of of 55 GPa for both tension and compression. For normal concrete (NC) the unit weight was taken as 2400 kg/m^3 and elastic properties were defined by a Poisson's ratio of 0.2 and a modulus of elasticity of 30 GPa. Steel plates have density of 7850 kg/m^3 and modulus of elasticity was taken as 200 GPa and Poisson's ratio of 0.3.

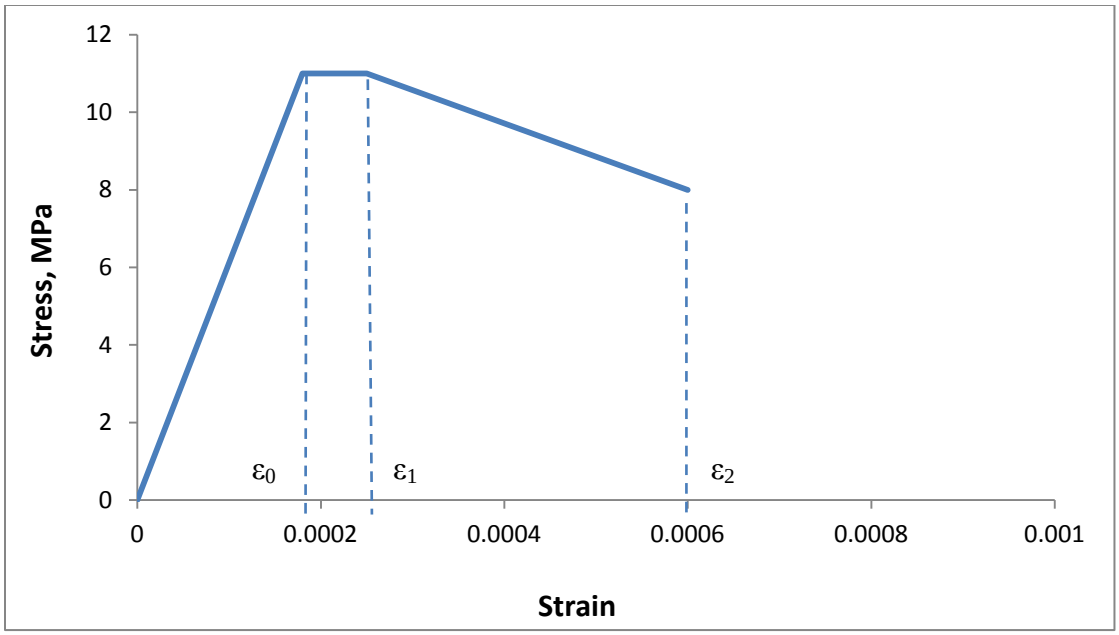

Figure 8.1: Idealized uniaxial tensile response of UHPC

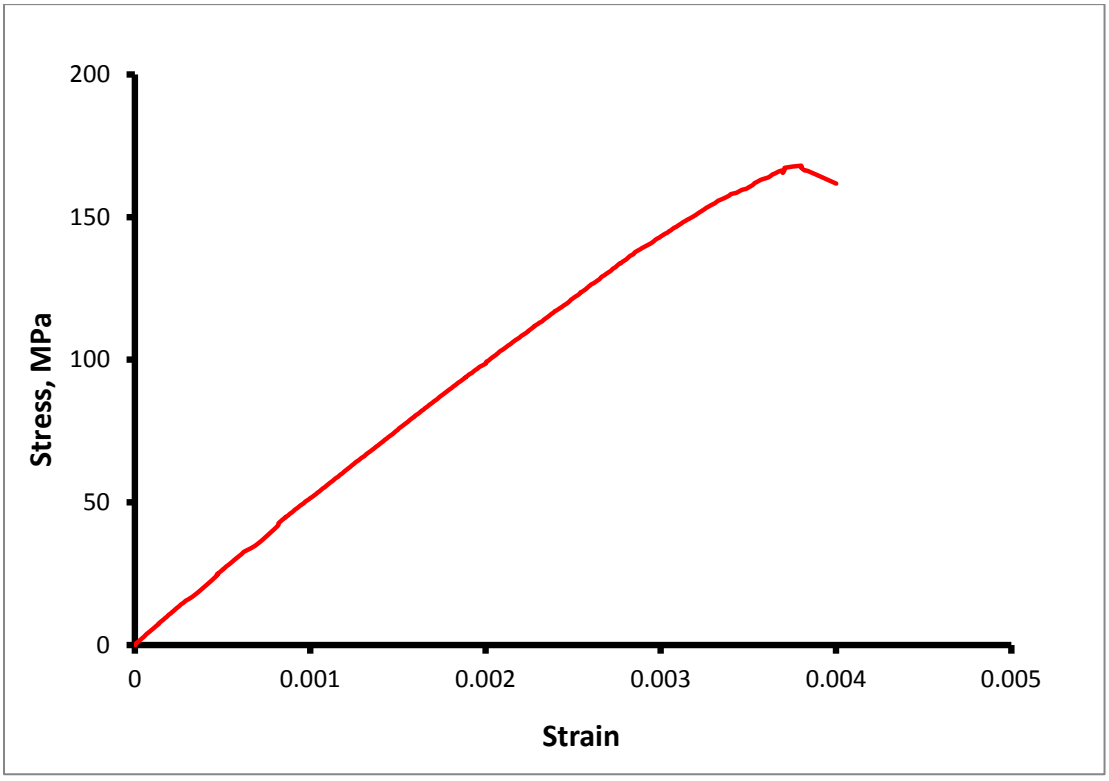

Figure 8.2: Compressive stress-strain behavior of UHPC

8.3. FE Analysis and Results

Up to the peak stress, the linear analysis and thereafter nonlinear analysis was carried out till the attainment of ε_1=0.00025. No attempt was made to carry out analysis after this limit as the section becomes cracked followed by strain softening with declining load, and post-cracking behavior has no practical interest.

8.3.1 Layered Beam

All the material used in FEM were considered homogeneous, and modeled as an elastic isotropic material. The elements had a uniform mesh size of about 10 mm. Full bond was assumed along the entire interacting surfaces of the different materials. The boundary conditions for all hybrid beams were identical, and consisted of a pin support at the left support and a roller support at the right support. The load was applied, as in the tests, into the specimen through a steel plate. This steel plate was also modeled as 3D-elements as shown in **Figure 8.3**.

As a typical example, **Figure 8.3** shows the FEM model for beam LS-A-C2. The following results are based on the linear FEA model using the material parameters in **Table 8.1**. The mesh model of hybrid beams LS-A-C2 is illustrated in **Figure 8.3**.

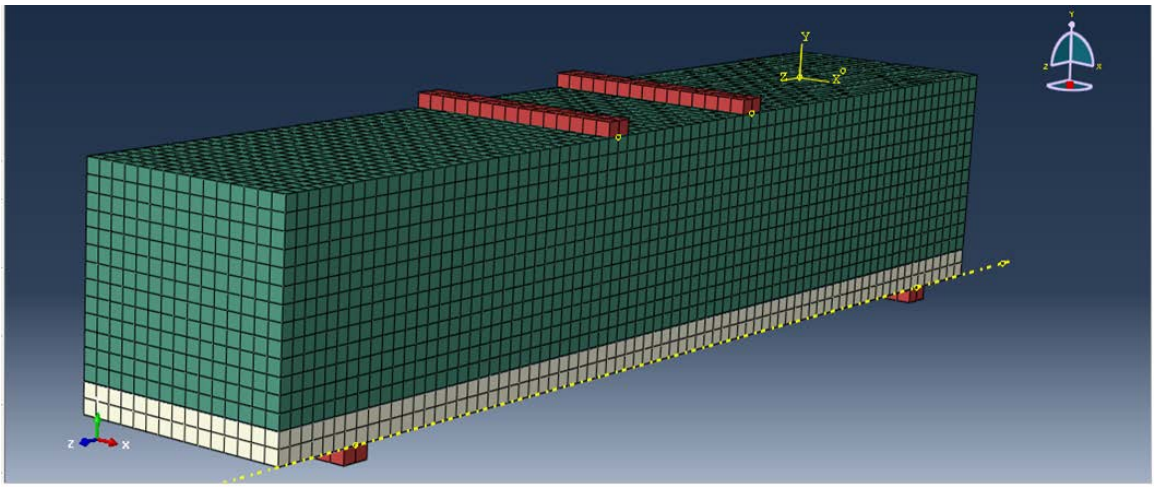

Figure 8.3: Meshing of layered hybrid beam LS-A-C2

A. Strain Distribution

The strain distribution along the depth at center of hybrid beam is shown in **Figure 8.4**. The longitudinal strains are corresponding to maximum tensile strain on the bottom surface and maximum compressive strain on the top surface of the hybrid beam. **Figure 8.5** demonstrates the comparison between the FEM and experimentally observed longitudinal strains on the top and bottom surfaces of layered beam. Tensile and compressive strains are well predicted by the FEM model in elastic regions.

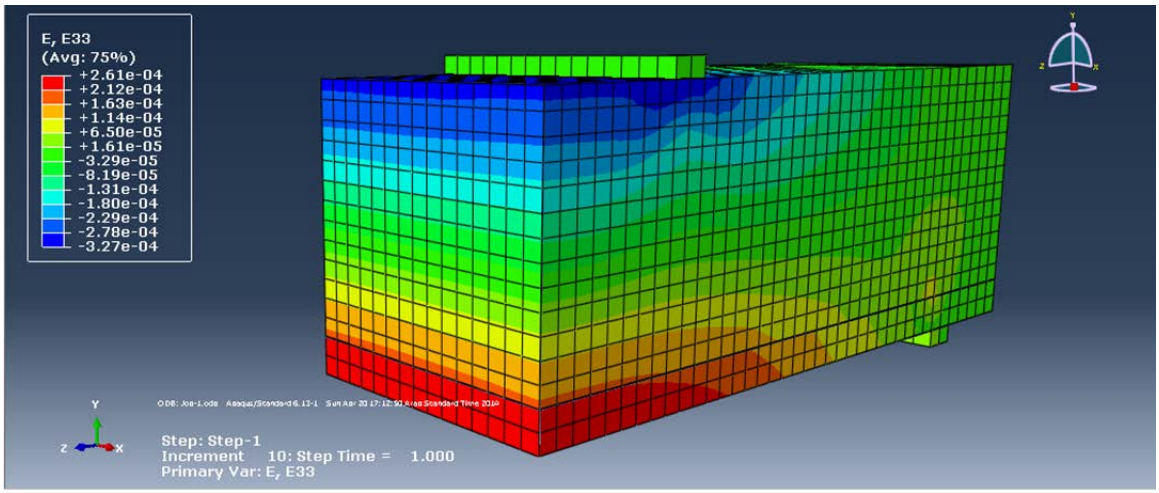

Figure 8.4: view of strain distribution along the depth at center of hybrid beam

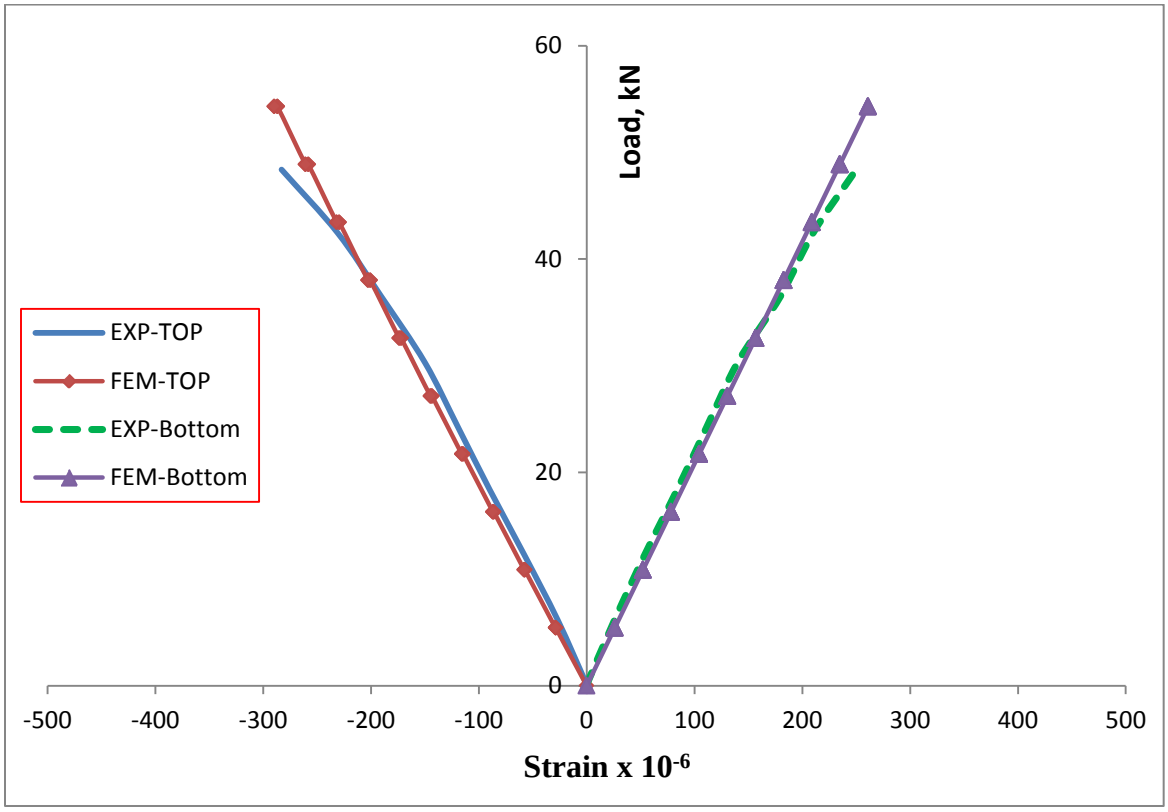

Figure 8.5: FEM vs. experimentally observed longitudinal strain on top and bottom faces of hybrid beam of specimen LS-A-C2

The experimental result demonstrated that the hybrid beam exhibits a tensile strain at the bottom close to the failure load of 258 x 10^{-6} compared to 276 x 10^{-6} predicted by FEM. Similarly, the experimental compressive strain at the top is 284 x 10^{-6} compared to 320 x 10^{-6} predicted by FEM. The agreement is reasonably good in both tension and compression strains of the hybrid beam.

Figure 8.6 illustrates the strain profile along beam depth of specimens LS-A-C2 at midspan with two different load levels: 50% P_U and 90% P_U for experimentally observed FEM strains.

The experimentally measured linear strain distribution along the depth of the hybrid beam was confirmed from the FEM (**Figure 8.6**).

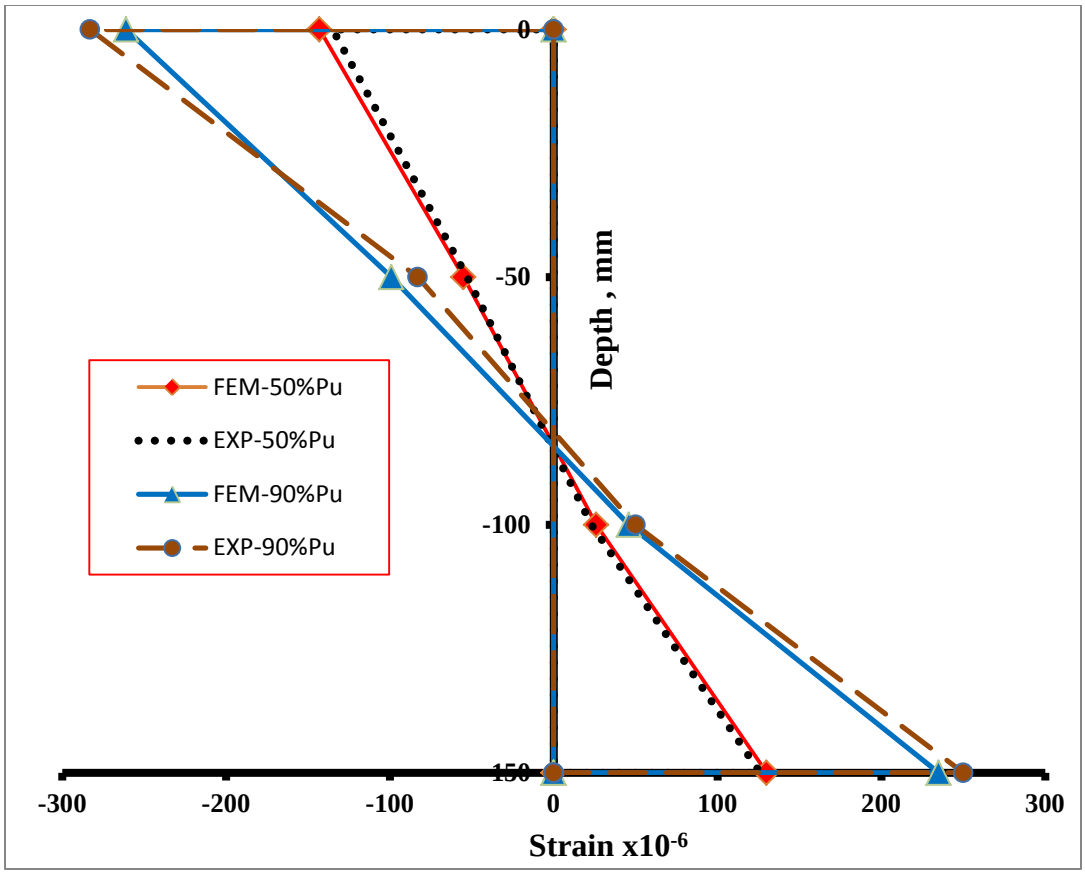

Figure 8.6: FEM vs. experimentally observed longitudinal strain along the depth at mid span

It can be observed that the strain profile between FEM and experiment agrees well with each other until 0.9 P_U. This strain distribution along the depth is almost identical at low load levels. However, little variations at higher load levels may be due to the unavoidable variation of experimental data during the loading and strain increment near the failure load. In the compression area, in most cases, it is noted that the FEM strain is almost similar to the experimental result on the top surface of the hybrid beams.

B. Stress Distribution

Figure 8.7 shows the longitudinal stress distribution in the hybrid beam. The maximum tensile stress developed in the tension zone of the hybrid beam was 15 MPa compared to 19 MPa achieved by measured strain and calculated stress based on the transformed section properties as shown in **Table 8.1**. The figure further indicates the distribution of low to high tensile and compressive stresses within in the beam.

A summary of the finite element and experimentally observed and calculated results for hybrid beams is presented in **Table 8.1**. FEM results of all other specimens are presented in **Appendix E**.

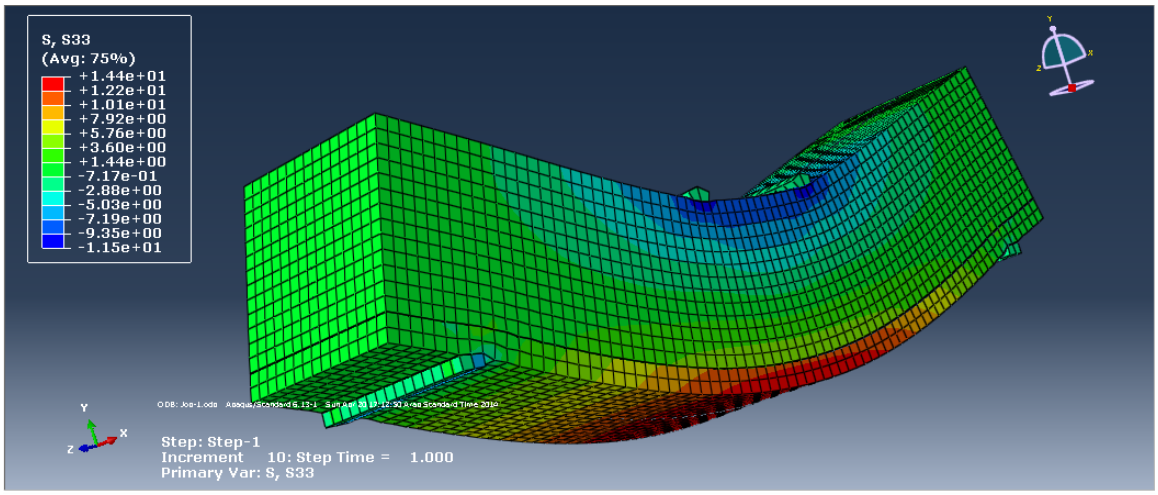

Figure 8.7: FEM longitudinal stress distribution

Table 8.1: Comparison of Finite Element Results with Experimental and Calculated Values for Layered specimens

Beam Designation	UHPC thick. (mm)	Load P (kN)	Strain x 10^{-6}				Stress (MPa)					
			Bottom		Top		Bottom			Top		
			Meas.*	FEM	Meas.*	FEM	Meas.#	Calc.‡	FEM	Meas.#	Calc.‡	FEM
LS-A-C2 150x150 x 760 (b × h × L)	20	48	350	261	-283	-327	19	19	15	-9	-9	-12
LS-C-C2 150x150 x 1000 (b × h × L)	20	20	173	146	-256	-187	10	13	9	-8	-6	-6
LS-D-C2 150x150 x 1000 (b × h × L)	40	32	223	222	-455	-302	12	14	12	-14	-10	-10
LS-H-C2 150x200 x 1200 (b × h × L)	50	40	318	253	-349	-331	17	12	13	-11	-11	-11

Meas.*: Measured strain experimentally, Meas.#: Measured stress from strain experimentally
Calc.‡: Calculated stress on the basis of transformed section

C. Deflection Comparison

The results presented in **Table 8.2** show the deflection of hybrid beams by three ways: experimentally observed deflection, Equation 5.3 given in section 5.6 (Chapter 5), and FEM for three selected load levels: 0.8 P_U and P_U.

Table 8.2: Comparison of Experimental, Theoretical, and FEM Deflection of Layered Hybrid Beams

Beam Designation	Failure load P_U (kN)	Experimental		Elastic formula		FEM	
		0.8 P_U	P_U	0.8 P_U	P_U	0.8 P_U	P_U
LS-A-C2 150x150 x 760 (b × h × L)	52	0.43	0.51	0.16	0.20	0.15	0.19
LS-C-C2 150x150 x 1000 (b × h × L)	21	0.37	0.41	0.18	0.22	0.15	0.19
LS-D-C2 150x150 x 1000 (b × h × L)	34	0.31	0.45	0.25	0.31	0.24	0.30
LS-H-C2 150x200 x 1200 (b × h × L)	51	0.46	0.59	0.29	0.38	0.31	0.40

Table 8.2 demonstrates that the FEM model accurately predicts the deflection calculated based on the theoretical elastic formula for the mid span vertical displacement of layered beam specimens in elastic range for the three load levels selected.

The deflections of the finite element models and deflections calculated using elastic deflection formula for layered beams were smaller than those measured experimentally.

It appears there may be two reasons for that: the first one may be because the UHPC bottom layer is more flexible in reality than in the model. Secondly, there might be some

rigid body rotation and therefore increasing discrepancy is observed. It appears that deflection of the supporting system on both seats of the specimen would have rigid body movement in a form of uniform vertical displacement, rotation, or combination of both. A uniform vertical displacement is assumed to be the primary rigid body movement although slight rotation due to different reaction force on the supporting system and/or different rigidity of the supporting system of each end is possible.

A nonlinear FE analysis for one specimen of hybrid NC-UHPC layered specimens was performed up to ε_1 =0.00025 as shown in **Figure 8.1**, although linear FE analysis and the experimental results showed that the proposed forms of constructions were almost linear up to failure.

Concrete damage plasticity (CDP) model in ABAQUS 6.13 was used for nonlinear behavior of the hybrid specimen using material properties extracted from uniaxial tensile and compressive tests as shown in **Figures 8.1** and **8.2** for UHPC and **Figure 5.14** for NC.

In the concrete damage plasticity model in ABAQUS, the fibers were assumed uniformly distributed in the matrix and the UHPC is thus modeled as a homogeneous material.

In the CDP model, five parameters required to be defined: (a) the dilation angle in degrees, (b) the flow potential eccentricity, (c) the ratio of initial equi-biaxial compressive yield stress to initial uniaxial compressive yield stress, (d) the viscosity parameter and (e) the ratio of the second stress invariant on the tensile meridian to that on the compressive meridian. Their default values of 34, 0.1, 1.16, 0.66 and 0.0, were used respectively for the above mentioned parameters.

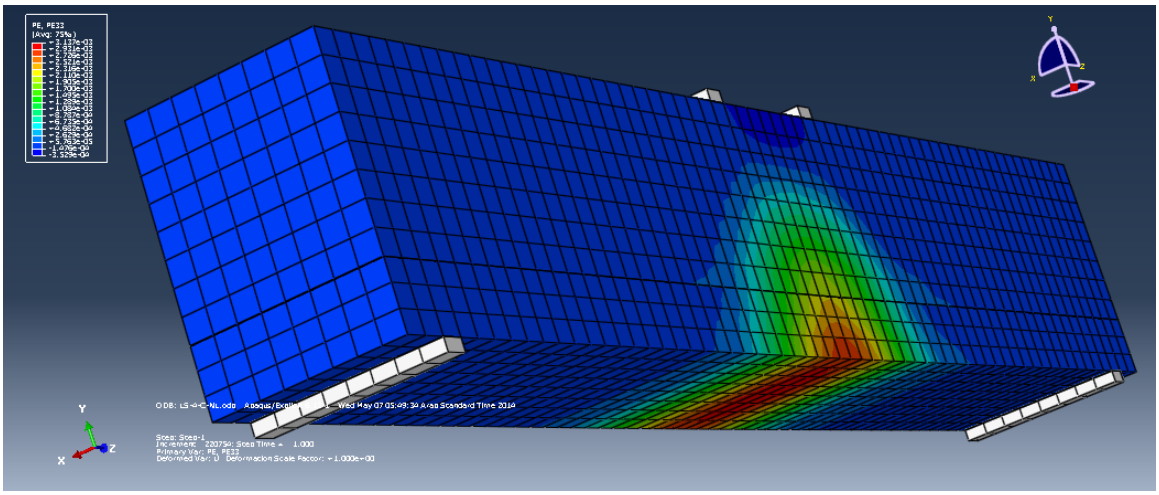

Figure 8.8: Nonlinear FEM showing the plastic strain distribution

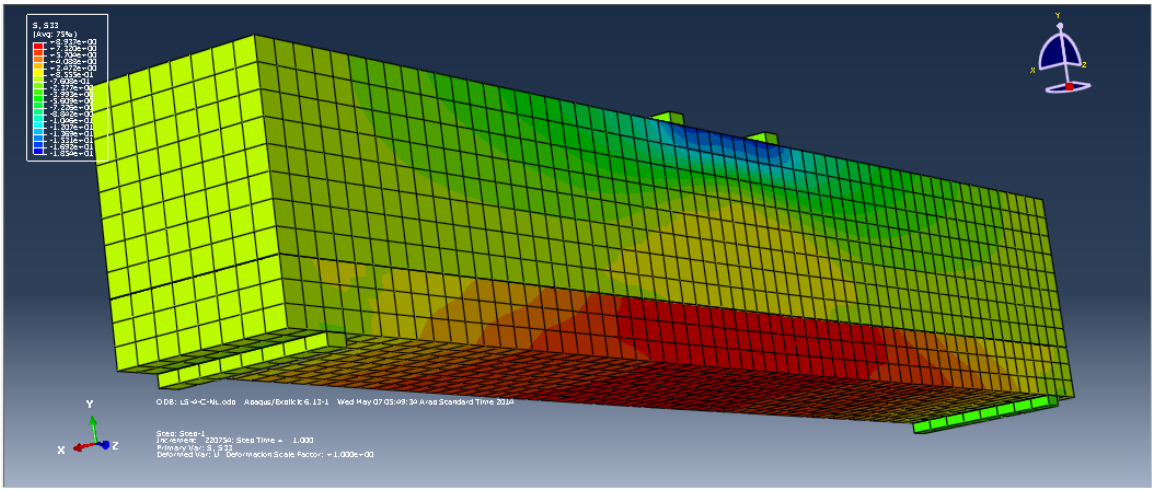

Figure 8.9: Nonlinear FEM showing longitudinal stress distribution

Figures 8.8 and **8.9** show the plastic strain distribution and longitudinal stress distribution of the hybrid beam tested respectively. The maximum tensile strength at the bottom of UHPC layer was found to be about 11 MPa compared to 13 achieved using linear FE analyses, which shows that the linear FE analysis was good enough to predict

the maximum tensile strength. However, nonlinear finite element can accurately predict the crack location and propagation.

8.3.2 Hollow Core Specimens

Similar to layered beam specimens, all the material used in FEM were considered homogeneous, and modelled as an elastic isotropic material. The elements had a uniform mesh size of about 10 mm. Full bond was assumed along the entire interacting surfaces of the different materials. The mesh geometry of the FEM model is shown in **Figure 8.10** for specimen HC-7-B as an example of beams used in hollow core specimens.

As in layered beams, the boundary conditions for all hollow core specimens were identical, and consisted of a pin support at the left support and a roller support at the right support. The load was applied, as in the tests, into the specimen through a steel plate. This steel plate was also modeled as 3D-elements as shown in **Figure 8.10**.

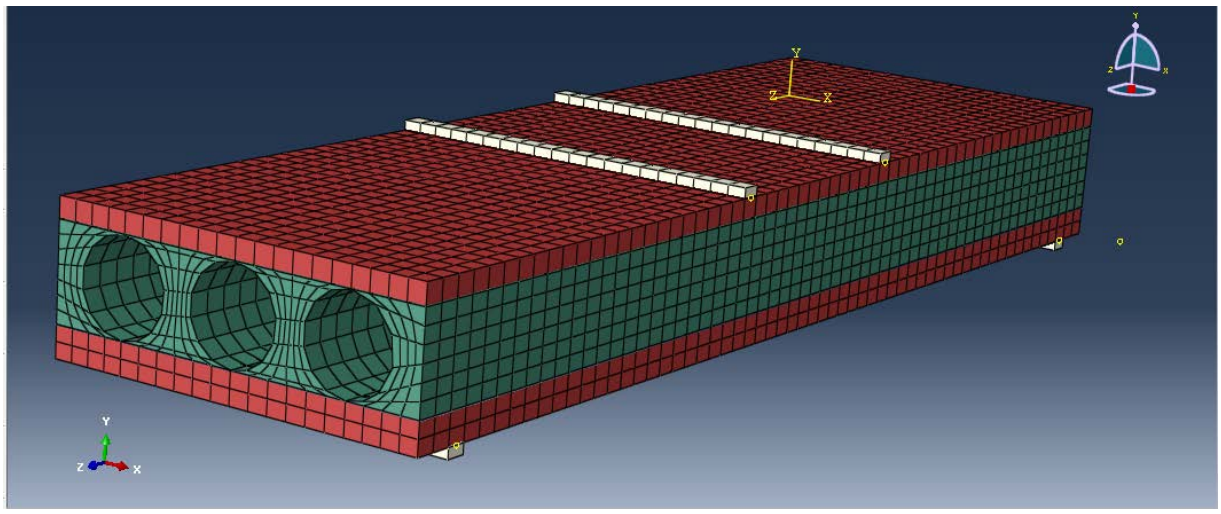

Figure 8.10: Meshing of hollow core specimen HC-7-B

8.3.2.1 Strain Distribution

Figure 8.11 shows the longitudinal section along the length showing the strain distribution of specimen HC-7-B at center of hybrid beam. **Figure 8.12** demonstrates the comparison between the FEM and experimentally observed longitudinal strains on the top and bottom surfaces of hollow core beam. Tensile and compressive strains are well predicted by the FEM model in elastic regions. The experimental result demonstrated that the hollow core beam exhibits a tensile strain at the bottom close to the failure load of 239 x 10^{-6} compared to 193 x 10^{-6} predicted by FEM. Similarly, the experimental compressive strain at the top is 186 x 10^{-6} compared to 214 x 10^{-6} predicted by FEM. The agreement is reasonably good in both tension and compression strains of the hybrid beam.

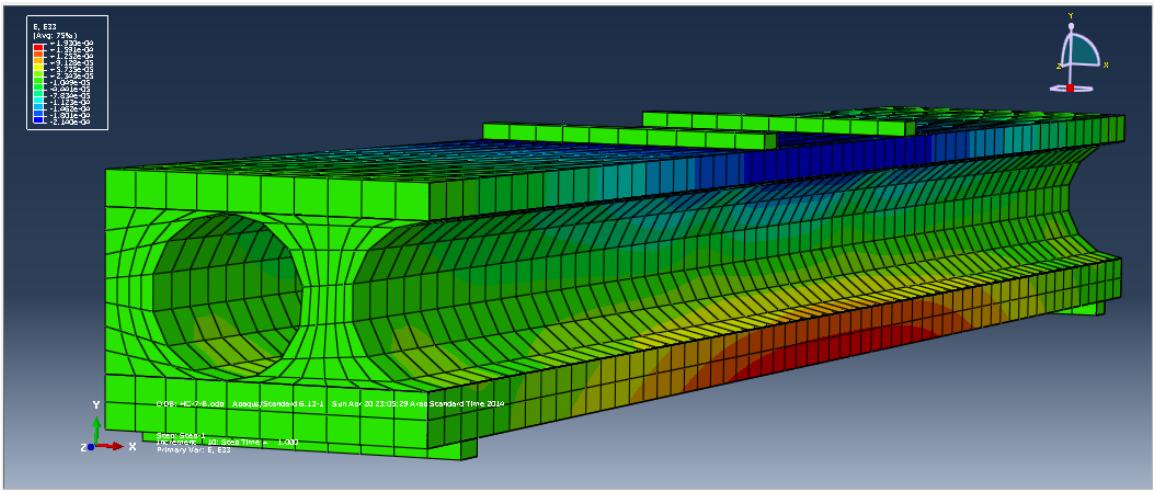

Figure 8.11: Longitudinal section along the length showing the strain distribution of HC-7-B

The strain profile along beam depth of specimens HC-7-B at midspan with two different load levels: 50% P_U and 90% P_U for experimentally observed FEM strains is illustrated in **Figure 8.13**.

The experimentally measured linear strain distribution along the depth of the hybrid beam was also confirmed from the FEM as shown in **Figure 8.13**. This strain distribution along the depth is almost identical at all load levels of hollow core specimens.

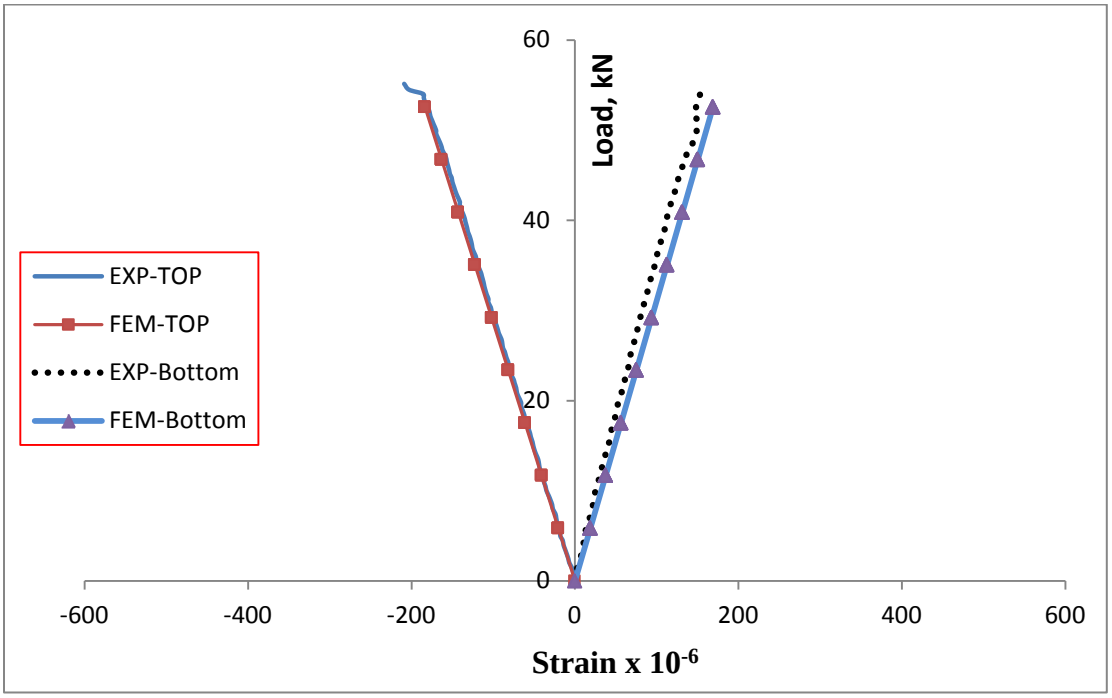

Figure 8.12: FEM vs. experimentally observed longitudinal strain on top and bottom faces of hybrid beam of specimen HC-7-B

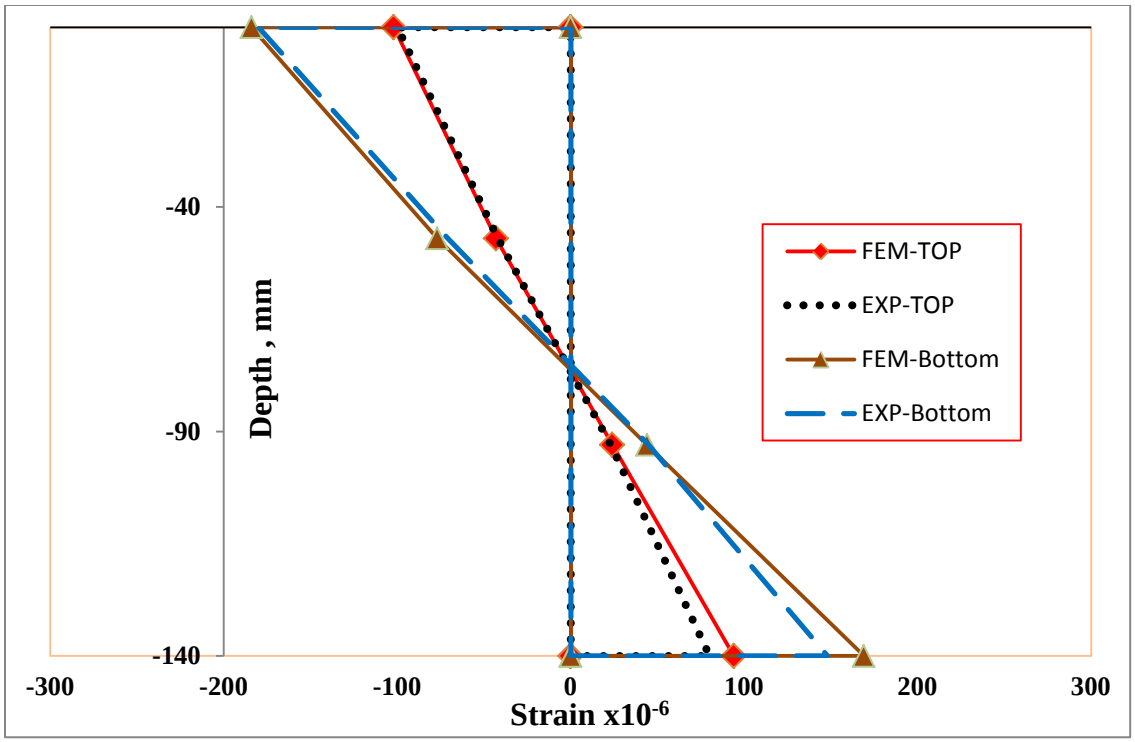

Figure 8.13: FEM vs. experimentally observed longitudinal strain along the depth at mid span of specimen HC-7-B

8.3.2.2 Stress Distribution

The FEM longitudinal stress distribution in the hybrid beam is shown in **Figure 8.14**. **Figure 8.14** indicates that the maximum tensile stress developed in the tension zone of hollow core beam was 11 MPa compared to 13 MPa achieved by measured strain experimentally and 12 MPa calculated stress based on the transformed section properties. The figure further indicates the distribution of low to high tensile and compressive stresses everywhere in the beam.

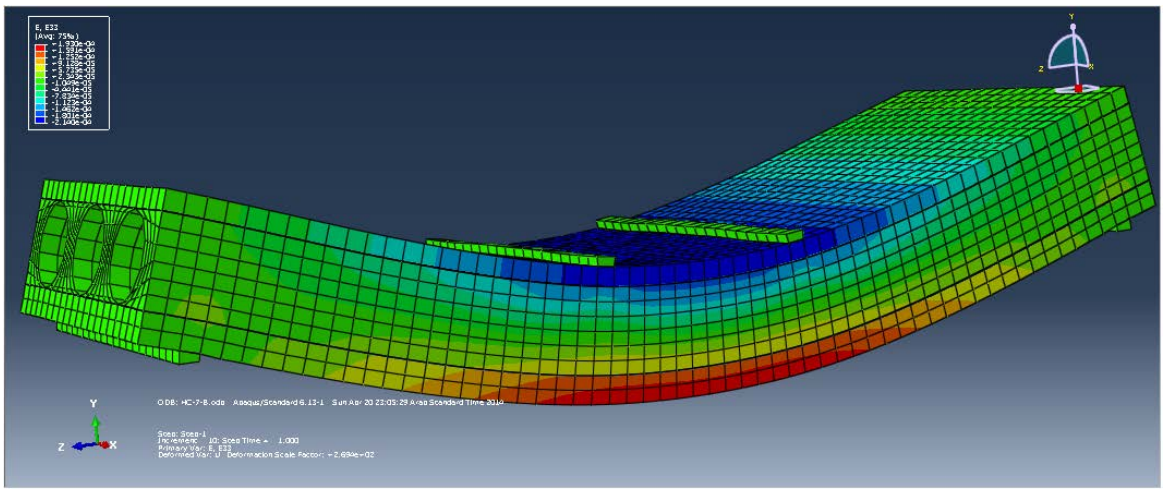

Figure 8.14: FEM longitudinal stress distribution of HC-7-B

A summary of the finite element and experimentally observed and calculated results for hybrid hollow core beams is presented in **Table 8.3**. FEM results of all other specimens are presented in **Appendix E**.

Table 8.3: Comparison of Finite Element Results with Experimental and Calculated Values for Hollow Core Specimens

Beam Designation	Load P (kN)	Strain x 10^{-6}				Stress (MPa)					
		Bottom		Top		Bottom			Top		
		Meas.*	FEM	Meas.*	FEM	Meas.#	Calc.‡	FEM	Meas.#	Calc.‡	FEM
HC-A-L3 (260 × 140) Span 1100	48	258	276	-284	-320	14	15	15	16	15	16
HC-B-L3 (330 × 175) Span 1100	59	220	180	-160	-204	12	12	10	9	12	12
HC-C-S2 (390 × 200) Span 900	107	180	169	-181	-195	10	11	10	10	10	12
HC-C-L2 (390 × 200) Span 1100	54	247	200	-204	-201	14	13	11	11	13	12
HC-D-L2 (380 × 140) Span 1100	103	239	193	-186	-214	13	12	11	10	12	12

Meas.*: Measured strain experimentally, Meas.#: Measured stress from strain experimentally
Calc.‡: Calculated stress on the basis of transformed section

The assumption that plane sections remain plane after bending was confirmed by the linearity of the measured and FEM longitudinal strains at mid span of both hybrid layered and hollow core specimens. The linear strain distribution measured experimentally and modeled by FEM across the depth of the hybrid section justified the assumption that

perfect bonds exist at the surface interfaces between UHPC and NC at the mid span section of the beam.

The good agreement between the FEM and experimental results presents the possibility of predicting the flexural stresses and capacity of hybrid beam by linear analysis of the hybrid sections. This aspect can help in optimizing the design of the hybrid beam dimensions to make full benefit of UHPC and NC. The FEM results of stresses at top and bottom of the hybrid beams are close to the experimental results using the measured stresses and calculated stresses on the basis of transformed section.

8.3.2.3 Deflection Comparison

The results presented in **Table 8.4** show the deflection of hybrid hollow core specimens by three ways: experimentally observed deflection, Equation 5.3 given in section 5.6 (Chapter 5), and FEM for two selected load levels: 0.8 P_U and P_U.

Table 8.4: Comparison of Experimental, Theoretical, and FEM Deflection Hollow Core Specimens

Beam Designation	Failure load P_U (kN)	Experimental		Elastic formula		FEM	
		0.8 P_U	P_U	0.8 P_U	P_U	0.8 P_U	P_U
HC-A-L3 (260 × 140) Span 1100	56	0.55	0.63	0.45	0.56	0.45	0.56
HC-B-L3 (330 × 175) Span 1100	65	0.19	0.23	0.24	0.30	0.28	0.35
HC-C-L2 (390 × 200) Span 1100	103	0.51	0.57	0.23	0.28	0.28	0.35
HC-D-L2 (380 × 140) Span 1100	58	0.41	0.49	0.33	0.40	0.36	0.45

Similar observation as in case layered specimens that the FEM model accurately predicts the deflection calculated based on the theoretical elastic formula for the mid span deflection of hollow core beam specimens in elastic range for the three load levels selected.

The deflections of the finite element models and deflections calculated using elastic deflection formula for layered beams were also smaller than those measured experimentally as explained in section 8.3.1-C above.

CHAPTER 9

POSSIBLE UTILIZATION OF THE PROPOSED HYBRID CONSTRUCTION

This exploratory study has confirmed that each of the three alternative forms of construction is structurally promising and can be utilized in designing simply supported precast floor slab units for residential and commercial buildings. As the design of one-way simply supported precast units is controlled by flexure, not shear, in common applications, each concept can be utilized as discussed herein.

9.1. Simply Supported One-Way Floor Slabs

Precast slab units of certain width are designed as a simply supported beam type element for which demand for flexure strength and deflection is the controlling design factor. For solid one-way slab the code specified minimum depth (unless deflection is calculated) is often controls the thickness, as the intensity of loading, both dead and live, is not high enough to demand higher depth. For common residential buildings, live would normally be less than 3.5 kN/m^2 and even with live load as high as 5.0 kN/m^2, the code specified minimum thickness would be sufficient for design. The following example lends support to this assertion.

For a simple span of 4.0 m, the ACI-specified minimum thickness, unless deflection is checked, is $l/20$ = 0.2 m=200 mm. Assuming superimposed dead load of 0.75 kN/m^2 and live load of 4.0 kN/m^2, the factored moment M_u = 1.2D + 1.6L = (1.2 x 5.55 + 1.6 x 4) x $4^2/8$ = 26.12 kNm/m. The elastic section modulus of unit width of slab = 1/6 x 1000 x 200^2 = 6.67 x 10^6 mm^3. The maximum flexural tensile stress at the bottom = 26.12 x 10^6/ 6.67 x 10^6 = 3.91 MPa.

For a concrete of f_c' = 4900 psi (33.8 MPa), the modulus of rupture is about 525 psi (3.62 MPa). The tensile stress barely exceeds the tensile strength of plain concrete. The tension steel (f_y = 420 MPa), A_s, for M_u = 26.12 kN.m is about 480 mm^2/m, slightly less than the ACI code specified minimum reinforcement for flexure which is 520 mm^2/m. The reinforcement area to be used is therefore not less than 520 mm^2/m, being greater than the shrinkage and thermal (S+T) requirement.

This is the normal scenario for design of one-way reinforced concrete (RC) slab for short to moderate span for which the depth of the slab is essentially controlled by the deflection criterion and the requirement of tension reinforcement is not high.

9.2. Hybrid Construction with UHPC

From the above presentation, it is clear that the tensile strength demand for simply supported one-way RC slab elements in flexure is small to at best modest. This recognition paves the way for hybrid construction in which the tensile strength demand can amply be met by UHPC. In the previous example of RC slab, the tensile force T= $A_s f_y$ = 520 x 420 N = 218.4 kN. This can easily be accommodated by a layer of UHPC of

20 mm, considered as the minimum thickness from practical viewpoint. The average tensile stress of 218.4x 10^3/ (20 x 1000) = 10.9 MPa is less than the flexural tensile strength of UHPC layer. Using transformed section properties, the bottom tensile stress will be less than 3.91 MPa calculated by using properties of RC section.

Likewise, the hybrid hollow-core section can be found structurally sufficient with ample reserve for the flexural capacity. For the RC slab considered above, the use of UHPC bars can also strengthen the slab by using 25 x 50 mm (50 mm depth) rectangular bars, the number of which has to be calculated. Because of the number of the bars and the clear spacing, the width of the section may not be enough to house all bars. Thus, a slight increase in depth than the layer or hollow-core section will be necessary in most cases. This has been illustrated with an example in section 9.4.

9.3. Design Approach for the Hybrid Units

The design of precast hybrid floor slab units is based on the following considerations:

- The nominal moment capacity is determined by using transformed section properties and linear stress and strain distribution for the transformed section. Thus, $M_n = S_b \cdot f_t / n$, when S_b= bottom section modulus for transformed section, f_t = flexural tensile strength of UHPC and n= modular ratio (E_U/E_C).
- Because of the expected high variability in the value of f_t, a lower reduction factor of $\phi = 0.7$ can be used for the average value of f_t determined from tests on similar size specimens. For UHPC bars, where the variation is expected to be smaller

because of smaller cross section of the bars, ϕ can be increased to 0.8. Design moment capacity ϕM_n must satisfy $\phi M_n \geq M_u$.

- Shear strength need not be considered for layered and UHPC bar reinforced units, as the slab thickness required to satisfy deflection would be sufficient. For hollow-core slab, the shear strength can be calculated from $V_n = 5\sqrt{f'c}\ b_w\ h$, using reduction factor of $\phi = 0.75$. Shear strength requirement is $\phi\ V_n \geq V_u$.
- ACI- specified minimum thickness for simple span one-way slab unit will also apply for hybrid units, unless deflection is checked.
- As precast units are topped with a thin cast-in-place concrete layer, this thickness can be deducted from the required depth to determine the depth of precast units, as the cast-in-place concrete will acts compositely with the hybrid precast units.
- The minimum tensile strength provided by UHPC layers or bars will correspond to the minimum (S + T) requirement for concrete slabs. For reinforcement steel yield stress f_y = 420 MPa, the tensile strength provided by the minimum (S+T) reinforcement equals $0.0018\ bhf_y$, where b = width and h is the height of the section in mm. The tensile strength of UHPC must therefore be greater than $0.0018\ bhf_y$.

9.4. Design Examples

The data given in section 9.1 will be used to find the three alternative designs for simply supported slab of span of 4.0 m, in addition to superimposed dead load = o.75 kN/m^2 and live load = 4.0 kN/m^2.

9.4.1 RC One-Way Slab

From section 9.1, the minimum thickness is 200 mm and the required M_u = 26.12 kN.m. The tension steel area A_s = 520 mm^2 / m (minimum requirement). This can be provided by 5 – 12 mm dia bars as shown in **Figure 123(a)**.

9.4.2 Layered Hybrid UHPC Unit

Consider 1.0 m width of the precast unit with a depth of 190 mm including 20 mm UHPC thickness of the bottom layer (**Figure 123(b)**). The slight reduction in depth from 200 mm is justified in view of the enhanced moment of inertia for the hybrid section. The factored moment M_u = (1.2 x 5.31 + 1.6 x 4) x 4^2/8 = 25.54 kN.m

For the uncracked transformed section with an assumed value of n= 1.8, the location of NA from the bottom = 88.4 mm, I = 666.3 x 10^6 mm^4 and the bottom section modulus S_b = 7.54 * 10^6 mm^3. The bottom tensile stress, f_t, at M_u = n. M_u / S_b = 6.1 MPa. This is much lower than the expected flexural tensile strength of greater than 12 MPa for the UHPC layer. Thus the section possesses ample reserved strength. Based on an assumed value of f_t = 12 MPa, the design strength is 0.7 x 12 x S_b / n = 35.2 kN.m versus the required M_u = 25.54 kN.m.

The tensile strength of UHPC layer = 0.7 x 12 x 1000 x 20 = 168 kN. This is greater than the minimum (S + T) requirement of 0.0018 * (190 - 20) * 1000 * 420 N = 128.5 kN.

9.4.3 Hollow-Core Section

Using the same depth of 190 mm as for the layered section, 20 mm thick top and bottom UHPC layers and 3 holes of diameter 150 mm as shown in **Figure 9.1(c)**, the transformed section I = 726.9 x 10^6 mm^4 and S_b = 7.65 x 10^6 mm^3. The required M_u = 22.5 kN.m. The design moment capacity, $\phi M_n = 0.7 * 12 * S_b / n$ = 35.7 kN.m, far greater than what is required. The solid web width of (1000 – 3x150) = 550 mm is ample to provide the required shear strength. The tensile strength of the two UHPC layers = 0.7 x 12 x 1000 x 20 x 2 = 336 kN, greater than the minimum for (S + T) requirement of 0.0018 x (190 - 40) x 1000 x420 = 113 kN.

9.4.4 Section Reinforced with UHPC Bars

Using 220 mm depth and 11 rectangular UHPC bars of 25x50 mm cross section (50 mm depth) at the bottom (**Figure 9.1(d)**), the transformed section I = 496.8 x 10^6 mm^4 and S_b = 3.46 x 10^6 mm^3. The required M_u = 27.2 kN.m. Based on assumed f_t = 18 MPa, and Ø=0.8, the design moment capacity, $\phi M_n = 0.8 * 18 * S_b / n$ = 27.72 kN.m, matching what is required. The tensile strength of the 11 UHPC bars = 0.8 x 18 x 25 x 50 x 11 = 198 kN, greater than the minimum for (S + T) requirement of 0.0018 x (1000x220 – 11x25x50) x 420 = 156 kN.

9.5. Possibilities and Prospects

Of the three alternative forms of floor slab construction, both layered and hollow-core section have the best prospects for utilization and have structural appeal. Both form of design will have ample flexural strength. In order to keep the material cost lower, the minimum thickness of UHPC has been kept at 20 mm (considered minimum from practical view point) to reduce the usage of UHPC. The increased cost due to UHPC usage is countered by a construction that is void of conventional steel reinforcement and offers an alternative.

While in this study, an economic assessment of the hybrid UHPC construction has not been the primary goal, it is the evident that the proposed alternatives forms are somewhat more expensive than the conventional RC construction. However, as the amount of UHPC needed is not that high, the increase in cost is not prohibitive. This study has made a strong case for adoption of hybrid sections using UHPC that eliminates the use of steel reinforcement. In corrosive environment, this may prove to have significant advantage worthy of consideration.

The concept of using precast UHPC bars as tension reinforcement is a new one. It draws attention to the future possibilities that concrete bars of superior tensile strength can be developed and used in some applications. With further advancement in fiber-reinforced UHPC and its casting with better dispersion of steel fibers to ensure better predictability of tensile strength, the possibility of replacing steel bars with UHPC bars as the tension reinforcement in some application is not an imaginary one. This exploratory study points to such possibility.

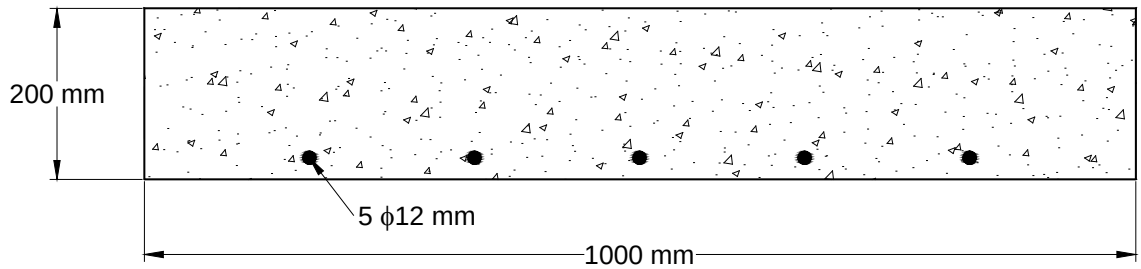

(a) RC slab section

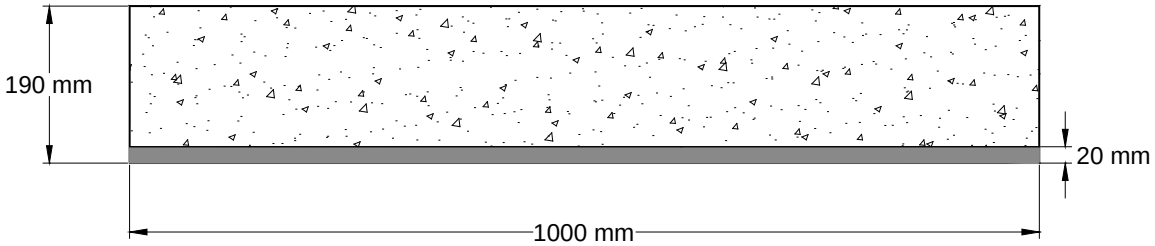

(b) Layered slab section

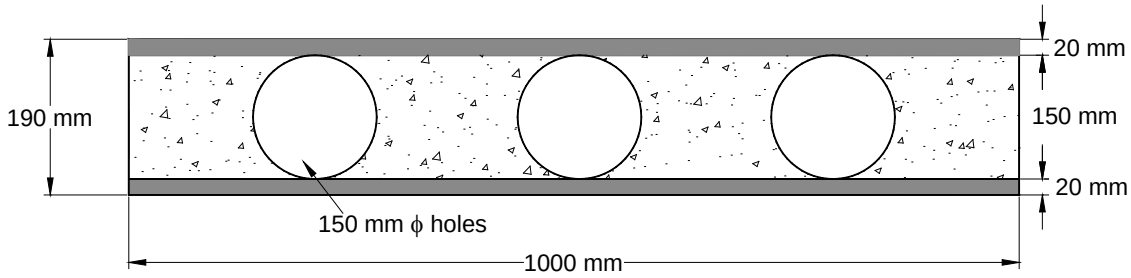

(c) Hollow-core slab section

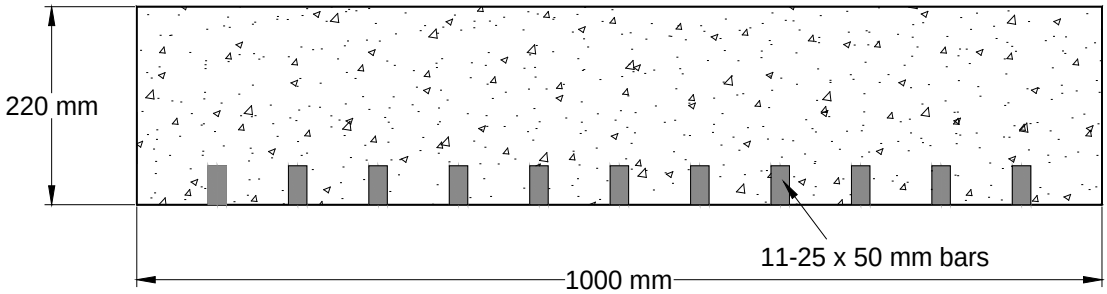

(d) UHPC bar reinforced section

Figure 9.1: Design sections

CHAPTER 10

CONCLUSIONS AND RECOMMENDATIONS

10.1. General

With the aim of seeking new applications of UHPC in concrete construction, an exploratory study has been undertaken to develop hybrid concrete floor slab construction utilizing the tensile strength of steel fiber-reinforced UHPC instead of steel reinforcement. Three concepts for one-way simply supported precast floor units were explored: (i) units with a layer of UHPC at the bottom tension face, (ii) units reinforced with precast UHPC deformed bars and (iii) hybrid hollow-core units with top and bottom faces cast with UHPC layers. Types (i) and (iii) do not require the use of any steel reinforcement. Test results using small size specimens have shown encouraging structural behavior and flexural strength that support their adequacy and invite further exploration. Further studies would add creditability to this study that reveals that the practical adoption of the proposed new forms of construction is a distinct possibility.

Based on this study, the following conclusions are drawn:

10.2. Conclusions

10.2.1 General

1. All three forms of hybrid construction are suitable for simple span one-way floor slab construction for which shear is not a critical design factor and they can be designed with adequate flexural strength.
2. The hybrid test specimens show linear behavior almost upto the peak load, permitting the use of transformed section properties to compute stress, deflection and flexural capacity.
3. All three forms of construction exhibit post-cracking softening with increased deformation under declining load as flexural crack advances through UHPC layers or bars. The post-cracking strength is provided by the uncracked ligament and the unpulled steel fibers across the crack.
4. The proposed forms of construction may offer some advances in the applications in corrosive environment as steel reinforcement bars are not necessary.
5. As flexural tensile strength of UHPC is dictated by the orientation and uniformity in dispersion of steel fibers, the estimate of flexural strength should be based on statistical significant number of tests on similar size of UHPC samples.

10.2.2 Hybrid Layered Construction

1. The UHPC layer should be partially cured, at least for two days, before the placement of normal concrete on top of it. In design, the thickness of UHPC

layers should preferable be kept low, as higher thickness is not proportionately fully effective as load carrying component.

2. When normal concrete is placed directly on the top surface of unfinished UHPC layer, the bond strength is adequate to develop full composite action with no bond slip at the interface.

10.2.3 UHPC Reinforced Beams

1. For efficient utilization of UHPC bars, the bars preferably should have larger width, rather than higher thickness, for identical areas.
2. Cracked concrete transformed section properties are applicable as concrete will crack due to tensile stress.
3. UHPC bars should be fully cured before placement in concrete for the development of full tensile strength.

10.2.4 Hybrid Hollow-Core Units

1. The surfaces of the UHPC layers in contact with normal concrete should left unfinished to provide good bond with normal concrete. The UHPC layers should be cured for at least two days.
2. For efficient utilization of UHPC layers, the thickness of the layers should preferably be small.
3. The required shear strength of the hollow-core units can be met by a judicious use of the holes to have the required net solid width of the section.

4. Limited test data on web-shear failure suggests that nominal shear strength to prevent web-shear failure can be estimated by $V_n = 5\sqrt{f'c}\, b_w d$.

10.2.5 Finite Element Modeling

The results of finite element modeling (FEM) of layered and hollow-core specimens show acceptable agreement with the experimental results for strain and stress at top and bottom of the specimens throughout the entire range of loading. The FEM predict the peak loads close to the experimental values.

10.3. Recommendations

The following recommendations for future work in this direction are made:

1. Undertake large-size testing of specimens using the suggested three forms of construction using UHPC to provide further experimental evidence to the observed behavior and performance in order to evaluate the possibility of construction of one-way floor slabs.
2. Undertake a large number of testing of UHPC bars and thin elements to observe the variation in strengths caused by inherent variation in construction caused by randomness of steel fiber dispersion within the mortar and develop a statistical model for strength distribution.
3. Construction methods needs to be developed to ensure more uniform dispersion of fibers within the mix, as this is highly critical for the predictability of the results.

REFERENCES

[1] Moallem, M., M.S thesis, "Flexural Redistribution in Ultra-High Performance Concrete Lab Specimens", Ohio University, June 2010.

[2] Yanni, V., "Multi-Scale Investigation of Tensile Creep of Ultra-High Performance Concrete for Bridge Applications", A Doctoral Thesis Dissertation, Georgia Institute of Technology, December 2009.

[3] Richard P, Cheyrezy M., "Reactive powder concretes with high ductility and 200–800 MPa compressive strength", ACI SP144-24:507–18, 1994.

[4] Richard, P. and Cheyrezy, M., "Composition of Reactive Powder Concretes", Cement and Concrete Research, Vol. 25, No. 7, pp. 1501-1511.1995.

[5] Behzad N., Raizal S. M. R., Mohd. S. J., Yen L. V., "A review on Ultra High Performance 'Ductile' Concrete (UHPdC) Technology " international journal of civil and structural engineering volume 2, no 3, 2012.

[6] Lukasik, J., "Concrete: A High-Tec material of the 21st Century", 8th Hitachi EU Science and Technology Forum, Athens, May 20-22, 2005.

[7] Henry N., P. and Kris R., P.," ULTRA-HIGH PERFORMANCE CONCRETE, with DUCTILITY", the world's first long-span roof in Ductal. The Joppa Clinker Dome Roof, 2nd Material Specialty Conference of the Canadian Society for Civil Engineering, Montréal, Québec, Canada, 5-8 juin 2002 / June 5-8, 2002.

[8] Murthy, R. S., "Design of joints for laterally loaded UHPC columns", MS thesis, Iowa State University, 2009.

[9] LEE, C. D., KIM, KI-B., CHOI, S "Application of Ultra-High Performance Concrete to Pedestrian Cable-Stayed Bridges" , Journal of Engineering Science and Technology Vol. 8, No. 3 (2013) , pp.296 – 305.

[10] Lubbers, A., "MS Thesis "Bond Performance of Ultra- High Performance Concrete and Prestressing Strands", Ohio University, August, 2003.

[11] **Azad, A. K.**, and Ahmad, S., "An Exploratory Study of a Newly-Developed Ultra High Performance Concrete (Ductal) for its Application in Saudi Arabia, Final Report, SABIC SB090016, April 2011.

[12] **Hakeem, I. Y.**, "Characterization of an Ultra-High Performance Concrete", MS Thesis, Department of Civil Engineering, King Fahd University of Petroleum and Minerals, Saudi Arabia, June, 2011.

[13] **Hakeem, I. Y., Azad, A. K and Ahmad, S**., "Effect of steel fibres and thermal cycles on fracture properties of ultra-high performance concrete", Journal of Testing and Evaluation, ASTM, Volume 41, No. 3, 2013.

[14] **Azad, A. K., Ahmad, S. and Hakeem, I. Y.**, "Effect of cyclic exposure and fiber content on tensile properties of ultrahigh performance concrete", Advances in Cement Research, U.K, Volume 25, Issue 5, October 2013 , pages 273 – 280.

[15] **Ahmad, S., Hakeem, I. Y. and Azad, A. K.**., "Effect of Curing Regime, Fiber Content and Cyclic Exposures on the Compressive Strength and Modulus of Elasticity of Ultra-High Performance Concrete" , Advances in Cement Research, U.K. In press (Accepted 03/02/2014).

[16] Collepardi S., Coppola, R., Troli L., and Collepardi, M., "Mechanical Properties of Modified Reactive Powder Concrete", International Conference on Super plasticizers and the Chemical Admixtures in Concrete, Rome, Italy, Farmingto Hills, ACI Publication SP-173. pp. 1-21. 1996.

[17] Buitenaar, P., "Ultra high performance concrete: developments and applications during 25 years", Plenary session international symposium on UHPC, Kassel, Germany; 2004.

[18] Cheyrezy, M., Behloul, M., Dowd, W., and Dauriac, C. "Reactive Powder Concrete (RPC) Application for Seismic Design." American Concrete Institute Convention, October 29, 1998, pp. 1-15, 1998.

[19] Habel, K., Charron, J.-R., Denarié, E., and E. Brühwiler, "Autogenous Deformations and Viscoelasticity of UHPFRC in Structures", Magazine of Concrete Research, Vol. 58, No. 3: 135-145. April 2006.

[20] Cheyrezy, M., and Behloul, M. "Creep and Shrinkage of Ultra-High Performance Concrete", Creep, Shrinkage and Durability Mechanisms of Concrete and other Quasi-Brittle Materials – Proceedings of the Sixth International Conference CONCREEP-6@MIT, Cambridge, MA, USA, 2001.

[21] Graybeal, B., "Material Property Characterization of Ultra-High Performance Concrete", FHWA-HRT-06-103, 2006.

[22] Loukili, A., Khelidj, A., and Richard P., "Hydration Kinetics, Change of Relative Humidity, and Autogenous Shrinkage of Ultra-High-Strength Concrete", Cement and Concrete Research, Vol. 29, No. 4: 577-584, April 1999.

[23] Tanaka, Y., Musya, H., Ootake, A., Shimoyama, Y., Kaneko, O., "Design and Construction of Sakata-Mirai Footbridge Using Reactive Powder Concrete," Proceedings of the First Fib Congress, Vol. 3, pp. 417-424, 2002.

[24] Cavill, B., "Ductal, An Ultra-high Performance Material for Resistance to Blasts, Safeguarding Australia", Canberra, 12-14 July, 2005.

[25] Gilliland, S., "Reactive Powder Concrete (RPC), A New Material for Prestressed Concrete Bridge Girders", Structures Congress – Proceedings,

Vol. 1, Building an International Community of Structural Engineers, pp. 125-132. 1996.

[26] Cwirzen, A., Penttala, V, and Vornanen, C., "Reactive powder based concretes: Mechanical properties, durability and hybrid use with OPC", Helsinki University of Technology, Laboratory of Building Materials Technology, Rakentajanaukio 5, FIN-02150 Espoo, Finland, 2008.

[27] Chang, T. P, Chen, B. T, Wang J. J. and Wu C. S., "Performance of Reactive Powder Concrete (RPC) with different curing conditions and its retrofitting effects on concrete member", Concrete Repair, Rehabilitation and Retrofitting II – Alexander et al (eds) © 2009 Taylor & Francis Group, London, ISBN 978-0-415-46850-3, 2009.

[28] Graybeal, B., and Hartmann, J., "Strength and Durability of Ultra-High Performance Concrete", Paper presented at the Concrete Bridge Conference, Portland Cement Association. , 2003.

[29] Perry, V., and Zakariasen, D., "First Use of Ultra-High Performance Concrete for an Innovative Train Station Canopy", Concrete Technology Today, Aug., Vol. 25, No. 2: 1-2. 2004.

[30] Heinz, D. and Ludwig, H., "Heat Treatment and the Risk of DEF Delayed Ettringite Formation in UHPC", Proceedings of the International Symposium on Ultra-High Performance Concrete, Kassel, Germany, Sept. 13-15, pp. 717-730, 2004.

[31] Graybeal, B., "Characterization of the Behavior of Ultra-High Performance Concrete", PhD Dissertation submitted to the Faculty of the Graduate School of the University of Maryland, 2005.

[32] Soutsos, N., Millar, G., and Karaiskos, K., "Mix Design, Mechanical Properties, and Impact Resistance of Reactive Powder Concrete (RPC)", International RILEM Workshop on High Performance Fiber Reinforced Cementitious Composites in Structural Applications, 2005.

[33] Magureanu, C. Sosa, I. Negrutiu, C. and Heghes, B. "Mechanical Properties and Durability of Ultra-High-Performance Concrete", ACI Materials Journal, V. 109, No. 2, March-April 2012.pp. 177-183.

[34] A.M.T. Hassan, S.W. Jones, G.H. Mahmud, "Experimental test methods to determine the uniaxial tensile and compressive behaviour of ultra high performance fibre reinforced concrete (UHPFRC)", Construction and Building Materials, 37 (2012) 874-882.

[35] Dugat, J., Roux, N., and G. Bernier. "Mechanical Properties of Reactive Powder Concretes", Materials and Structures, May, Vol. 29: 233-240, 1996.

[36] Reineck, K., and Greiner S., "Tests on ultra-high performance fibre reinforced concrete designing hot-water tanks and UHPFRC-shells", Proceedings of the International Symposium on Ultra High Performance Concrete, Kassel, Germany, pp. 361-374, Sept. 2004.

[37] VandeVoort, M. Suleiman, S. Sritharan, “Design and Performance Verification of UHPC Piles for Deep Foundations”, (Final report of project entitled Use of Ultra-High Performance Concrete in Geotechnical and Substructure Applications), 2008.

[38] Dong J. K., Seung H. P., Gum S. R., Kyung T. K., “Comparative flexural behavior of Hybrid Ultra High Performance Fiber Reinforced Concrete with different macro fibers “ Construction and Building Materials - CONSTR BUILD MATER 01/2011; 25(11):4144-4155.

[39] Duy Liem Nguyen Dong Joo Kim Gum Sung Ryu Kyung Taek Koh,” Size effect on flexural behavior of ultra-high-performance hybrid fiber-reinforced concrete “ Composites Part B , 2013 , 45 (1) 1104-1116 .

[40] Akkya Y, Shah SP, Ankenman B. Effect of fiber dispersion on multiple cracking of cement composites. J Eng Mech 2001;127(4):311–6.

[41] Tue NV, Henze S. Determination of the distribution and orientation of fibers in steel fiber reinforced UHPC by photographic method. In Proceedings of 2nd international symposium on ultra-high performance concrete. 2008. p. 505–12.

[42] In Hwan Yanga,1, Changbin Joh b, Byung Suk Kimb “Structural behavior of ultra-high performance concrete beams subjected to bending”, Engineering Structures 32 (2010) 3478–3487.

[43] Stephanie J. Barnett, Jean-Francois Lataste , Tony Parry • Steve G. Millard , Marios N. Soutsos, “Assessment of fiber orientation in ultra-high performance fibre reinforced concrete and its effect on flexural strength”, Materials and Structures (2010) 43:1009–1023.

[44] Su Tae Kang a, Bang Yeon Lee b, Jin-Keun Kim c, Yun Yong Kim ,” The effect of fibre distribution characteristics on the flexural strength of steel fibre-reinforced ultra-high strength concrete”, Construction and Building Materials 25 (2011) 2450–2457.

[45] Graybeal, B., “UHPC in the U.S. highway transportation system, “Ultra High Performance Concrete (UHPC)”, in: Fehling, et al., (Eds.), 2nd International Symposium on Ultra High Performance Concrete, 5–7 March, Kassel, Germany, Kassel,, pp. 11–17, 2008.

[46] Doo-Yeol Yoo a, Joo-Ha Lee b, Young-Soo Yoon, “Effect of fiber content on mechanical and fracture properties of ultra-high performance fiber reinforced cementitious composites] [D.-Y. Yoo et al. / Composite Structures 106 (2013) 742–753]

[47] Kang ST, Lee Y, Park YD, Kim JK. Tensile fracture properties of an ultra high performance fiber reinforced concrete (UHPFRC) with steel fiber. Comp Struct 2010;92(1):61–71.

[48] Kwon SH, Lee SK, Park SY, Cho KH, Cho KR. Tensile stress-crack opening relationship of ultra high performance cementitious composites (UHPCC) used for bridge decks (in Korean). J Korea Inst Struct Maint Insp 2013;17(1):46–54.

[49] Ryu GS, Kang ST, Park JJ, Koh KT, Kim SW. Mechanical behavior of UHPC (ultra high performance concrete) according to hybrid use of steel fibers. Adv Mater Res 2011;287–290:453–7.

[50] Park SH, Kim DJ, Ryu GS, Koh KT. Tensile behavior of ultra high performance hybrid fiber reinforced concrete. Cem Concr Compos 2012;34(2):172–84.

[51] Wille K, Kim DJ, Naaman AE. "Strain-hardening UHP-FRC with low fiber contents. Mat Struct 2011;44(3): pp.583–98.

[52] Kang ST, Kim JK. Investigation on the flexural behavior of UHPCC considering the effect of fiber orientation distribution. Const Build Mater 2012; 28(1):57–65.

[53] Habel, K., Denarié, E., and Brühwiler, E., "Time dependent behavior of elements combining ultra-high performance fiber reinforced concretes, UHPRFC and reinforced concrete." Mater. Struct., 39, 557–569, 2006.

[54] Duy Liem Nguyen a, Gum Sung Ryu b, Kyung Taek Koh b, Dong Joo Kim , "Size and geometry dependent tensile behavior of ultra-high-performance fiber-reinforced concrete", Composites: Part B 58 (2014) 279–292.

[55] Kay Wille , Dong Joo Kim , Antoine E. Naaman, "Strain-hardening UHP-FRC with low fiber contents", Materials and Structures (2011) 44:583–598.

[56] Azad, A. K. and Hakeem, I. Y. "Development of Hybrid Concrete construction Eliminating Traditional Steel Reinforcements", Final Report, SB111001, King Fahd University of Petroleum and Minerals, Saudi Arabia, October, 2013.

[57] Azad, A. K. and Hakeem, I. Y., "Flexural Behavior of Hybrid High Performance Concrete construction", Proceedings of the first Australasia and South-East Asia Structural Engineering and construction, ASEA-SEC-1, Perth, Nov. 28-Dec.2, **2012.**

[58] Hakeem, I. Y., and Azad, A.K., "Flexural Performance of Hybrid Concrete Construction Utilizing Developed UHPC", 9th International Concrete Conference &Exhibition, Kingdom of Bahrain, 11th - 13th February, 2013.

[59] Azad, A. K. and Hakeem, I. Y**.**, "Flexural Behaviour of Hybrid Concrete Beams Reinforced with Ultra-High Performance Concrete Bars", Construction & Building Materials, volume 49, Pages 128–133, December 2013.

[60] Azad, A. K. and Hakeem, I. Y., "Ultra-High Performance Concrete Reinforcement Bars", Patent Pending, Docket No. 34000.41, Patent Application No. 13/737,876, 2013.

[61] Elmahdy, R. El-Hacha and Shrive N., "Flexural behaviour of hybrid composite girders in bridge construction", Fourth International Conference on FRP Composites in Civil Engineering (CICE2008) 22-24July 2008, Zurich, Switzerland, 2008.

[62] Donna Chen, Raafat El-Hacha, “Flexural Behaviour Of Hybrid FRP-UHPC Girders Under Static Loading”, Proceedings of 8th International Conference on Short and Medium Span Bridge, Niagara Falls, Canada, 2010.

[63] Ferrier E., Labossière, P., and Neale, K. W. “Mechanical Behavior of an Innovative Hybrid Beam Made of Glulam and Ultrahigh-Performance Concrete Reinforced with FRP or Steel”, Journal of Composites for Construction ASCE / March/April 2010, 14:217-223, 2010.

[64] Petr Hajek, Magdalena Kynclova, Ctislav Fiala, “Timber – UHPC composite floor structures – environmental study”, http://www.ctislav.wz.cz/publ/2012_01_UHPC-Kassel_Hajek.pdf.

[65] Martin Schäfers, Werner Seim, “Investigation on bonding between timber and ultra-high performance concrete (UHPC)”, Construction and Building Materials, 25 (2011) 3078-3088.

[66] Bassam A., Tayeh, B. H., Abu Bakar, M. A., MegatJohari, Yen Lei Voo, “Mechanical and permeability properties of the interface between normal concrete substrate and ultra-high performance fiber concrete overlay”, Construction and Building Materials, 538-548, 2012.

[67] Georges Youssef, Louisa Loulou, Sylvain Chataigner, Sabine Caré, André “Analysis of the behaviour of a bonded joint between laminated wood and ultra-high performance fibre reinforced concrete using push-out test”, Construction and Building Materials 53 (2014) 381–391.

[68] Benjamin A. Graybeal and Florent Baby, “Development of Direct Tension Test Method for Ultra-High- Performance Fiber-Reinforced Concrete”, ACI Materials Journal, V. 110, No. 2, March-April 2013.

[69] Anastasia Nezhentseva, Eigil V. Sørensen, Lars V. Andersen, Frank Schuler, “Distribution and Orientation of Steel Fibres in UHPFRC”, DCE Technical Report No. 151, Aalborg University, Department of Civil Engineering, Division for Structures, Materials and Geotechnics, April 2013.

[70] Spasojević A. (2008), “Structural Implications of Ultra-High Performance Fibre-Reinforced Concrete in Bridge Design”, Ingénieur Civil Diplômée de l'Université de Niš, Serbie et de Nationalitéserbe.

APPENDIX A: MATERIAL PROPERTIES

A1. Compressive stress-strain diagrams of Normal concrete [75x150 mm cylinders], each plot shows one specimens.

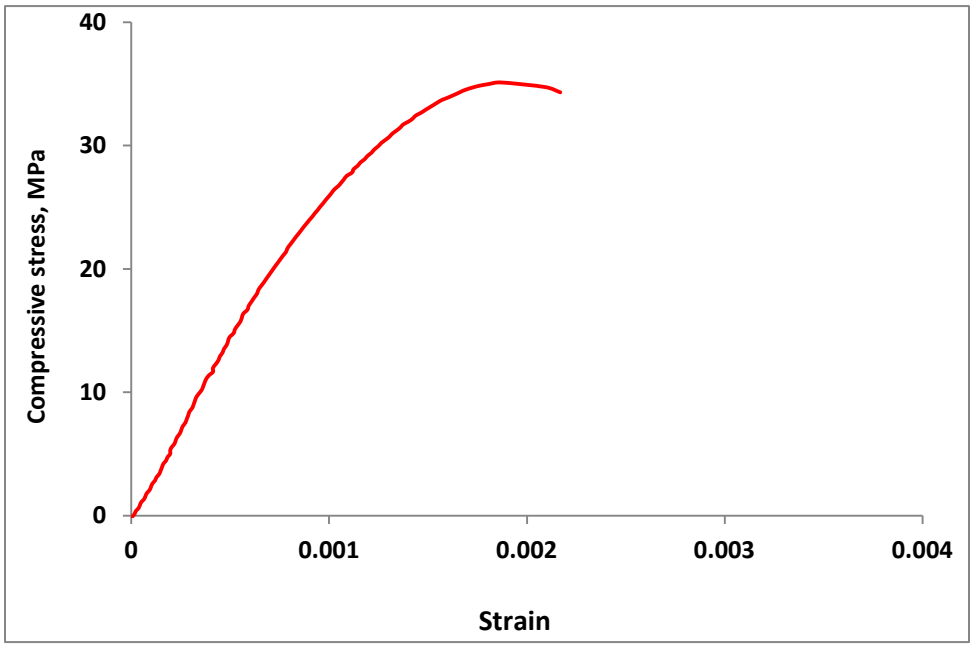

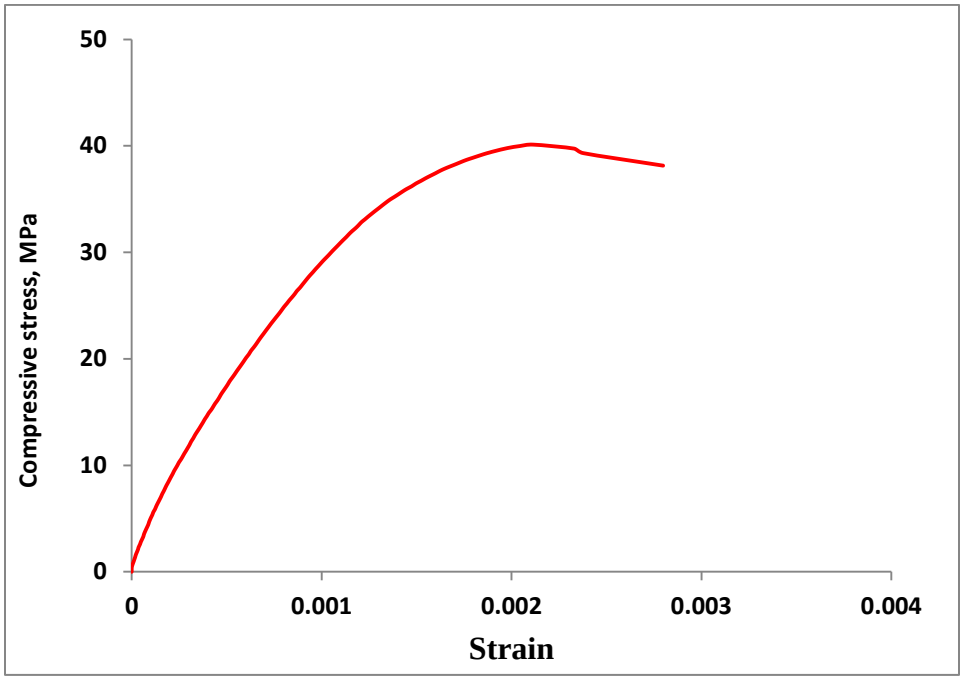

A2. Compressive stress-strain diagrams of UHPC [75x150 mm cylinders], each plot shows two specimens.

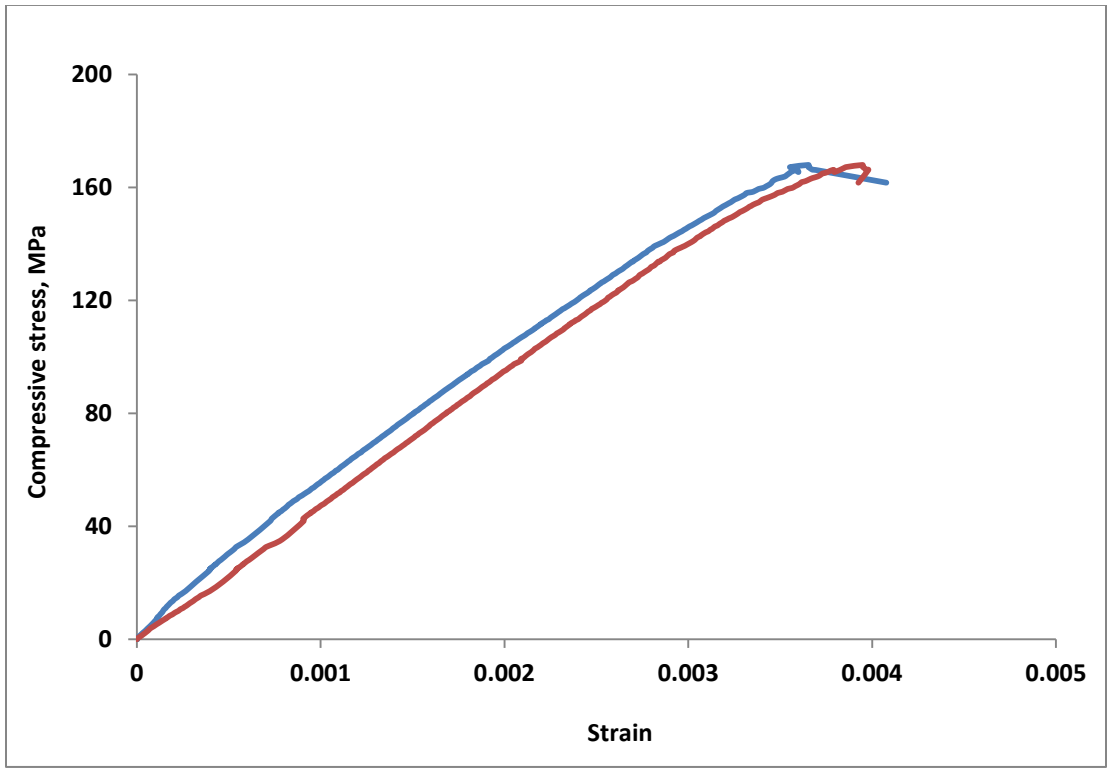

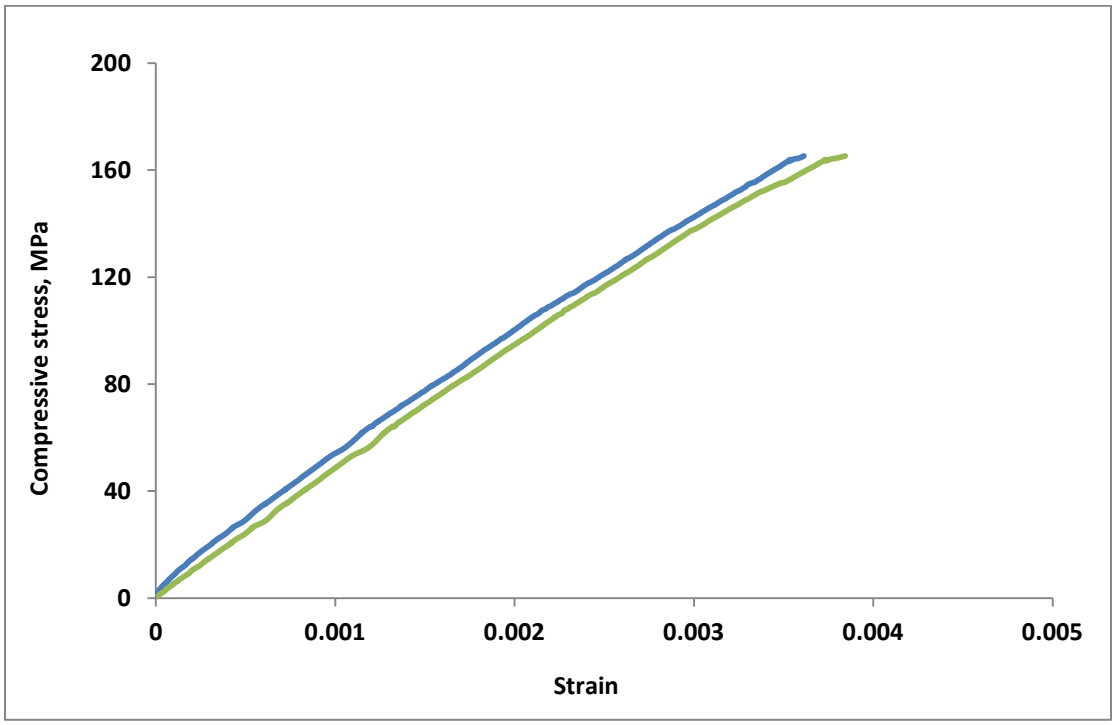

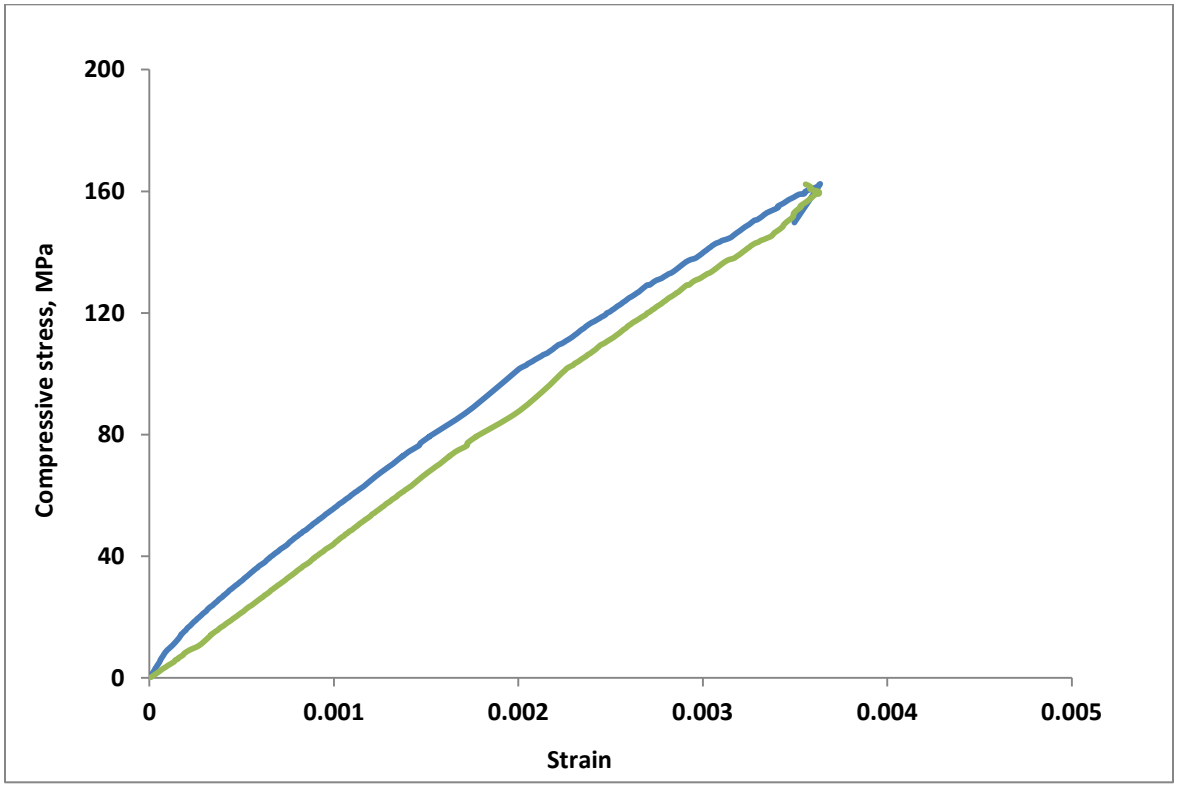
200
160
120
80
40
0
Compressive stress, MPa
0
0.001
0.002
0.003
0.004
0.005
Strain

A3. Flexural strength of UHPC prisms [40x40x160 mm prisms]. (Load-deflections curves), each plot shows three specimens from same mix.

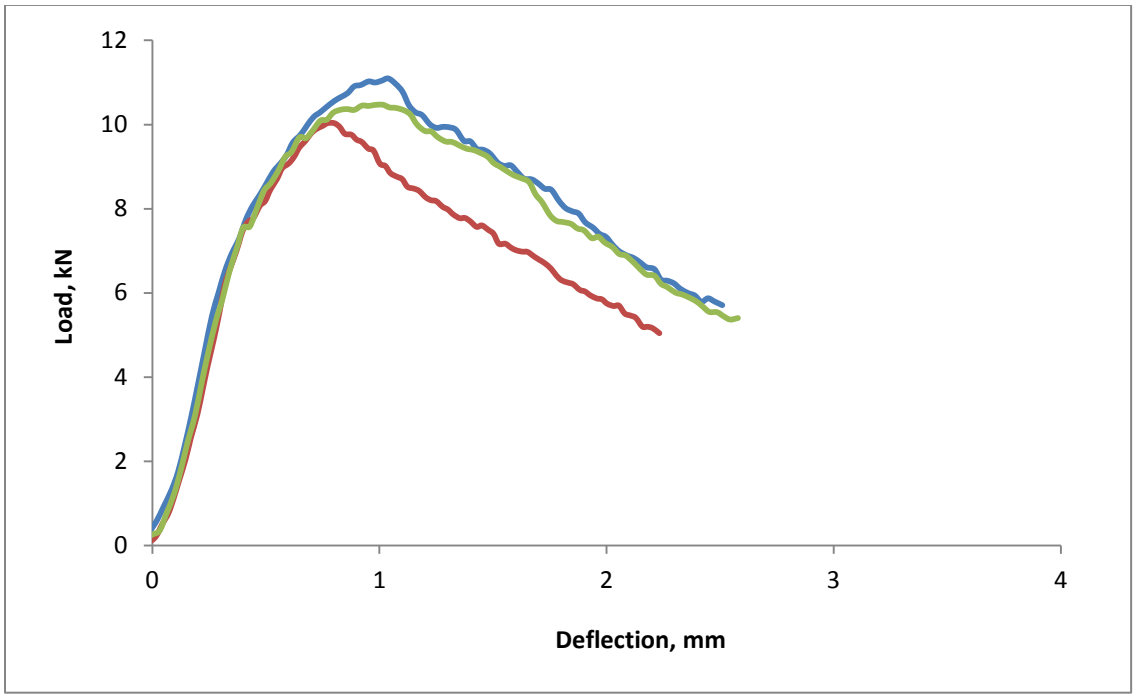

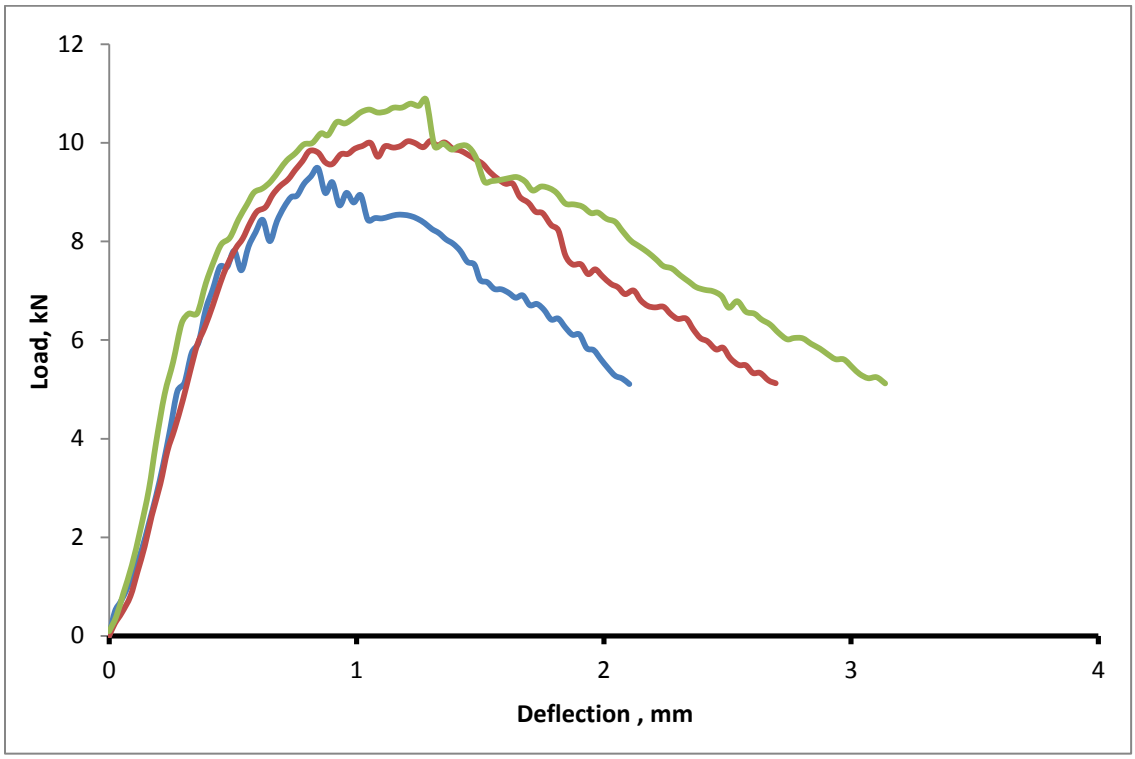

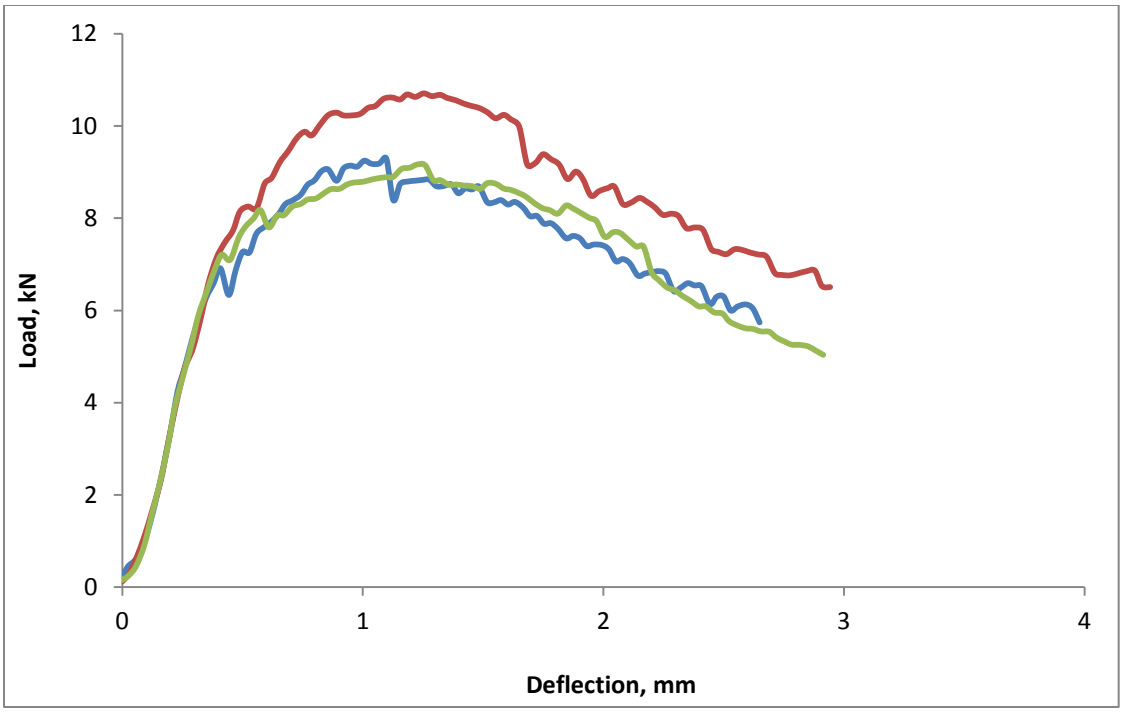
12
10
8
6
4
2
0
Load, kN
0
1
2
3
4
Deflection, mm

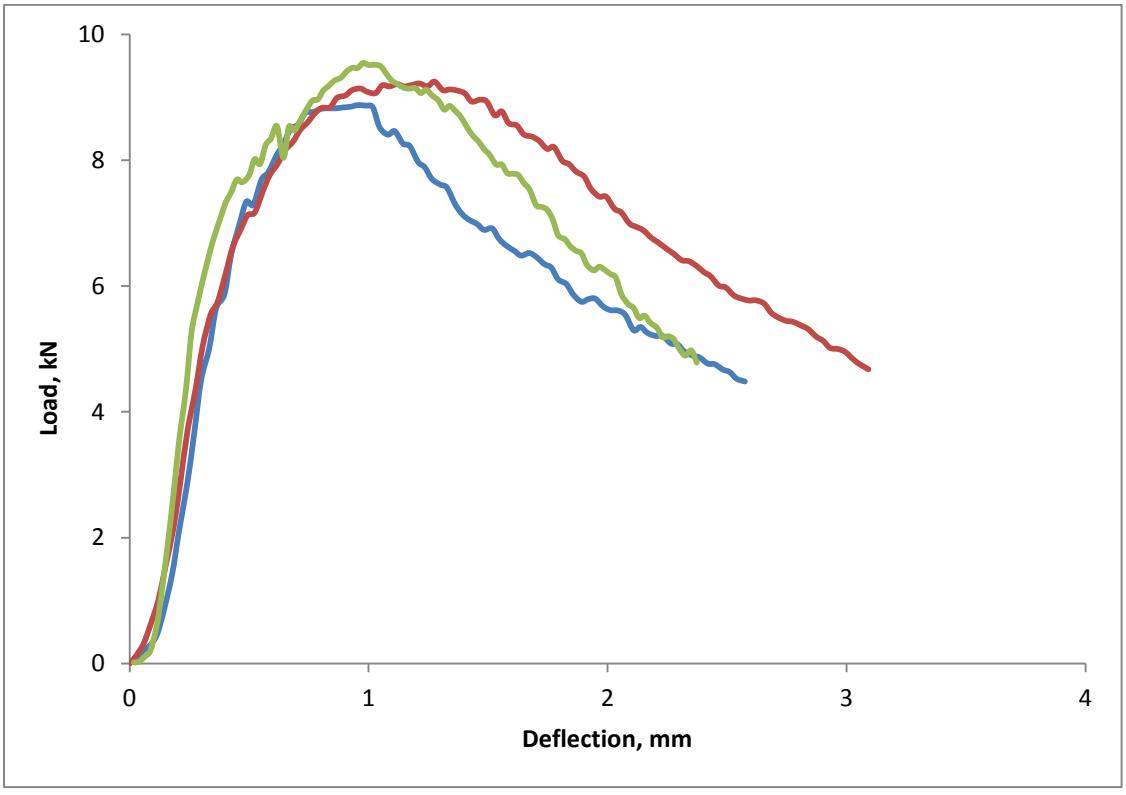
10
8
6
4
2
0
Load, kN
0
1
2
3
4
Deflection, mm

APPENDIX B: HYBRID NC-UHPC LAYERED SPECIMENS

B.1.1: Load-deflections curve for three specimens of Group A with 20 mm thick UHPC layer of beam size 150x150x760 mm.

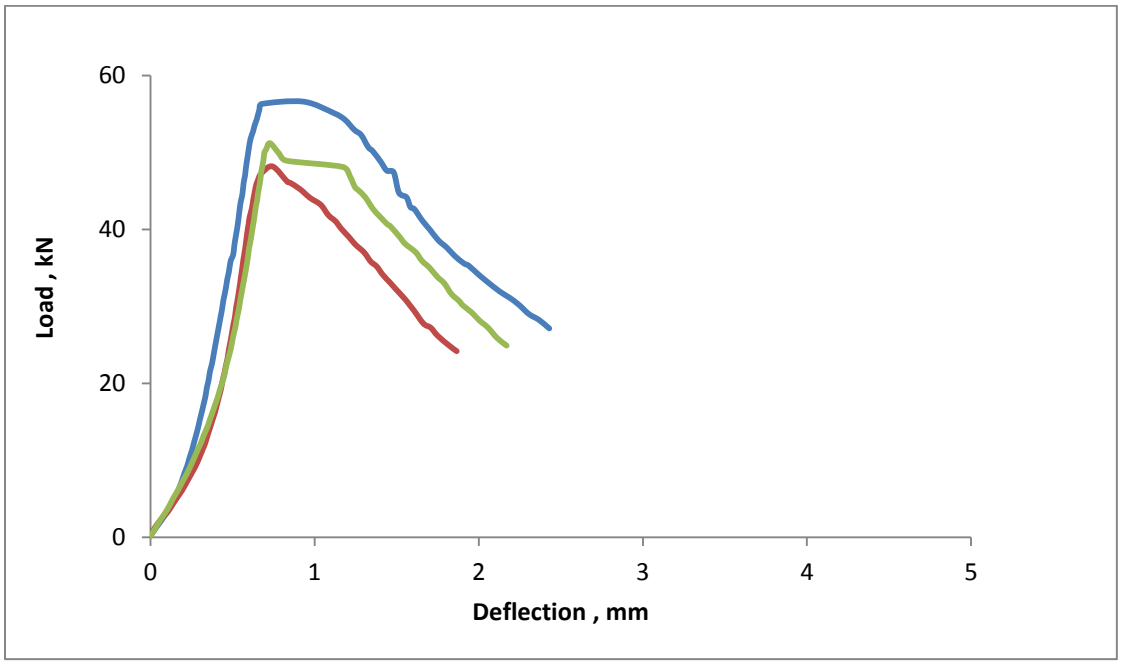

B.1.2: Load-deflections curve for three specimens of Group A with 40 mm thick UHPC layer of beam size 150x150x760 mm.

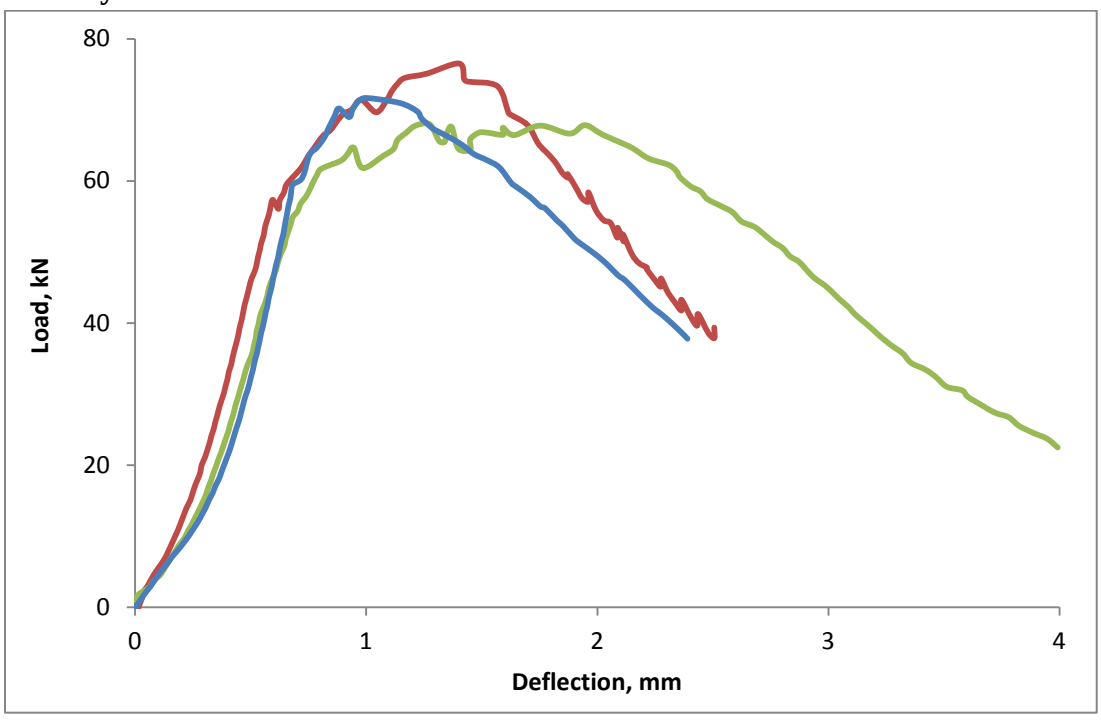

B.1.3: Load-deflections curve for three specimens of Group B with 20 mm thick UHPC layer of beam size 150x150x1000 mm.

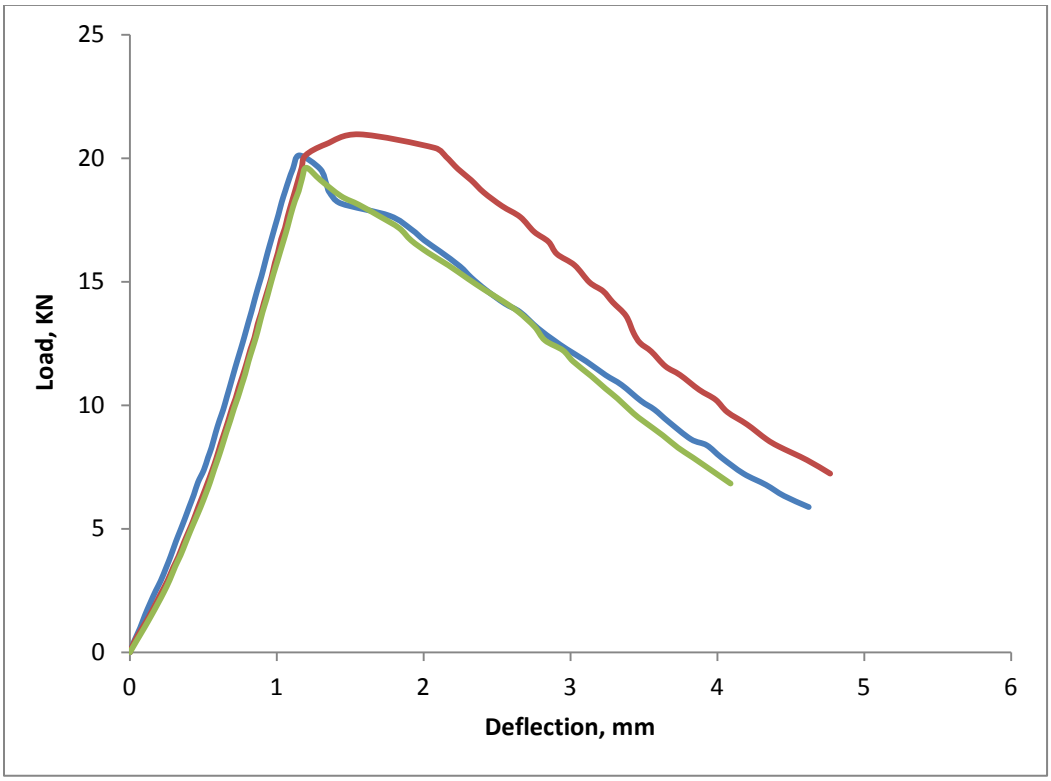

B.1.4: Load-deflections curve for three specimens of Group B with 40 mm thick UHPC layer of beam size 150x150x1000 mm.

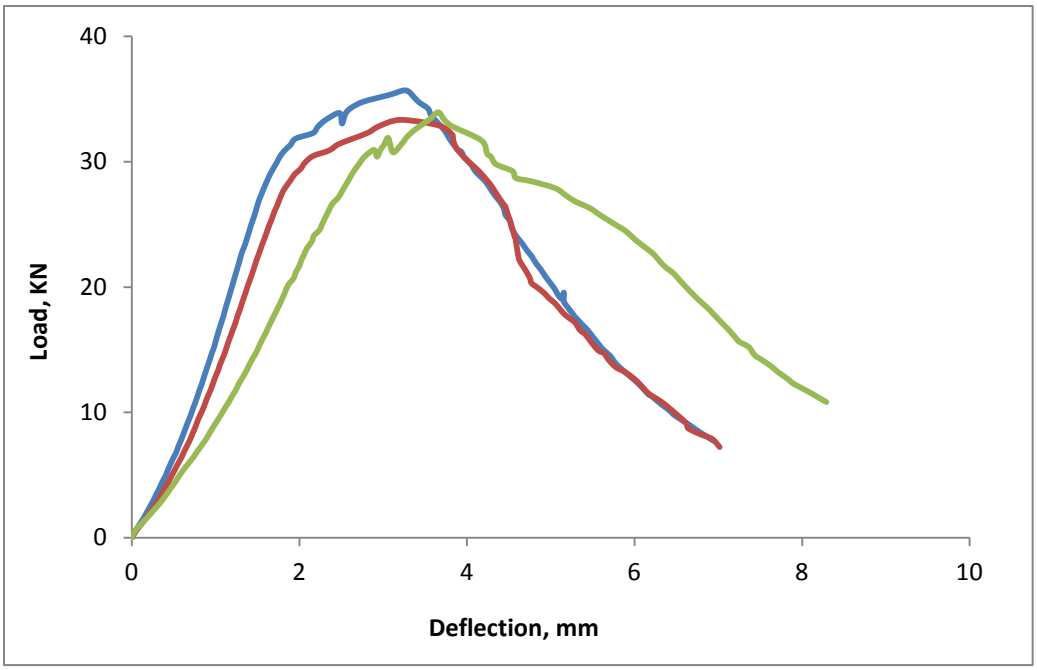

B.1.5: Load-deflections curve for three specimens of Group C with 25 mm thick UHPC layer of beam size 150x200x900 mm.

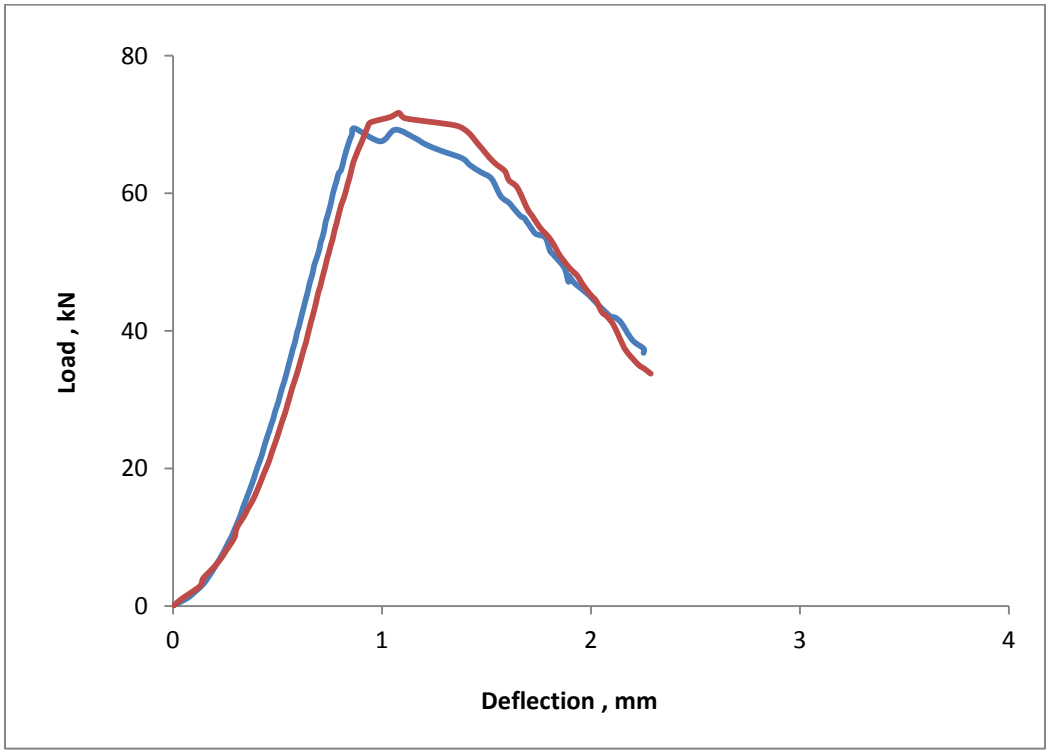

B.1.6: Load-deflections curve for three specimens of Group C with 50 mm thick UHPC layer of beam size 150x200x900 mm.

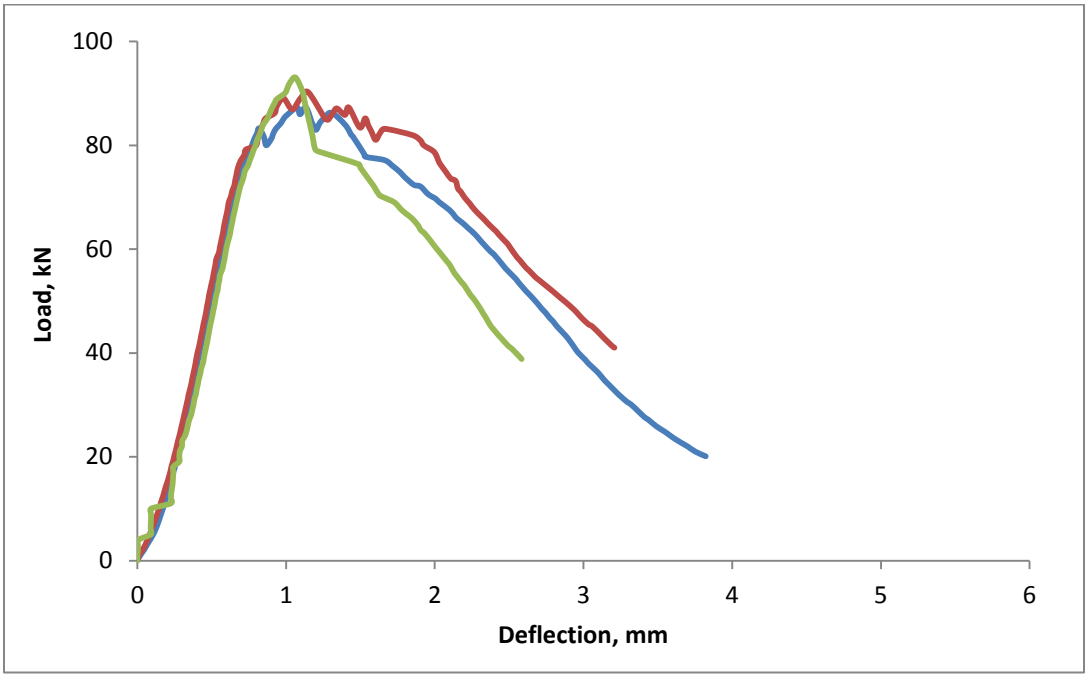

B.1.7: Load-deflections curve for three specimens of Group D with 25 mm thick UHPC layer of beam size 150x200x1200 mm.

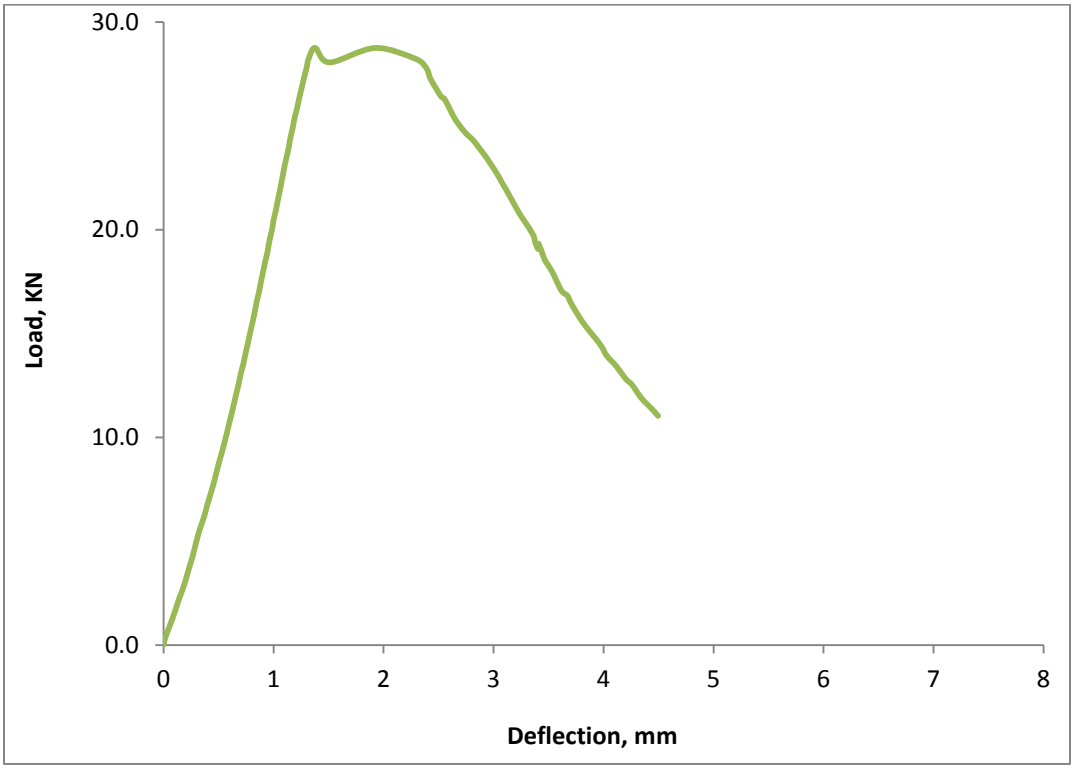

B.1.8: Load-deflections curve for three specimens of Group D with 50 mm thick UHPC layer of beam size 150x200x1200 mm.

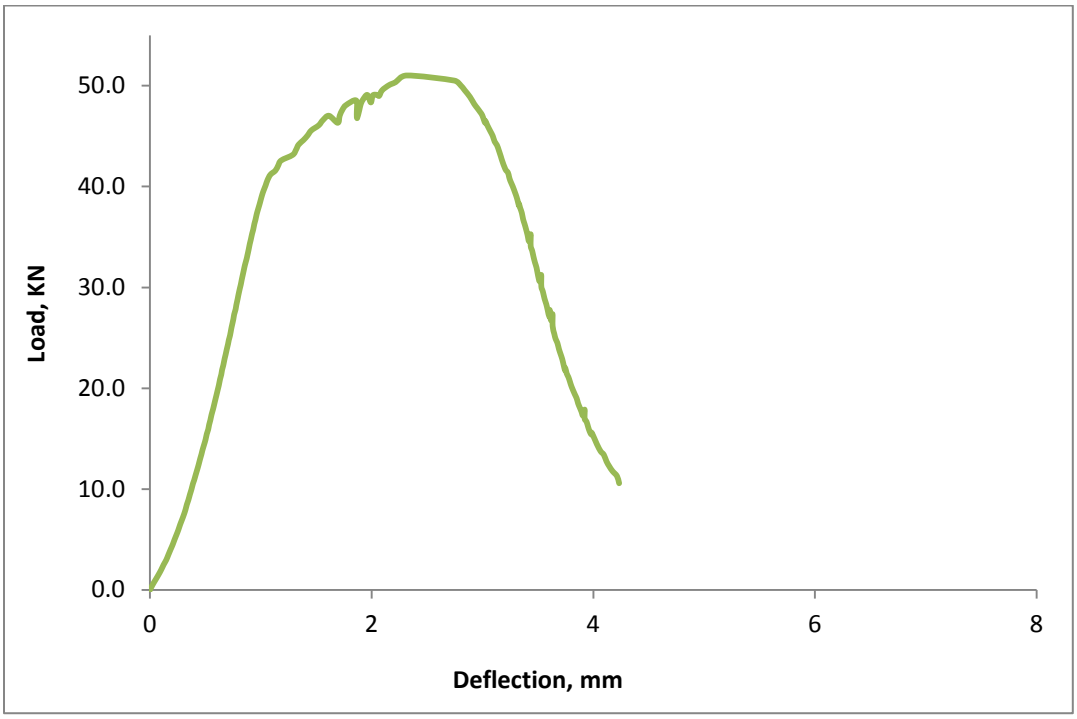

B.2.1: Load-strain curve for three specimens of Group B with 20 mm thick UHPC layer of beam size 150x150x1000 mm. Each plot shows one specimens with 4 strain location.

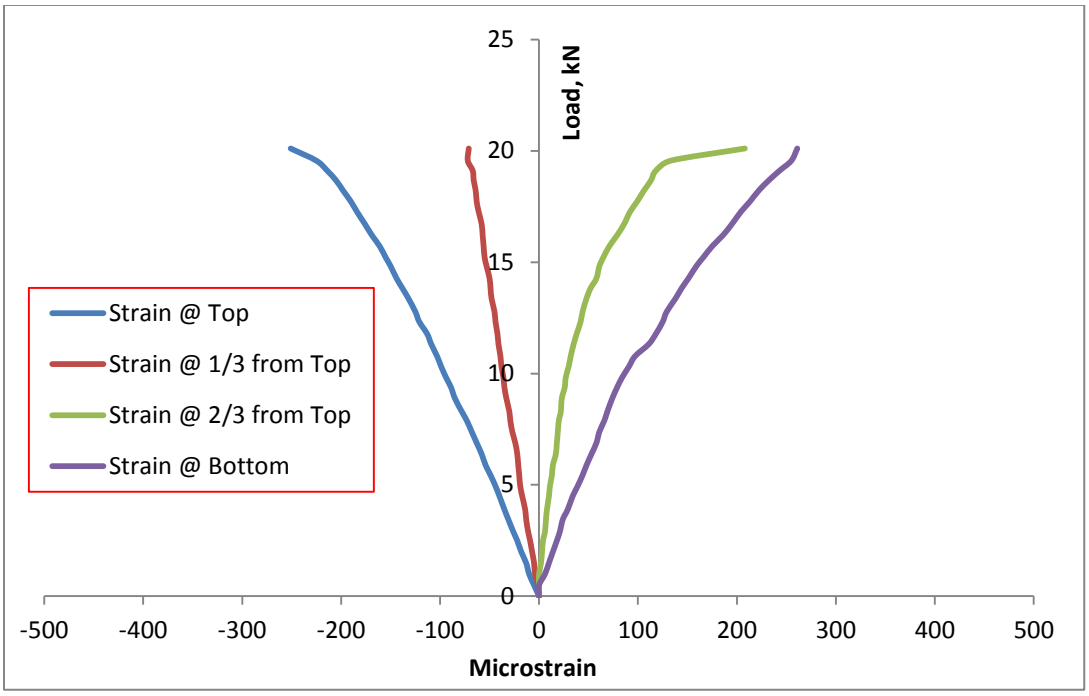

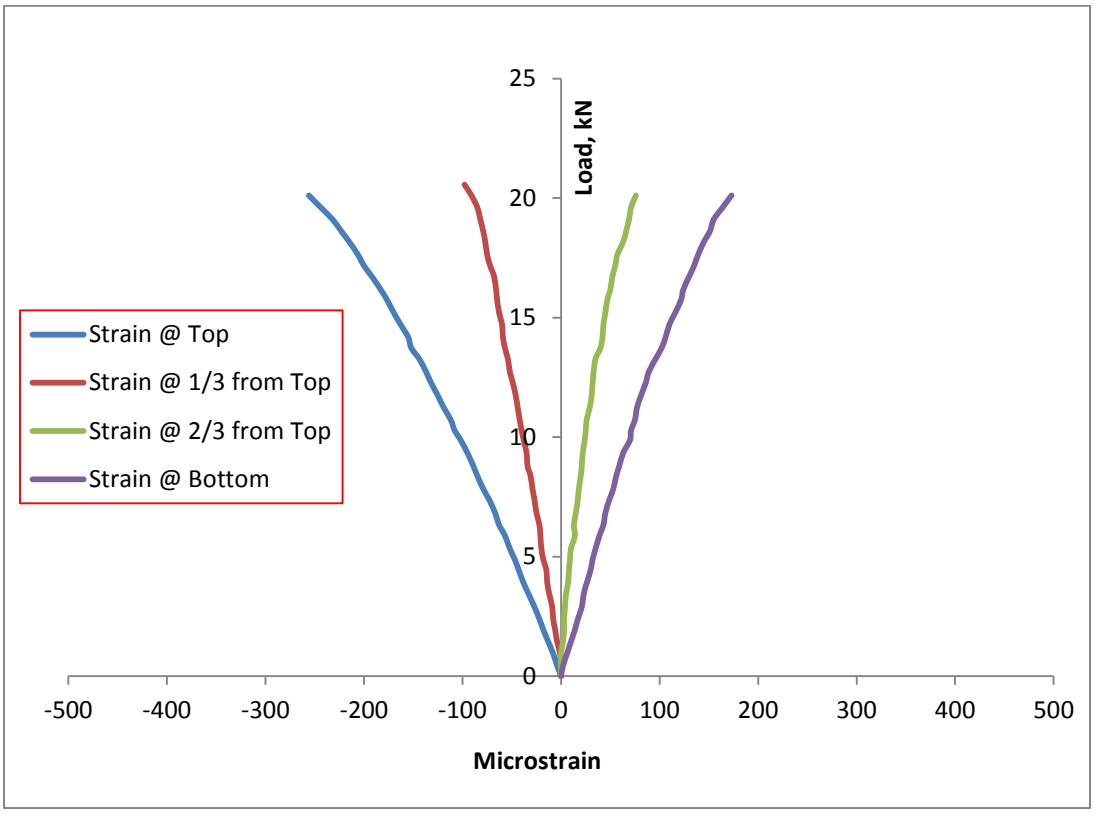

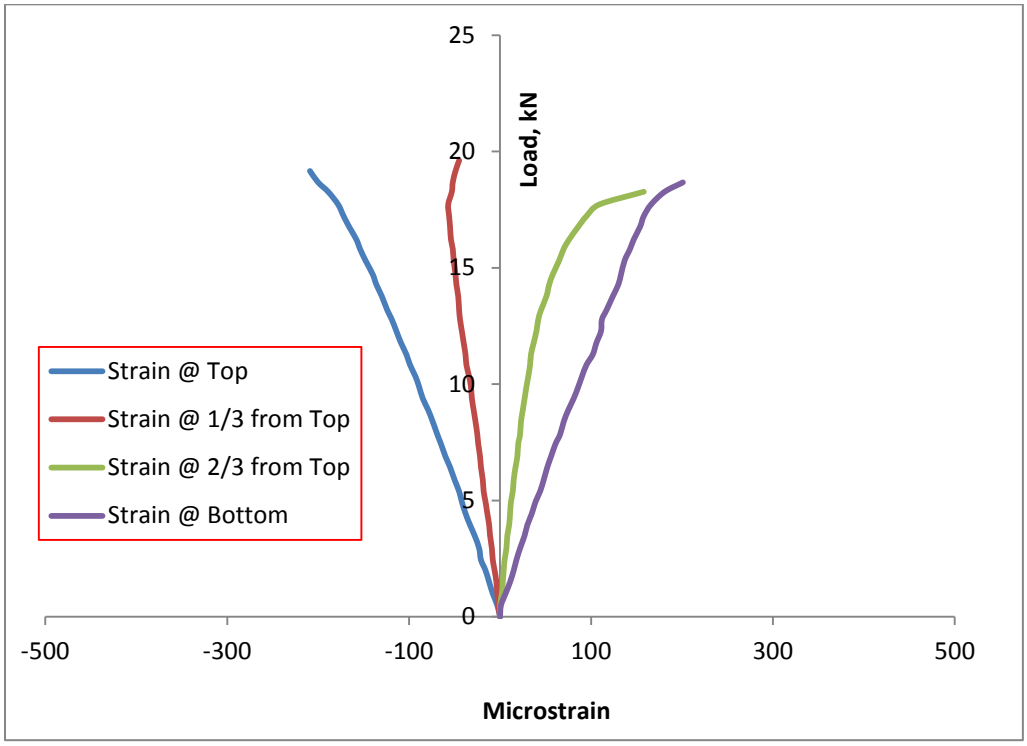

B.2.3: Load-strain curve for three specimens of Group D with 25 mm thick UHPC layer of beam size 150x200x1200 mm. Each plot shows one specimens with 4 strain location.

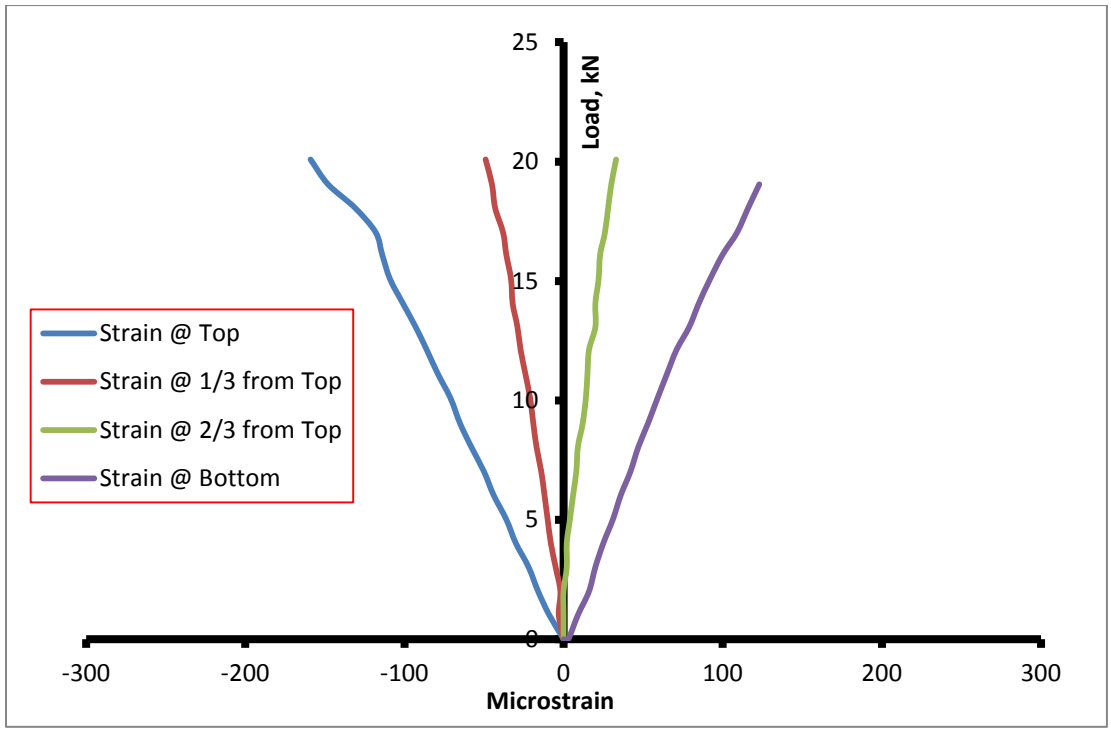

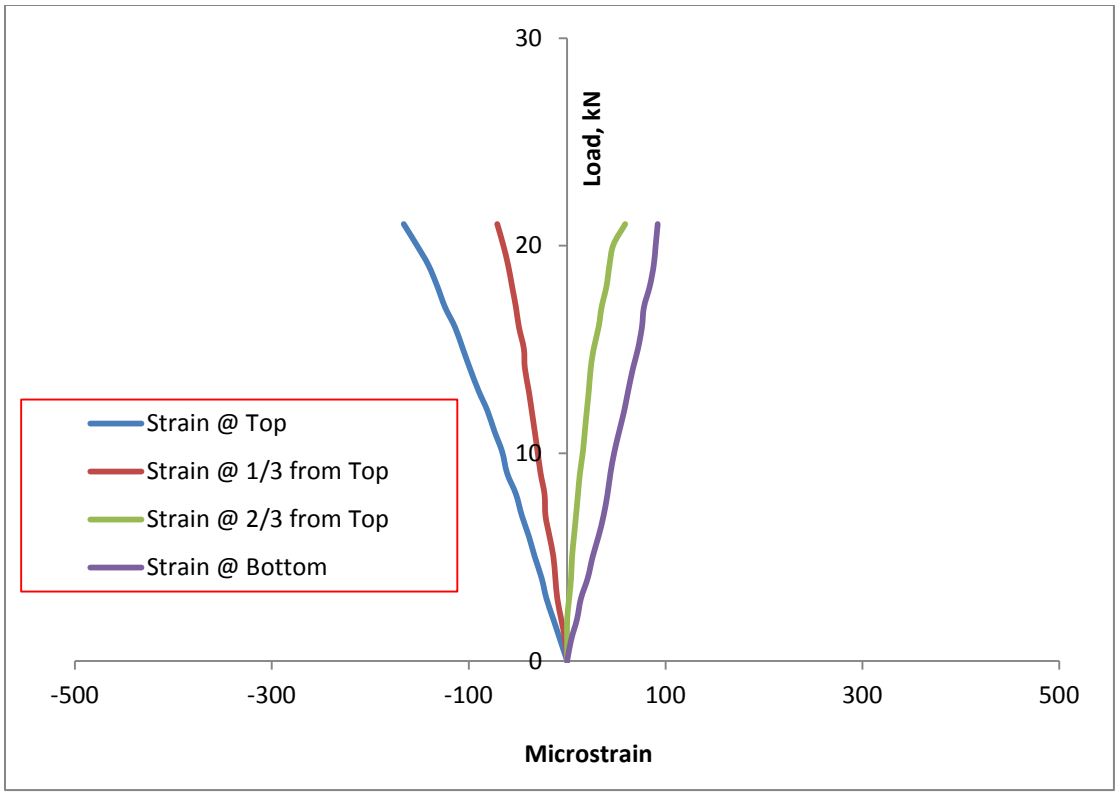

B.2.4: Load-strain curve for three specimens of Group D with 50 mm thick UHPC layer of beam size 150x200x1200 mm. Each plot shows one specimens with 4 strain location.

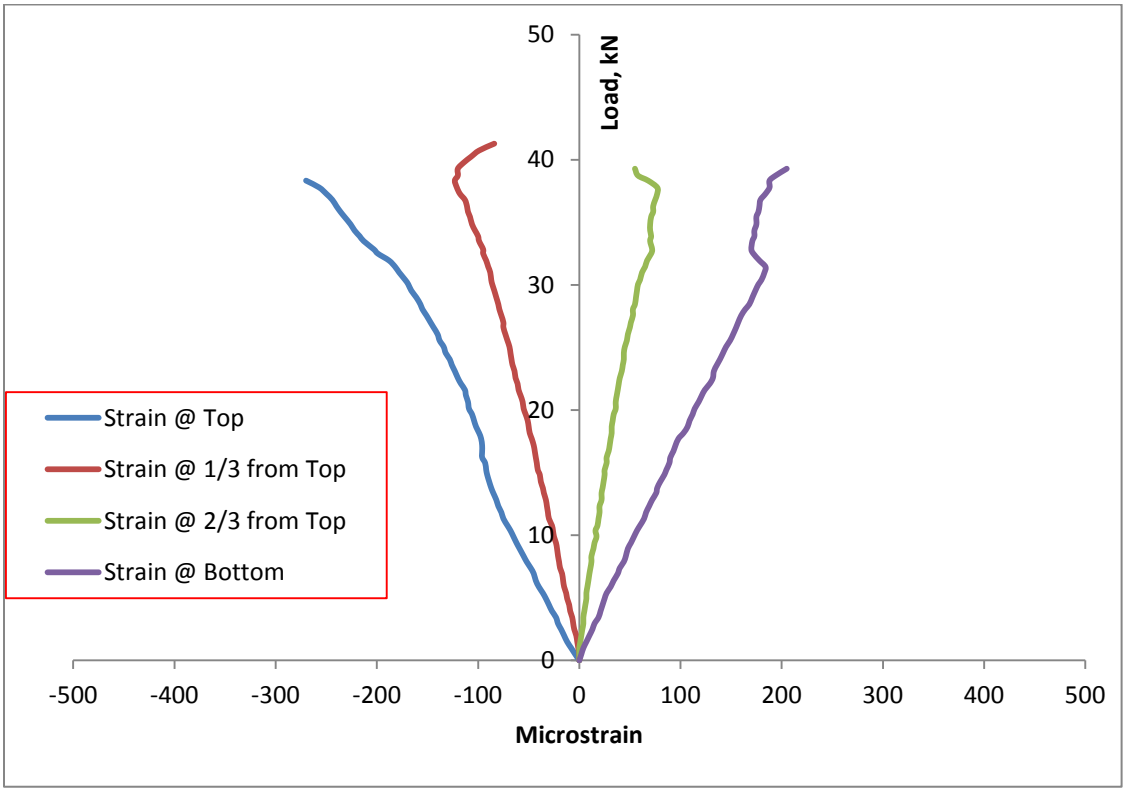

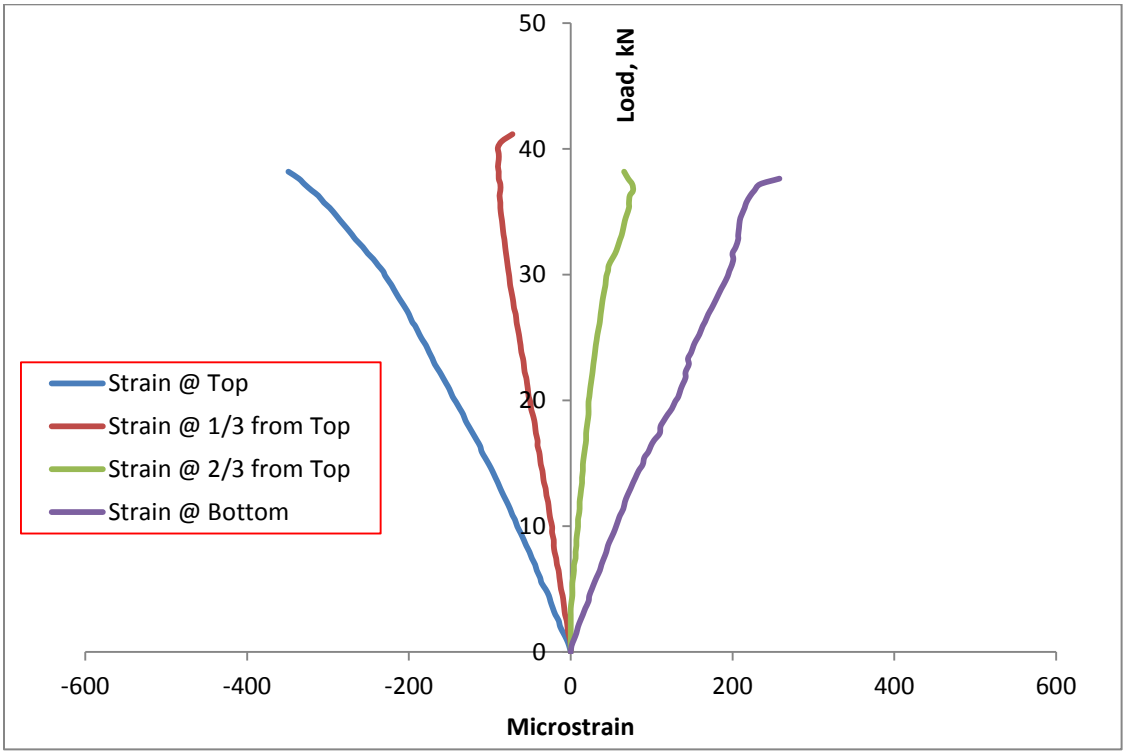

B.3.1: Strain profile along the depth for three specimens of Group B with 20 mm thick UHPC layer of beam size 150x150x1000 mm. Each plot shows one specimens.

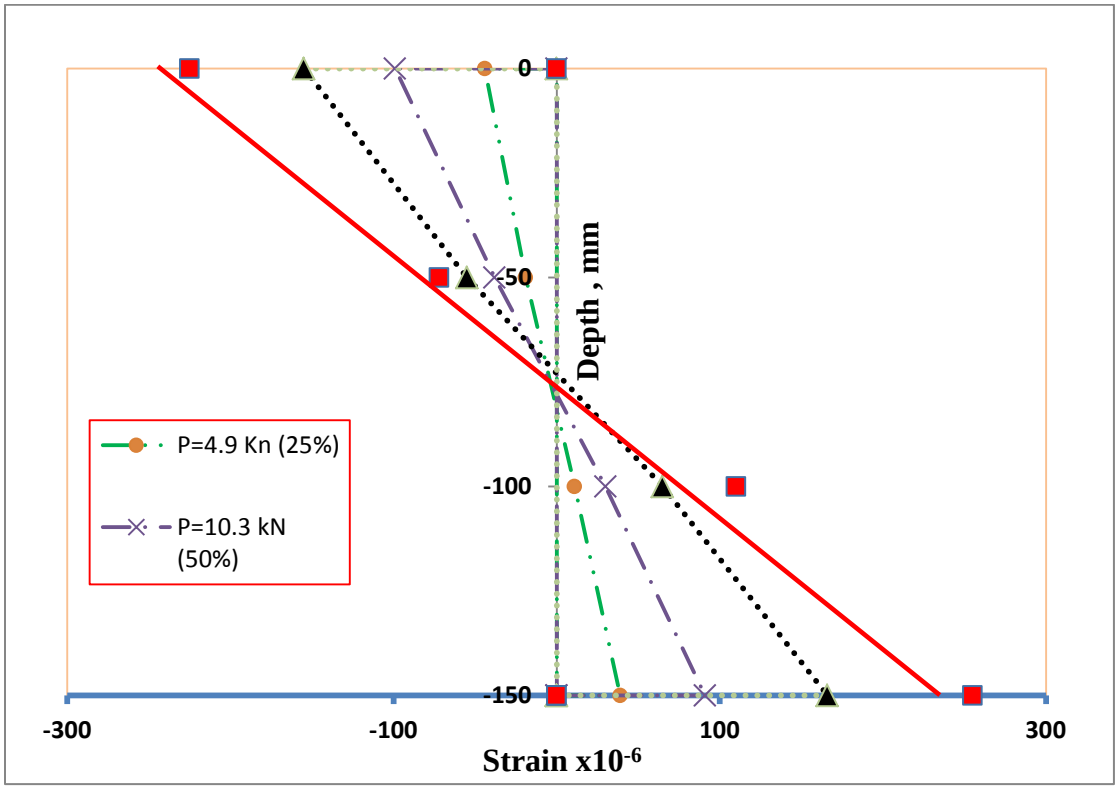

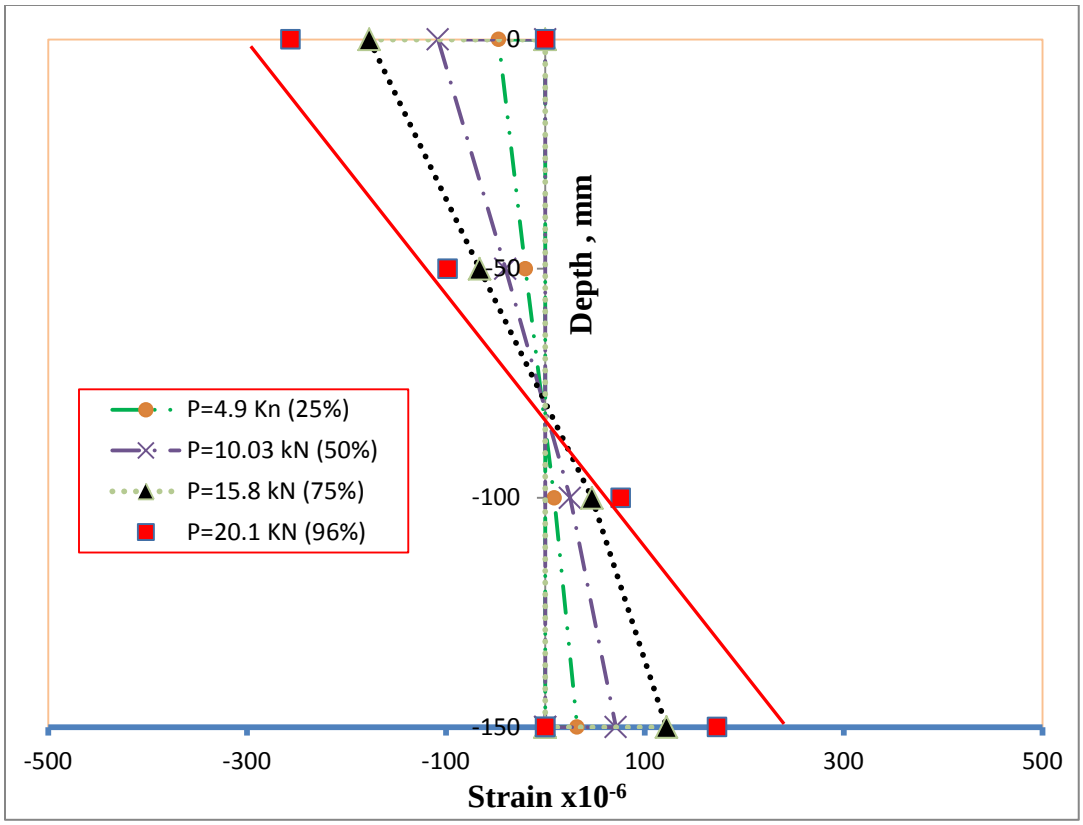
0
-50
-100
-150
Depth , mm
P=4.9 Kn (25%)
P=10.03 kN (50%)
P=15.8 kN (75%)
P=20.1 KN (96%)
-500
-300
-100
100
300
500
Strain x10-6

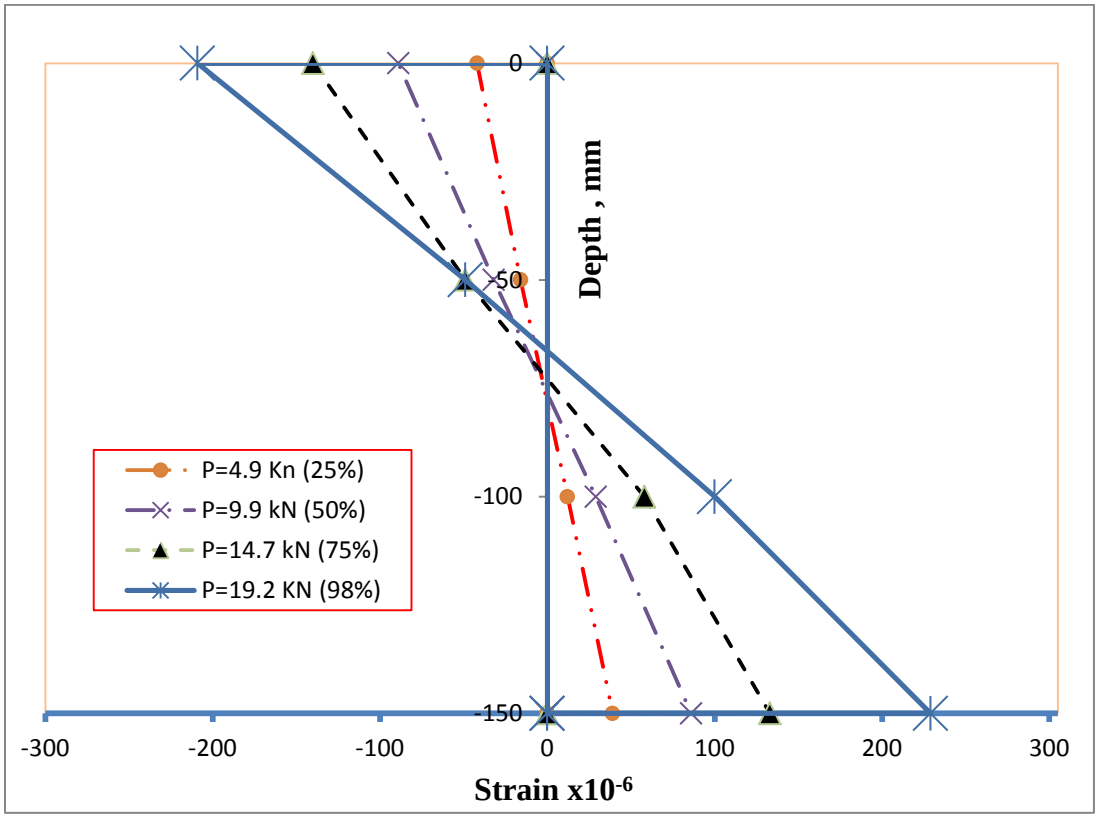
0
-50
-100
-150
Depth , mm
P=4.9 Kn (25%)
P=9.9 kN (50%)
P=14.7 kN (75%)
P=19.2 KN (98%)
-300
-200
-100
0
100
200
300
Strain x10-6

B.3.2: Strain profile along the depth for three specimens of Group B with 40 mm thick UHPC layer of beam size 150x150x1000 mm. Each plot shows one specimens

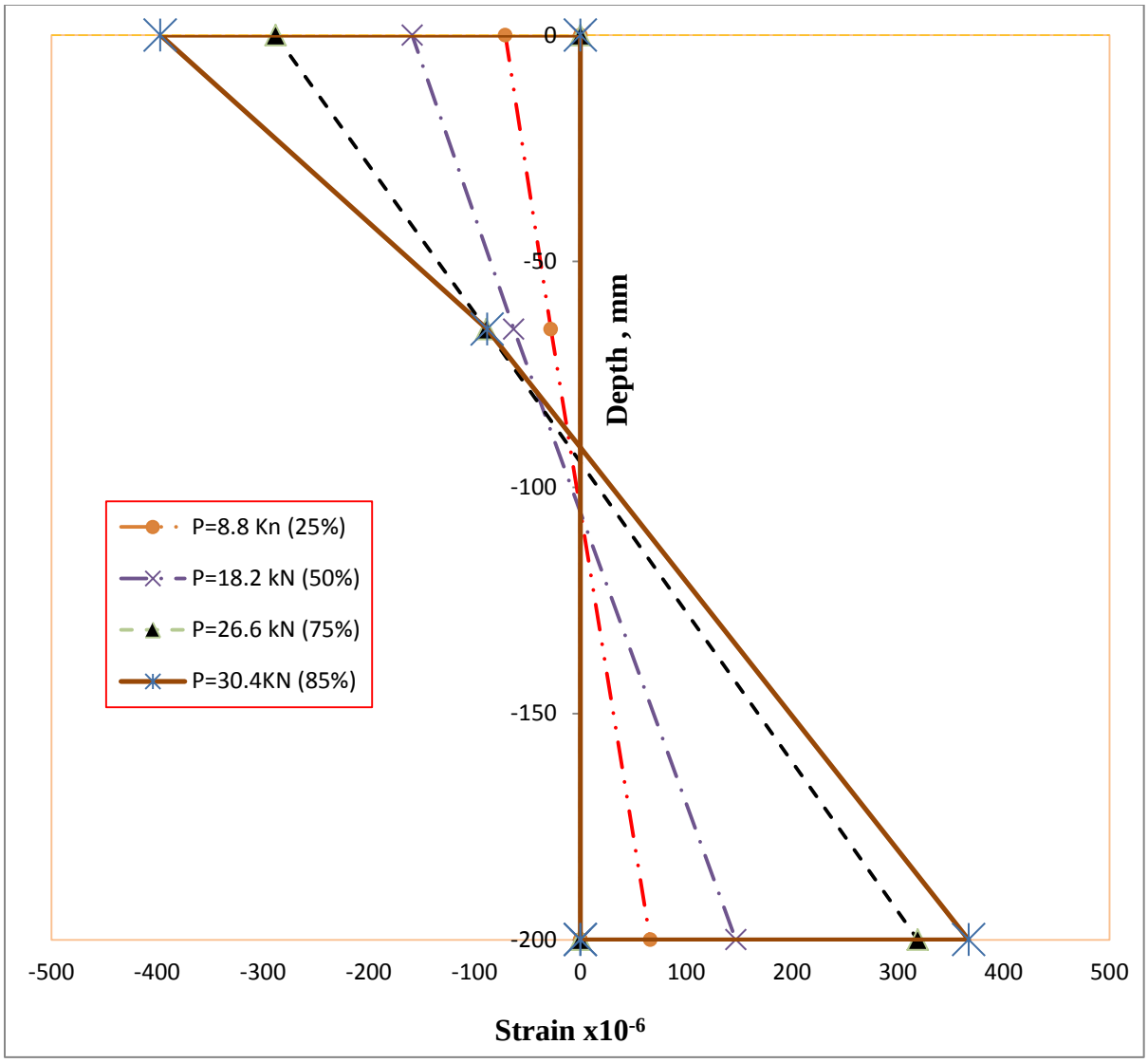

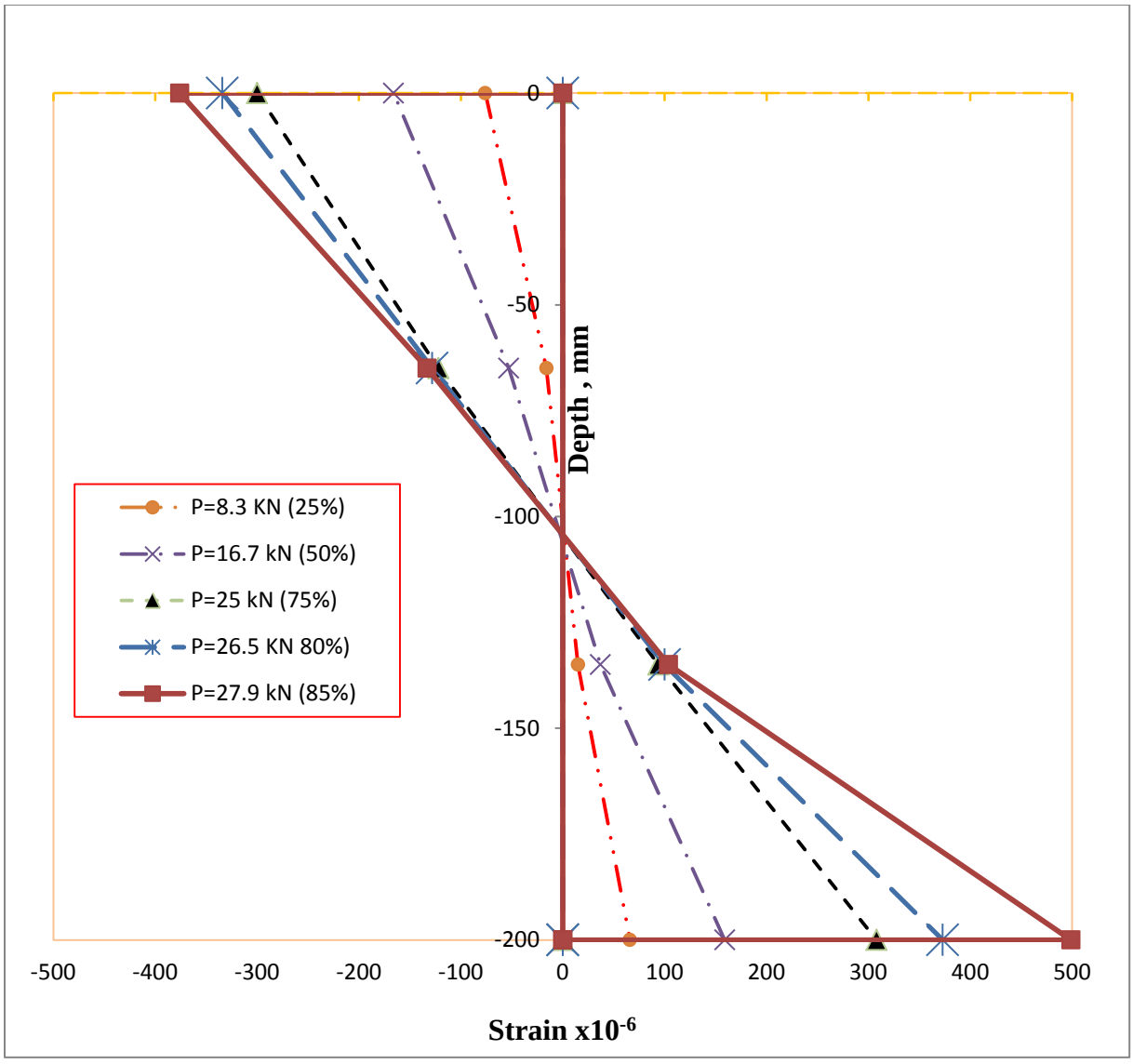
0
-50
-100
-150
-200
Depth , mm
-500
-400
-300
-200
-100
0
100
200
300
400
500
Strain x10-6
P=8.3 KN (25%)
P=16.7 kN (50%)
P=25 kN (75%)
P=26.5 KN 80%)
P=27.9 kN (85%)

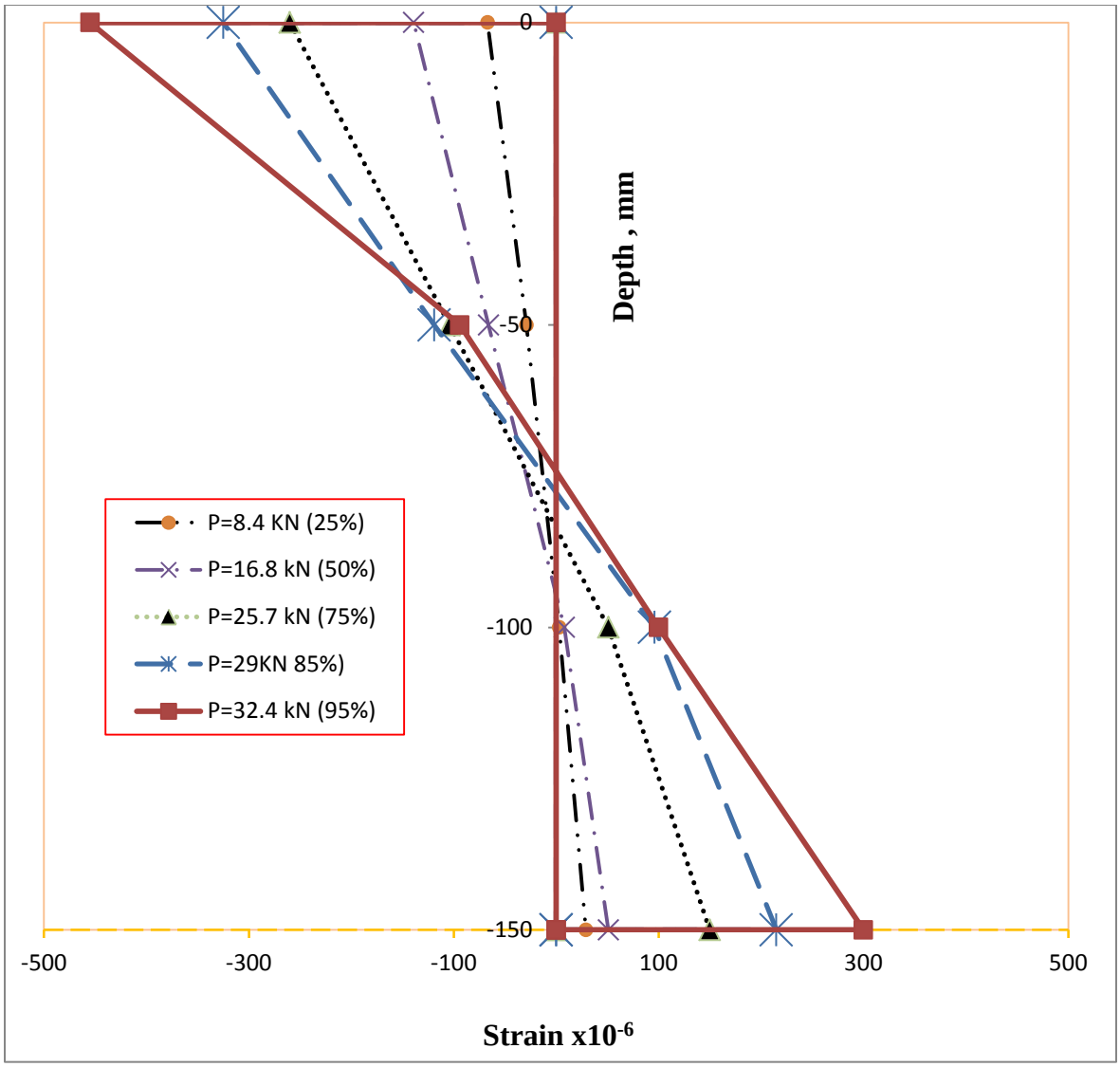
0
-50
-100
-150
Depth , mm
-500
-300
-100
100
300
500
Strain x10-6
P=8.4 KN (25%)
P=16.8 kN (50%)
P=25.7 kN (75%)
P=29KN 85%)
P=32.4 kN (95%)

B.3.3: Strain profile along the depth for three specimens of Group D with 25 mm thick UHPC layer of beam size 150x200x1200 mm. Each plot shows one specimens

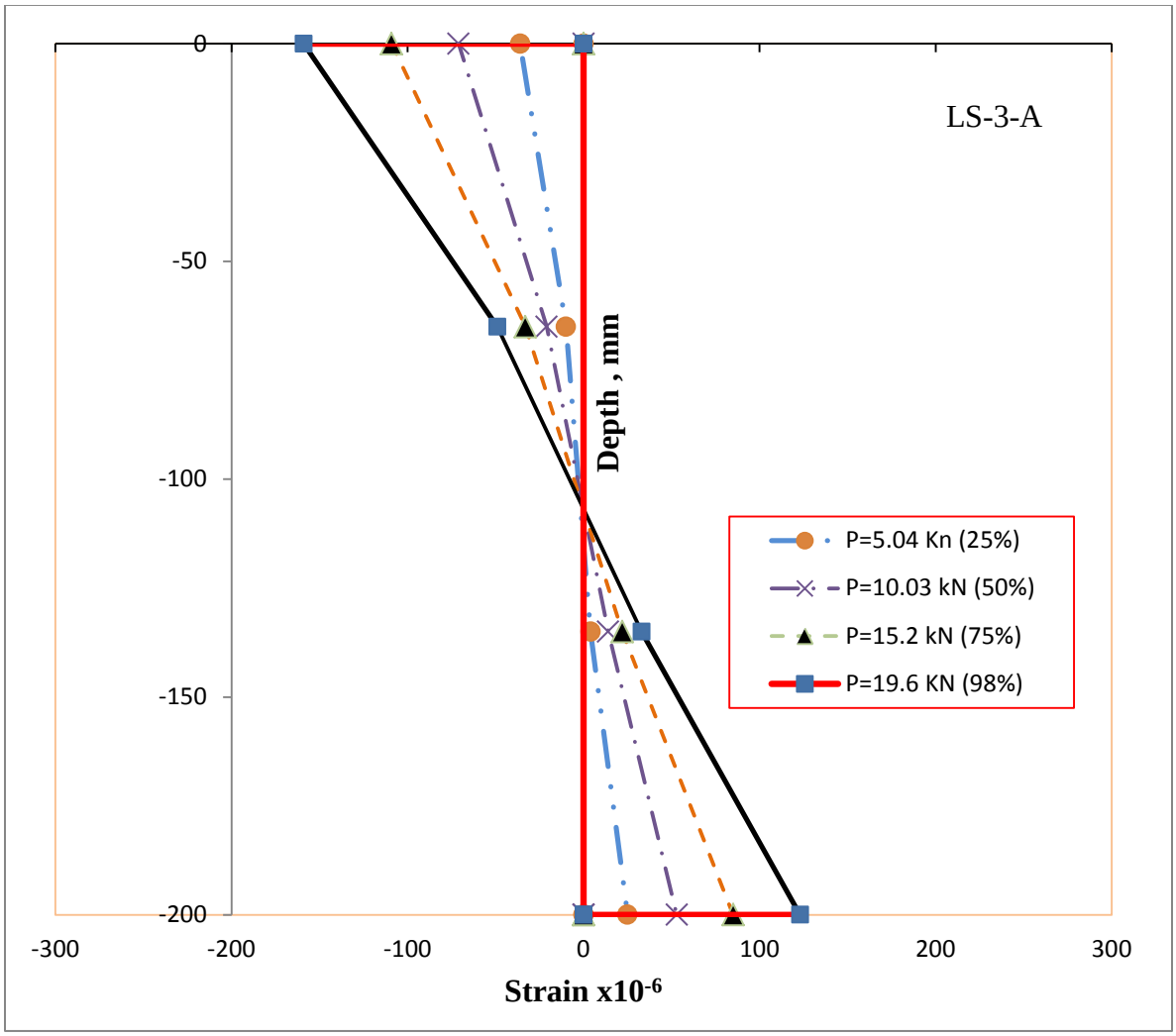

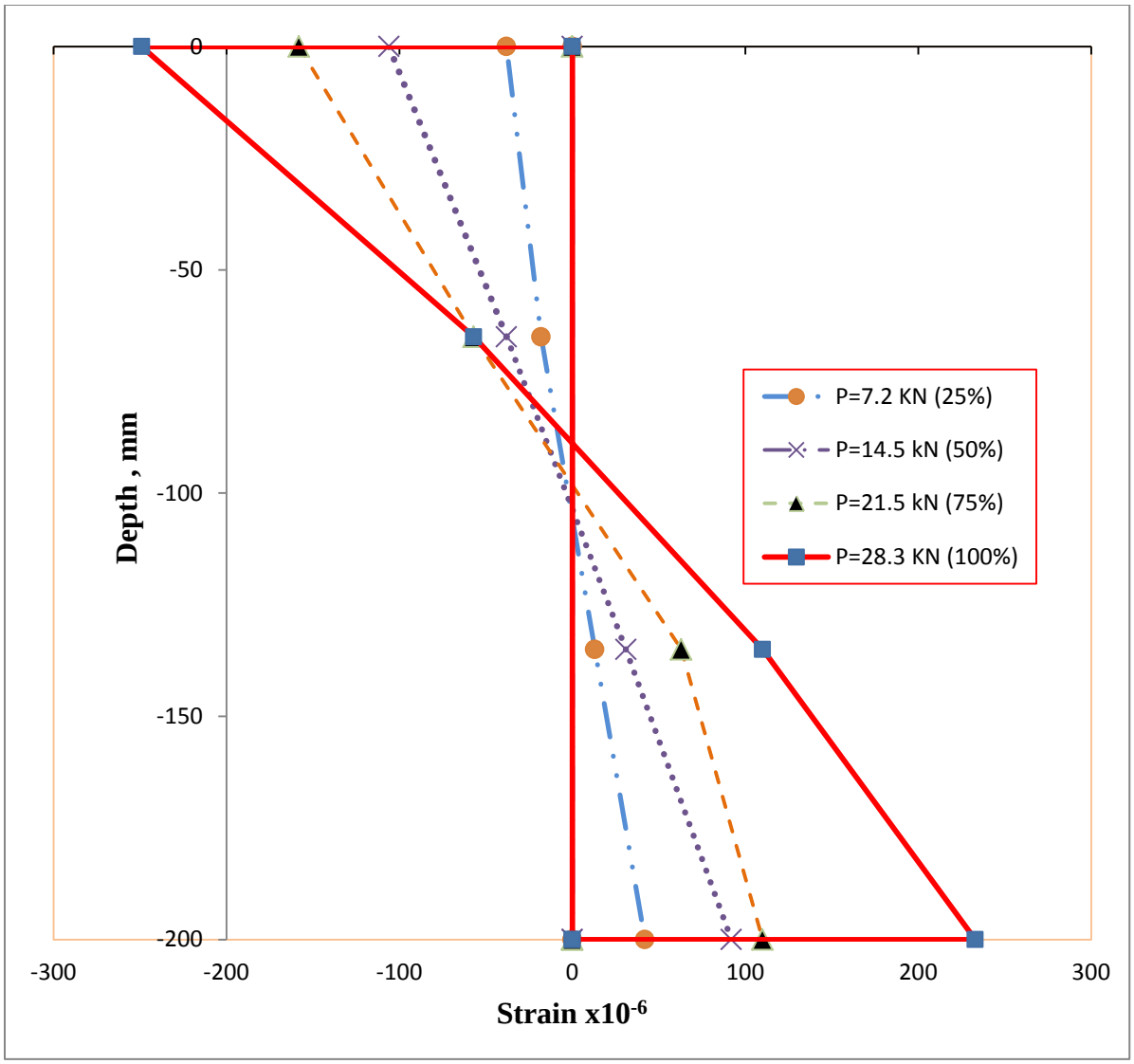
0
-50
-100
-150
-200
Depth , mm
-300
-200
-100
0
100
200
300
Strain x10-6
P=7.2 KN (25%)
P=14.5 kN (50%)
P=21.5 kN (75%)
P=28.3 KN (100%)

B.3.4: Strain profile along the depth for three specimens of Group D with 50 mm thick UHPC layer of beam size 150x200x1200 mm. Each plot shows one specimens.

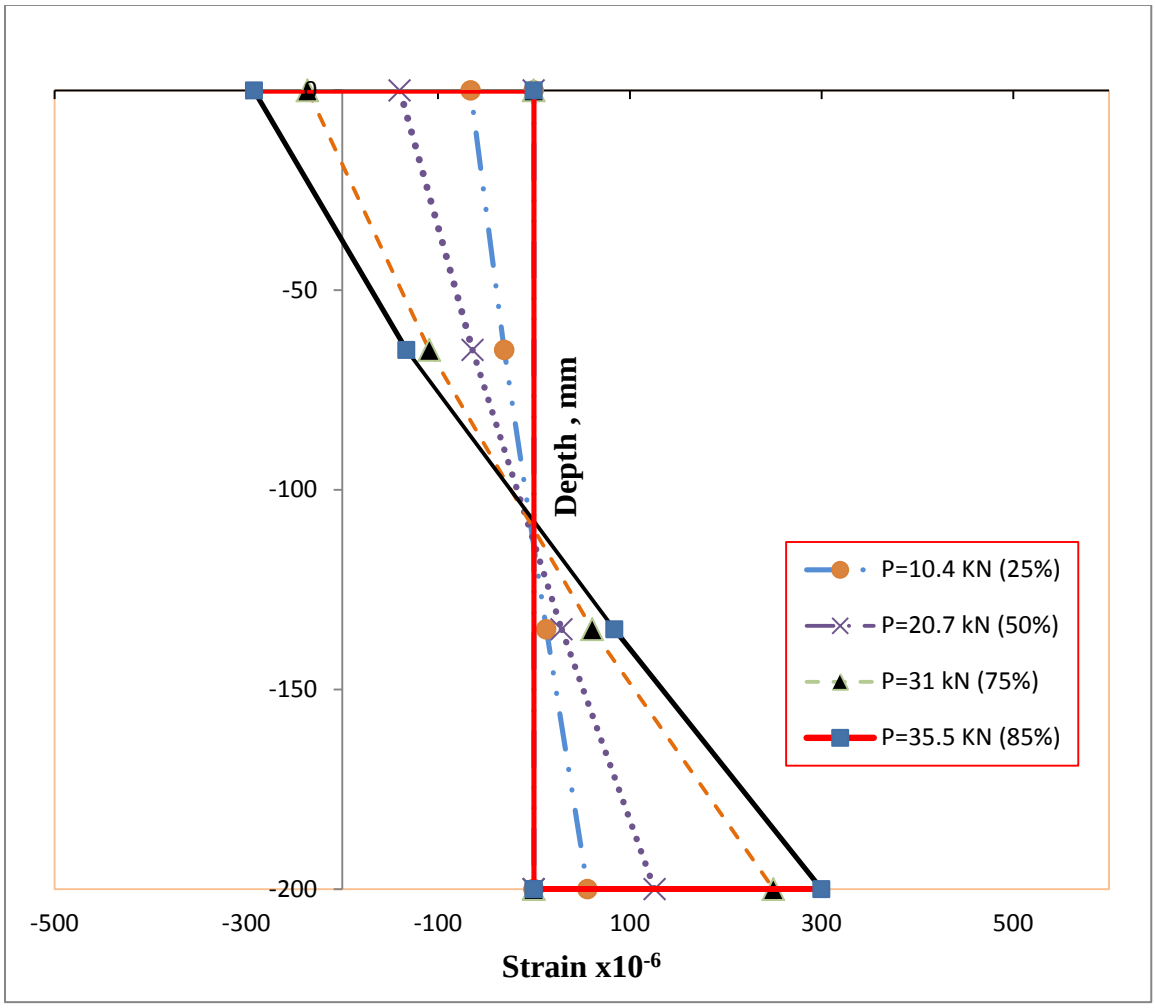

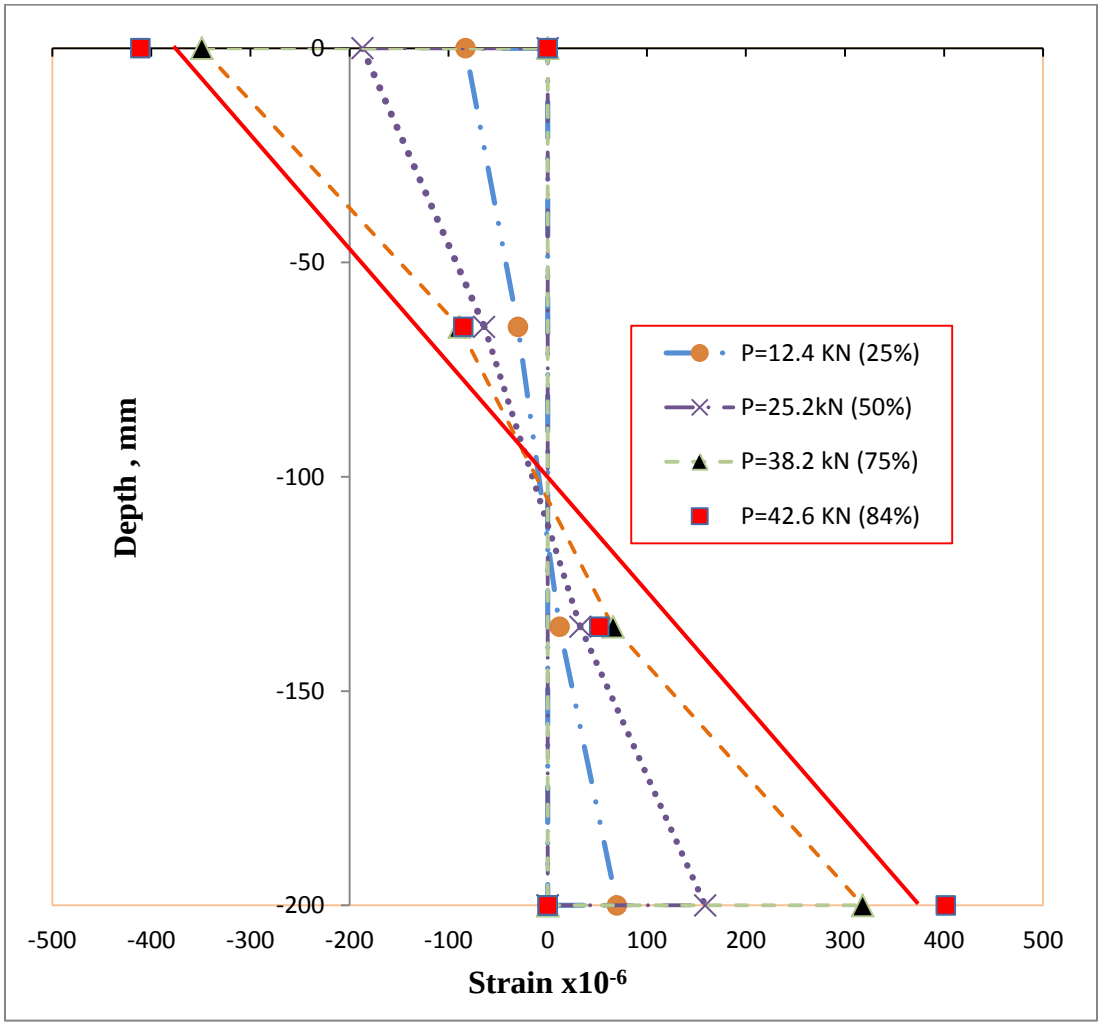
0
-50
-100
-150
-200
Depth , mm
-500
-400
-300
-200
-100
0
100
200
300
400
500
Strain x10-6
P=12.4 KN (25%)
P=25.2kN (50%)
P=38.2 kN (75%)
P=42.6 KN (84%)

B.4.1: Load levels and strain values for three specimens of Group A with 20 mm thick UHPC layer of beam size 150x150x760 mm.

Beam ID	UHPC thickness mm	Size mm	load level, KN	% of P_U	Measured strain, microstrain				X, from Top, mm	
					Top	1/3 from top	2/3 from top	Bottom	Measured	Calculated
LS-A-C2-S1	20	150x150x760	12.15	25	-21	-8	14	22	69	81
			24.15	50	-47	-15	27	35	68	81
			36.49	75	-69	-23	43	52	67	81
			41.13	85	-81	-29	60	102	65	81
			47.15	98	-89	-56	310	327	58	71
			48.3	100	-80	-59	399	393	57	71
LS-A-C2-S2	20	150x150x760	12.3	25	-58	-24	8	54	81	81
			24.17	50	-119	-47	20	111	81	81
			36.56	75	-119	-70	36	262	72	81
			42.46	85	-231	-80	56	355	69	81
			48.39	90	-283	-83	112	461	65	71
			54.3	100	-	-	-	-	-	71

B.4.2: Measured and computed stresses for selected load levels of beams for three specimens of Group A with 20 mm thick UHPC layer of beam size 150x150x760 mm.

Beam ID	UHPC thick., mm	Size , mm	load level, KN	% of load	Measured stress , Mpa		Calculated stress, MPa			
							Bottom		Top	
					Bottom	Top	Cracked	Uncracked	Cracked	Uncracked
LS-A-C2-S1	20	150x150x760	12.15	25	1.2	0.63	-	3.6	-	2.3
			24.15	50	1.9	1.41	-	7.1	-	4.6
			36.49	75	2.9	2.1	-	10.6	-	7
			41.13	85	5.6	2.43	-	12	-	7.8
			47.15	98	18	2.7	-	13.8	-	9
			48.3	100	21.6	2.4	19	-	9.3	-
LS-A-C2-S2	20	150x150x760	12.3	25	2.97	1.74	-	3.6	-	2.3
			24.17	50	6.11	3.6	-	7.1	-	4.6
			36.56	75	14.4	5.73	-	10.7	-	7
			42.46	85	19.53	7	-	12.4	-	8
			48.39	90	25.4	8.5	-	14.1	-	9.2
			54.3	100	F	13.83	21.4	-	10.5	-

B.4.3: Load levels and strain values for three specimens of Group B with 20 mm thick UHPC layer of beam size 150x150x1000 mm.

Beam ID	UHPC thickness mm	Size, mm	load level KN	% of load	Measured strain, microstrain				X, from Top, mm	
					Top	1/3 from top	2/3 from top	Bottom	Measured	Calculated
LS-C-C2-S1	20	150x150x1000	4.9	25	-44	-19	11	39	81	81
			10.3	50	-99	-38	30	91	78.1	81
			15.2	75	-155	-55	65	166	72.6	68
			19.6	98	-225	-72	133	255	68.1	69
			20.1	100	-251	-71	208	261	65	69
LS-C-C2-S2	20	150x150x1000	4.9	25	-47	-20	9	32	84	81
			10.3	50	-108	-40	25	71	81	81
			15.8	75	-177	-66	47	122	78	81
			20.1	96	-256	-98	76	173	77	68
			20.6	98	-377	-43	8	228	67	68
			21	100	-	-	-	-	-	68
LS-C-C2-S3	20	150x150x1000	4.9	25	-42	-16	12	39	78.3	81
			9.9	50	-89	-32	29	86	76.3	81
			14.7	75	-140	-49	58	133	74.7	81
			19.2	98	-209	-49	234	229	61	69
			19.6	100	-224	-45	303	288	56	69

B.4.4: Measured and computed stresses for selected load levels of beams for three specimens of Group A with 20 mm thick UHPC layer of beam size 150x150x1000 mm.

Beam ID	UHPC thickness mm	Size mm	load level KN	% of P_U	Measured stress , MPa		Calculated stress, Mpa			
							Bottom		Top	
					Bottom	Top	Cracked	Uncracked	Cracked	Uncracked
LS-C-C2-S1	20	150x150x1000	4.9	25	2.15	1.32	-	2.3	-	1.5
			10.3	50	5.01	3	-	4.8	-	3.1
			15.2	75	9.13	4.7	-	7.1	-	4.52
			19.6	98	14	6.8		9.1	-	5.8
			20.1	100	14.4	7.53	13.9	-	6.3	-
LS-C-C2-S2	20	150x150x1000	4.9	25	1.8	1.41	-	2.3	-	1.5
			10.3	50	4.91	3.24	-	4.8	-	3.1
			15.8	75	6.71	5.31	-	7.33	-	4.7
			20.1	96	9.52	7.7	-	9.33	-	6
			20.6	98	12.54	11.31	-	9.6	-	6.12
			21	100	35	16.4	14	-	6.5	-
LS-C-C2-S3	20	150x150x1000	4.9	25	2.15	1.26	-	2.3	-	1.5
			9.9	50	4.73	2.7	-	4.6	-	2.94
			14.7	75	7.32	4.2	-	6.82	-	4.4
			19.2	98	12.6	6.3	-	8.91	-	5.71
			19.6	100	15.8	6.72	13.5	-	6	-

B.4.5: Load levels and strain values for three specimens of Group B with 40 mm thick UHPC layer of beam size 150x150x1000 mm.

Beam ID	UHPC thickness mm	Size, mm	load level KN (%)	Measured strain, microstrain				X, from Top, mm	
				Top	1/3 from top	2/3 from top	Bottom	Measured	Calculated
LS-D-C2-S1	40	150x150x1000	8.8 (25%)	-71	-28	588	66	83	85
			18.2 (50%)	-159	-63	593	147	83	85
			26.6 (75%)	-288	-89	518	319	81	82
			30.4 (85%)	-397	-88	-296	367	76	82
			33.9 (95%)	-760	5	-804	1118	63	82
			35.7 (100%)	-	-	-	-	-	82
LS-D-C2-S2	40	150x150x1000	8.3 (25%)	-76	-16	15	66	78	85
			16.7 (50%)	-166	-53	37	159	78	85
			25 (75%)	-300	-122	94	308	76	85
			26.5 (80%)	-334	-128	100	373	74	82
			27.9 (85%)	-376	-133	104	499	73	82
			31.4 (95%)	-748	351	640	1613	53	82
			33.3 (100%)	-	-	-	-	-	82
LS-D-C2-S2	40	150x150x1000	8.4 (25%)	-67	-29	3	29	95	85
			16.8 (50%)	-139	-66	8	51	95	85
			25.7 (75%)	-260	-104	51	150	89	85
			29 (85%)	-323	-119	96	215	84	82
			32.4 (95%)	-455	-94	228	223	80	82
			33.9 (100%)	-505	-85	249	267	78	82

B.4.6: Measured and computed stresses for selected load levels of beams for three specimens of Group A with 40 mm thick UHPC layer of beam size 150x150x1000 mm.

Beam ID	Failure mode	Size , mm	load level KN (%)	Measured stress , Mpa		Calculated stress, Mpa			
						Bottom		Top	
				Bottom	Top	Cracked	Uncracked	Cracked	Uncracked
LS-D-C2-S1	Flexure	150x150x1000	8.8 (25%)	3.63	2.13	3.9	3.62	2.6	2.57
			18.2 (50%)	8.09	4.8	8	7.5	5.3	5.3
			26.6 (75%)	17.5	8.6	11.7	11	7.8	7.8
			30.4 (85%)	20.2	11.91	13.4	12.5	8.9	8.9
			33.9 (95%)	-	-	15	14	10	9.9
			35.7 (100%)	-	-	15.8	14.7	10.5	10.4
LS-D-C2-S2	Flexure	150x150x1000	8.3 (25%)	3.63	2.3	3.7	3.4	2.4	2.42
			16.7 (50%)	8.75	5	7.4	6.84	4.9	4.9
			25 (75%)	16.94	9	11	10.3	7.3	7.3
			26.5 (80%)	20.52	10.02	11.7	10.9	7.8	7.75
			27.9 (85%)	27.45	11.3	12.3	11.4	8.2	8.2
			31.4 (95%)	-	-	13.9	12.9	9.2	9.2
			33.3 (100%)	-	-	14.7	13.6	9.8	9.73
LS-D-C2-S3	Flexure	150x150x1000	8.4 (25%)	1.6	2	3.7	3.44	2.5	2.45
			16.8 (50%)	2.8	4.2	7.4	6.9	4.9	4.9
			25.7 (75%)	8.3	7.8	11.4	10.5	7.5	7.5
			29 (85%)	11.83	9.8	12.8	11.9	8.5	8.5
			32.4 (95%)	12.3	13.7	14.3	13.3	9.5	9.5
			33.9 (100%)	14.7	15.2	15	13.9	10	10

B.4.7: Load levels and strain values for three specimens of Group D with 25 mm thick UHPC layer of beam size 150x200x1200 mm.

Beam ID	Failure mode	Size, mm	load level KN (%)	Measured strain, microstrain				X, from Top, mm	
				Top	1/3 from top	2/3 from top	Bottom	Measured	Calculated
LS-G-C-S1	Flexure	150x200x1200	5.02 (25%)	-36	-10	4	25	114	108
			10.09 (50%)	-71	-21	14	53	107	108
			15.08 (75%)	-109	-33	22	85	107	108
			20.1 (100%)	-159	-49	33	123	107	91
LS-G-C-S2	Flexure	150x200x1200	5.04 (25%)	-33	-14	5	26	114	108
			11.084 (50%)	-74	-33	18	53	114	108
			15.05 (75%)	-106	-44	27	72	109	108
			21.05 (100%)	-166	-71	59	92	103	91
LS-G-C-S3	Flexure	150x200x1200	7.2 (25%)	-38	-18	13	42	105	108
			14.5 (50%)	-106	-38	31	92	105	108
			21.5 (75%)	-158	-57	63	110	98	108
			28.3 (98%)	-249	-57	236	233	86	91
			28.8 (100%)	-311	-19	569	433	-	91

B.4.8: Measured and computed stresses for selected load levels of beams for three specimens of Group D with 25 mm thick UHPC layer of beam size 150x200x1200 mm.

Beam ID	Failure mode	Size , mm	load level KN (%)	Measured stress , Mpa		Calculated stress, Mpa			
						Bottom		Top	
				Bottom	Top	Cracked	Uncracked	Cracked	Uncracked
LS-G-C-S1	Flexure	150x200x1200	5.02 (25%)	1.4	1.1	2.4	1.7	1.1	1.1
			10.09 (50%)	3	2.13	4.9	3.4	2.2	2.14
			15.08 (75%)	4.7	3.3	7.3	5.03	4.7	3.21
			20.1 (100%)	6.8	4.8	10	6.7	4.4	4.3
LS-G-C-S2	Flexure	150x200x1200	5.04 (25%)	1.43	1.0	2.5	1.7	1.1	1.1
			11.084 (50%)	3	2.22	5.4	3.7	2.4	2.4
			15.05 (75%)	4	3.2	7.3	5.03	3.3	3.2
			21.05 (100%)	5.1	5.0	10.3	7.03	4.7	4.5
LS-G-C-S3	Flexure	150x200x1200	7.2 (25%)	2.31	1.14	3.5	2.4	1.6	1.53
			14.5 (50%)	5.1	3.2	7.1	4.83	3.2	3.1
			21.5 (75%)	6.1	4.8	10.5	7.2	4.7	4.6
			28.3 (98%)	13	7.5	14	9.43	6.2	6.0
			28.8 (100%)	-	-	14	9.6	6.3	6.11

B.4.9: Load levels and strain values for three specimens of Group D with 50 mm thick UHPC layer of beam size 150x200x1200 mm.

Beam ID	UHPC thickness (mm)	Size , mm	load level KN (%)	% of P_U	Measured strain 10^{-6}				X, from Top, mm	
					Top	1/3 from top	2/3 from top	Bottom	Measured	Calculated
LS-H-C2-S1	50	150x200x1200	10.4 (25%)	25	-66	-31	13	56	112	113
			20.7 (50%)	50	-140	-64	29	126	111	113
			31 (75%)	75	-236	-109	61	250	107	113
			35.5 (85%)	85	-292	-133	84	300	106	113
			39.8 (95%)	95	-	-	-	-	-	109
			41.8 (100%)	100	-	-	-	-	-	109
LS-H-C2-S2	50	150x200x1200	11.3 (25%)	25	-75	-30	19	64	108	113
			22.6 (50%)	50	-120	-63	40	132	107	113
			33.9 (75%)	75	-217	-100	71	173	109	113
			39.3 (87%)	85	-282	-120	55	205	111	113
			42.7 (95%)	95	-283	6	418	1209	70	109
			45.1 (100%)	100	-	-	-	-	-	109
LS-H-C2-S3	50	150x200x1200	12.4 (25%)	25	-83	-30	12	70	110	113
			25.2 (50%)	50	-187	-64	33	159	109	113
			38.2 (75%)	75	-349	-89	66	318	104	113
			42.6 (84%)	85	-531	-37	0	563	100	113
			46.1 (90%)	90	-	-	-	-	-	109
			48.5 (95%)	95	-	-	-	-	-	109
			51 (100%)	100	-	-	-	-	-	113

B.4.10: Measured and computed stresses for selected load levels of beams for three specimens of Group D with 50 mm thick UHPC layer of beam size 150x200x1200 mm.

Beam ID	UHPC thickness (mm)	Size (mm)	load level KN (%)	% of P_U	Measured stress (MPa)		Calculated stress, MPa			
							Bottom		Top	
					Bottom	Top	Cracked	Uncracked	Cracked	Uncracked
LS-H-C2-S1	50	150x200x1200	10.4	25	3.1	2	3.3	3.1	2.2	2.2
			20.7	50	6.93	4.2	6.6	6.1	4.3	4.3
			31	75	20.9	7.1	9.9	9.15	6.5	6.4
			35.5	85	29.5	8.8	11.4	10.5	7.4	7.4
			39.8	95	-	18.6	12.7	11.74	8.3	8.3
			41.8	100	-	-	13.4	12.33	8.7	8.7
LS-H-C2-S2	50	150x200x1200	11.3	25	3.52	2.3	3.6	3.33	2.4	2.35
			22.6	50	7.3	3.6	7.2	6.7	4.7	4.7
			33.9	75	9.52	6.5	10.9	10	7.1	7
			39.3	85	11.3	8.5	12.6	11.6	8.2	8.2
			42.7	95	-	8.5	13.7	12.6	8.9	8.9
			45.1	100	-	-	14.4	13.3	9.4	9.4
LS-H-C2-S3	50	150x200x1200	12.4	25	3.85	2.49	4	3.7	2.6	2.6
			25.2	50	8.75	5.61	8.1	7.4	5.2	5.2
			38.2	75	17.49	10.47	12.2	11.3	8	7.93
			42.6	85	30.97	15.93	13.6	12.6	8.9	8.85
			46.1	90	-	27.3	14.8	13.6	9.6	9.6
			48.5	95	-	34.6	15.5	14.31	10.1	10.1
			51	100	-	42	16.3	15.1	10.6	10.6

APPENDIX C: UHPC REINFORCED SPECIMENS

C.1.1: Load-deflections curve for three specimens of Beam UB-1 with 2-25x25 mm UHPC bars of beam size 150x150x760 mm.

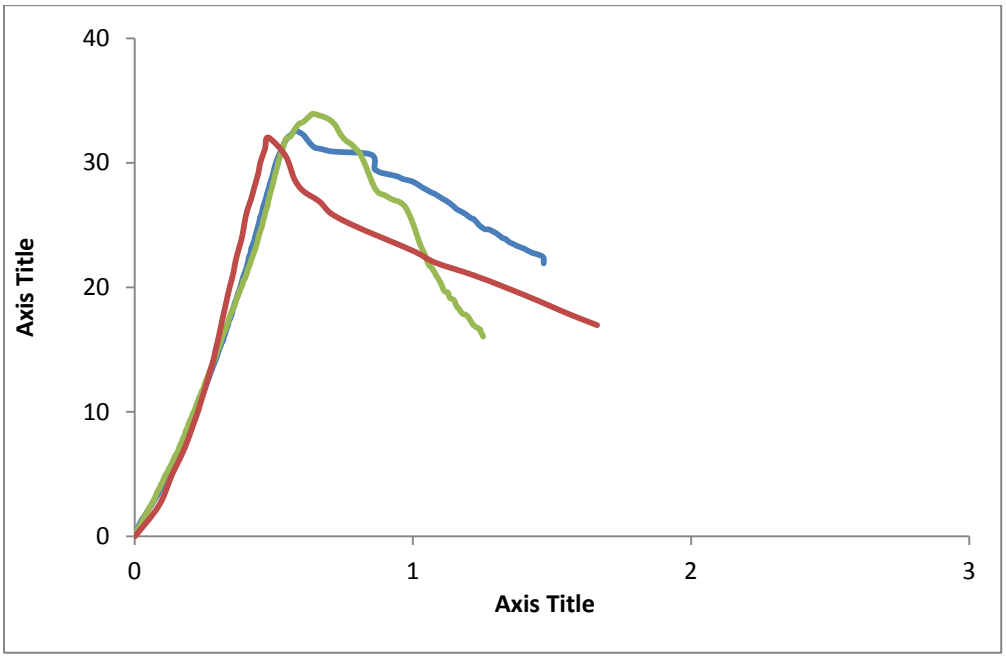

C.1.2: Load-deflections curve for three specimens of Beam UB-2 with 3-25x25 mm UHPC bars of beam size 150x150x760 mm.

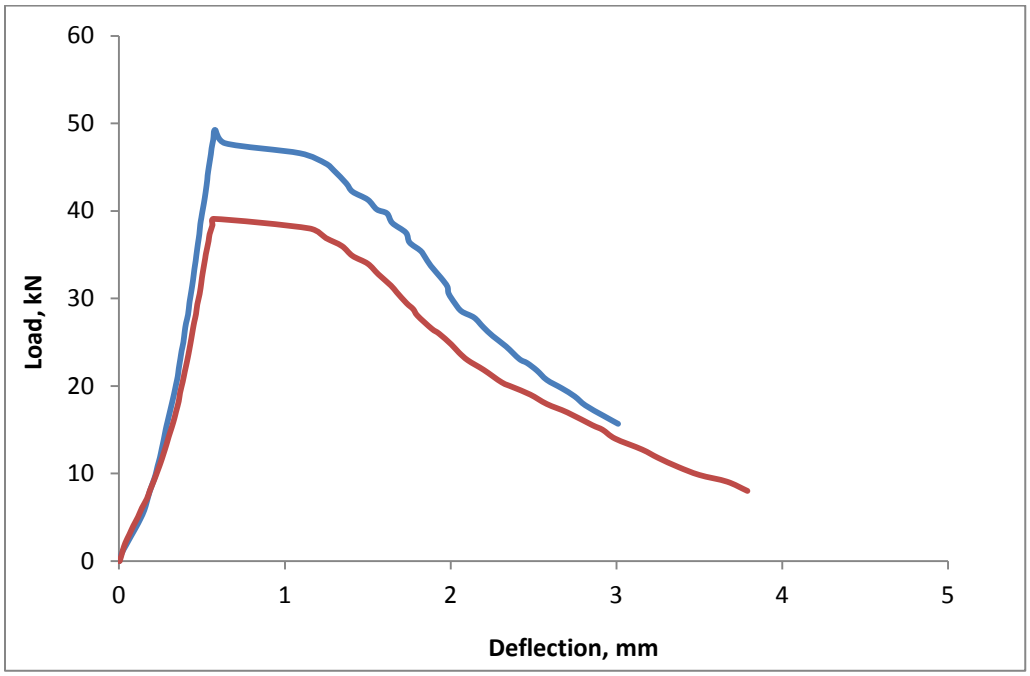

C.1.3: Load-deflections curve for three specimens of Beam UB-3 with 3-25x50 mm UHPC bars of beam size 150x150x760 mm.

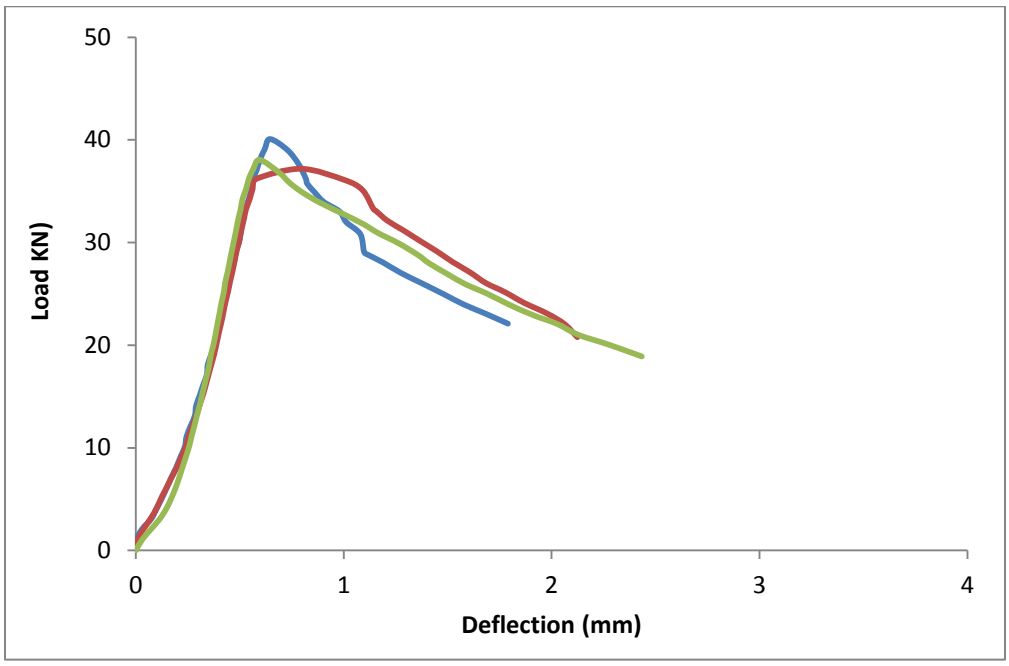

C.1.4: Load-deflections curve for three specimens of Beam UB-4 with 2-50x50 mm UHPC bars of beam size 150x150x760 mm.

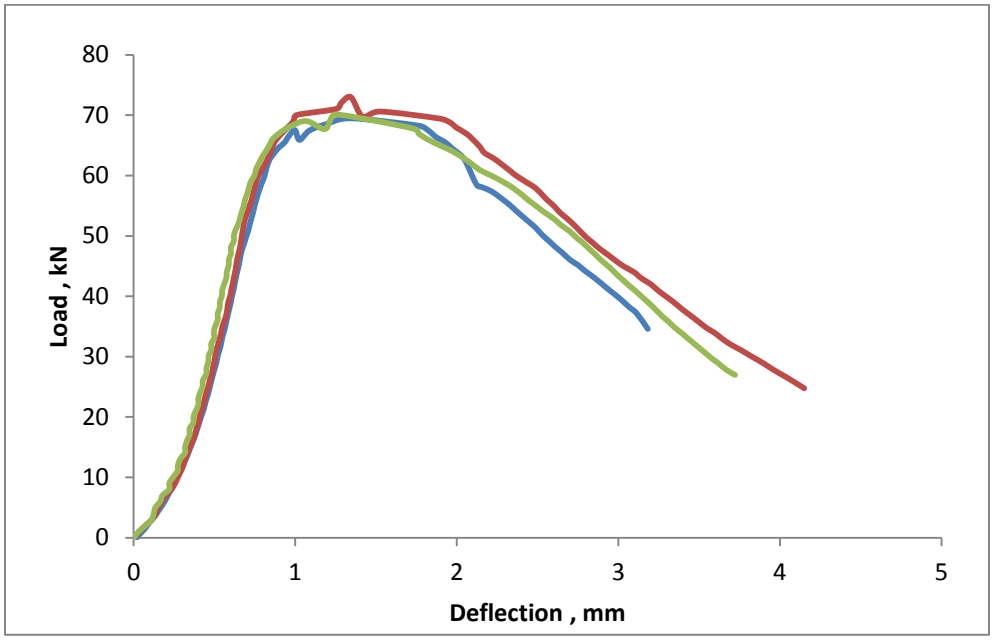

C.1.5: Load-deflections curve for three specimens of Beam UB-5 with 2-25x25 mm UHPC bars of beam size 150x200x900 mm (200 mm depth).

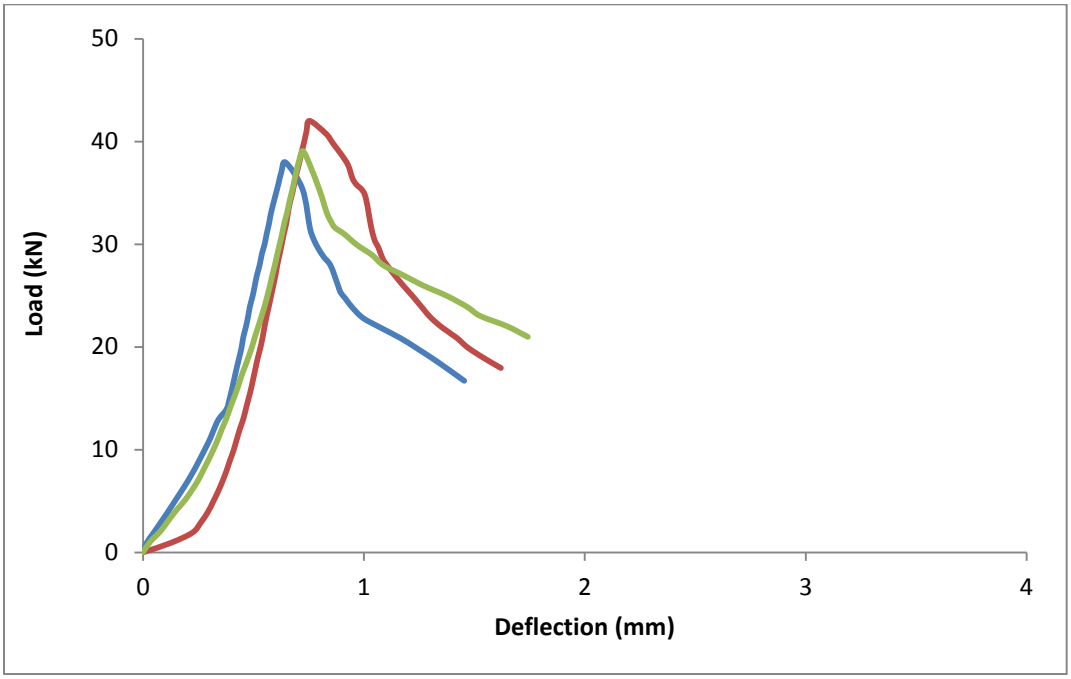

C.1.6: Load-deflections curve for three specimens of Beam UB-6 with 2-50x50 mm UHPC bars of beam size 150x220x760 mm (220 mm depth).

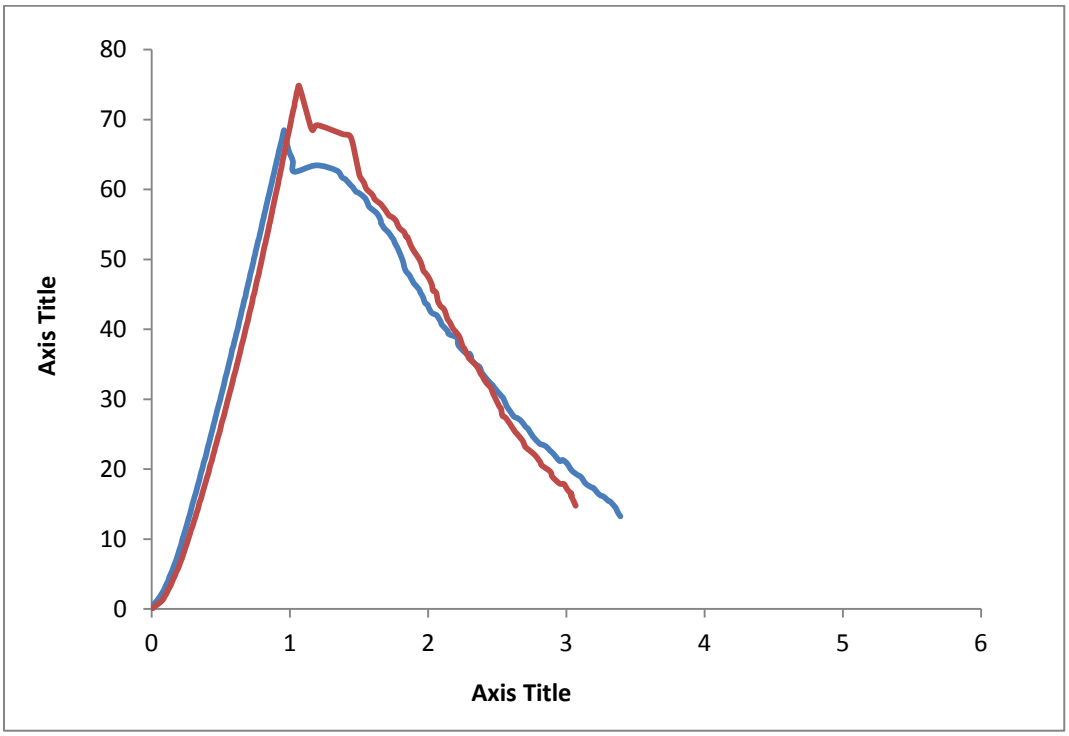

C.1.7: Load-deflections curve for three specimens of Beam UB-7 with 2-50x50 mm UHPC bars of beam size 200x270x1000 mm (270 mm depth).

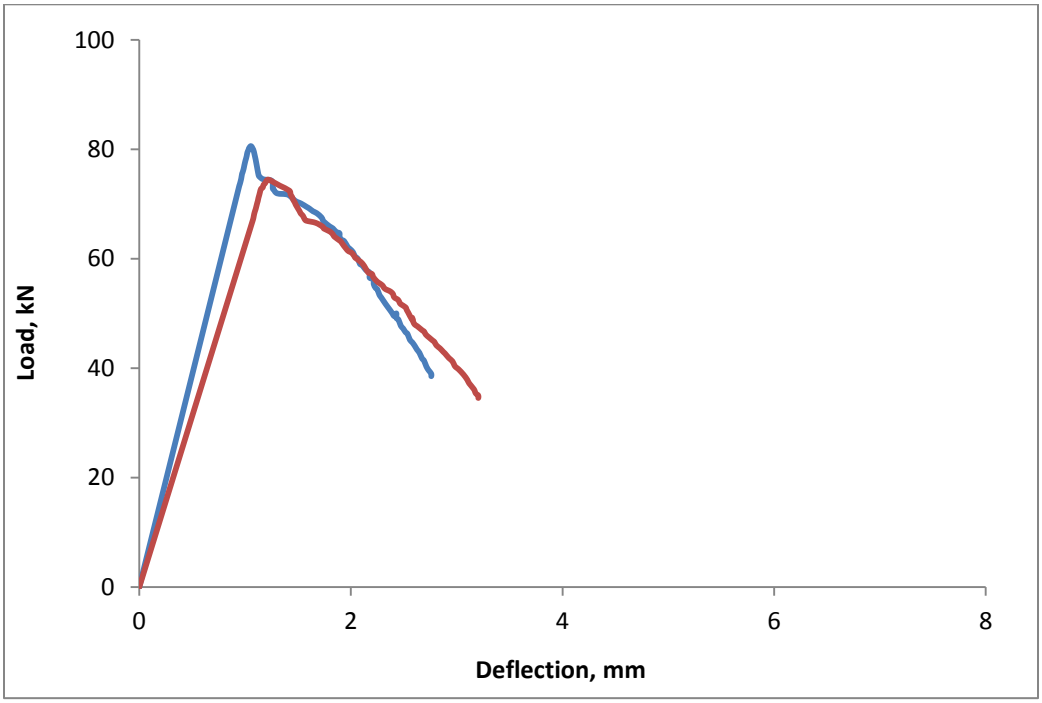

C.1.8: Load-deflections curve for three specimens of Beam UB-8 with 2-50x50 mm UHPC bars of beam size 200x220x1000 mm (220 mm depth).

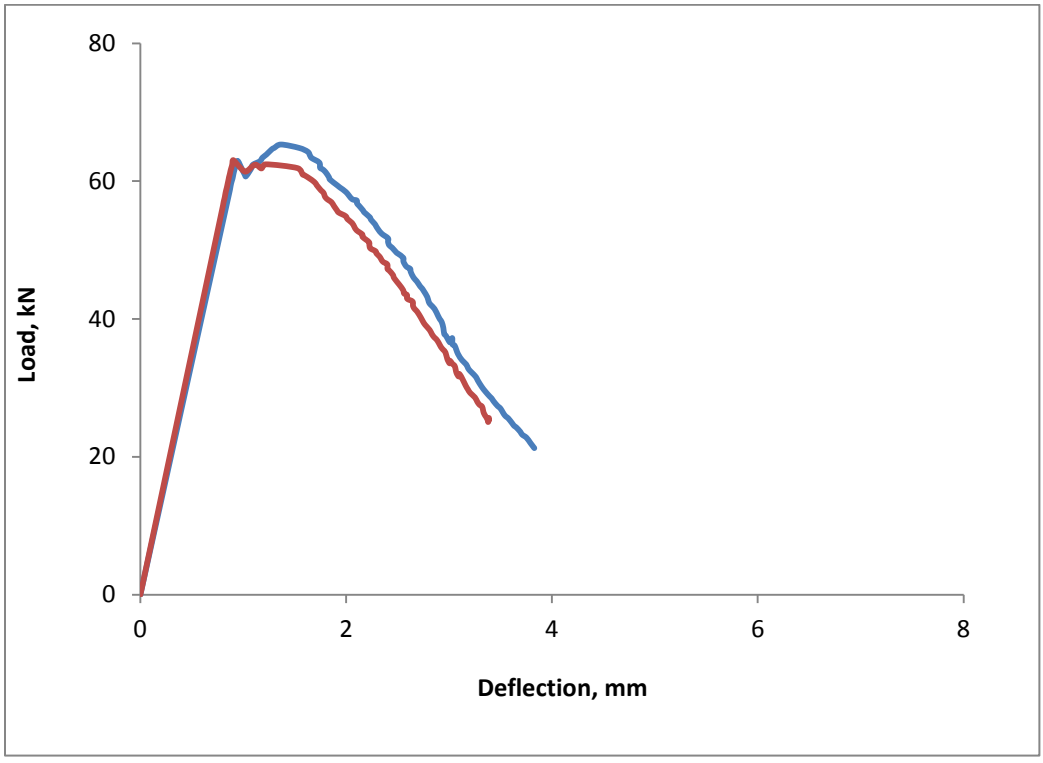

C.1.9: Load-deflections curve for three specimens of Beam UB-9 with 4-25x25 mm UHPC bars of beam size 200x310x1000 mm (310 mm depth).

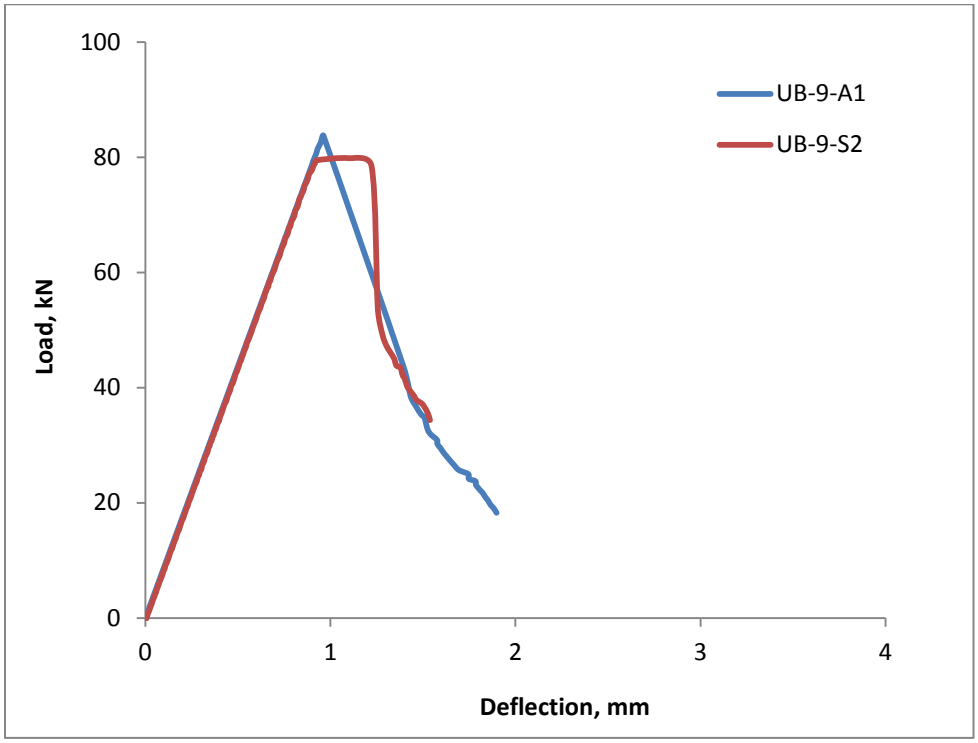

C.2.1: Load-strain curve for two specimen of Beam UB-2 with 3-25x25 mm UHPC bars of beam size 150x150x7600 mm. Each plot shows one specimens with 4 strain location.

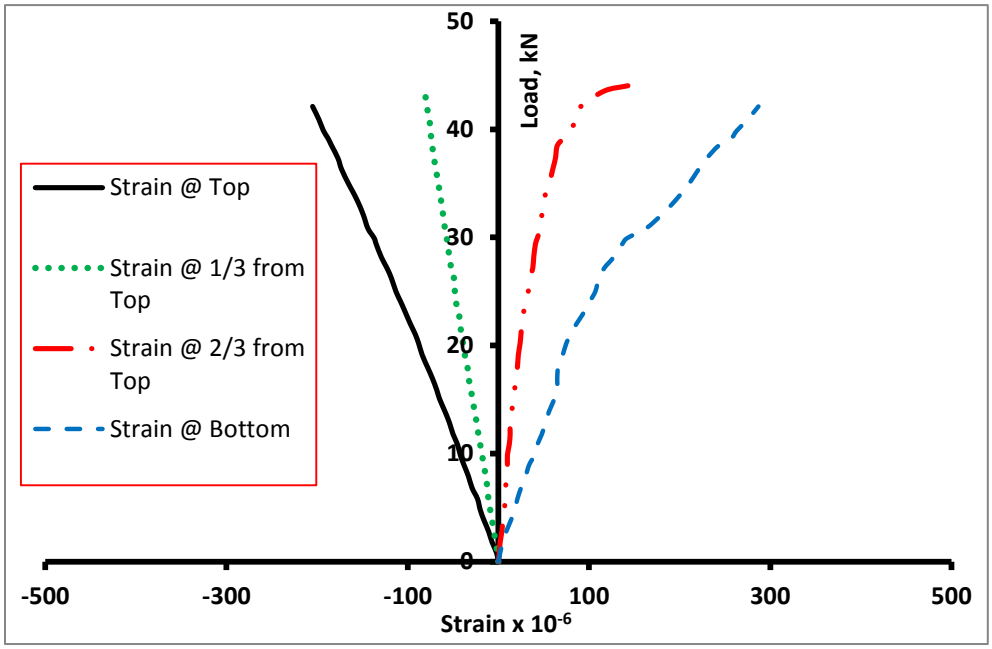

C.2.2: Load-strain curve for two specimen of Beam UB-6 with 2-50x50 mm UHPC bars of beam size 150x220x7600 mm. Each plot shows one specimens with 4 strain location.

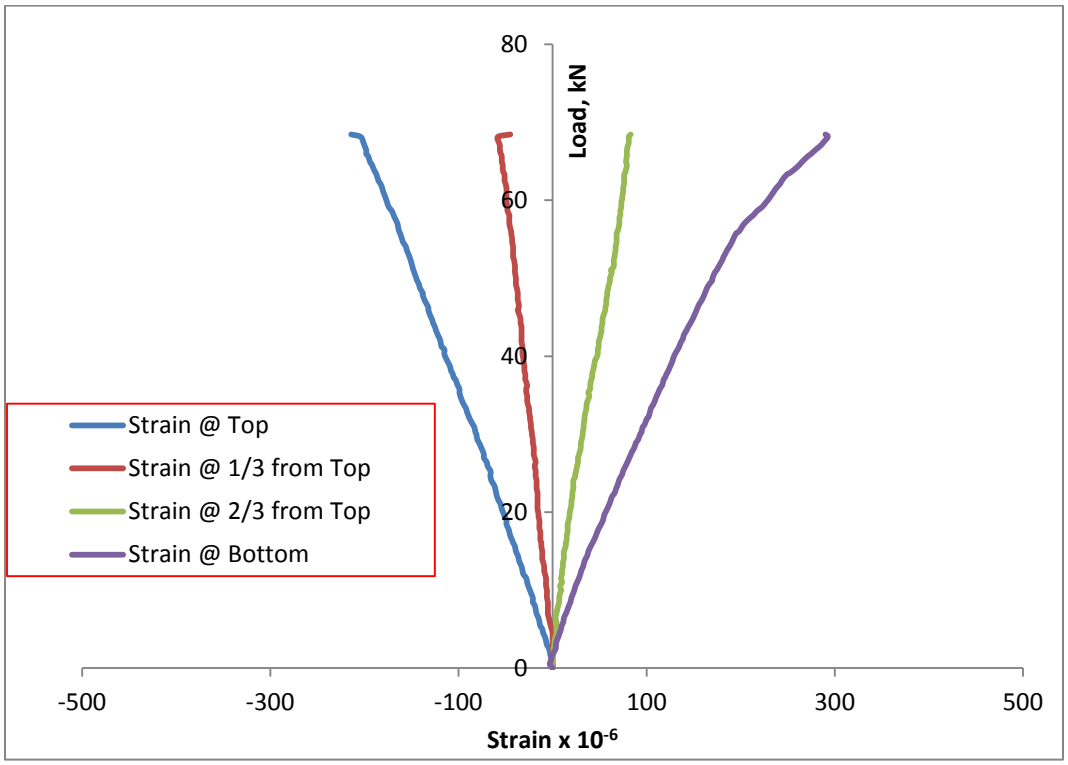

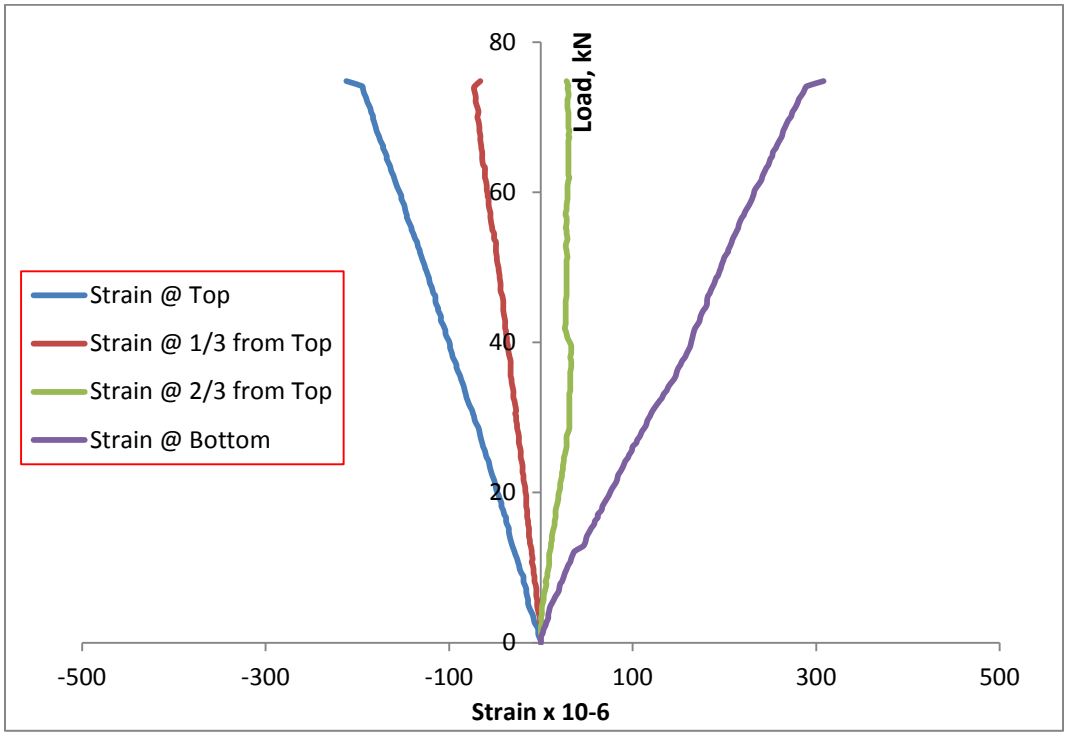

C.2.3: Load-strain curve for two specimen of Beam UB-7 with 2-50x50 mm UHPC bars of beam size 200x270x1000 mm. Each plot shows one specimens with 4 strain location.

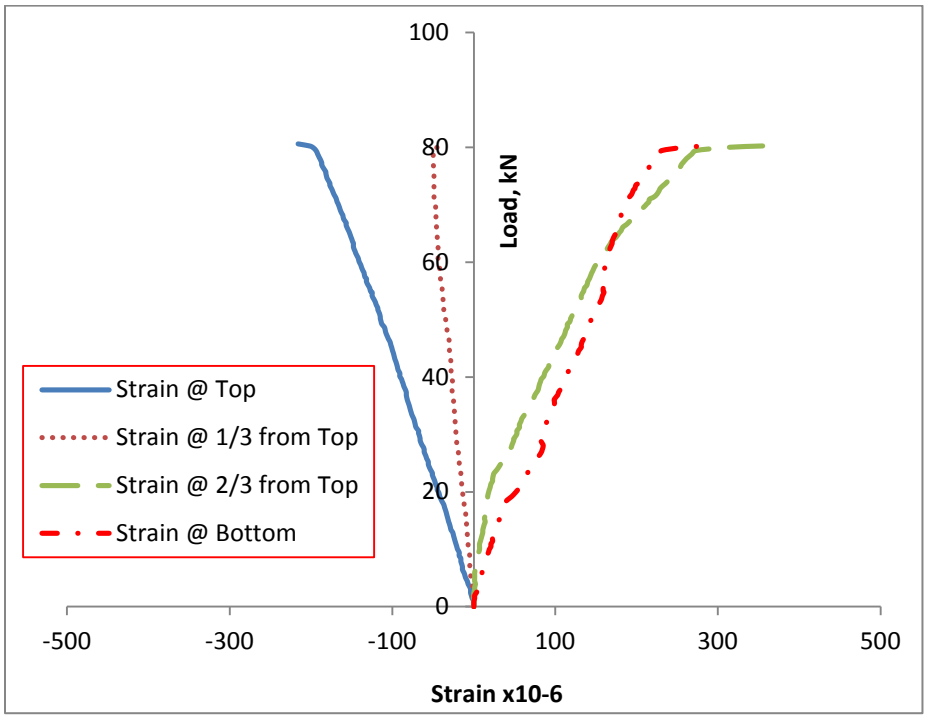

C.2.4: Load-strain curve for two specimen of Beam UB-8 with 2-50x50 mm UHPC bars of beam size 200x220x1000 mm. Each plot shows one specimens with 4 strain location.

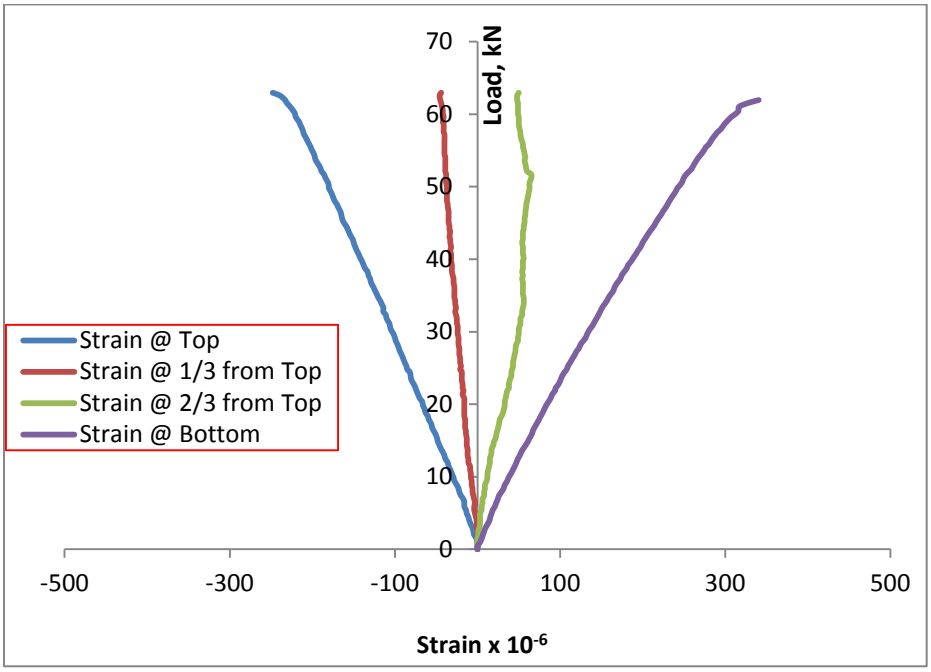

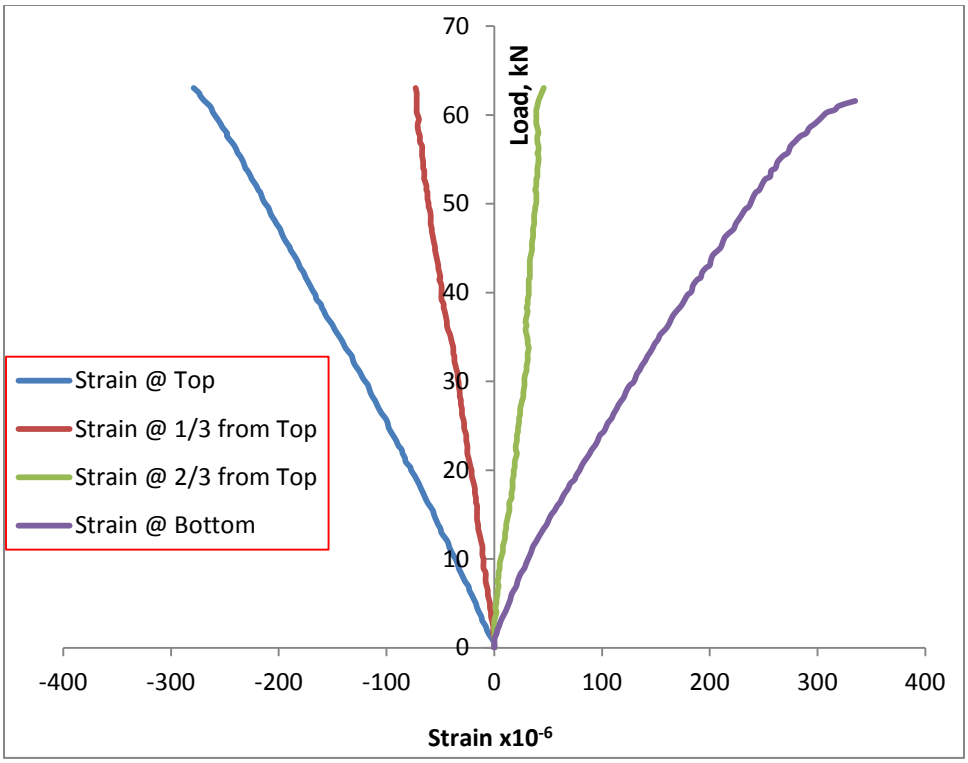

C.2.5: Load-strain curve for two specimen of Beam UB-9 with 4-25x25 mm UHPC bars of beam size 200x310x1000 mm. Each plot shows one specimens with 4 strain location.

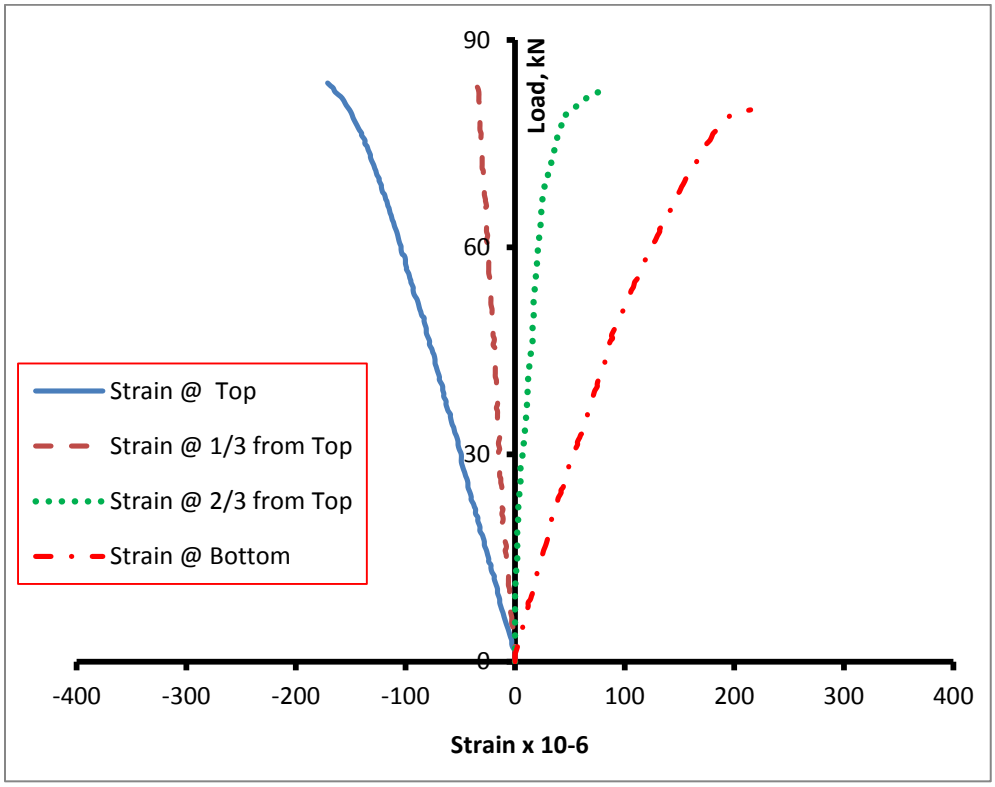

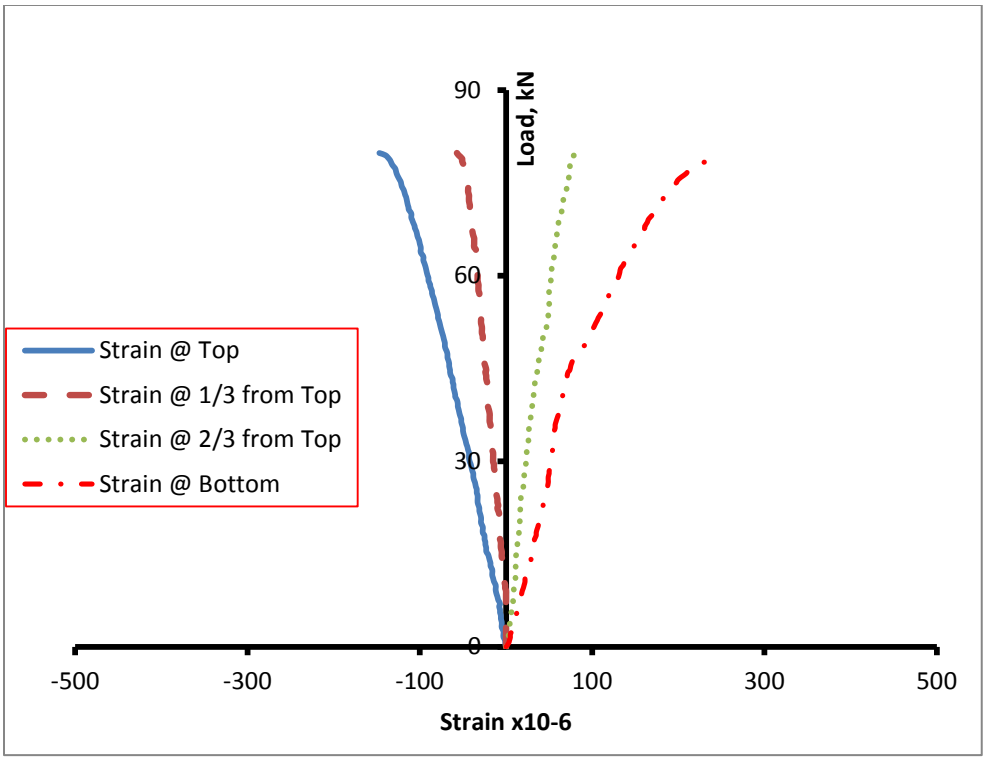

C.3.1: Strain profile along the depth for two specimen of Beam UB-2 with 3-25x25 mm UHPC bars of beam size 150x150x7600 mm. Each plot shows one specimen.

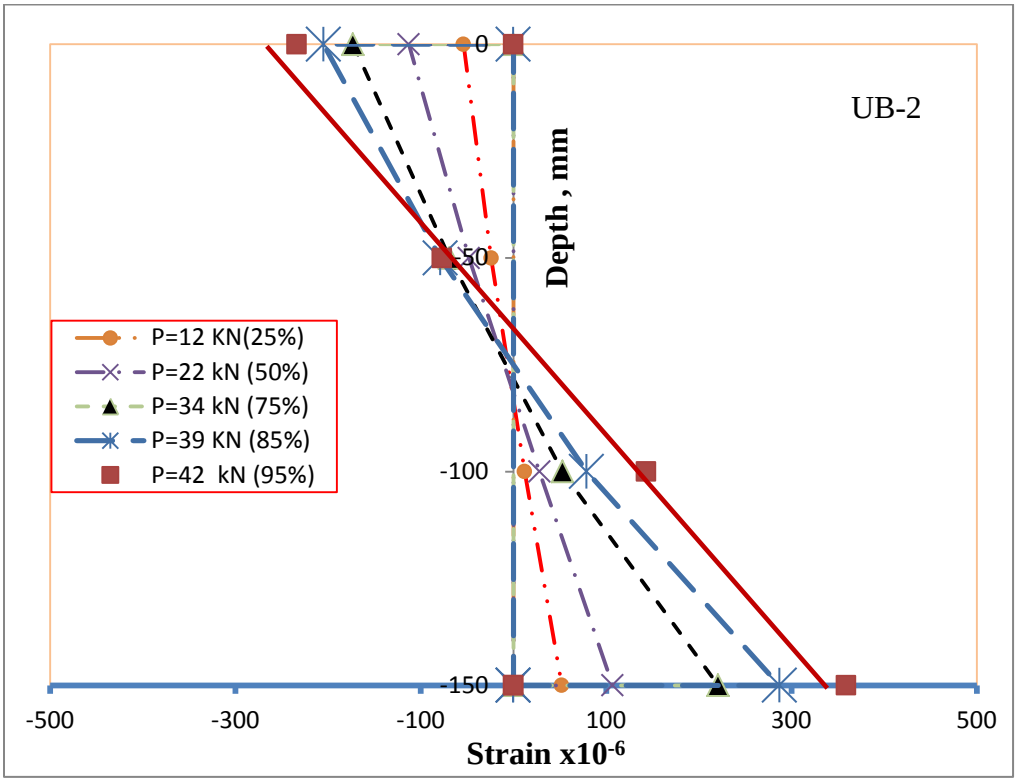

C.3.5: Strain profile along the depth for two specimens of Beam UB-9 with 4-25x25 mm UHPC bars of beam size 200x310x1000 mm (310 mm depth). Each plot shows one specimen.

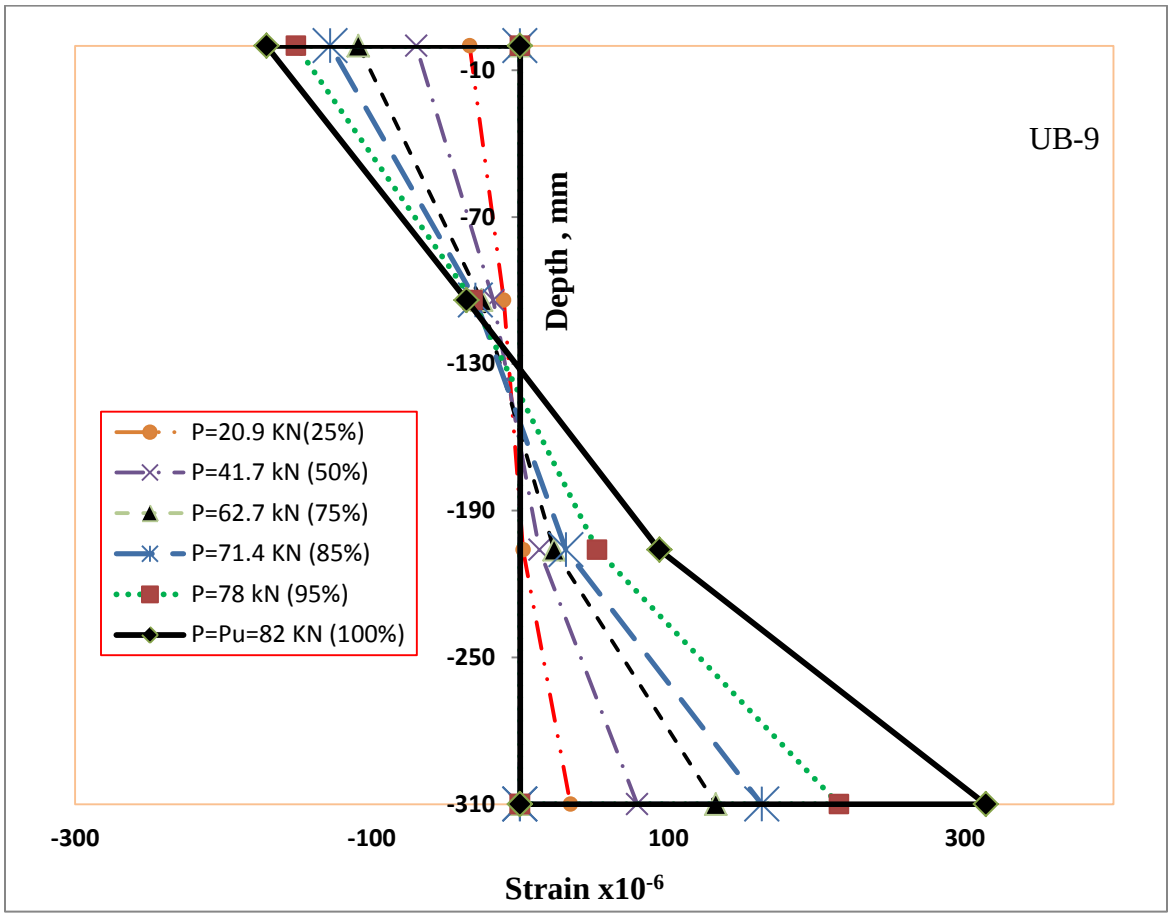

C.4.1: Load levels and strain values for two specimens of beam UB-2 with 3-25x25 mm UHPC bars of beam size 150x150x760 mm.

Beam Designation	UHPC bar size mm	load P (kN)	% of P_U	Measured strain, (x 10^6)				Depth of N.A from top, (mm)	
				Top	1/3 from top	2/3 from top	Bottom	Measured	Calculated
UB-2-S1 (150x150x760) (b x h x L)	3- 25 x 25	11	25	-54	-24	12	52	80	79
		22	50	-113	-48	28	107	79	79
		33	75	-173	-69	53	221	78	79
		37	85	-205	-79	79	287	75	79
		42	95	-234	-77	143	359	63	60
		44	100	-259	-61	259	498	59	60
UB-2-S2 (150x150x760) (b x h x L)	3- 25 x 25	10.3	25	-45	-28	9	-	87	79
		19.2	50	-90	-45	18	-	85	79
		29.3	75	-146	-66	27	-	85	79
		33.3	85	-170	-75	33	-	84	79
		37.3	95	-200	-93	32	-	87	79
		39.1	100	-223	-106	33	-	88	60

C.4.2: Measured and computed stresses for selected load levels of two specimens beam UB-2 with 3-25x25 mm UHPC bars of beam size 150x150x760 mm.

Beam Designation	UHPC bar size (mm)	load P (kN)	% of P_U	Measured stress (MPa)		Calculated stress, (MPa)			
						Bottom		Top	
				Bottom	Top	Cracked	Uncracked	Cracked	Uncracked
UB-2-S1 (150x150x760) (b x h x L)	3- 25 x 25	11	25	2.9	1.6	-	4.2	-	2.6
		22	50	5.9	3.4	-	8.1	-	4.9
		33	75	12.2	5.2	--	11.8	-	7.2
		37	85	15.8	6.2	-	13.7	-	8.3
		42	95	19.7	7.0	-	15.2	-	9.2
		44	100	27.4	7.8	31.1	-	11.2	-
UB-2-S2 (150x150x760) (b x h x L)	3- 25 x 25	10.3	25	-	1.4	-	3.4	-	2.0
		19.2	50	-	2.7	-	6.3	-	3.8
		29.3	75	-	4.4	-	9.5	-	5.8
		33.3	85	-	5.1	-	10.9	-	6.6
		37.3	96	-	6.0	-	12.2	-	7.4
		39.1	100	-	6.7	24.7	-	9.0	7.7

C.4.3: Load levels and strain values for two specimens of beam UB-6 with 2-50x50 mm UHPC bars of beam size 200x220x760 mm.

Beam Designation	UHPC bar size mm	load P (kN)	% of P	Measured strain, (x 10^6)				Depth of N.A from top, (mm)	
				Top	1/3 from top	2/3 from top	Bottom	Measured	Calculated
UB-6-S1 (150x220x760) (b x h x L)	2- 50 x 50	17.0	25	-45	-13	15	40	112	119
		34.2	50	-96	-27	37	109	104	119
		51.5	75	-149	-40	65	177	101	119
		58.1	85	-169	-46	72	214	102	119
		64.9	95	-194	-54	78	265	104	119
		68.5	100	-214	-45	83	290	100	105
UB-6-S2 (150x220x760) (b x h x L)	2- 50 x 50	18.6	25	-43	-16	18	69	107	119
		37.5	50	-94	-33	33	154	110	119
		56.6	75	-146	-55	28	219	104	119
		63.7	85	-165	-63	30	248	104	119
		71.2	95	-186	-69	29	277	103	119
		74.8	100	-212	-66	28	308	100	105

C.4.4: Measured and computed stresses for selected load levels of beam UB-6 with 2-50x50 mm UHPC bars of beam size 200x220x760 mm.

Beam Designation	UHPC bar size mm	load P (kN)	% of P	Measured stress (MPa)		Calculated stress, (MPa)			
						Bottom		Top	
				Bottom	Top	Cracked	Uncracked	Cracked	Uncracked
UB-6-S1 (150x220x760) (b x h x L)	2- 50 x 50	17.0	25	2.5	1.4	3.6	2.6	1.8	1.7
		34.2	50	6.0	2.9	7.2	5.2	3.6	3.4
		51.5	75	9.7	4.5	10.9	7.9	5.4	5.1
		58.1	85	11.8	5.1	12.3	8.9	6.1	5.8
		64.9	95	14.6	5.8	13.7	9.9	6.8	6.4
		68.5	100	16.0	6.4	14.5	10.5	7.2	6.8
UB-6-S2 (150x220x760) (b x h x L)	2- 50 x 50	18.6	25	3.8	1.3	3.9	2.8	2.0	1.8
		37.5	50	8.5	2.8	7.9	5.7	3.9	3.7
		56.6	75	12.1	4.4	12.0	8.7	6.0	5.6
		63.7	85	13.6	5.0	13.5	9.7	6.7	6.3
		71.2	96	15.2	5.6	15.1	-	7.5	-
		74.8	100	16.9	6.4	15.8	-	7.9	-

C.4.5: Load levels and strain values for two specimens of beam UB-7 with 2-50x50 mm UHPC bars of beam size 200x270x1000 mm.

Beam Designation	UHPC bar size mm	load P (kN)	% of P	Measured strain, ($x 10^6$)				Depth of N.A from top, (mm)	
				Top	1/3 from top	2/3 from top	Bottom	Measured	Calculated
UB-7-S1 (200x270x1000) (b x h x L)	2- 50 x 50	20.4	25	-45	-14	19	54	128	143
		40.7	50	-91	-28	87	115	126	143
		60.6	75	-142	-44	115	165	127	143
		68.4	85	-162	-45	198	181	127	143
		77	95	-187	-50	255	216	125	143
		80.2	99	-202	-39	355	287	112	111
		83.8	100	-216	-14	528	404	95	111
UB-7-S2 (200x270x1000) (b x h x L)	2- 50 x 50	18.6	25	-42	-13	20	35	135	143
		37.5	50	-95	-27	43	64	141	143
		55.8	75	-148	-39	56	156	132	143
		63.21	85	-168	-46	68	190	127	143
		70.6	95	-191	-49	110	236	119	143
		73.1	98	-215	-48	257	322	100	111
		79.84	100	-	-	-	-	-	111

C.4.6: Measured and computed stresses for two specimens of beam UB-7 with 2-50x50 mm UHPC bars of beam size 200x270x1000 mm.

Beam Designation	UHPC bar size (mm)	load P (kN)	% of P	Measured stress (MPa)		Calculated stress, (MPa)			
						Bottom		Top	
				Bottom	Top	Cracked	Uncracked	Cracked	Uncracked
UB-7-S1 (200x270x1000) (b x h x L)	2- 50 x 50	20.4	25	3.0	1.4	4.4	2.4	1.7	1.5
		40.7	50	6.3	2.7	8.7	4.7	3.3	2.9
		60.6	75	9.1	4.3	13.0	7.1	4.9	4.3
		68.4	85	10	4.9	14.6	8.0	5.6	4.9
		77	95	11.9	5.6	16.5	9.0	6.3	5.5
		80.2	99	15.8	6.1	17.2	9.3	6.5	5.7
		83.8	100	22.2	6.5	17.2	9.4	6.6	5.8
UB-7-S2 (200x270x1000) (b x h x L)	2- 50 x 50	18.6	25	1.9	1.3	4.0	2.2	1.5	1.3
		37.5	50	3.5	2.9	8.0	4.4	3.1	2.7
		55.8	75	8.6	4.4	11.9	6.5	4.5	4.0
		63.21	85	10.5	5.0	13.5	7.4	5.1	4.5
		70.6	95	13.0	5.7	15.1	8.2	5.7	5.0
		73.1	98	17.7	6.5	15.6	8.5	6.0	5.2
		79.84	100	27.2	7.7	15.8	8.7	6.1	5.3

C.4.7: Load levels and strain values for two specimens of beam UB-8 with 2-50x50 mm UHPC bars of beam size 200x220x1000 mm.

Beam Designation	UHPC bar size mm	load P (kN)	% of P	Measured strain, (x 10^6)				Depth of N.A from top, (mm)	
				Top	1/3 from top	2/3 from top	Bottom	Measured	Calculated
UB-8-S1 (200x220x1000) (b x h x L)	2- 50 x 50	16.3	25	-53	-14	24	67	101	117
		32.8	50	-114	-27	54	149	97	117
		49.1	75	-177	-37	62	239	98	117
		55.5	85	-202	-40	55	277	99	117
		61.9	95	-233	-45	48	341	99	96
		65.3	100	-522	-	-	-	-	-
UB-8-S2 (200x220x1000) (b x h x L)	2- 50 x 50	15.5	25	-57	-16	14	59	113	117
		31.3	50	-126	-35	30	137	112	117
		47.29	75	-199	-58	36	224	110	117
		53.7	85	-229	-65	40	261	109	117
		61.0	97	-264	-72	40	335	106	96
		63.1	100	-279	-73	46	406	102	96

C.4.8: Measured and computed stresses for two specimens of beam UB-8 with 2-50x50 mm UHPC bars of beam size 200x220x1000 mm.

Beam Designation	UHPC bar size mm	load P (kN)	% of P_U	Measured stress (MPa)		Calculated stress, (MPa)			
						Bottom		Top	
				Bottom	Top	Cracked	Uncracked	Cracked	Uncracked
UB-8-A (200x220x1000) (b x h x L)	2- 50 x 50	16.3	25	3.7	1.6	4.7	2.8	2.0	1.7
		32.8	50	8.2	3.4	9.4	5.7	4.0	3.5
		49.1	75	13.1	5.3	14.1	8.5	5.9	5.3
		55.5	85	15.2	6.1	16.0	9.6	6.7	6.0
		61.9	95	18.8	7.0	17.8	10.7	7.4	6.7
		65.3	100	-	-	18.8	11.2	7.9	7.0
UB-8-B (200x220x1000) (b x h x L)	2- 50 x 50	15.5	25	3.2	1.7	4.5	2.7	1.9	1.7
		31.3	50	7.5	3.8	9.0	5.4	3.8	3.4
		47.29	75	12.3	6.0	13.6	8.1	5.7	5.1
		53.7	85	14.4	6.9	15.4	9.2	6.5	5.8
		61.0	96	18.4	7.9	17.6	10.5	7.4	6.6
		63.1	100	22.3	8.4	18.1	10.9	7.6	6.8

C.4.9: Load levels and strain values for two specimens of beam UB-9 with 4-25x25 mm UHPC bars of beam size 200x310x1000 mm.

Beam Designation	UHPC bar size mm	load P (kN)	% of P_U	Measured strain, ($x 10^6$)				Depth of N.A from top, (mm)	
				Top	1/3 from top	2/3 from top	Bottom	Measured	Calculated
UB-9-S1 (200x310x1000) (b x h x L)	4- 25 x 25	20.91	25	-34	-11	2	34	165	160
		41.73	50	-70	-18	13	79	162	160.
		62.7	75	-109	-26	23	132	157	160
		71.4	85	-128	-30	31	163	154	160
		79.9	95	-151	-32	52	215	137	96
		83.8	100	-171	-36	94	314	123	96
UB-9-B (200x310x1000) (b x h x L)	4- 25 x 25	20	25	-29	-8	16	38	138	160
		39.9	50	-57	-22	31	64	146	160.
		60	75	-91	-33	53	131	143	160
		67.74	85	-106	-39	60	161	144	160
		75.91	95	-125	-45	73	203	131	96
		79.84	100	-147	-57	88	242	131	96

C.4.10: Measured and computed stresses two specimens of beam UB-9 with 4-25x25 mm UHPC bars of beam size 200x310x1000 mm.

Beam Designation	UHPC bar size mm	load P (kN)	% of P_U	Measured stress (MPa)		Calculated stress, (MPa)			
						Bottom		Top	
				Bottom	Top	Cracked	Uncracked	Cracked	Uncracked
UB-9-A (200x310x1000) (b x h x L)	4- 25 x 25	20.91	25	1.9	1.0	6.3	2.0	1.5	1.2
		41.73	50	4.3	2.1	12.5	4.1	3.1	2.3
		62.7	75	7.3	3.3	18.8	6.0	4.6	3.5
		71.4	85	9.0	3.8	21.4	6.9	5.2	4.0
		79.9	95	11.8	4.5	24.0	7.7	5.9	4.5
		83.8	100	17.3	5.1	25.1	8.1	6.2	4.7
UB-9-B (200x310x1000) (b x h x L)	4- 25 x 25	20	25	2.1	0.90	6.0	1.9	1.5	1.1
		39.9	50	3.5	1.7	12.0	3.8	3.0	2.2
		60	75	7.2	2.7	18.0	5.8	4.4	3.3
		67.74	85	8.9	3.2	20.3	6.5	5.0	3.8
		75.91	96	11.2	3.8	22.8	7.3	5.6	4.2
		79.84	100	13.3	4.4	24.0	7.7	5.9	4.5

APPENDIX D: HYBRID HOLLOW CORE SPECIMENS

D.1.1: Load-deflections curve for three specimens of Group (i) of beam size 260x140x1000 mm (140 mm depth) of span 900 mm.

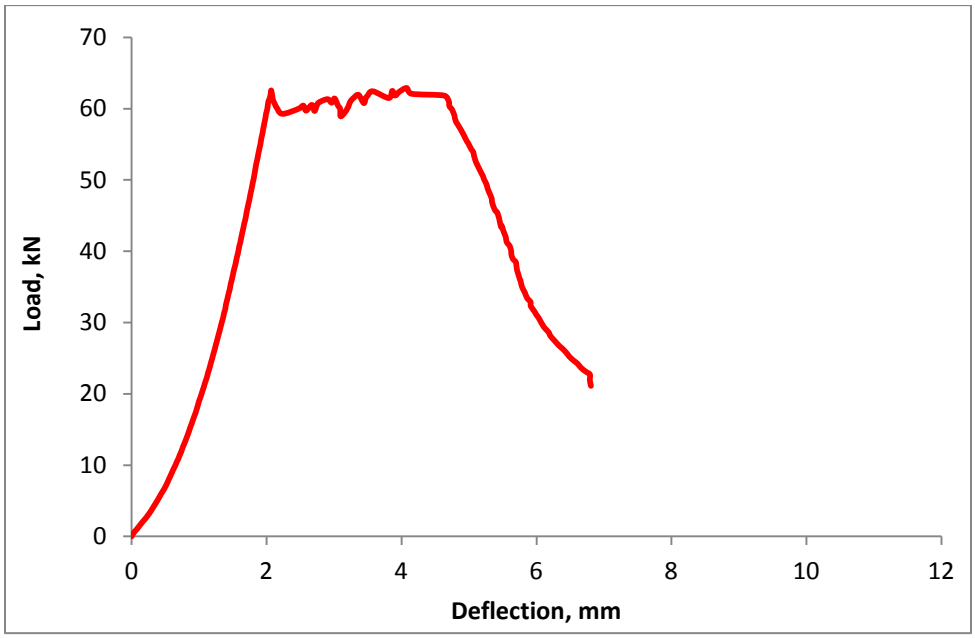

Specimen HC-A-S1

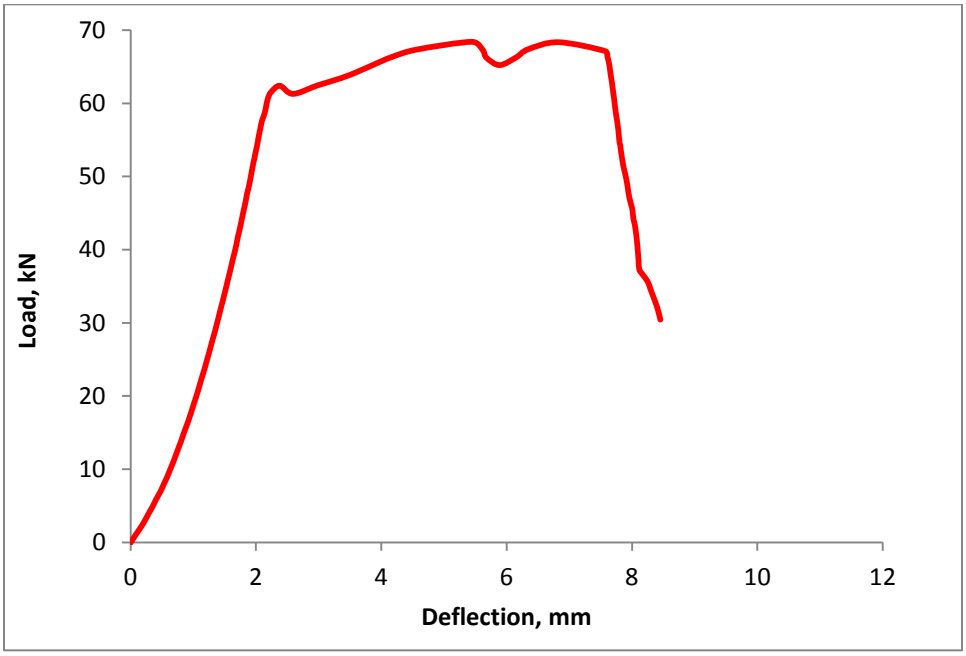

Specimen HC-A-S2

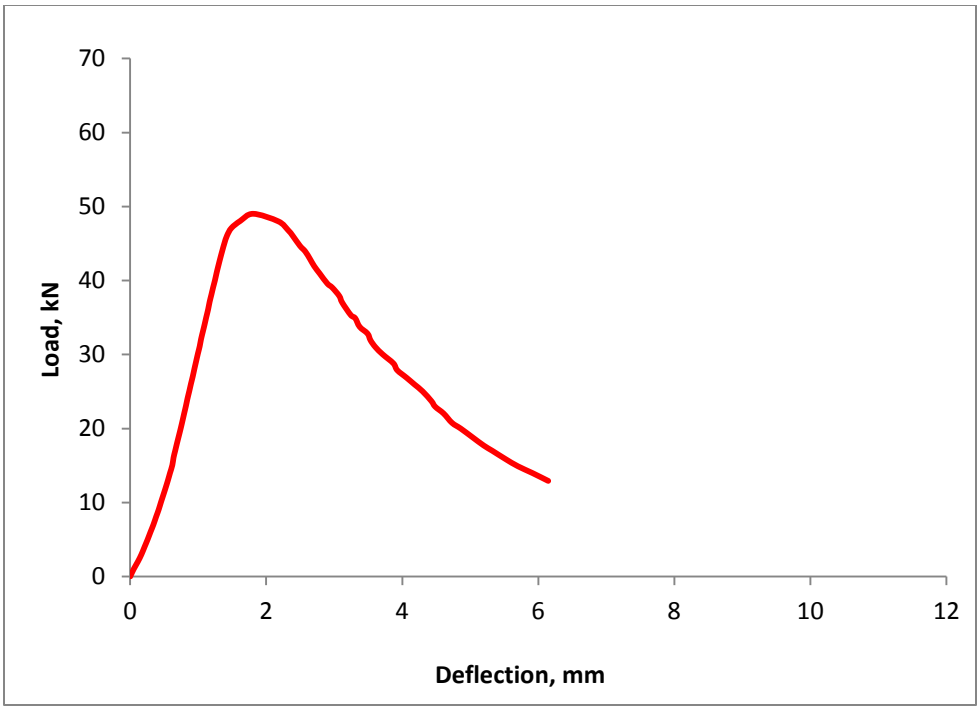

Specimen HC-A-S3

D.1.2: Load-deflections curve for three specimens Group (i) of beam size 260x140x1200 mm (140 mm depth) of span 1100 mm.

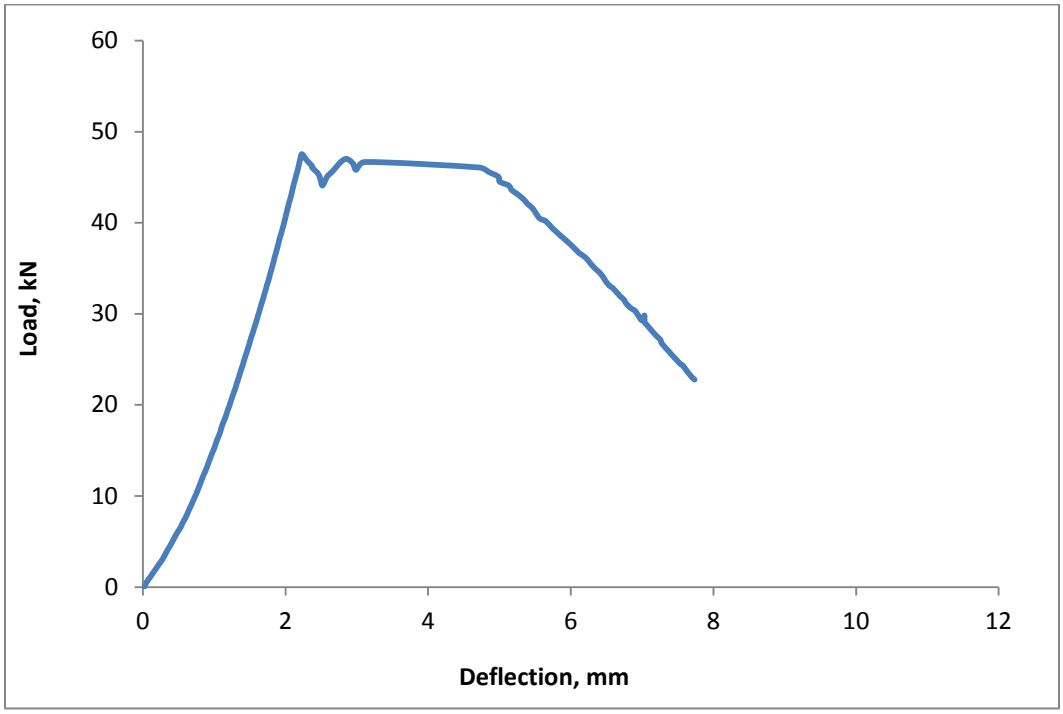

Specimen HC-A-L1

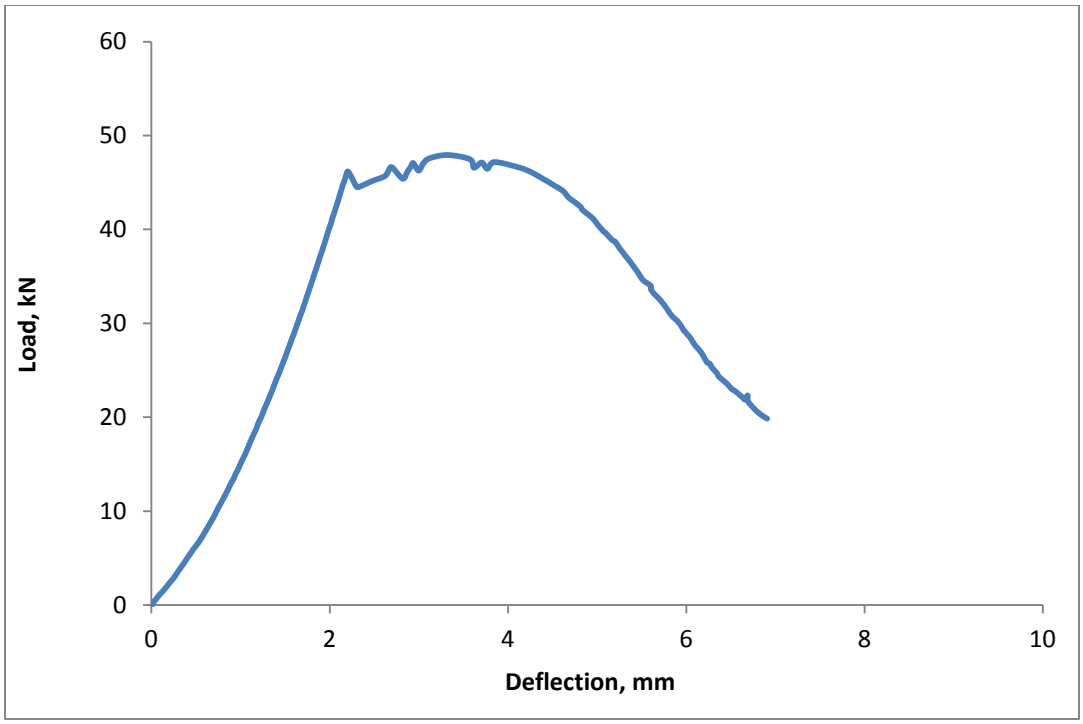

Specimen HC-A-L2

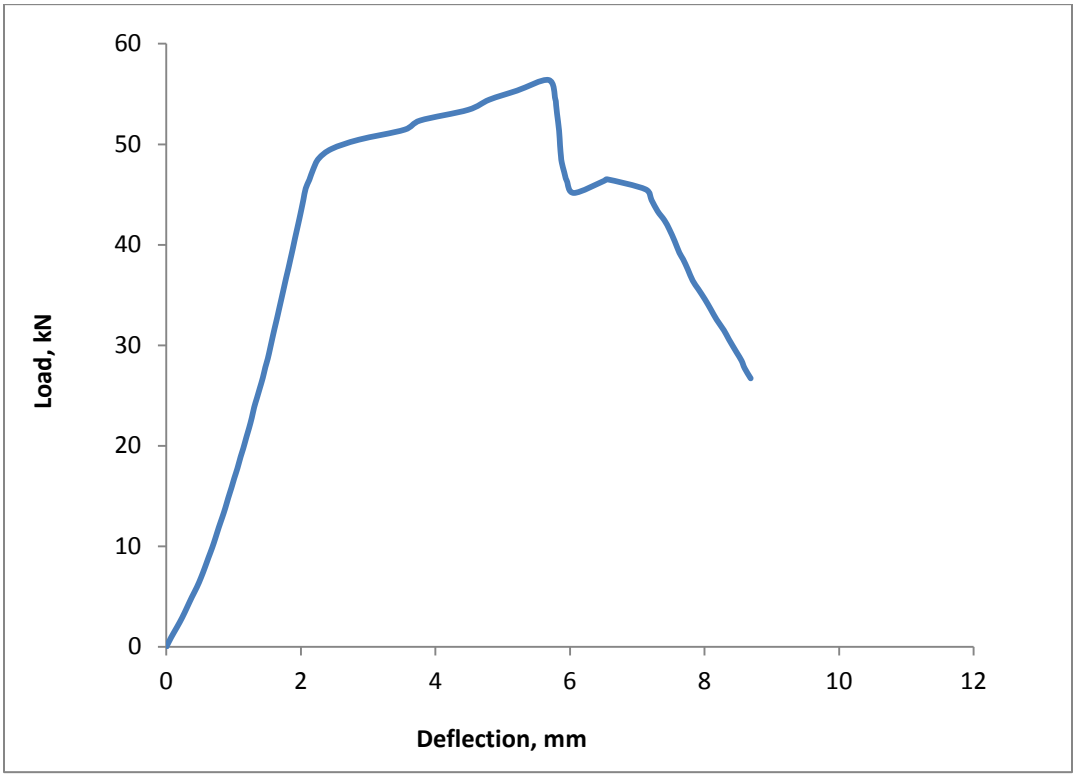

Specimen HC-A-L3

D.1.3: Load-deflections curve for three specimens Group (ii) of beam size 330x175x1000 mm (175 mm depth) of span 900 mm.

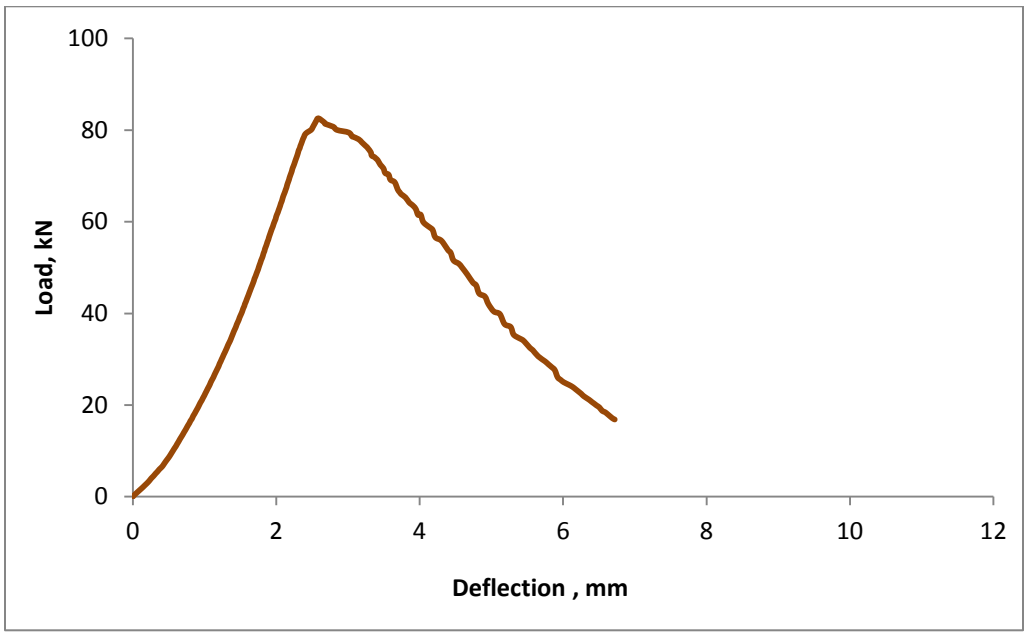

Specimen HC-B-S1

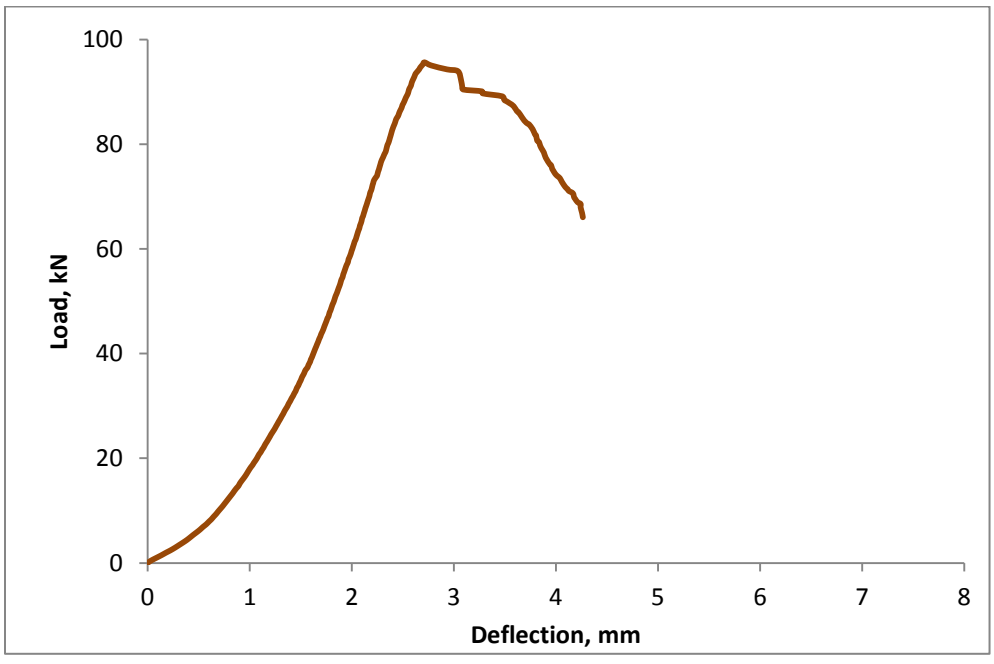

Specimen HC-B-S3

D.1.4: Load-deflections curve for three specimens Group (ii) of beam size 330x175x1200 mm (175 mm depth) of span 1100 mm.

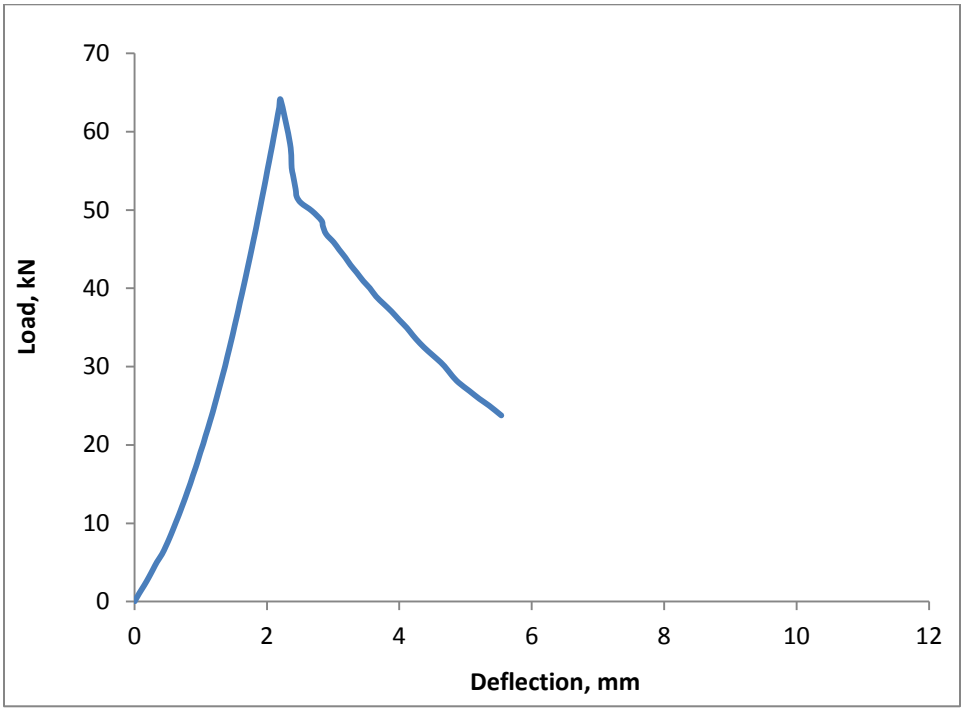

Specimen HC-B-L1

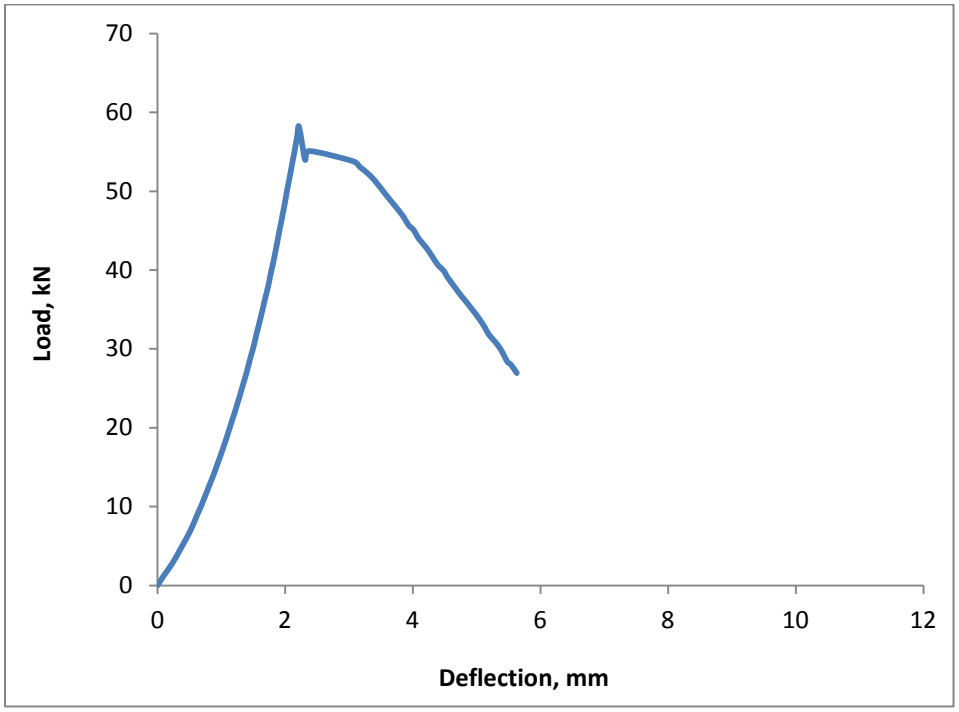

Specimen HC-B-L2

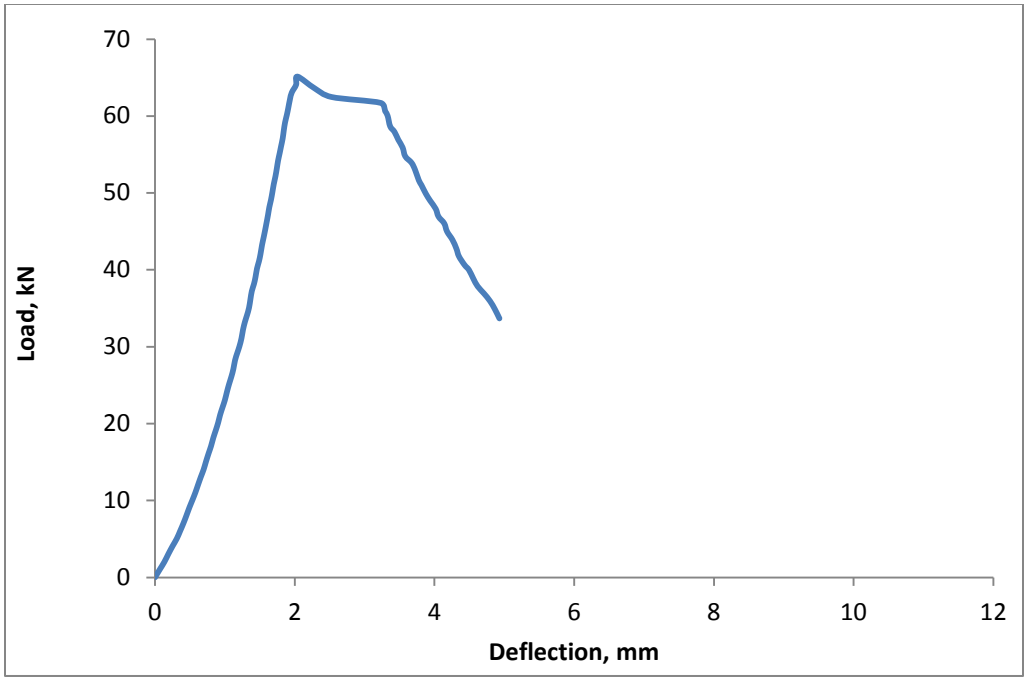

Specimen HC-B-L3

D.1.5: Load-deflections curve for three specimens of Group (iii) of beam size 390x200x1000 mm (200 mm depth) of span 900 mm.

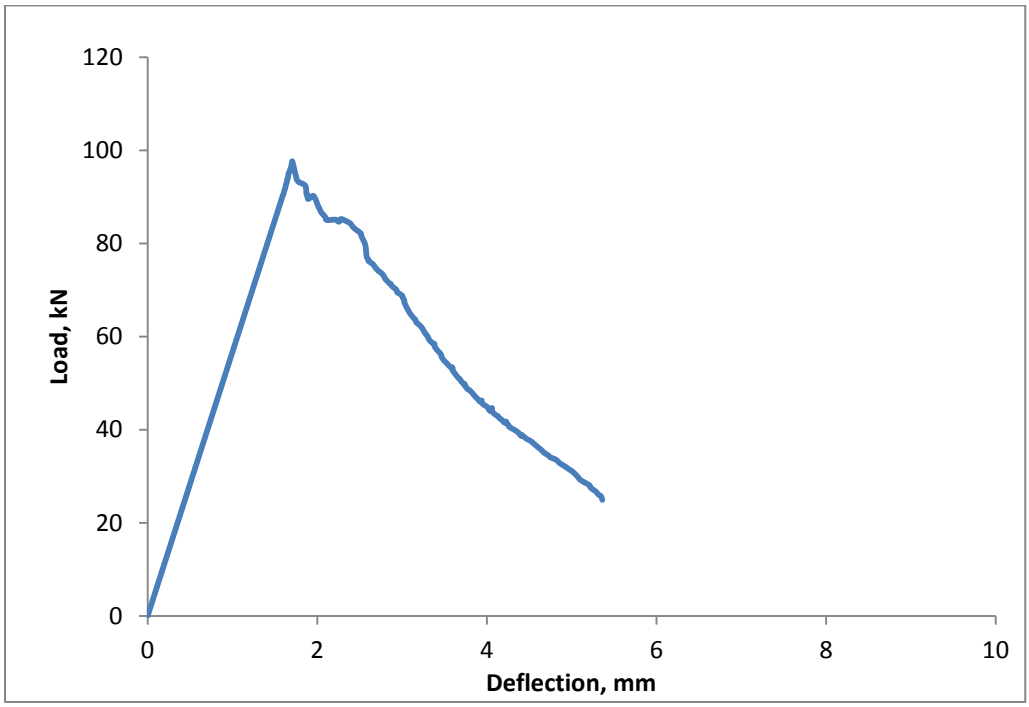

Specimen HC-C-S1

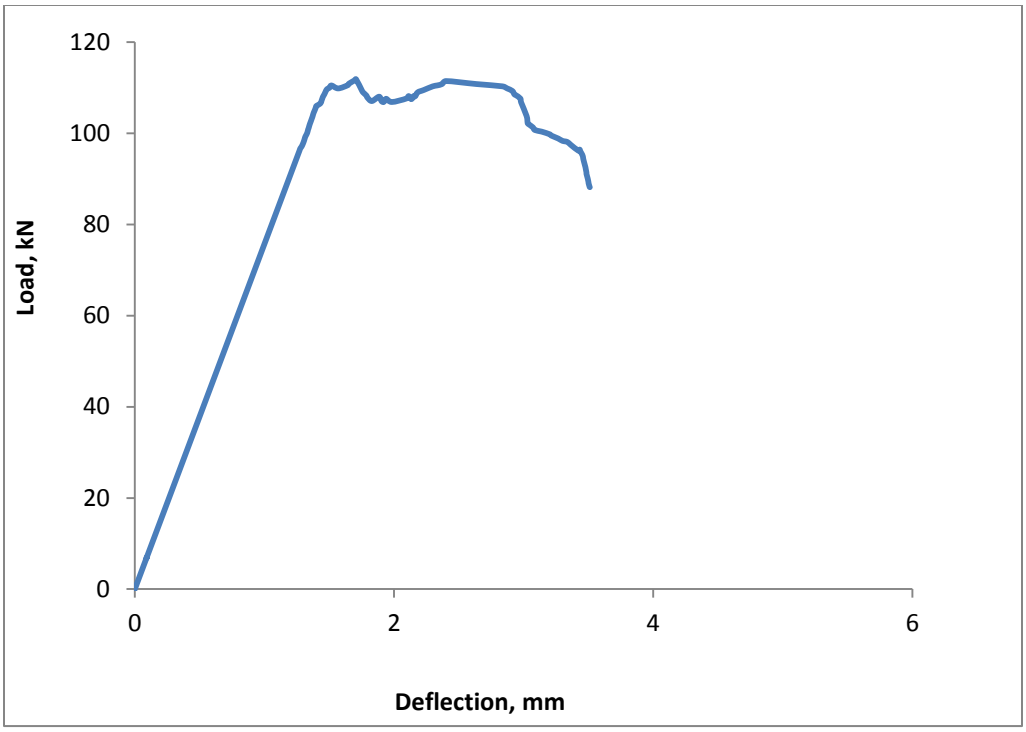

Specimen HC-C-S2

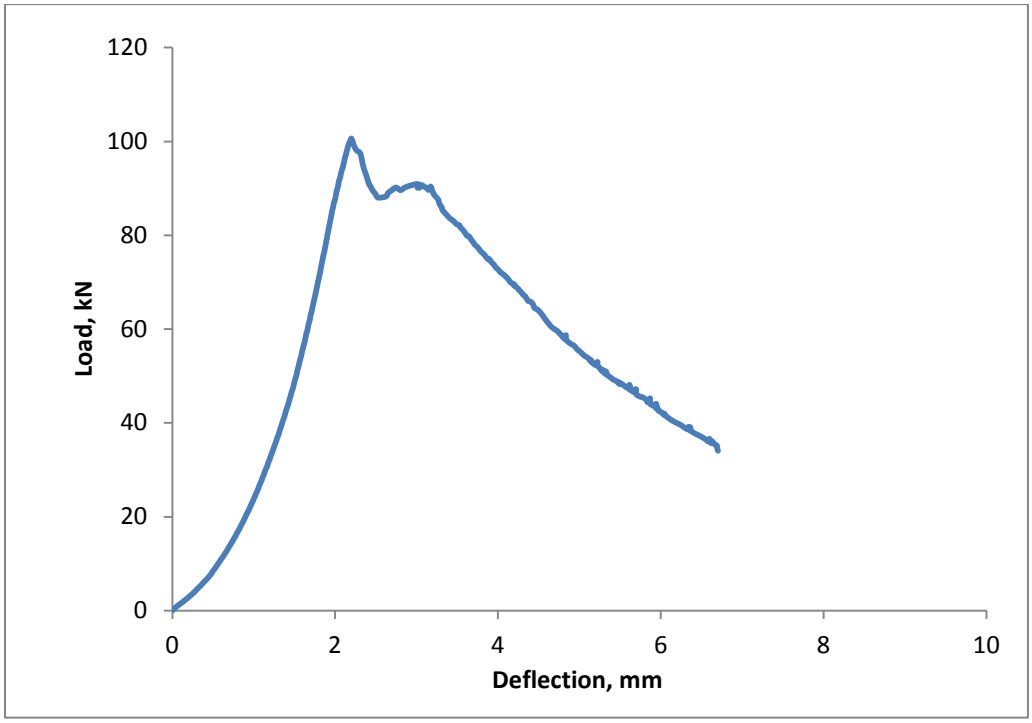

Specimen HC-C-S3

D.1.6: Load-deflections curve for three specimens of Group (iii) of beam size 390x200x1200 mm (200 mm depth) of span 1100 mm.

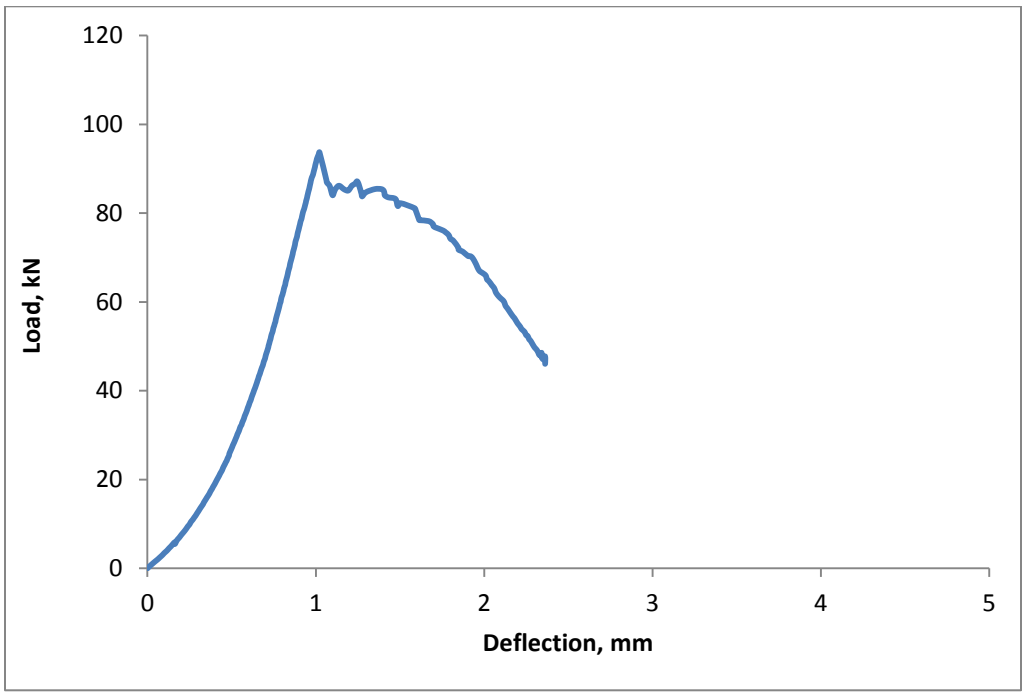

Specimen HC-C-L1

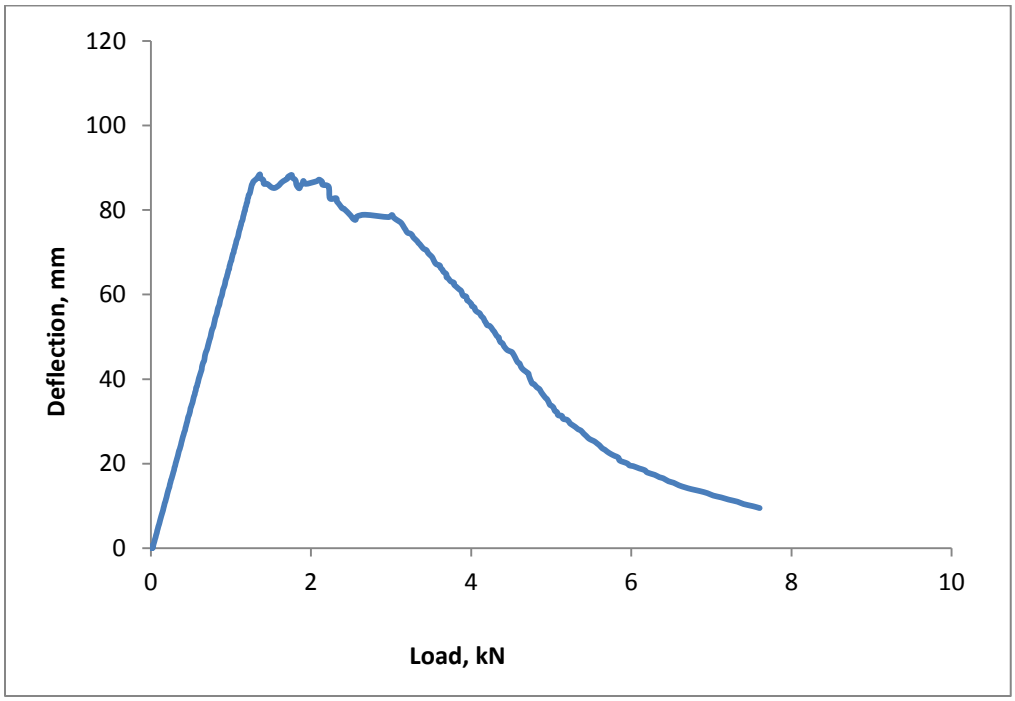

Specimen HC-C-L2

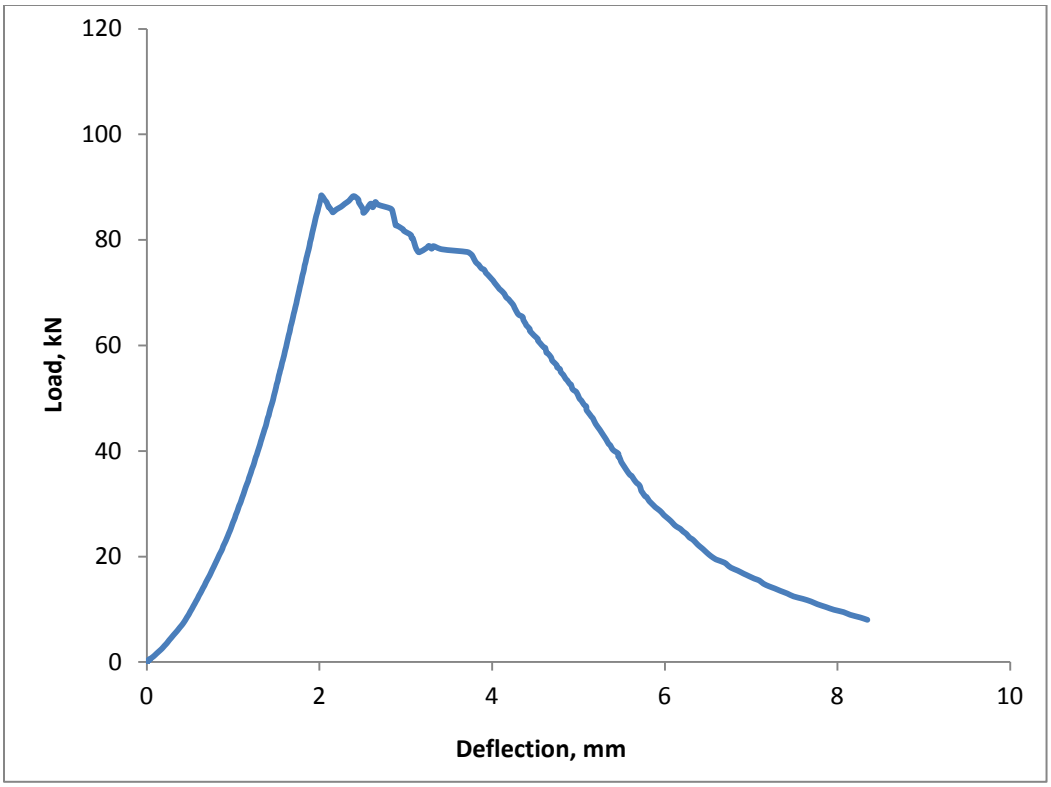

Specimen HC-C-L3

D.1.7: Load-deflections curve for three specimens of Group (iv) of beam size 380x140x1200 mm (140 mm depth) of span 1100 mm.

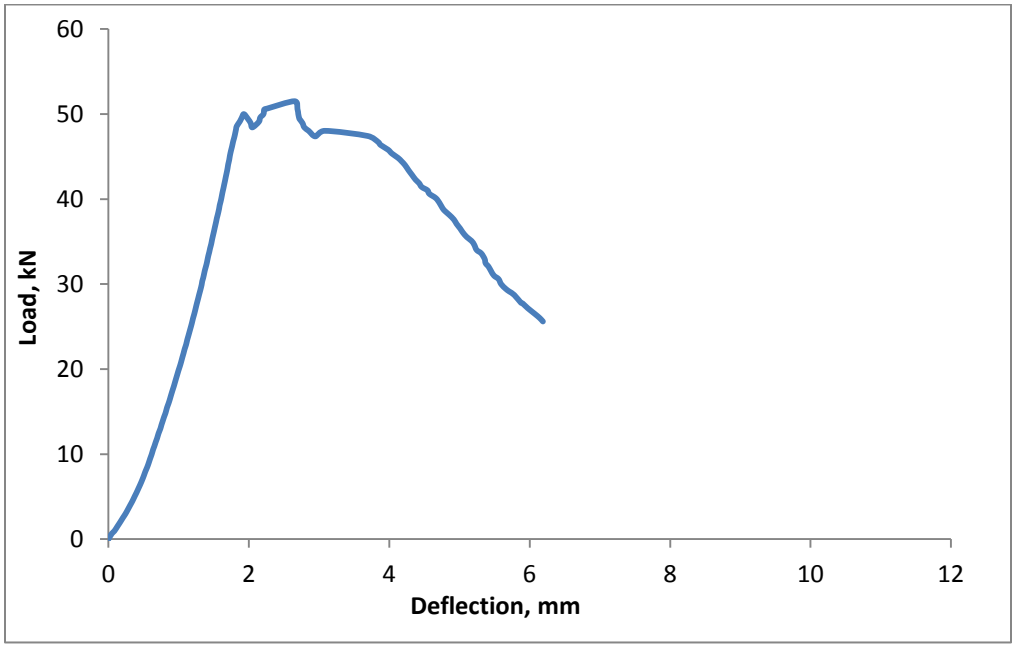

Specimen HC-D-L1

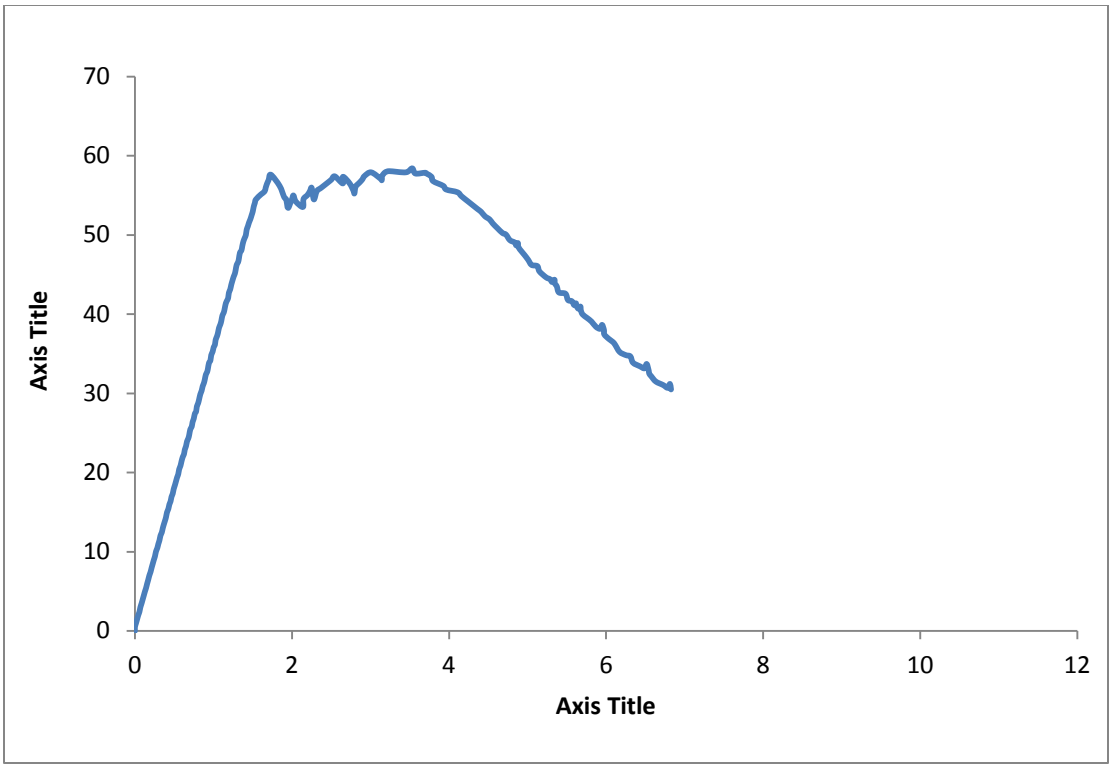

Specimen HC-D-L2

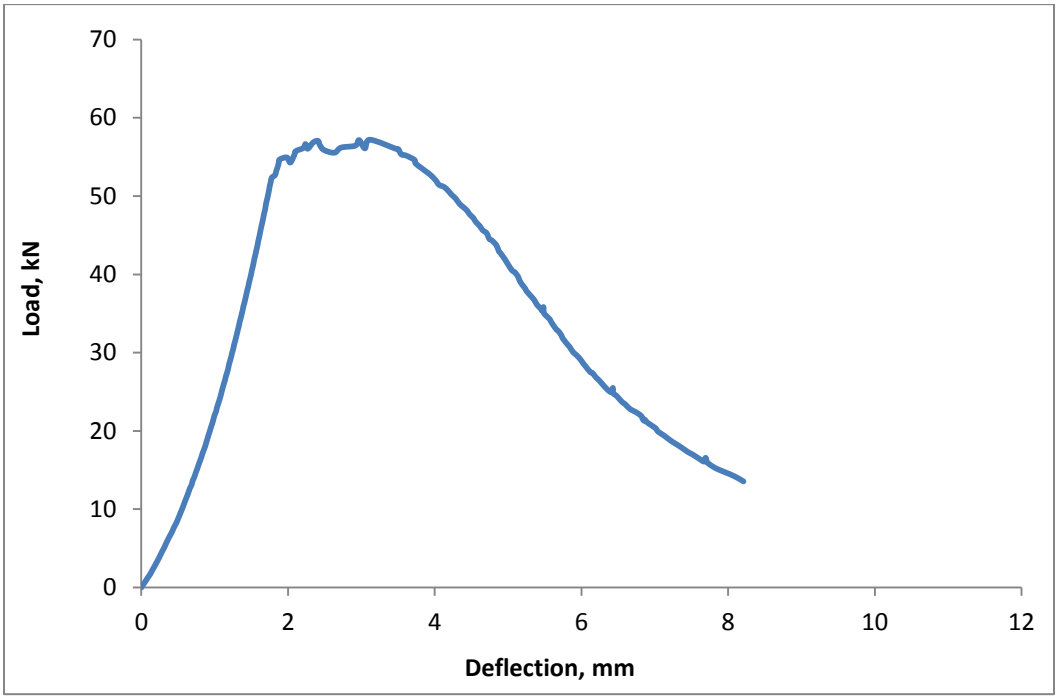

Specimen HC-D-L3

D.1.8: Load-deflections curve for three specimens of Group (v) of beam size 260x140x1000 mm (140 mm depth) of span 900 mm.

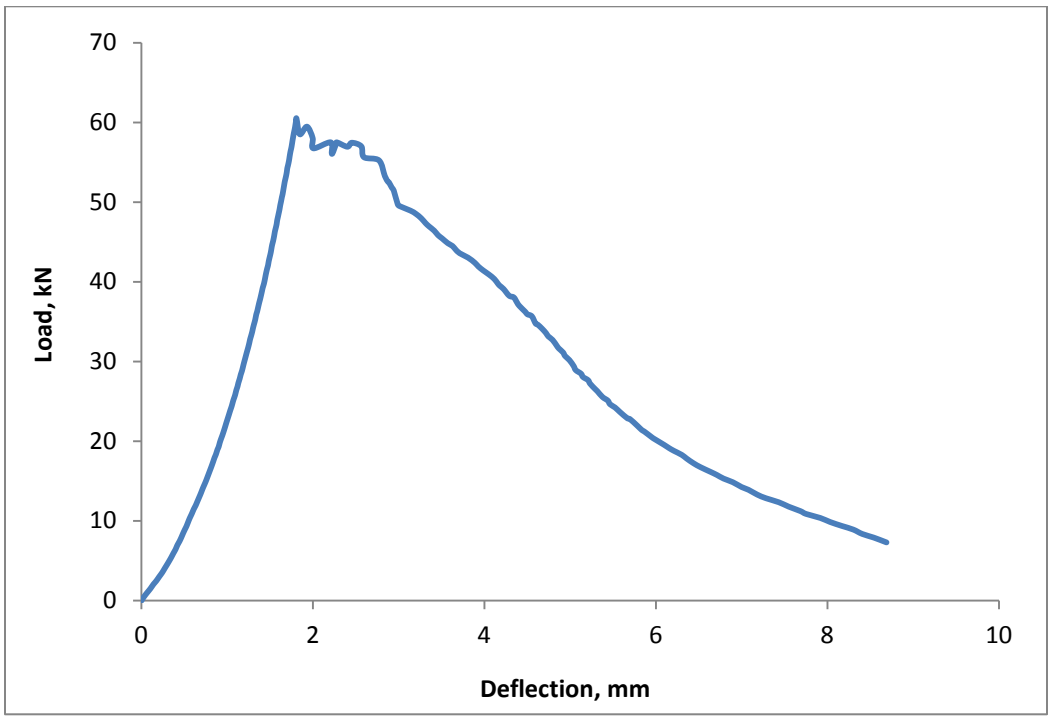

Specimen HC-E-S1

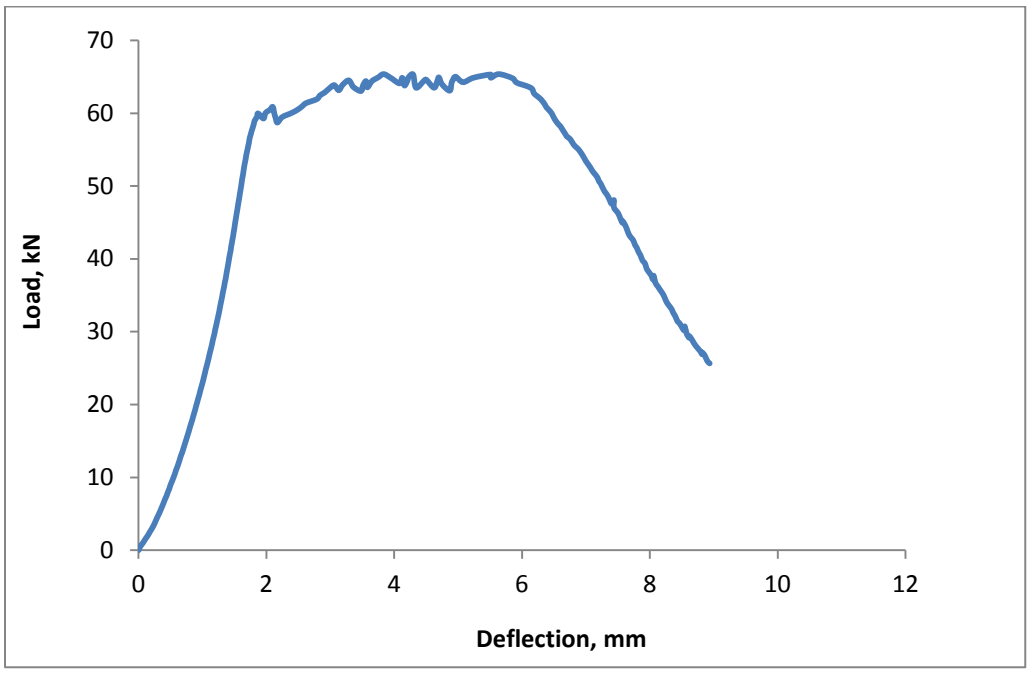

Specimen HC-E-S2

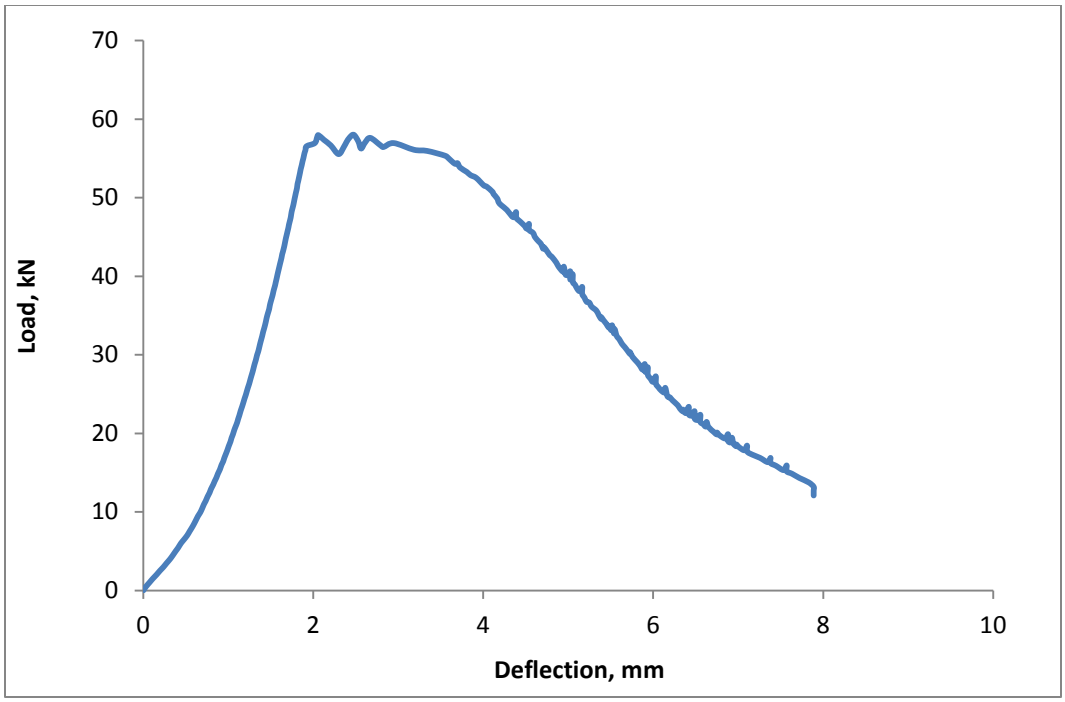

Specimen HC-E-S3

D.2.1: Load-strain curve for three hollow core specimens of Group (i) of size 260x140x1000 mm (140 mm depth) of span 900 mm.

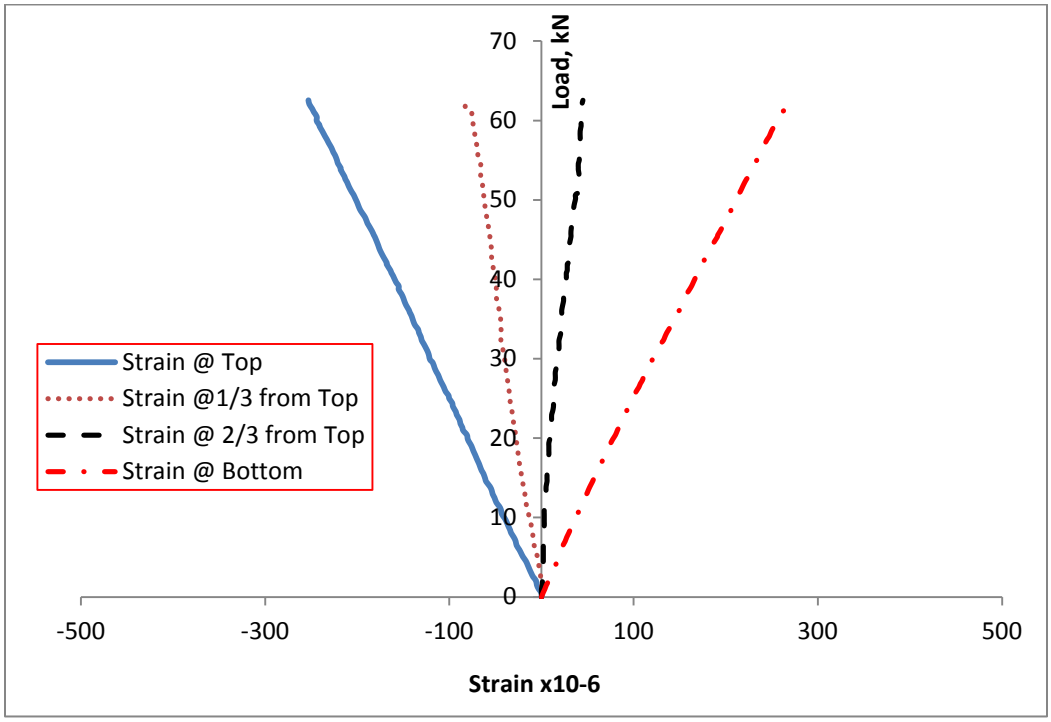

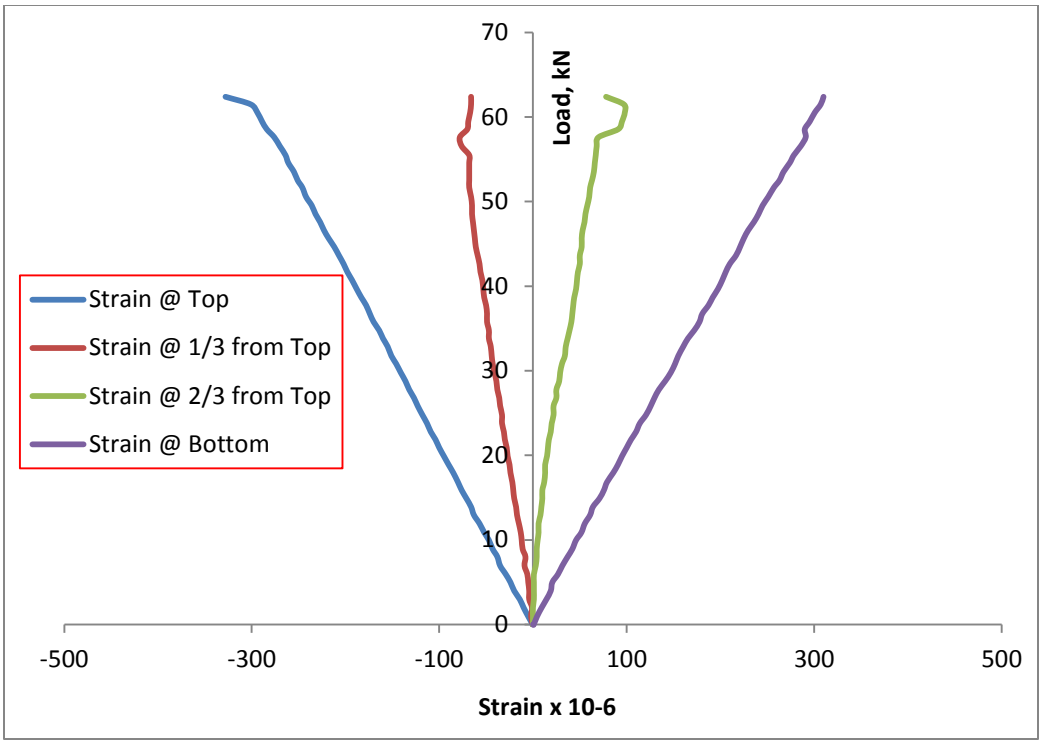
70
60
50
40
30
20
10
0
Load, kN
Strain @ Top
Strain @ 1/3 from Top
Strain @ 2/3 from Top
Strain @ Bottom
-500
-300
-100
100
300
500
Strain x 10-6

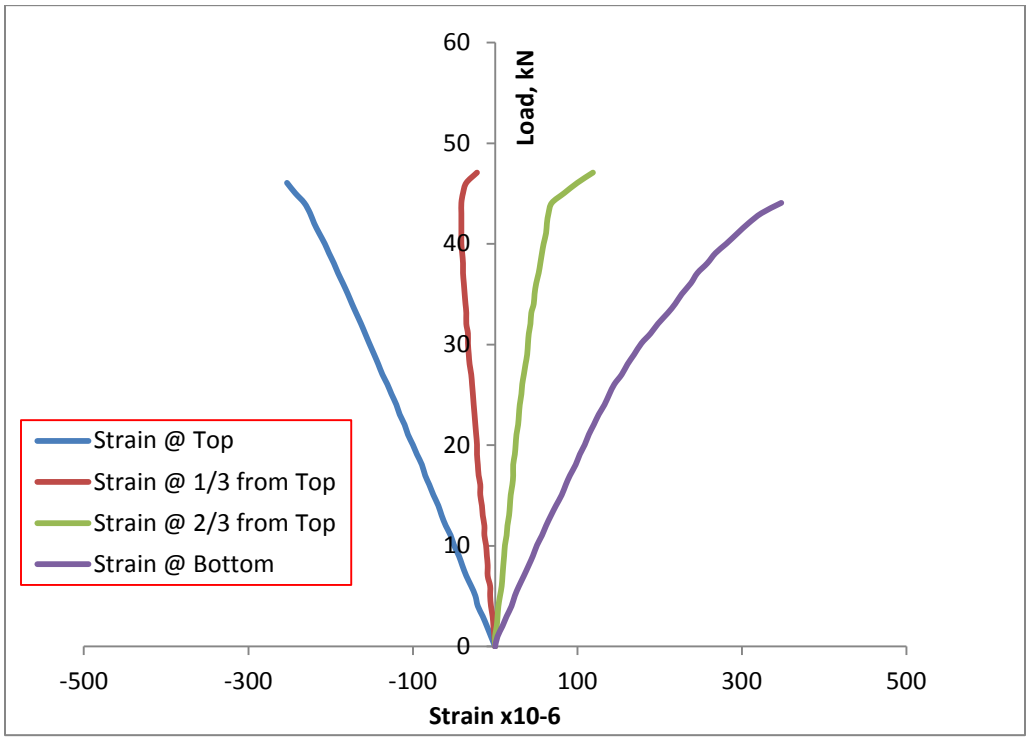
60
50
40
30
20
10
0
Load, kN
Strain @ Top
Strain @ 1/3 from Top
Strain @ 2/3 from Top
Strain @ Bottom
-500
-300
-100
100
300
500
Strain x10-6

D.2.2: Load-strain curve for three hollow core specimens of Group (i) of size 260x140x1200 mm (140 mm depth) of span 1100 mm.

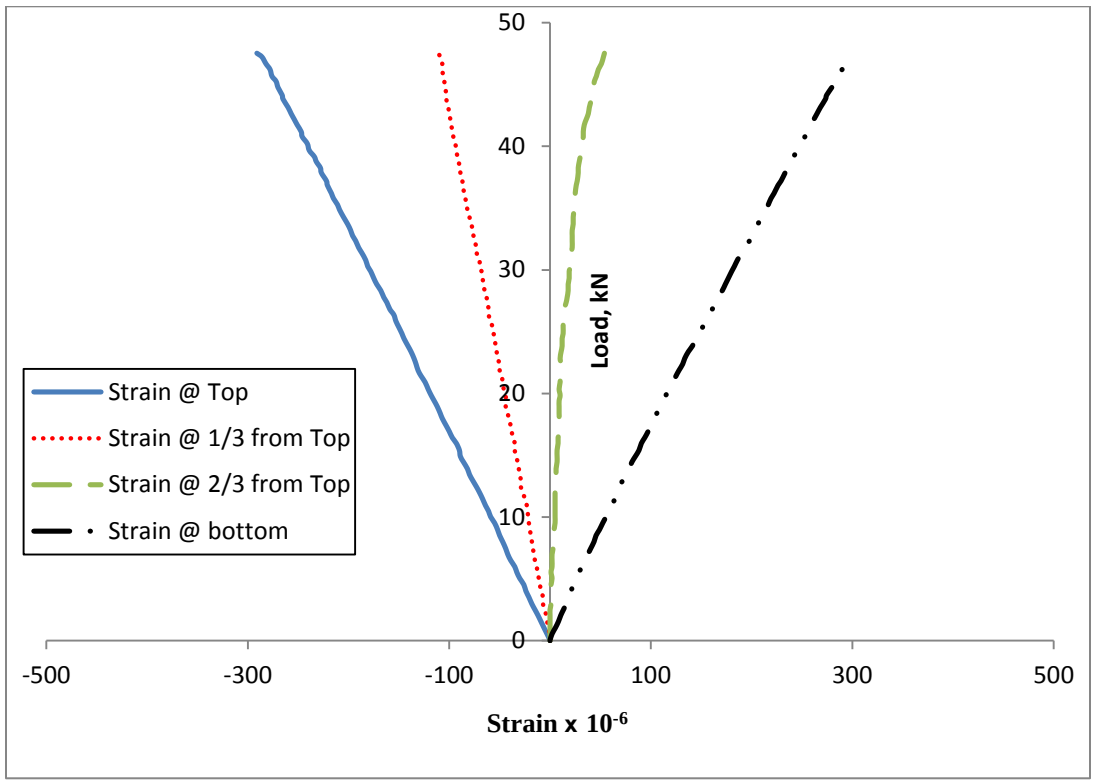

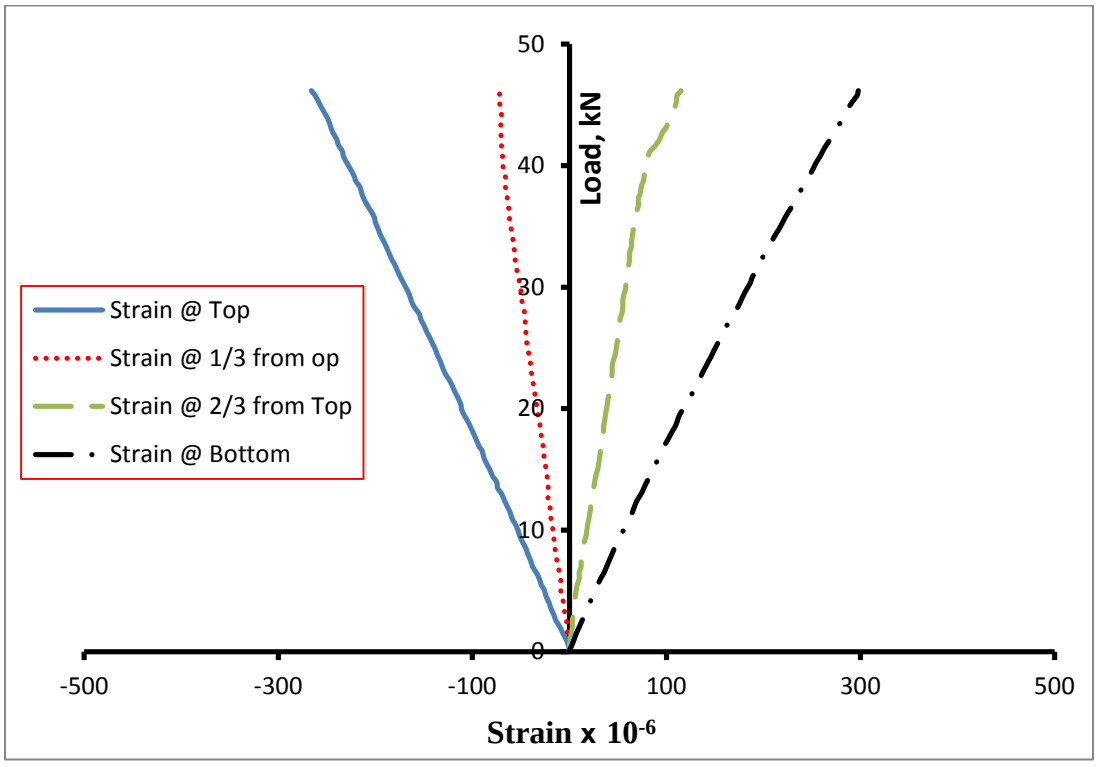

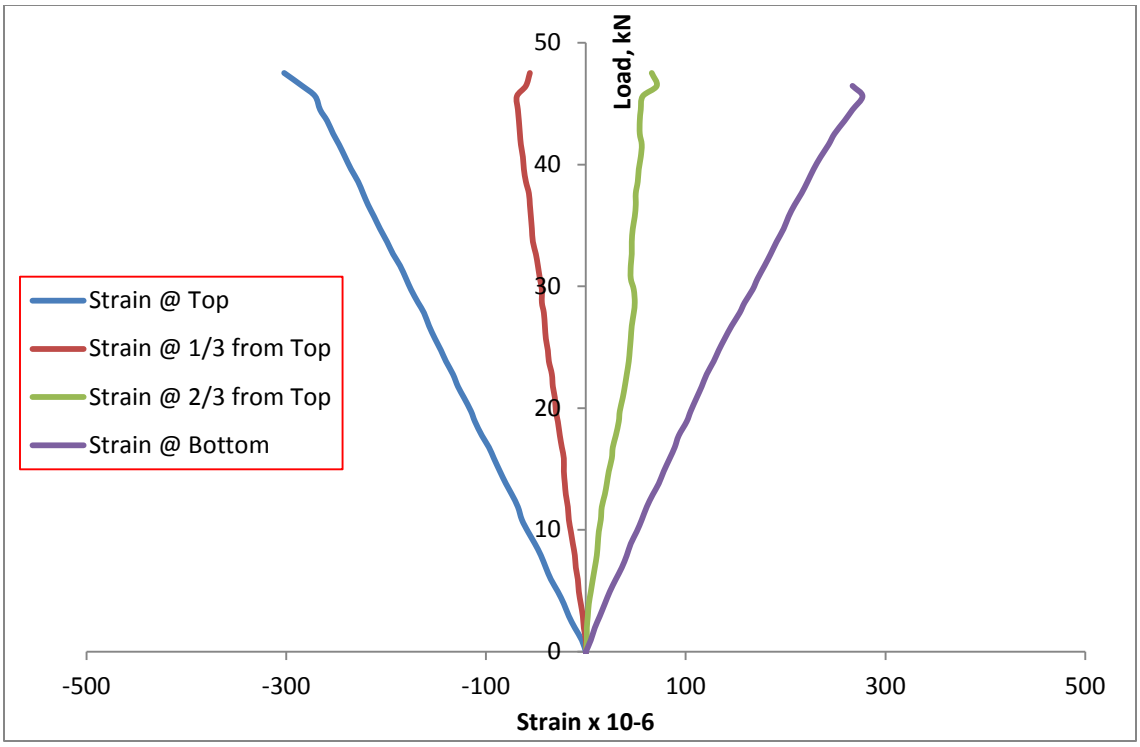

D.2.3: Load-strain curve for three hollow core specimens of Group (ii) of size 330x175x1000 mm (175 mm depth) of span 900 mm.

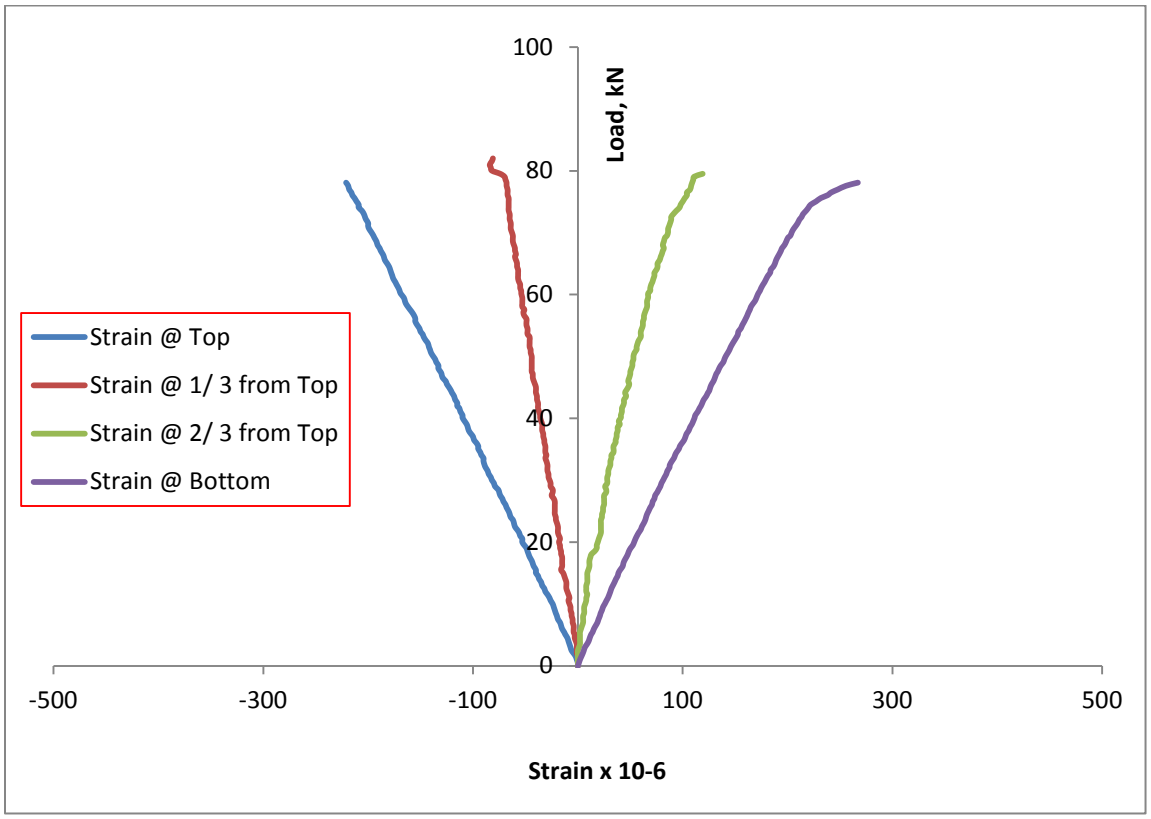

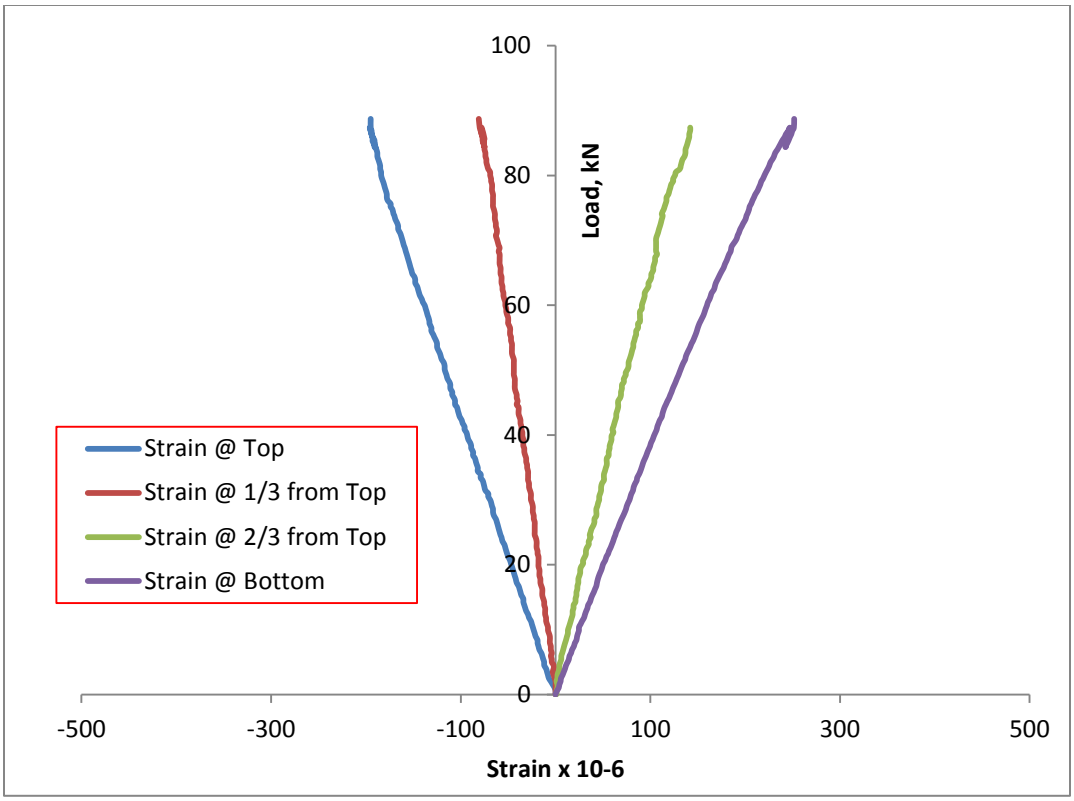
100
80
60
40
20
0
Load, kN
Strain @ Top
Strain @ 1/3 from Top
Strain @ 2/3 from Top
Strain @ Bottom
-500
-300
-100
100
300
500
Strain x 10-6

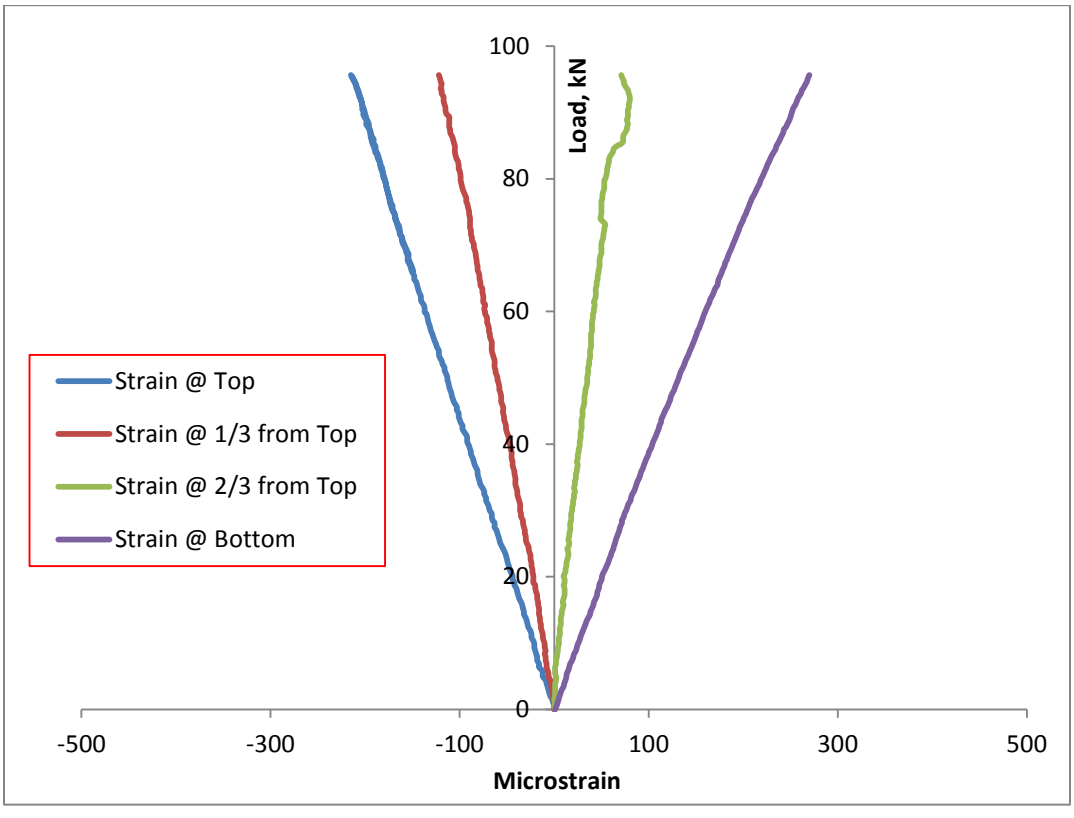
100
80
60
40
20
0
Load, kN
Strain @ Top
Strain @ 1/3 from Top
Strain @ 2/3 from Top
Strain @ Bottom
-500
-300
-100
100
300
500
Microstrain

D.2.4: Load-strain curve for three hollow core specimens of Group (ii) of size 330x175x1200 mm (175 mm depth) of span 1100 mm.

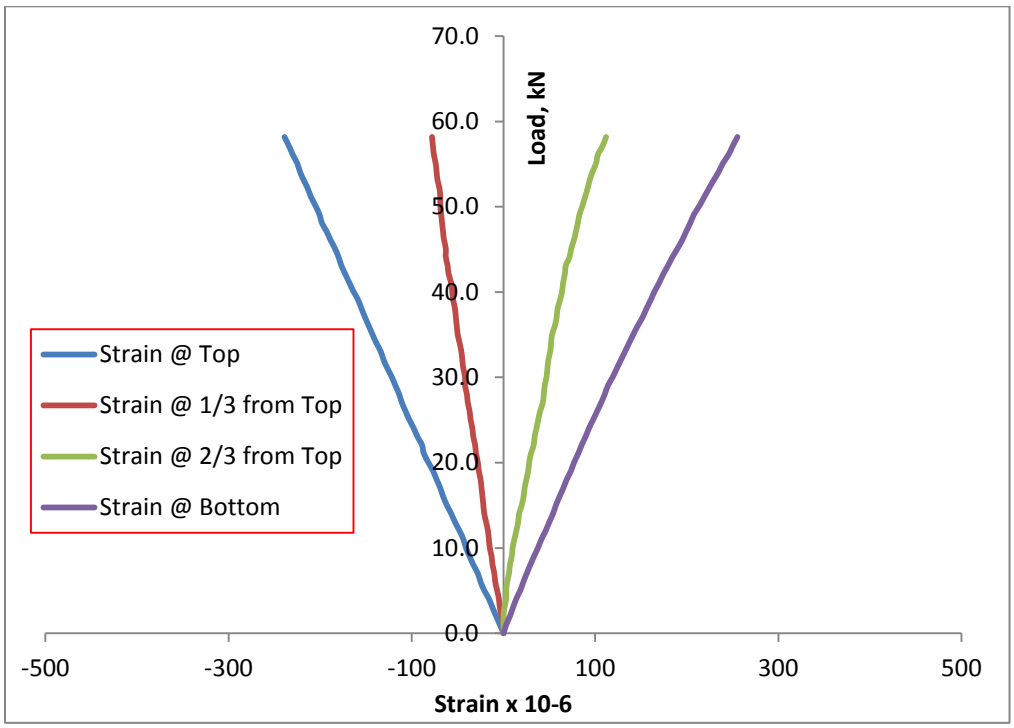

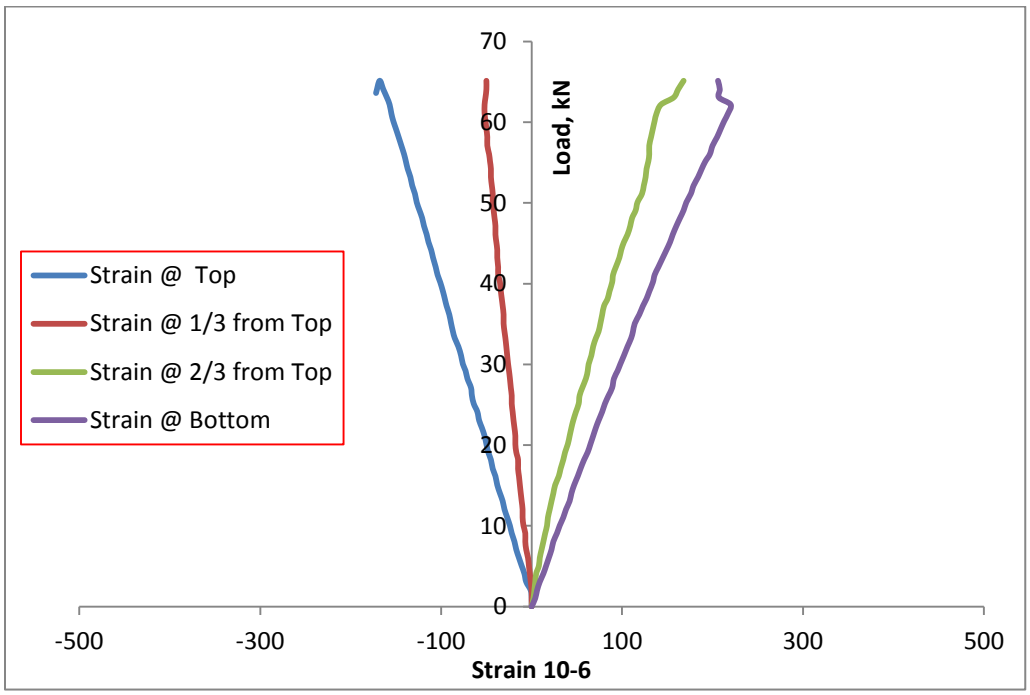

D.2.5: Load-strain curve for three hollow core specimens of Group (iii) of size 390x200x1000 mm (200 mm depth) of span 900 mm.

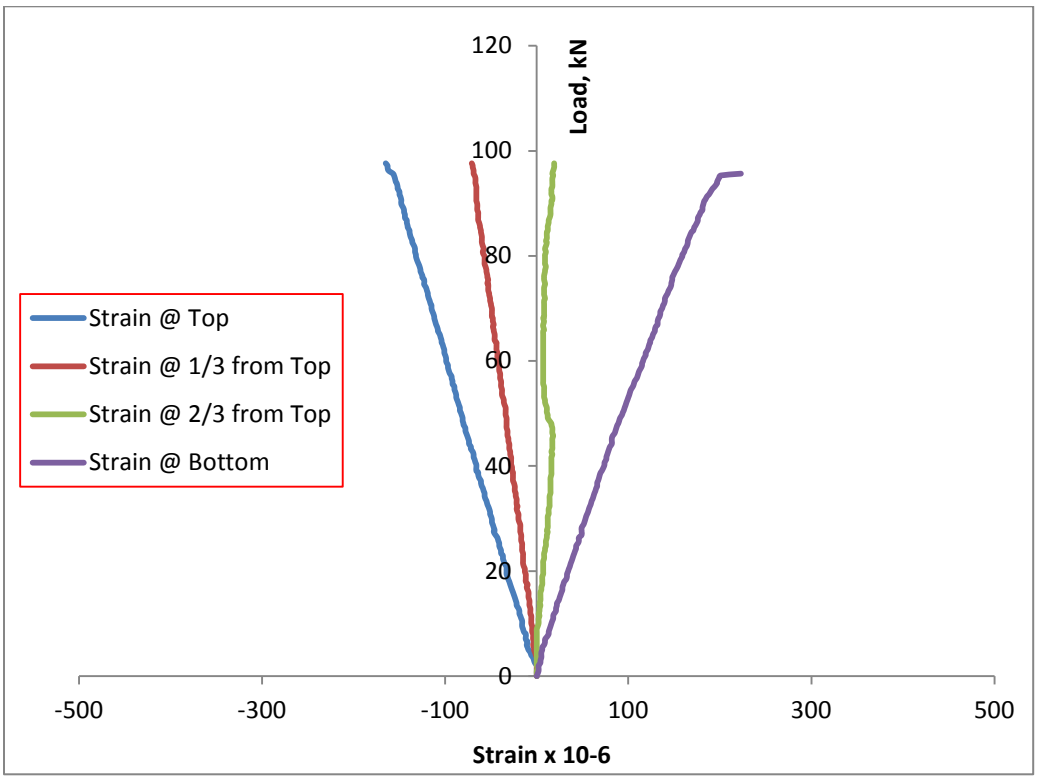

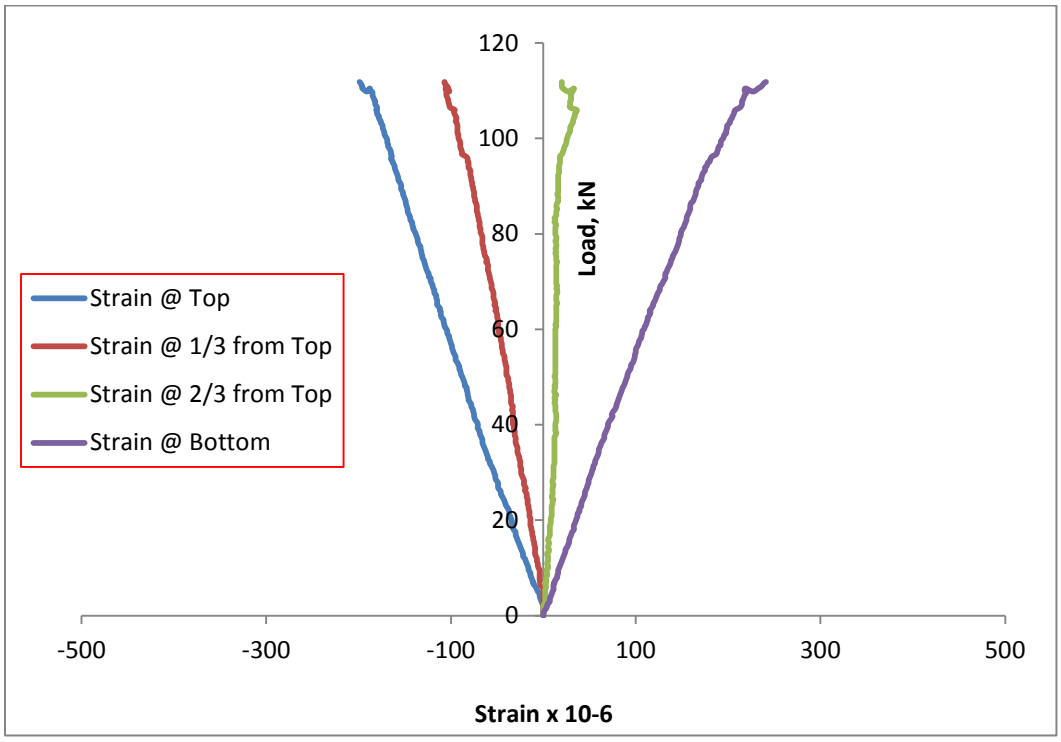

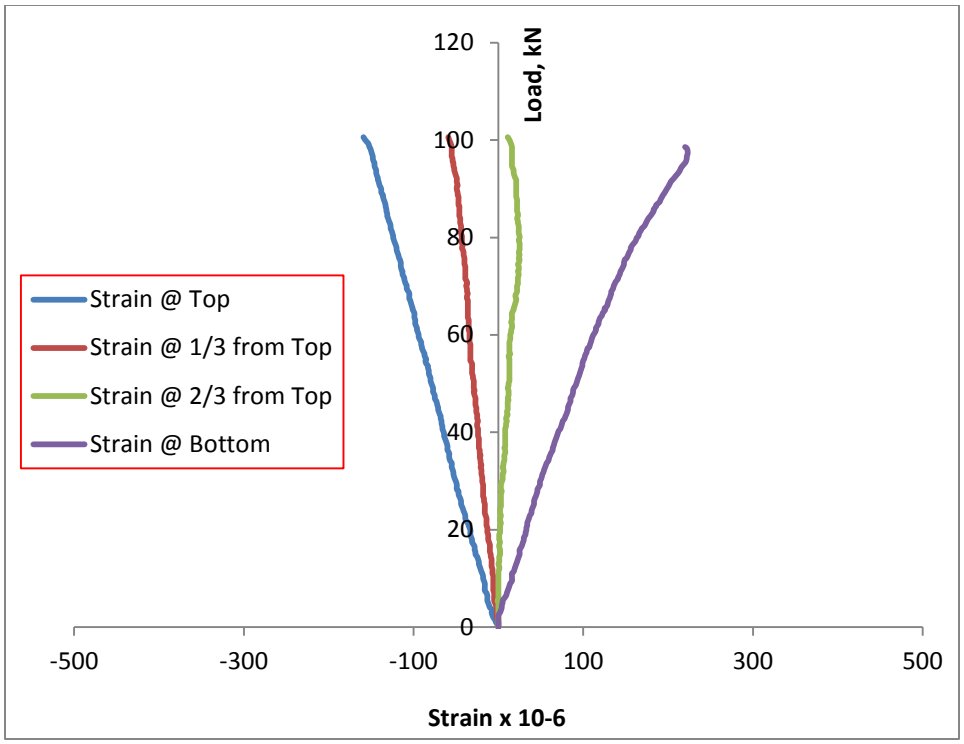

D.2.6: Load-strain curve for three hollow core specimens of Group (iii) of size 390x200x1200 mm (200 mm depth) of span 1100 mm.

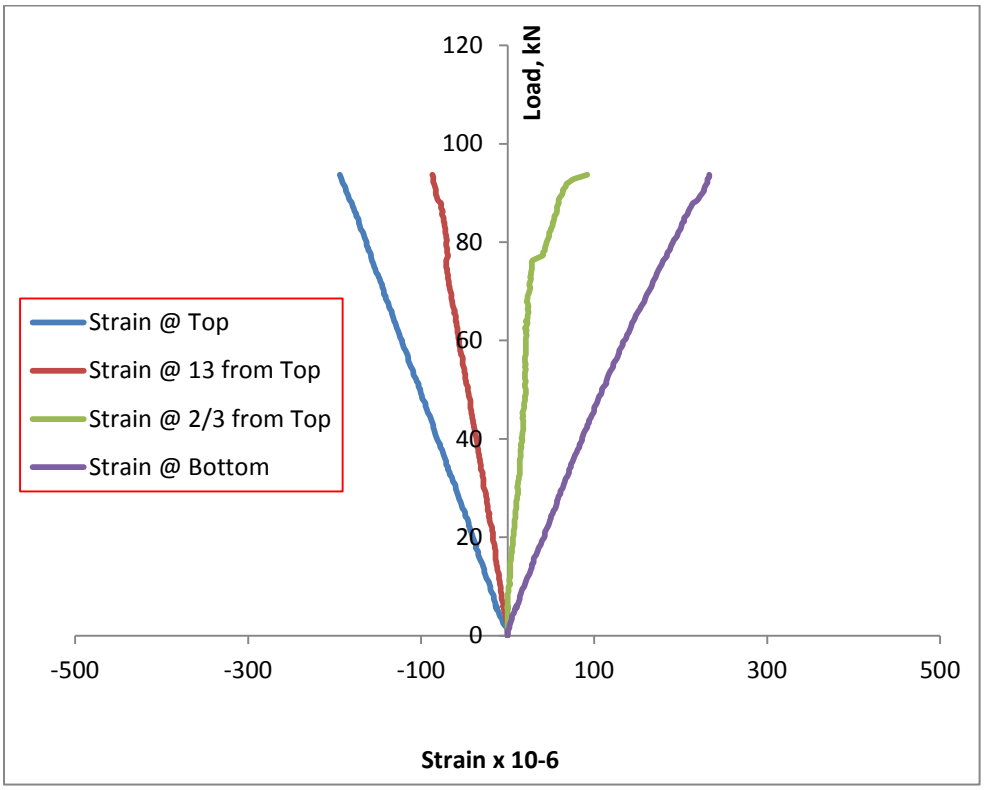

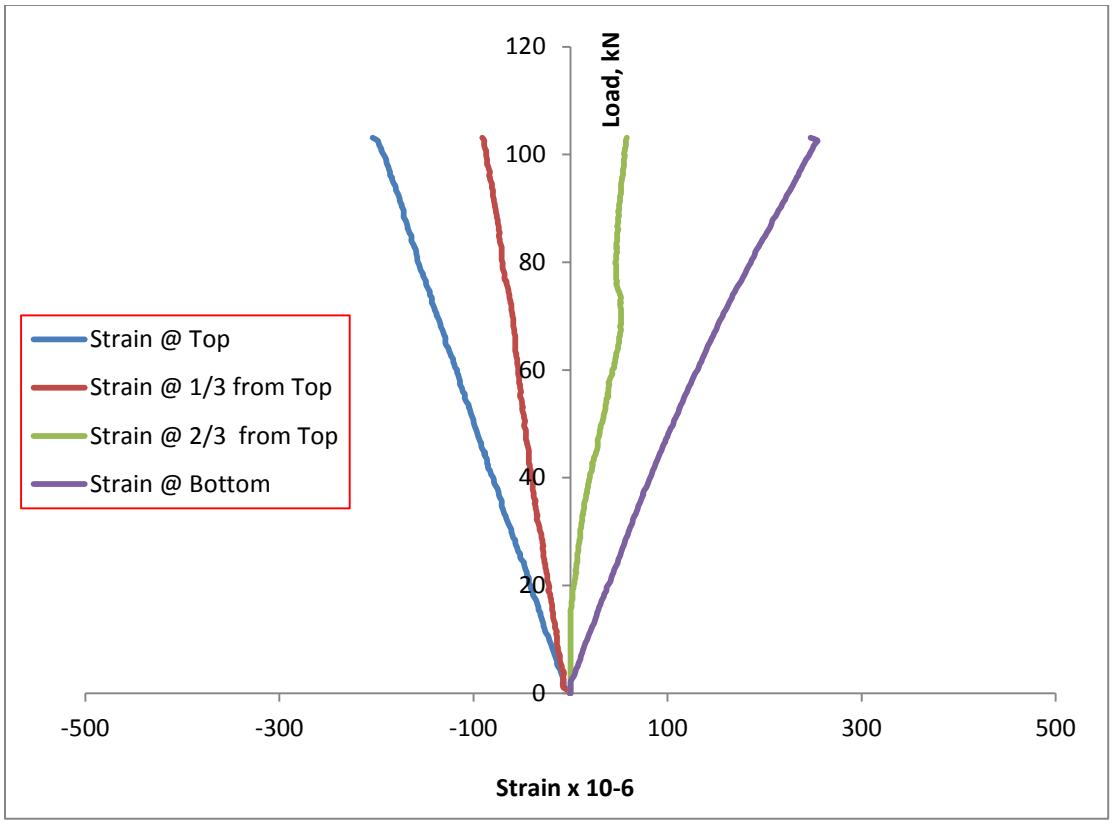
120
100
80
60
40
20
0
Load, kN
Strain @ Top
Strain @ 1/3 from Top
Strain @ 2/3 from Top
Strain @ Bottom
-500
-300
-100
100
300
500
Strain x 10-6

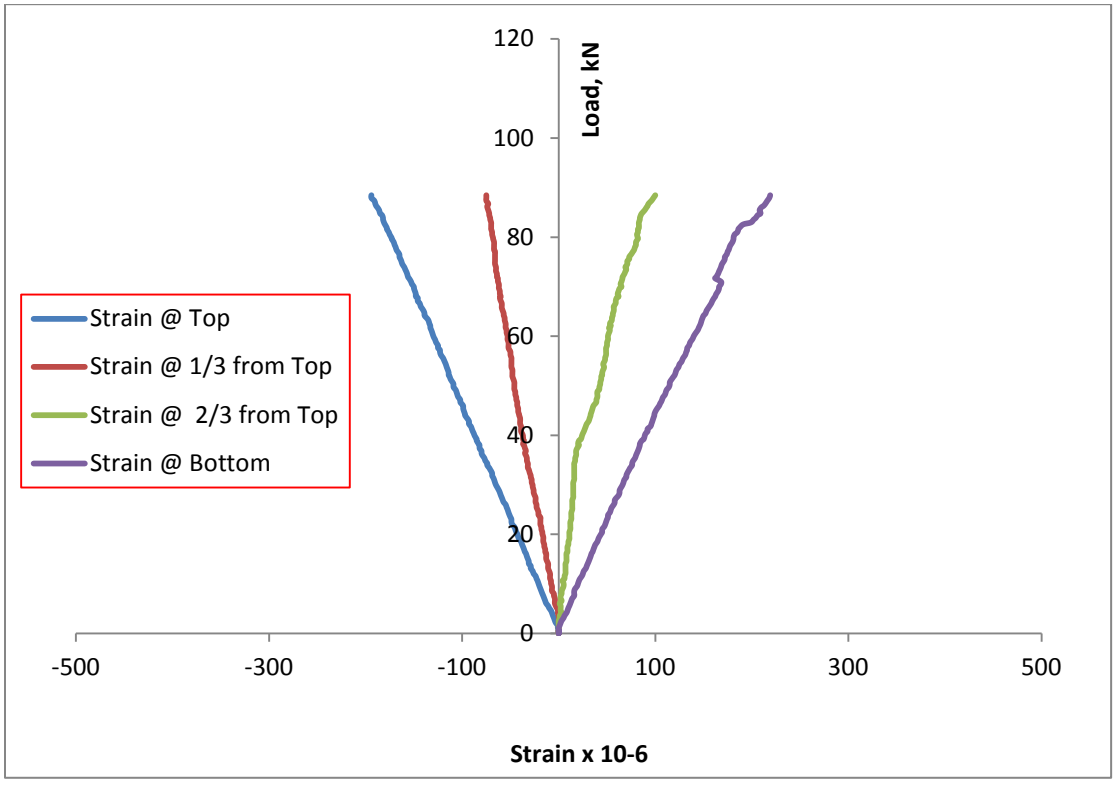
120
100
80
60
40
20
0
Load, kN
Strain @ Top
Strain @ 1/3 from Top
Strain @ 2/3 from Top
Strain @ Bottom
-500
-300
-100
100
300
500
Strain x 10-6

D.2.7: Load-strain curve for three hollow core specimens of Group (iv) of size 380x140x1200 mm (140 mm depth) of span 1100 mm.

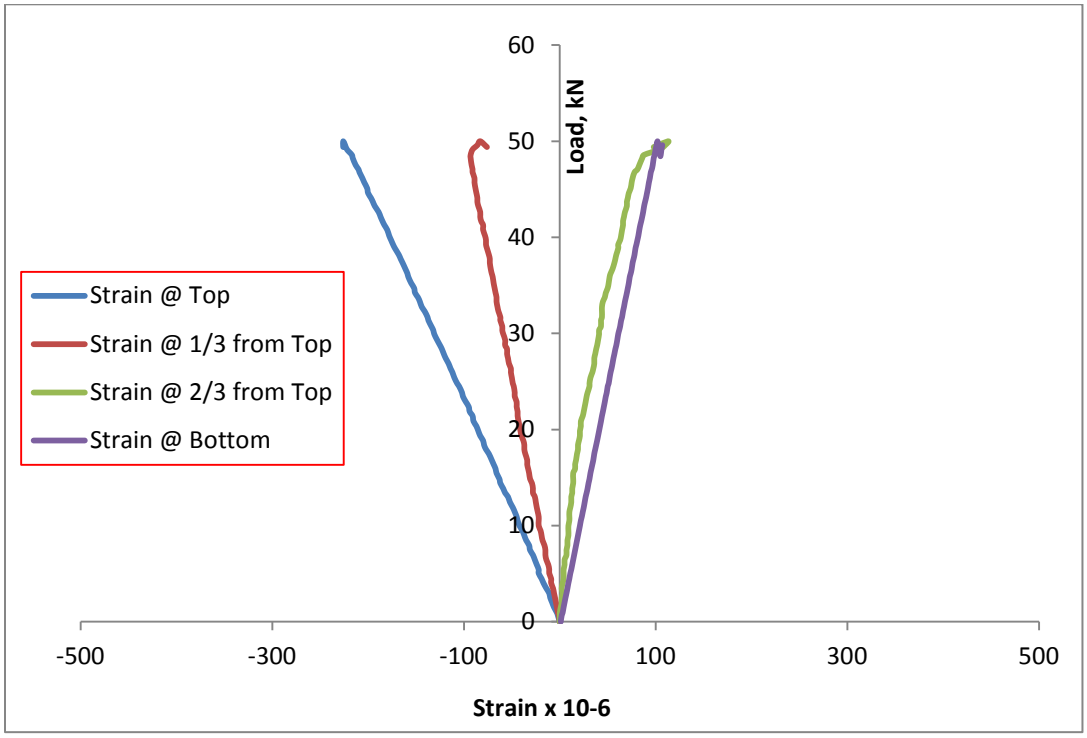

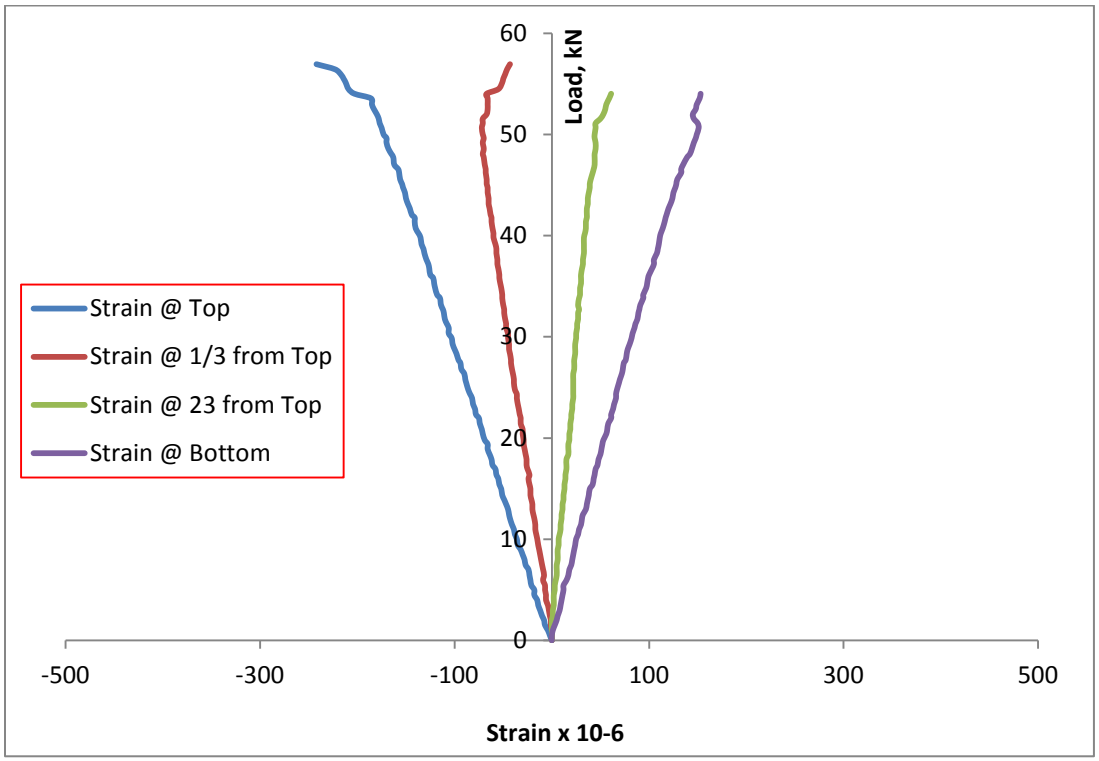

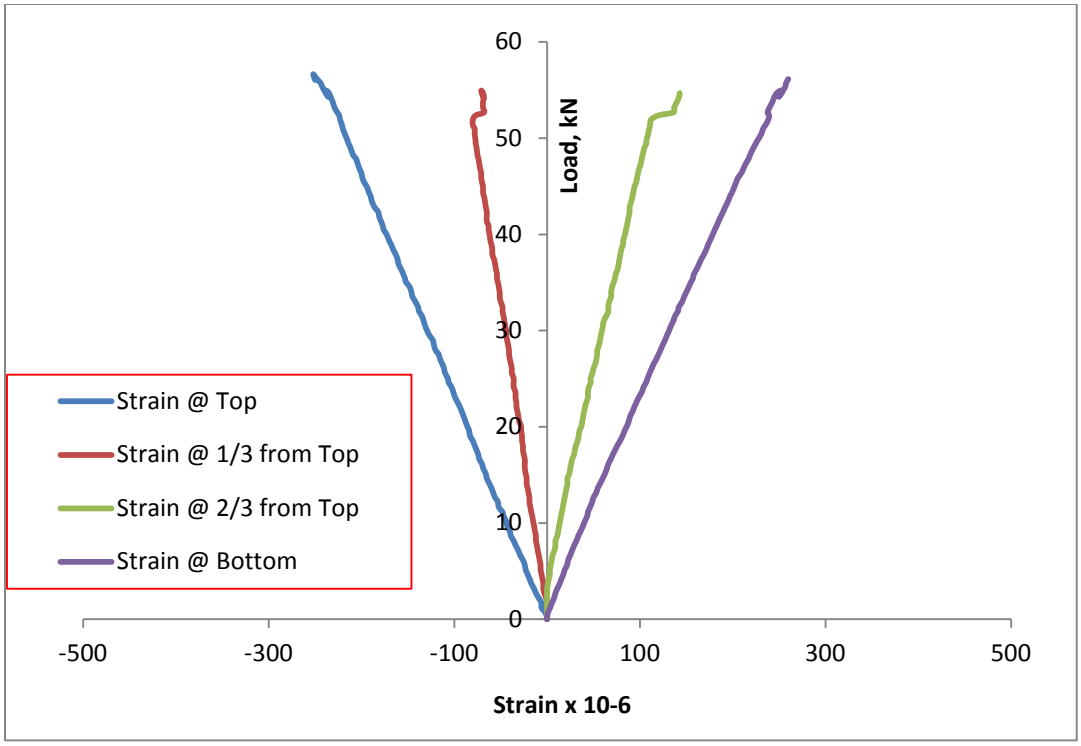

D.2.8: Load-strain curve for three hollow core specimens of Group (v) of size 260x140x1000 mm (140 mm depth) of span 900 mm.

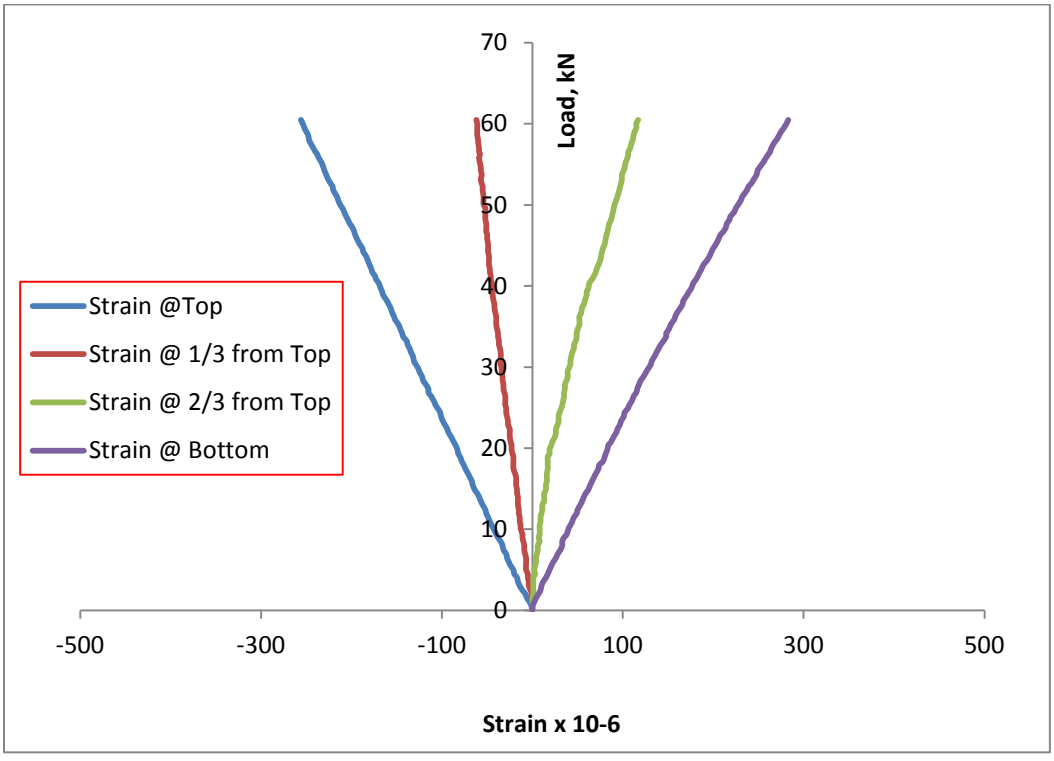

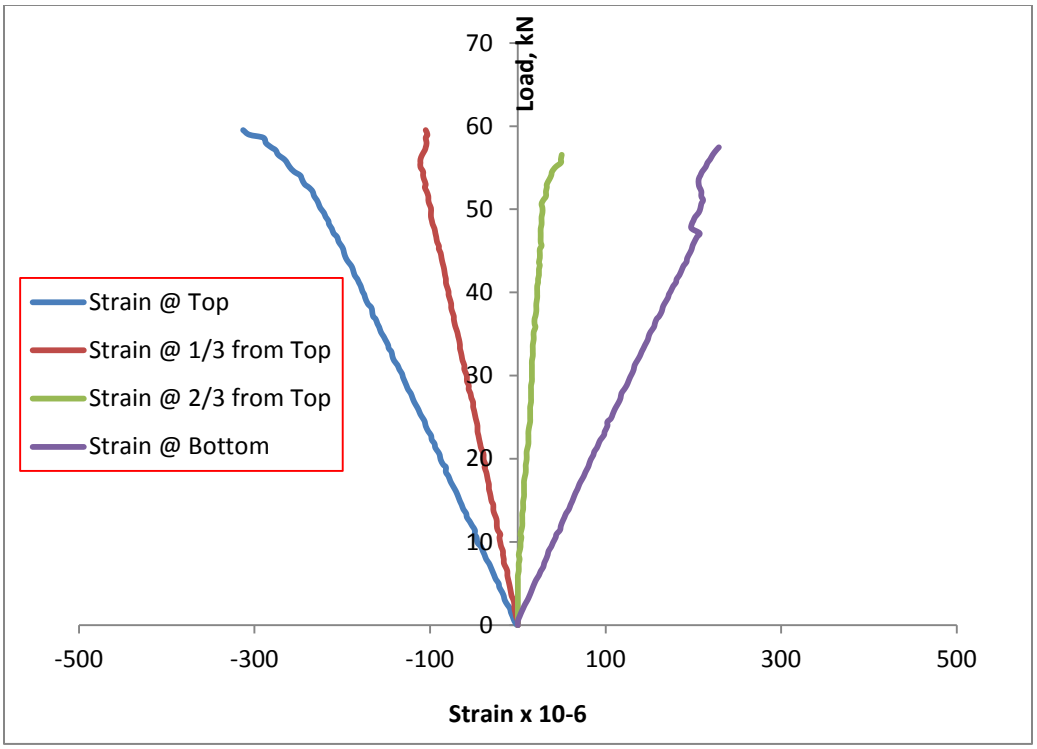
Load, kN
70
60
50
40
30
20
10
0
-500
-300
-100
100
300
500
Strain @ Top
Strain @ 1/3 from Top
Strain @ 2/3 from Top
Strain @ Bottom
Strain x 10-6

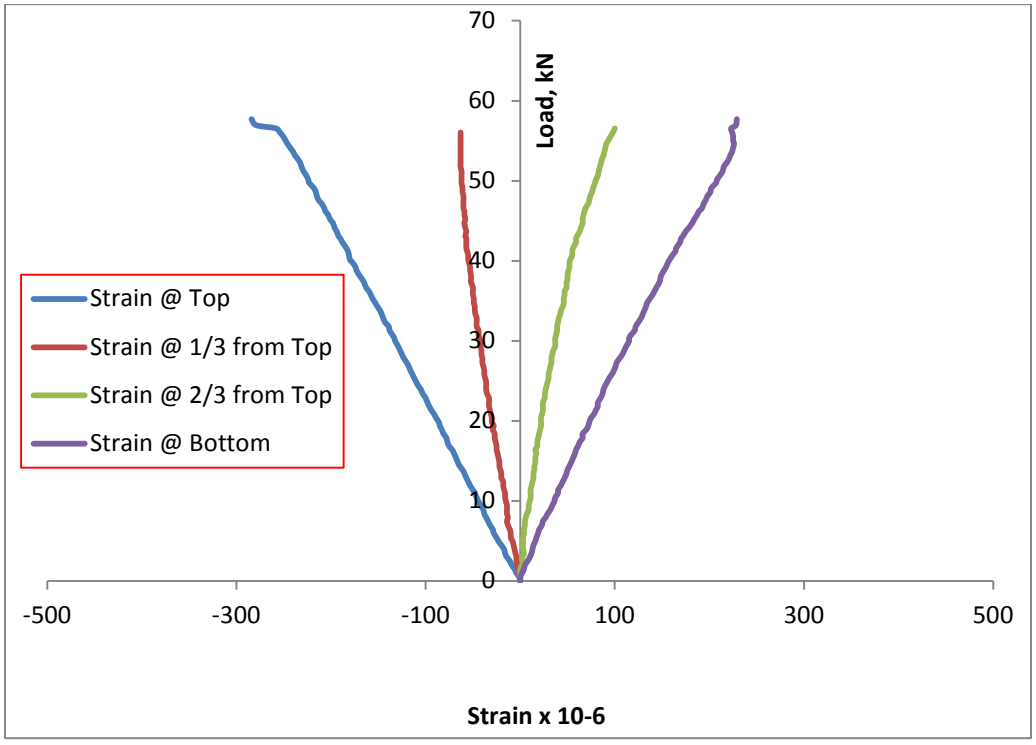
Load, kN
70
60
50
40
30
20
10
0
-500
-300
-100
100
300
500
Strain @ Top
Strain @ 1/3 from Top
Strain @ 2/3 from Top
Strain @ Bottom
Strain x 10-6

D.3.1: Strain profile along the depth for three hollow core specimens of Group (i) of size 260x140x1000 mm (140 mm depth) of span 900 mm. Each plot shows one specimen.

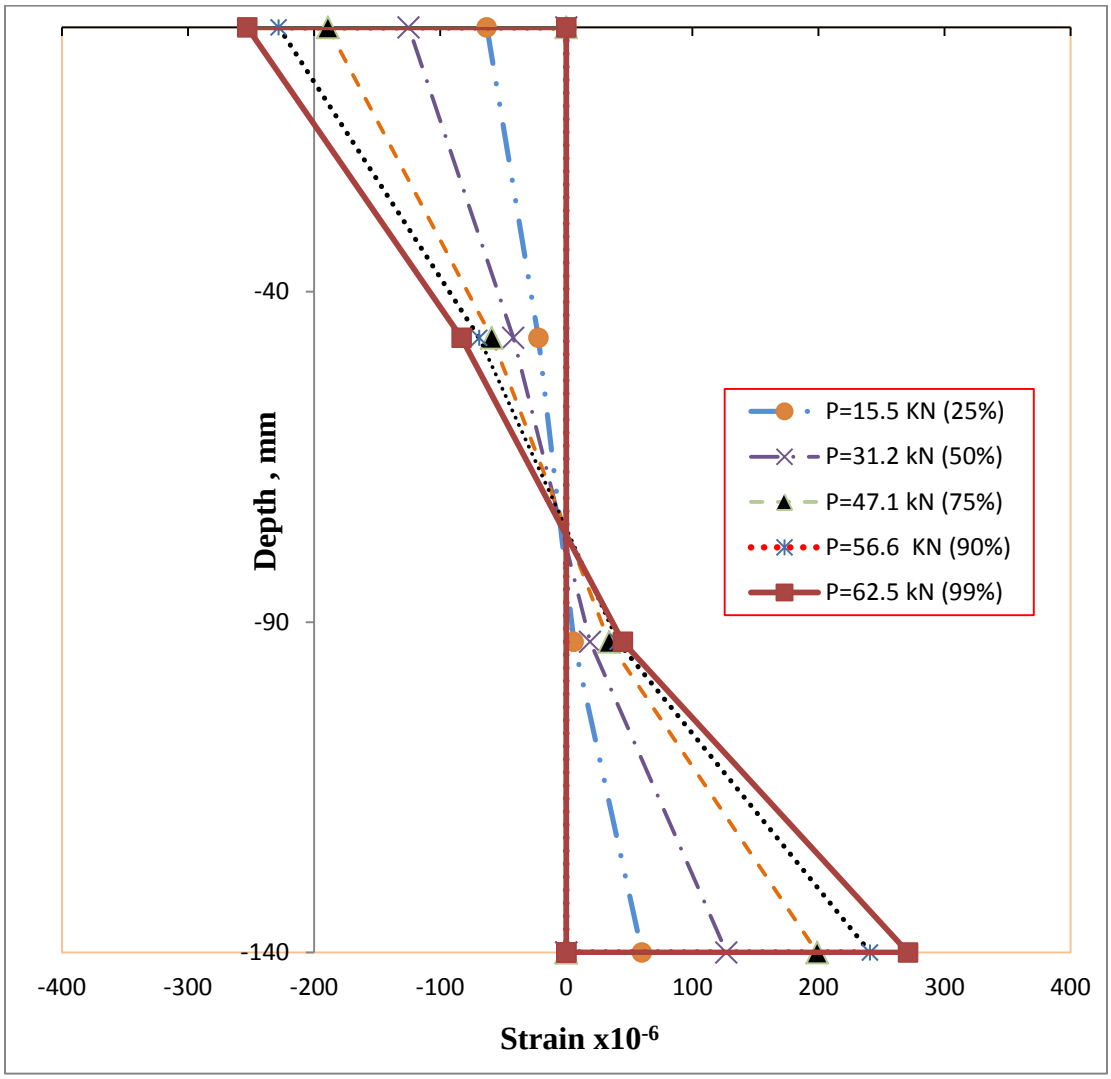

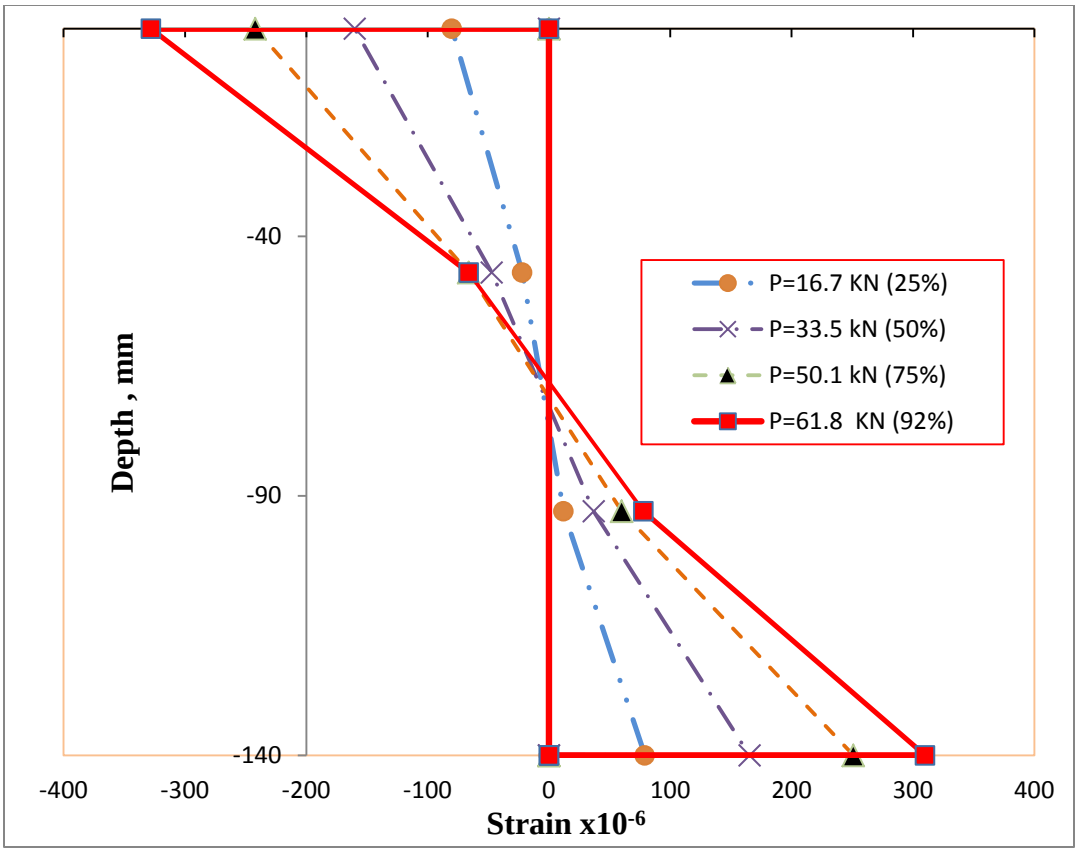
-40
-90
-140
Depth , mm
-400
-300
-200
-100
0
100
200
300
400
Strain x10-6
P=16.7 KN (25%)
P=33.5 kN (50%)
P=50.1 kN (75%)
P=61.8 KN (92%)

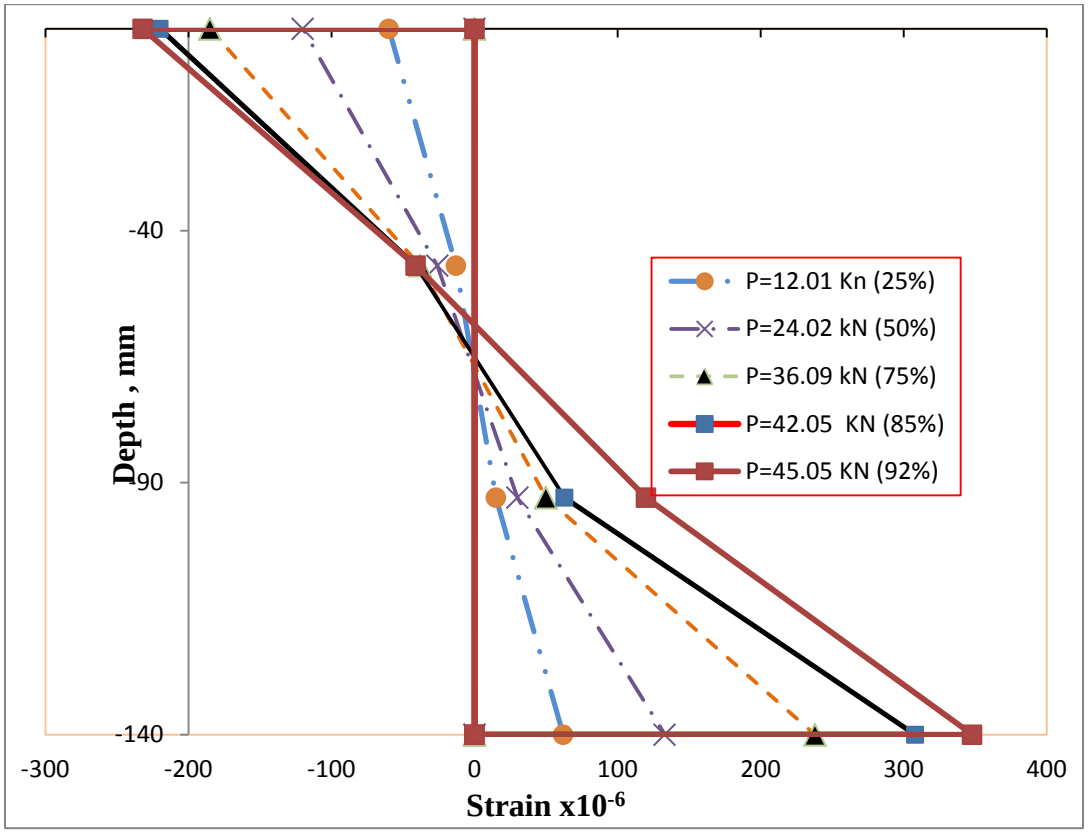
-40
-90
-140
Depth , mm
-300
-200
-100
0
100
200
300
400
Strain x10-6
P=12.01 Kn (25%)
P=24.02 kN (50%)
P=36.09 kN (75%)
P=42.05 KN (85%)
P=45.05 KN (92%)

D.3.2: Strain profile along the depth for three hollow core specimens of Group (i) of size 260x140x1200 mm (140 mm depth) of span 1100 mm. Each plot shows one specimen.

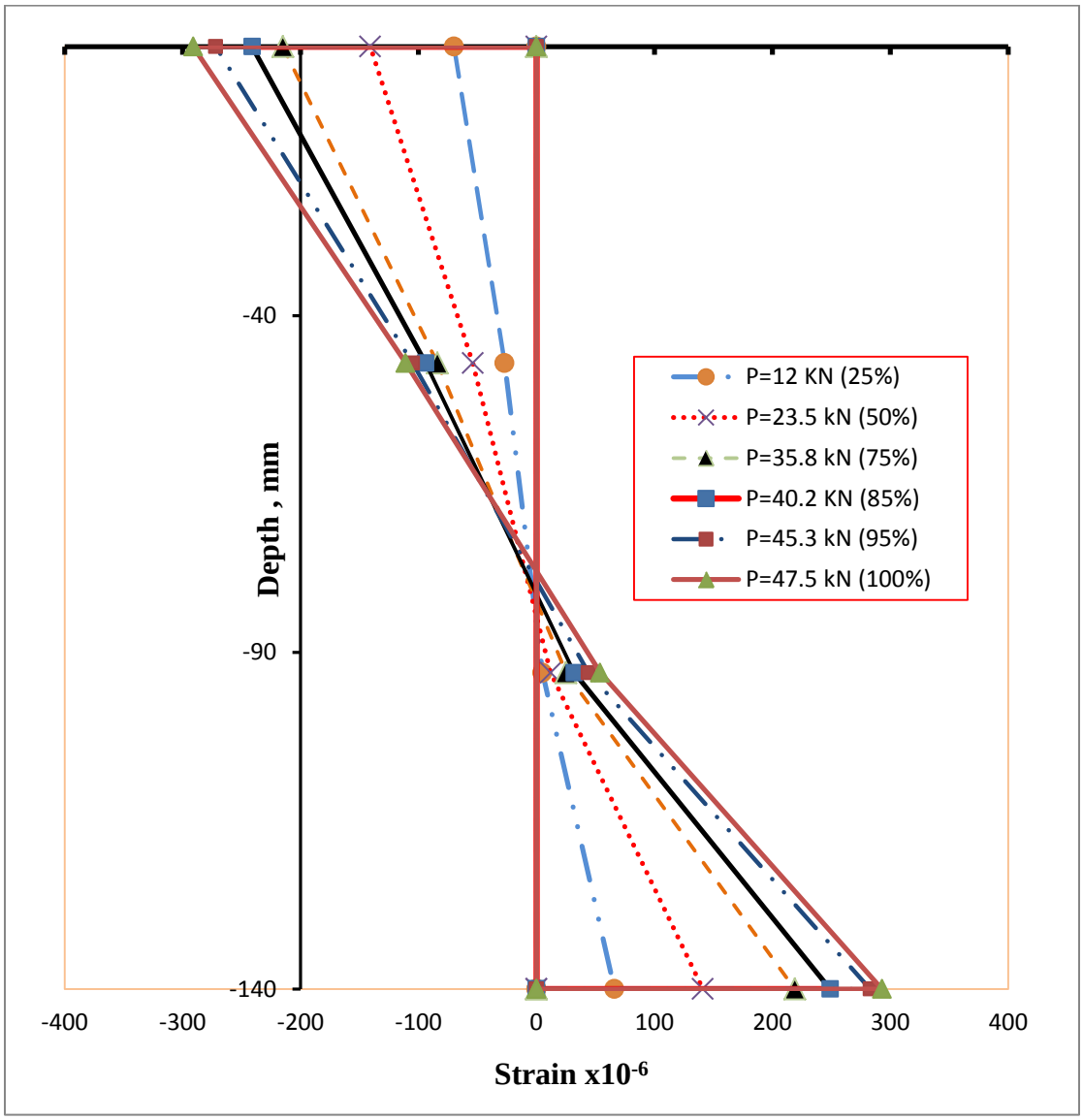

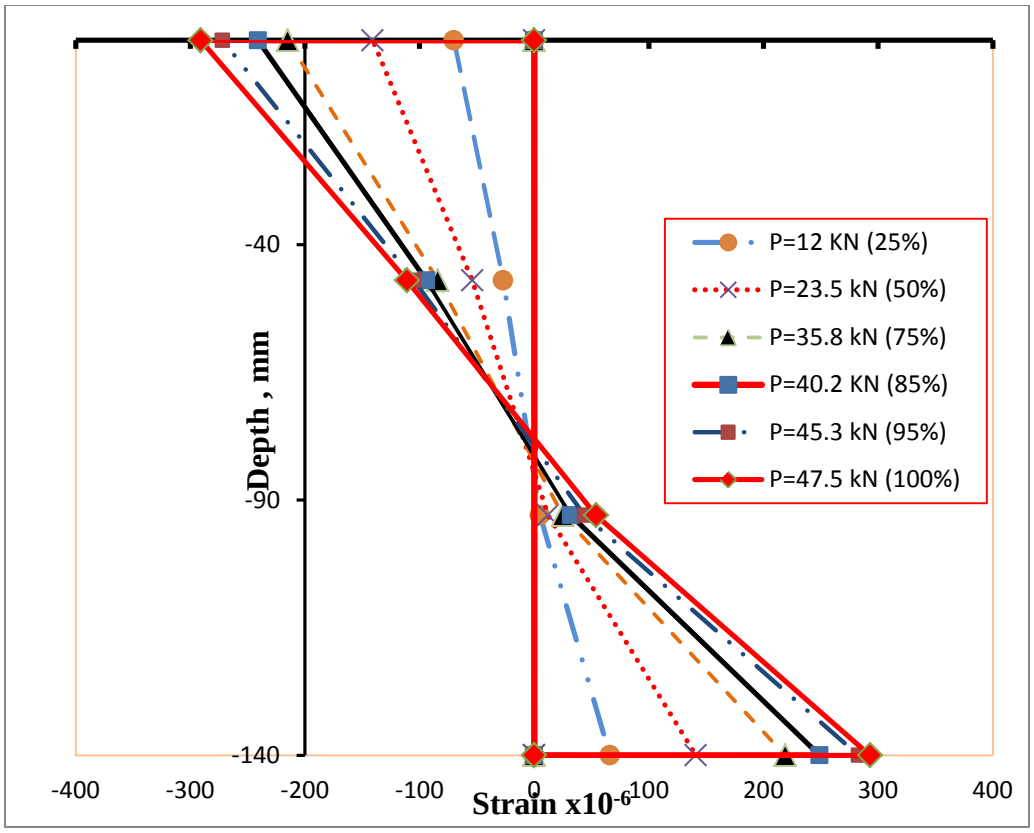
-40
-90
-140
Depth , mm
-400
-300
-200
-100
0
100
200
300
400
Strain x10-6
P=12 KN (25%)
P=23.5 kN (50%)
P=35.8 kN (75%)
P=40.2 KN (85%)
P=45.3 kN (95%)
P=47.5 kN (100%)

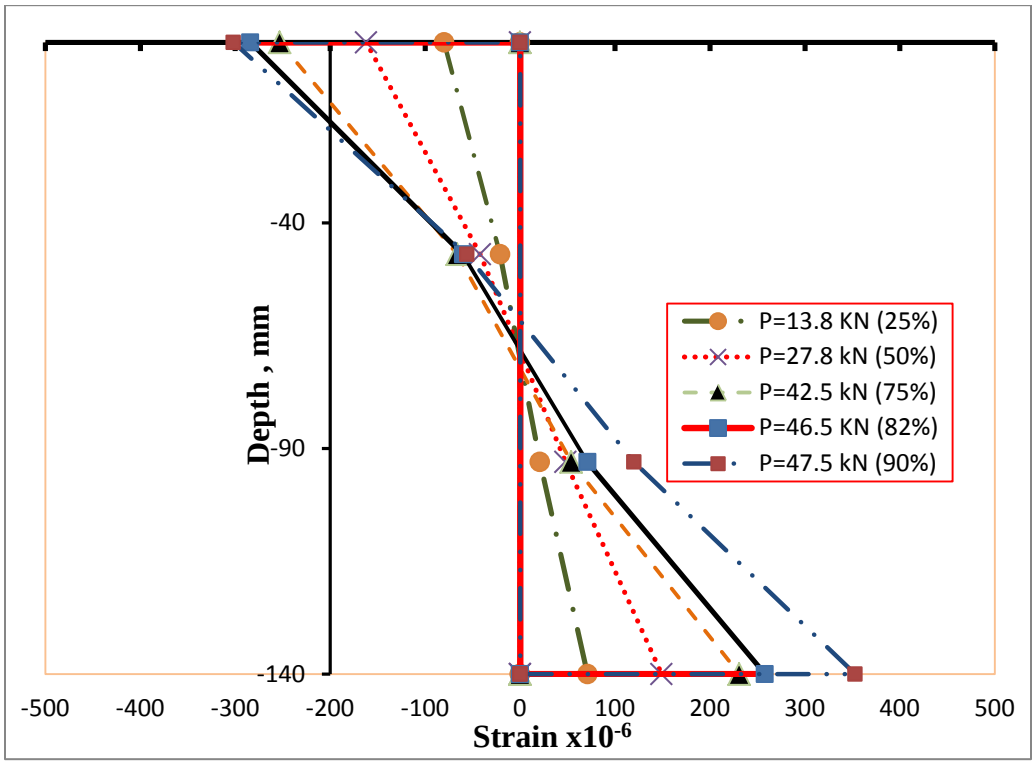
-40
-90
-140
Depth , mm
-500
-400
-300
-200
-100
0
100
200
300
400
500
Strain x10-6
P=13.8 KN (25%)
P=27.8 kN (50%)
P=42.5 kN (75%)
P=46.5 KN (82%)
P=47.5 kN (90%)

D.4.1: Load levels and strain values for three hollow core specimens of shorter span specimens Group (i) of size 260x140x1000 mm (140 mm depth) of span 900 mm.

Beam Designation	Failure Mode	Load P (kN)	% of P_U	Measured Strain, (x 10^6)				Depth of N.A from top, (mm)		Concrete Cracking Load P_{conc} (kN)
				Top	1/3 from top	2/3 from top	Bottom	Measured	Calculated	
HC-A-S1 (260x140) Span 1100 mm	Web-shear	15.5	25	-63	-22	6	60	75	74	62.2
		31.2	50	-125	-42	19	127	73	74	
		47.1	75	-189	-59	34	199	71	74	
		56.6	90	-228	-69	41	241	71	71	
		62.5	99	-253	-83	45	271	71	71	
HC-A-S2 (260x140) Span 1100 mm	Web-shear	16.8	25	-80	-22	12	79	72	74	62.2
		33.8	50	-160	-47	37	165	71	74	
		50.6	75	-242	-66	60	251	70	74	
		62.4	91	-328	-66	78	310	70	71	
HC-A-S3 (260x140) Span 1100 mm	Flexure	12.01	25	-60	-13	15	62	69	74	62.2
		24.02	50	-120	-26	30	133	68	74	
		36.1	75	-185	-38	50	238	65	74	
		42.1	85	-220	-41	63	308	63	74	
		44.1	90	-232	-41	69	348	61	74	

D.4.2: Measured and computed stresses for three hollow core specimens of shorter span specimens Group (i) of size 260x140x1000 mm (140 mm depth) of span 900 mm.

Beam Designation	Failure mode	load P (kN)	% of P_U	Measured stress , (MPa)		Concrete cracking load P_{conc} (kN)	Calculated stress, (MPa)			
							Bottom		Top	
				Bottom	Top		Cracked	Uncracked	Cracked	Uncracked
HC-A-S1 (260x140) Span 1100 mm	Web-shear	15.5	25	3.3	3.5	62.2	3.7	3.4	3.8	3.8
		31.2	50	7.0	6.9		7.4	6.8	7.6	7.7
		47.1	75	11.0	10.4		11.2	10.3	11.5	11.6
		56.6	90	13.3	12.6		13.5	12.3	13.8	14.0
		62.5	99	15.0	14.0		14.9	13.6	15.2	15.4
		62.9	100	-	-		15.0	13.7	15.3	15.5
HC-A-S2 (260x140) Span 1100 mm	Web-shear	16.8	25	4.3	4.4	62.2	4.0	3.7	4.1	4.1
		33.8	50	9.1	8.8		8.1	7.4	8.2	8.3
		50.6	75	13.8	13.3		12.0	11.0	12.3	12.5
		62.4	91	17.1	18		15.0	13.6	15.2	15.4
		68.4	100	-	-		16.3	15.0	16.7	16.9
HC-A-S3 (260x140) Span 1100 mm	Flexure	12.01	25	3.4	3.3	62.2	2.9	2.62	3.0	3.0
		24.02	50	7.3	6.6		5.7	5.2	5.9	5.92
		36.1	75	13.1	10.2		8.6	7.9	8.8	8.9
		42.1	85	16.9	12.1		10.0	9.2	10.3	10.4
		44.1	90	19.1	12.8		10.5	9.6	10.8	10.9
		46.1	95	25.2	14		11.0	10.1	11.2	11.4

D.4.3: Load levels and strain values for three hollow core specimens of longer span specimens Group (i) of size 260x140x1200 mm (140 mm depth) of span 1100 mm.

Beam Designation	Failure Mode	Load P (kN)	% of P_U	Measured Strain, (x 10^6)				Depth of N.A from top, (mm)		Concrete Cracking Load P_{conc} (kN)
				Top	1/3 from top	2/3 from top	Bottom	Measured	Calculated	
HC-A-L1 (260x140) Span 1100 mm	Flexure	12	25	-70	-27	5	66	77	74-Uncrac.	47.5
		23.8	50	-141	-54	12	141	75	74- Uncrac.	
		35.8	75	-215	-84	25	219	74	74 Uncrac.	
		40.2	85	-241	-94	32	249	74	74 Uncrac.	
		45.3	95	-272	-105	44	283	73	71-Crac.	
HC-A-L2 (260x140) Span 1100 mm	Flexure	11.9	25	-64	-20	22	67	69	74-Uncrac.	47.5
		23.9	50	-133	-40	45	143	68	74- Uncrac.	
		35.7	75	-201	-62	68	222	68	74 Uncrac.	
		40.8	85	-233	-69	81	258	68	74 Uncrac.	
		46.2	96	-266	-68	115	298	65	71-Crac.	
HC-A-L3 (260x140) Span 1100 mm	Flexure	13.8	25	-80	-21	21	71	72	74-Uncrac.	47.5
		27.8	50	-162	-42	48	149	71	74- Uncrac.	
		42.5	75	-253	-66	54	231	72	74 Uncrac.	
		46.5	82	-284	-60	71	258	71	74 Uncrac.	
		47.5	95	-302	-56	66	353	67	71-Crac.	

D.4.4: Measured and computed stresses for three hollow core specimens of longer span specimens Group (i) of size 260x140x1200 mm (140 mm depth) of span 1100 mm.

Beam Designation	Failure mode	load P (kN)	% of P_U	Measured stress , (MPa)		Concrete cracking load P_{conc} (kN)	Calculated stress, (MPa)			
							Bottom		Top	
				Bottom	Top		Cracked	Uncracked	Cracked	Uncracked
HC-A-L1 (260x140) Span 1100 mm	Flexure	12	25	3.6	3.9	47.5	3.7	3.4	3.8	3.9
		23.8	50	7.8	7.8		7.4	6.8	7.6	7.7
		35.8	75	12.1	11.8		11.1	10.2	11.4	11.5
		40.2	85	13.7	13.3		12.5	11.4	12.8	13.0
		45.3	95	15.6	15.0		14.1	12.9	14.4	14.6
		47.5	100	16.1	16.0		14.8	13.6	15.1	15.3
HC-A-L2 (260x140) Span 1100 mm	Flexure	11.9	25	3.7	3.5	47.5	3.7	3.4	3.8	3.9
		23.9	50	7.9	7.3		7.4	6.8	7.6	7.7
		35.7	75	12.2	11.1		11.1	10.2	11.4	11.5
		40.8	85	14.2	12.8		12.7	11.6	13.0	13.2
		46.2	96	16.4	14.6		14.4	13.2	14.7	14.9
		47.9	100	25.5	21.6		14.9	13.7	15.3	15.4
HC-A-L3 (260x140) Span 1100 mm	Flexure	13.8	25	3.9	4.4	47.5	4.3	3.9	4.4	4.5
		27.8	50	8.2	8.9		8.7	7.9	8.9	9.0
		42.5	75	12.7	13.9		13.2	12.1	13.5	13.7
		46.5	82	14.2	15.6		14.5	13.3	14.8	15.0
		47.5	95	19.4	16.6		14.8	13.6	15.1	15.3
		56.4	100	-	-		17.6	16.1	18	18.2

D.4.5: Load levels and strain values for three hollow core specimens of shorter span specimens Group (ii) of size 330x175x1000 mm (175 mm depth) of span 900 mm.

Beam Designation	Failure Mode	Load P (kN)	% of P_U	Measured Strain, (x 10^6)				Depth of N.A from top, (mm)		Concrete Cracking Load P_{conc} (kN)
				Top	1/3 from top	2/3 from top	Bottom	Measured	Calculated	
HC-B-S1 (330x175) Span 900 mm	Flexure	20.6	25	-53	-17	20	55	85	93-Uncrac.	96.0
		41.1	50	-112	-37	42	114	85	93-Uncrac.	
		62	75	-174	-56	71	178	85	93-Uncrac.	
		70.1	85	-197	-63	86	204	84	93-Uncrac.	
		74.5	90	-209	-66	98	222	80	93-Uncrac.	
		78.1	95	-221	-68	109	267	80	93-Uncrac.	
HC-B-S2 (330x175) Span 900 mm	Web-shear	22.1	25	-52	-19	32	56	81	93-Uncrac.	96.0
		44.3	50	-104	-39	66	115	80	93-Uncrac.	
		66.3	75	-154	-59	104	179	79	93-Uncrac.	
		75.2	85	-174	-66	115	205	79	93-Uncrac.	
		84.4	95	-190	-75	138	236	77	93-Uncrac.	
		87.4	98	-196	-78	142	247	77	87-Crac.	
HC-B-S3 (330x175) Span 900 mm	Web-shear	23.6	25	-52	-26	15	61	88	93-Uncrac.	96.0
		47.8	50	-109	-57	33	126	88	93-Uncrac.	
		71.6	75	-163	-88	52	193	88	93-Uncrac.	
		81.2	85	-182	-100	56	223	87	93-Uncrac.	
		90.8	95	-202	-115	79	253	86	87-Crac.	

D.4.6: Measured and computed stresses for three hollow core specimens of shorter span specimens Group (ii) of size 330x175x1000 mm (175 mm depth) of span 900 mm.

Beam Designation	Failure mode	load P (kN)	% of P_U	Measured stress , (MPa)		Concrete cracking load P_{conc} (kN)	Calculated stress, (MPa)			
							Bottom		Top	
				Bottom	Top		Cracked	Uncracked	Cracked	Uncracked
HC-B-S1 (330x175) Span 900 mm	Flexure	20.6	25	3.0	2.92	96	2.84	2.5	2.8	2.8
		41.1	50	6.3	6.2		5.7	5.0	5.6	5.7
		62	75	9.8	9.6		8.6	7.5	8.4	8.5
		70.1	85	11.2	10.8		9.7	8.5	9.5	9.6
		74.5	90	12.2	11.5		10.3	9.0	10.2	10.7
		78.1	95	14.7	12.2		10.8	9.4	10.6	10.7
		82.6	100	-	16.6		11.4	10.0	11.2	11.4
HC-B-S2 (330x175) Span 900 mm	Web-shear	22.1	25	3.1	2.9	96	3.0	2.7	3.0	3.0
		44.3	50	6.3	5.7		6.1	5.3	6.0	6.1
		66.3	75	9.9	8.5		9.2	8.0	9.0	9.1
		75.2	85	11.3	9.6		10.4	9.1	10.2	10.3
		84.4	95	13.0	10.5		11.6	10.2	11.5	11.6
		87.4	98	13.6	10.8		12.1	10.5	11.9	12.0
		88.7	100	13.9	10.7		12.2	10.7	12.1	12.2
HC-B-S3 (330x175) Span 900 mm	Web-shear	23.6	25	3.4	2.9	96	3.3	2.9	3.2	3.2
		47.8	50	6.9	6.0		6.6	5.8	6.5	6.6
		71.6	75	10.6	9.0		9.9	8.6	9.7	9.8
		81.2	85	12.3	10.0		11.2	9.8	11.0	11.2
		90.8	95	13.9	11.1		12.5	11.0	12.3	12.5
		95.7	100	14.9	11.8		13.2	11.54	13.0	13.2

D.4.7: Load levels and strain values for three hollow core specimens of longer span specimens Group (ii) of size 330x175x1200 mm (175 mm depth) of span 1100 mm.

Beam Designation	Failure Mode	Load P (kN)	% of P_U	Measured Strain, (x 10^6)				Depth of N.A from top, (mm)		Concrete Cracking Load P_{conc} (kN)
				Top	1/3 from top	2/3 from top	Bottom	Measured	Calculated	
HC-B-L1 (330x175) Span 1200 mm	Flexure	16.1	25	-66		13	63	92	93-Uncrac.	73.4
		32.1	50	-125		16	135	91	93-Uncrac.	
		48.1	75	-184		22	215	89	93-Uncrac.	
		54.1	85	-207		27	245	89	93-Uncrac.	
		61.1	95	-234		35	280	88	93-Uncrac.	
HC-B-L2 (330x175) Span 1200 mm	Flexure	14.0	25	-57	-21	17	54	90	93-Uncrac.	73.4
		29	50	-118	-42	45	114	88	93-Uncrac.	
		43.1	75	-177	-61	68	180	86	93-Uncrac.	
		49.1	85	-201	-68	83	208	85	93-Uncrac.	
		55.1	95	-225	-74	101	239	84	87-Crac.	
HC-B-L3 (330x175) Span 1200 mm	Flexure	16.1	25	-43	-14	30	51	77	93-Uncrac.	73.4
		32.2	50	-85	-28	68	106	75	93-Uncrac.	
		49.1	75	-127	-42	115	168	74	93-Uncrac.	
		55.1	85	-141	-46	129	192	74	93-Uncrac.	
		62.2	95	-160	-52	143	220-F	74	87-Crac.	

D.4.8: Measured and computed stresses for three hollow core specimens of longer span specimens Group (ii) of size 330x175x1200 mm (175 mm depth) of span 1100 mm.

Beam Designation	Failure mode	load P (kN)	% of P_U	Measured stress , (MPa)		Concrete cracking load P_{conc} (kN)	Calculated stress, (MPa)			
							Bottom		Top	
				Bottom	Top		Cracked	Uncracked	Cracked	Uncracked
HC-B-L1 (330x175) Span 1200 mm	Flexure	16.1	25	3.5	3.6	73.4	2.9	2.5	2.9	2.9
		32.1	50	7.4	6.9		5.8	5.1	5.7	5.8
		48.1	75	11.8	10.1		8.7	7.6	8.6	8.65
		54.1	85	13.5	11.4		9.8	8.5	9.6	9.7
		61.1	95	15.4	12.9		11.0	9.6	10.9	11.0
		64.1	100	16.3	13.5		11.6	10.1	11.4	11.5
HC-B-L2 (330x175) Span 1200 mm	Flexure	14.0	25	3.0	3.1	73.4	2.5	2.2	2.5	2.51
		29	50	6.3	6.5		5.2	4.6	5.2	5.2
		43.1	75	10	9.6		7.8	6.8	7.7	7.75
		49.1	85	11.4	11.1		8.9	7.7	8.7	8.8
		55.1	95	13.2	12.4		10.0	8.7	9.8	9.9
		58.2	100	14.0	13.1		10.5	9.2	10.3	10.5
HC-B-L3 (330x175) Span 1200 mm	Flexure	16.1	25	2.81	2.4	73.4	2.9	2.5	2.9	2.9
		32.2	50	5.8	4.7		5.8	5.1	5.7	5.8
		49.1	75	9.2	7.0		8.9	7.7	8.7	8.8
		55.1	85	10.6	7.8		10.0	8.7	9.8	9.9
		62.2	95	12.1	8.8		11.2	9.8	11.1	11.2
		65.1	100	11.3	9.5		11.8	10.3	11.6	11.7

D.4.9: Load levels and strain values for three hollow core specimens of shorter span specimens Group (iii) of size 390x200x1000 mm (200 mm depth) of span 900 mm.

Beam Designation	Failure Mode	Load P (kN)	% of P_U	Measured Strain, (x 10^6)				Depth of N.A from top, (mm)		Concrete Cracking Load P_{conc} (kN)
				Top	1/3 from top	2/3 from top	Bottom	Measured	Calculated	
HC-C-S1 (390x200) Span 900 mm	Flexure	24.3	25	-40	-16	9	43	102	106-Uncrac.	131.7
		48.6	50	-81	-33	14	90	103	106-Uncrac.	
		73.4	75	-120	-53	8	144	104	106-Uncrac.	
		82.9	85	-136	-60	10	165	103	106-Uncrac.	
		93.1	95	-152	-66	17	194	101	106-Uncrac.	
		95.7	98	-157	-69	17	223	98	98-Crac.	
HC-C-S2 (390x200) Span 900 mm	Web-shear	27.82	25	-49	-21	10	49	106.0	106-Uncrac.	131.7
		56.2	50	-99	-45	13	110	107	106-Uncrac.	
		83.87	75	-145	-71	14	156	107	106-Uncrac.	
		95.16	85	-163	-82	18	180	107	106-Uncrac.	
		106.6	95	-181	-96	36	208	104	106-Uncrac.	
		110.49	99	-188	-106	33	219	105	98-Crac.	
HC-C-S3 (390x200) Span 900 mm	Web-shear	25.3	25	-44	-16	3	42	109	106-Uncrac.	131.7
		50.05	50	-79	-29	12	92	101	106-Uncrac.	
		75.46	75	-116	-40	25	149	97	106-Uncrac.	
		85.44	85	-132	-46	22	183	96	106-Uncrac.	
		95.61	95	-147	-54	16	221	95	98-Crac.	

D.4.10: Measured and computed stresses for three hollow core specimens of shorter span specimens Group (iii) of size 390x200x1000 mm (200 mm depth) of span 900 mm.

Beam Designation	Failure mode	load P (kN)	% of P_U	Measured stress , (MPa)		Concrete cracking load P_{conc} (kN)	Calculated stress, (MPa)			
							Bottom		Top	
				Bottom	Top		Cracked	Uncracked	Cracked	Uncracked
HC-C-S1 (390x200) Span 900 mm	Flexure	24.3	25	2.4	2.2	131.7	2.4	2.0	2.25	2.3
		48.6	50	5.0	4.5		4.73	4.0	4.51	4.55
		73.4	75	7.92	6.6		7.14	6.0	6.8	6.9
		82.9	85	9.1	7.5		8.1	6.81	7.7	7.8
		93.1	95	10.7	8.4		9.1	7.65	8.63	8.71
		95.7	98	12.3	8.64		9.31	7.9	8.9	8.95
		97.6	100	20.6	9.1		9.5	8.02	9.1	9.13
HC-C-S2 (390x200) Span 900 mm	Web-shear	27.82	25	2.7	2.7	131.7	2.71	2.3	2.6	2.6
		56.2	50	5.6	5.45		5.5	4.62	5.2	5.3
		83.87	75	8.6	8.0		8.2	6.9	7.8	7.85
		95.16	85	9.9	9.0		9.3	7.81	8.82	8.9
		106.6	95	11.44	10.0		10.4	8.75	9.9	10
		110.49	99	12.0	10.34		10.75	9.1	10.24	10.4
		111.84	100	13.3	11.0		11.0	9.2	10.4	10.5
HC-C-S3 (390x200) Span 900 mm	Web-shear	25.3	25	2.3	2.4	131.7	2.5	2.1	2.3	2.4
		50.05	50	5.0	4.3		4.9	4.1	4.6	4.7
		75.46	75	8.2	6.4		7.3	6.2	7.0	7.1
		85.44	85	10.1	7.3		8.3	7.0	7.92	8.0
		95.61	95	12.2	8.1		9.3	7.9	8.9	9.0
		100.6	100	11.2	8.7		10	8.3	9.3	9.4

D.4.11: Load levels and strain values for three hollow core specimens of longer span specimens Group (iii) of size 390x200x1200 mm (200 mm depth) of span 1100 mm.

Beam Designation	Failure Mode	Load P (kN)	% of P_U	Measured Strain, (x 10^6)				Depth of N.A from top, (mm)		Concrete Cracking Load P_{conc} (kN)
				Top	1/3 from top	2/3 from top	Bottom	Measured	Calculated	
HC-C-L1 (390x200) Span 1200 mm	Flexure	23.5	25	-46	-21	8	49	105	106-Uncrac.	100.0
		46.7	50	-95	-43	19	101	105	106-Uncrac.	
		70	75	-143	-66	25	163	103	106-Uncrac.	
		79.9	85	-163	-71	45	191	100	106-Uncrac.	
		89.3	95	-184	-82	61	222	98	98-Crac.	
HC-C-L2 (390x200) Span 1200 mm	Flexure	25.9	25	-52	-28	7	52	100	106-Uncrac.	100.0
		51.6	50	-102	-48	34	109	100	106-Uncrac.	
		77.5	75	-152	-68	47	179	99	106-Uncrac.	
		87.8	85	-170	-75	49	208	98	106-Uncrac.	
		97.8	95	-188	-85	55	239	98	98-Crac.	
HC-C-L3 (390x200) Span 1200 mm	Flexure	21.92	25	-48	-19	12	48	104	98-Crac.	100.0
		44.2	50	-97	-41	33	99	102	98-Crac.	
		66.63	75	-144	-59	59	158	98	106-Uncrac.	
		75.15	85	-163	-66	71	171	98	106-Uncrac.	
		83.87	95	-182	-71	84	204	96	98-Crac.	

D.4.12: Measured and computed stresses for three hollow core specimens of longer span specimens Group (iii) of size 390x200x1200 mm (200 mm depth) of span 1100 mm.

Beam Designation	Failure mode	load P (kN)	% of P_U	Measured stress , (MPa)		Concrete cracking load P_{conc} (kN)	Calculated stress, (MPa)			
							Bottom		Top	
				Bottom	Top		Cracked	Uncracked	Cracked	Uncracked
HC-C-L1 (390x200) Span 1200 mm	Flexure	23.5	25	2.7	2.5	100.0	3.0	2.52	2.9	2.9
		46.7	50	5.6	5.2		6.0	5.0	5.7	5.7
		70	75	9.0	7.9		9.0	7.52	8.5	8.6
		79.9	85	10.5	9.0		10.2	8.6	9.7	9.8
		89.3	95	12.2	10.1		11.4	9.6	10.83	10.92
		93.7	100	12.8	10.7		12.0	10.1	11.4	11.5
HC-C-L2 (390x200) Span 1200 mm	Flexure	25.9	25	2.9	2.9	100.0	3.3	2.8	3.1	3.2
		51.6	50	6.0	5.6		6.6	5.54	6.3	6.3
		77.5	75	9.85	8.4		9.9	8.32	9.4	9.5
		87.8	85	14.4	9.4		11.2	9.43	10.6	10.74
		97.8	95	13.2	10.3		12.4	10.5	11.9	12.0
		103.1	100	13.6	11.2		13.1	11.10	12.5	12.61
HC-C-L3 (390x200) Span 1200 mm	Flexure	21.92	25	2.6	2.64	100.0	2.8	2.4	2.7	2.7
		44.2	50	5.5	5.4		5.62	4.75	5.4	5.41
		66.63	75	8.7	7.92		8.5	7.2	8.1	8.15
		75.15	85	9.4	9.0		9.6	8.1	9.1	9.2
		83.87	95	11.2	10.0		10.7	9.0	10.2	10.3
		88.5	100	12.1	10.7		11.3	9.5	10.73	10.83

D.4.13: Load levels and strain values for three hollow core specimens of longer span specimens Group (iv) of size 380x140x1200 mm (140 mm depth) of span 1100 mm.

Beam Designation	Failure Mode	Load P (kN)	% of P_U	Measured Strain, (x 10^6)				Depth of N.A from top, (mm)		Concrete Cracking Load P_{conc} (kN)
				Top	1/3 from top	2/3 from top	Bottom	Measured	Calculated	
HC-D-L1 (380x140) Span 1200 mm	Flexure	13.0	25	-54	-26	12	68	70	74-Uncrac.	68.0
		25.4	50	-110	-50	32	145	68	74-Uncrac.	
		38.9	75	-172	-76	61	218	67	74-Uncrac.	
		43.7	85	-195	-86	70	237	68	74-Uncrac.	
		49.4	95	-226	-76	98	283	65	71-Crac.	
HC-D-L2 (380x140) Span 1200 mm	Flexure	14.4	25	-49	-22	12	78	65(76)	74-Uncrac.	68.0
		29.3	50	-100	-44	24	135	68(76)	74-Uncrac.	
		43.7	75	-148	-65	37	197	68(76)	74-Uncrac.	
		49.2	85	-168	-71	45	222	68(75)	74-Uncrac.	
		54	95	-186	-67	61	239	66(71)	74-Uncrac.	
		57.0	98	-223	-43	310	370	-	71-Crac.	
HC-D-L3 (380x140) Span 1200 mm	Flexure	14.1	25	-62	-22	22	57	71	74-Uncrac.	68.0
		28.5	50	-122	-42	56	125	68	74-Uncrac.	
		42.8	75	-186	-66	89	192	67	74-Uncrac.	
		48.2	85	-209	-75	103	219	67	74-Uncrac.	
		54.3	95	-236	-69	147	250	64	71-Crac.	
		56.5	98	-278	-24	291	257	57	71-Crac.	

D.4.14: Measured and computed stresses three hollow core specimens of longer span specimens Group (iv) of size 380x140x1200 mm (140 mm depth) of span 1100 mm.

Beam Designation	Failure mode	load P (kN)	% of P_U	Measured stress , (MPa)		Concrete cracking load P_{conc} (kN)	Calculated stress, (MPa)			
							Bottom		Top	
				Bottom	Top		Cracked	Uncracked	Cracked	Uncracked
HC-D-L1 (380x140) Span 1200 mm	Flexure	13.0	25	3.7	3.0	68.0	2.8	2.6	2.9	2.9
		25.4	50	8.0	6.1		5.5	5.0	5.6	5.7
		38.9	75	12	9.5		8.3	7.7	8.6	8.7
		43.7	85	12.4	10.7		9.4	8.6	9.6	9.75
		49.4	95	15	12.4		10.6	9.72	10.9	11.0
		51.5	100	-	15.5		11.1	10.13	11.4	11.5
HC-D-L2 (380x140) Span 1200 mm	Flexure	14.4	25	4.3	2.7	68.0	3.1	2.83	32	3.21
		29.3	50	7.4	5.5		6.3	5.8	6.5	6.54
		43.7	75	10.8	8.1		9.4	8.6	9.6	9.75
		49.2	85	12.2	9.2		10.6	9.7	10.9	11.0
		54	95	13.2	10.2		11.6	10.7	11.92	12.0
		57.0	98	20.4	12.3		12.2	11.22	12.6	12.8
		58.4	100	13.6	27.8		12.53	11.5	12.9	13.0
HC-D-L3 (380x140) Span 1200 mm	Flexure	14.1	25	3.2	3.4	68.0	3.0	2.8	3.1	3.15
		28.5	50	6.9	6.7		6.1	5.61	6.3	6.4
		42.8	75	10.6	10.2		9.2	8.43	9.5	9.6
		48.2	85	12.0	11.5		10.34	9.5	10.64	10.8
		54.3	95	13.8	13.0		11.65	10.7	12.0	12.1
		56.5	98	14.1	15.3		12.2	11.12	12.5	12.6

D.4.15: Load levels and strain values for three hollow core specimens of shorter span specimens Group (v) (solid section) of size 260x140x1000 mm (140 mm depth) of span 900 mm.

Beam Designation	Failure Mode	Load P (kN)	% of P_U	Measured Strain, (x 10^6)				Depth of N.A from top, (mm)		Concrete Cracking Load P_{conc} (kN)
				Top	1/3 from top	2/3 from top	Bottom	Measured	Calculated	
HC-E-S1 (260x140) Span 900 mm	Flexure	14.91	25	-64	-17	15	62	71	72-Uncrac.	62.0
		30.34	50	-129	-35	42	131	69	72-Uncrac.	
		45.16	75	-191	-49	80	203	66	72-Uncrac.	
		51.76	85	-220	-55	96	237	66	72-Uncrac.	
		57.76	95	-246	-60	110	268	65	67Crac.	
HC-E-S2 (260x140) Span 900 mm	Flexure	16.38	25	-70	-33	7	68	77	72-Uncrac.	62.0
		32.86	50	-143	-65	17	141	76	72-Uncrac.	
		49.09	75	-216	-99	27	202	77	72-Uncrac.	
		55.59	85	-260	-111	49	216	77	72-Uncrac.	
		58.61	90	-287	-105	24	237	79	72-Uncrac.	
		59.48	91	-347	-110	0	290	79	72-Uncrac.	
		62.45	95	-420	-130	-18	872 -F	62	67Crac.	
HC-E-S3 (260x140) Span 900 mm	Flexure	14.36	25	-64	-22	15	52	75	72-Uncrac.	62.0
		29.33	50	-129	-42	37	112	73	72-Uncrac.	
		43.69	75	-194	-57	63	175	71	72-Uncrac.	
		49.09	85	-218	-61	77	202	70	72-Uncrac.	
		55.04	95	-248	-63	93	225	69	72-Uncrac.	
		57.71	99	-283	-42	82	229	70	67Crac.	

D.4.16: Measured and computed stresses three hollow core specimens of shorter span specimens Group (v) (solid section) of size 260x140x1000 mm (140 mm depth) of span 900 mm.

Beam Designation	Failure mode	load P (kN)	% of P_U	Measured stress , (MPa)		Concrete cracking load P_{conc} (kN)	Calculated stress, (MPa)			
							Bottom		Top	
				Bottom	Top		Cracked	Uncracked	Cracked	Uncracked
HC-E-S1 (260x140) Span 900 mm	Flexure	14.91	25	3.41	3.52	62.0	3.6	3.15	3.3	3.4
		30.34	50	7.21	7.1		7.32	6.4	6.71	6.8
		45.16	75	11.2	10.51		11.0	9.5	10.0	10.1
		51.76	85	13.1	12.1		12.5	11.0	11.5	11.6
		57.76	95	14.74	13.53		14	12.2	12.8	13.0
		60.49	100	15.6	14.1		14.6	12.8	13.4	13.6
HC-E-S2 (260x140) Span 900 mm	Flexure	16.38	25	3.74	3.9	62.0	3.95	3.5	3.63	3.67
		32.86	50	7.8	7.9		7.93	7.0	7.3	7.36
		49.09	75	11.11	11.9		11.85	10.4	10.9	11.0
		55.59	85	11.9	14.3		13.4	11.73	12.3	12.45
		58.61	90	13.0	15.8		14.1	12.4	13.0	13.12
		59.48	91	16.0	19.1		14.4	12.6	13.2	13.3
		62.45	95	-	23.1		15.1	13.2	13.82	14.0
		65.38	100	-	29.5		15.8	13.8	14.5	14.64
HC-E-S3 (260x140) Span 900 mm	Flexure	14.36	25	2.9	3.5	62.0	3.5	3.0	3.2	3.2
		29.33	50	6.2	7.1		7.1	6.2	6.5	6.6
		43.69	75	9.6	10.7		10.5	9.2	9.7	9.8
		49.09	85	11.1	12.0		11.9	10.4	10.9	11
		55.04	95	12.4	13.64		13.3	11.62	12.2	12.3
		57.71	99	12.6	15.6		14.0	12.2	12.8	13.0
		58.0	100	11.7	16.7		14.0	12.3	13.0	13.0

APPENDIX E: FINITE ELEMENT MODELING

E.1 HYBRID NC-UHPC LAYERED SPECIMENS

(i) Hybrid specimen LS-A-C2 of 20 mm thick UHPC layer of beam size 150x150x760 mm (span=630)

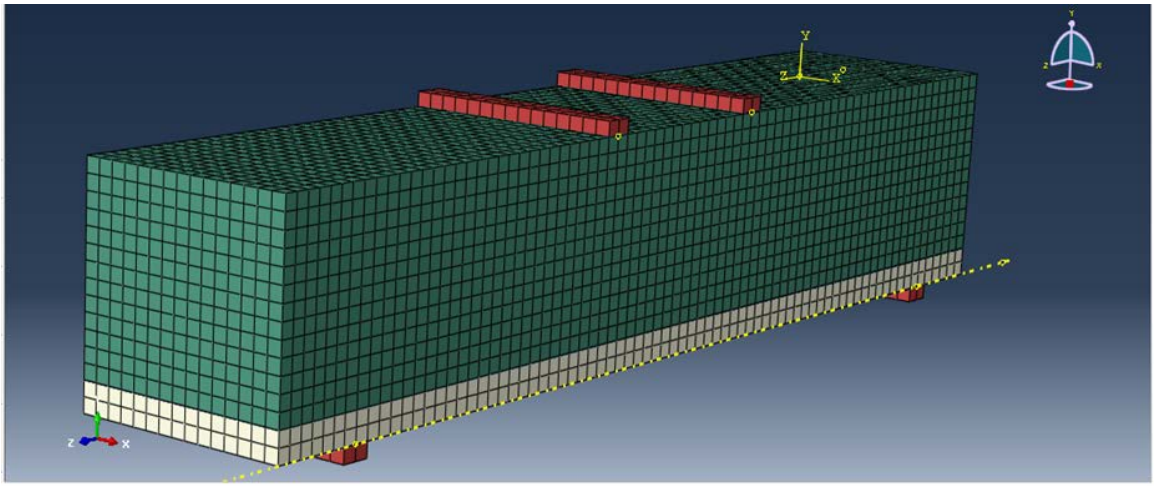

Meshing of layered hybrid specimen LS-A-C2

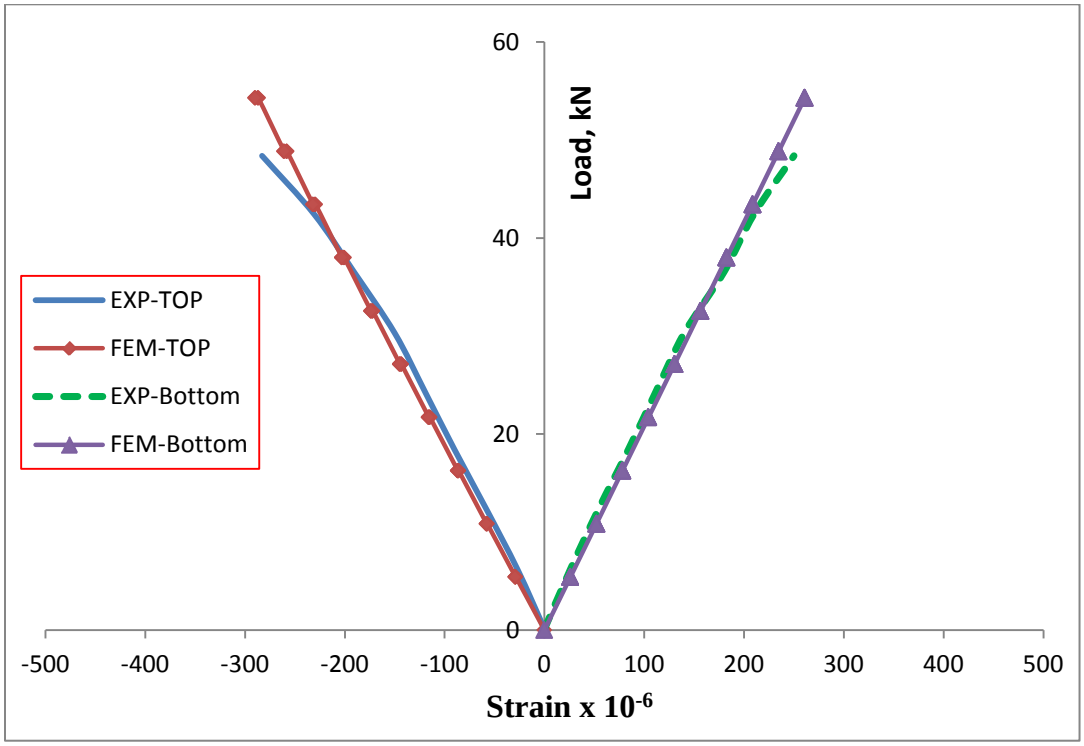

FEM vs. experimentally observed longitudinal strain on top and bottom faces of hybrid beam of specimen LS-A-C2.

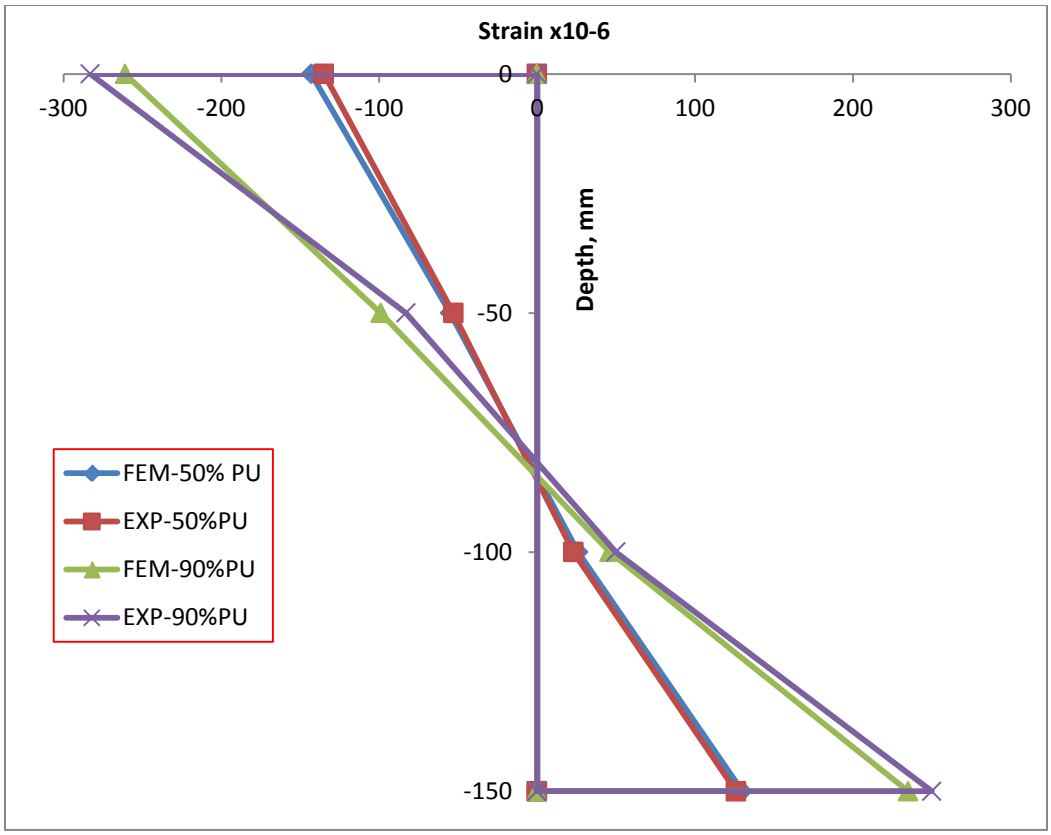

FEM vs. experimentally observed longitudinal strain along the depth at mid span LS-A-C2

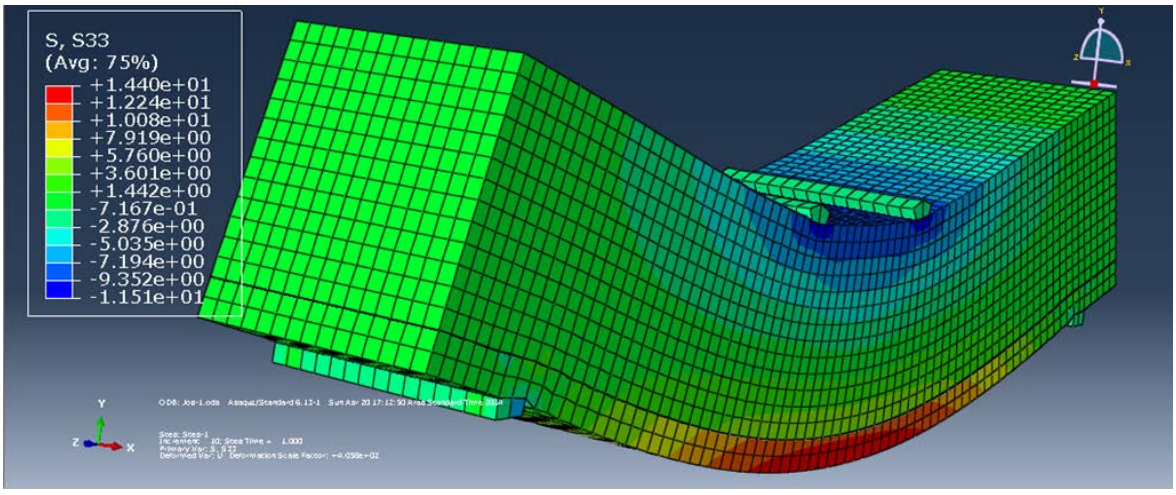

FEM longitudinal stress distribution of specimen LS-A-C2

(ii) Hybrid specimen LS-C-C2 of 20 mm thick UHPC layer of beam size 150x150x1000 mm (span=900)

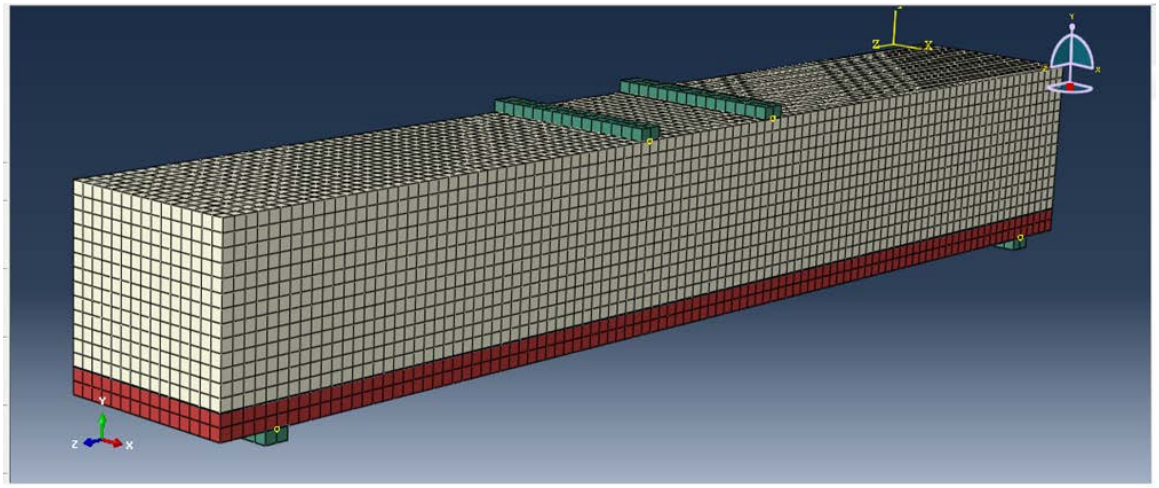

***Meshing of layered hybrid specimen* LS-C-C2**

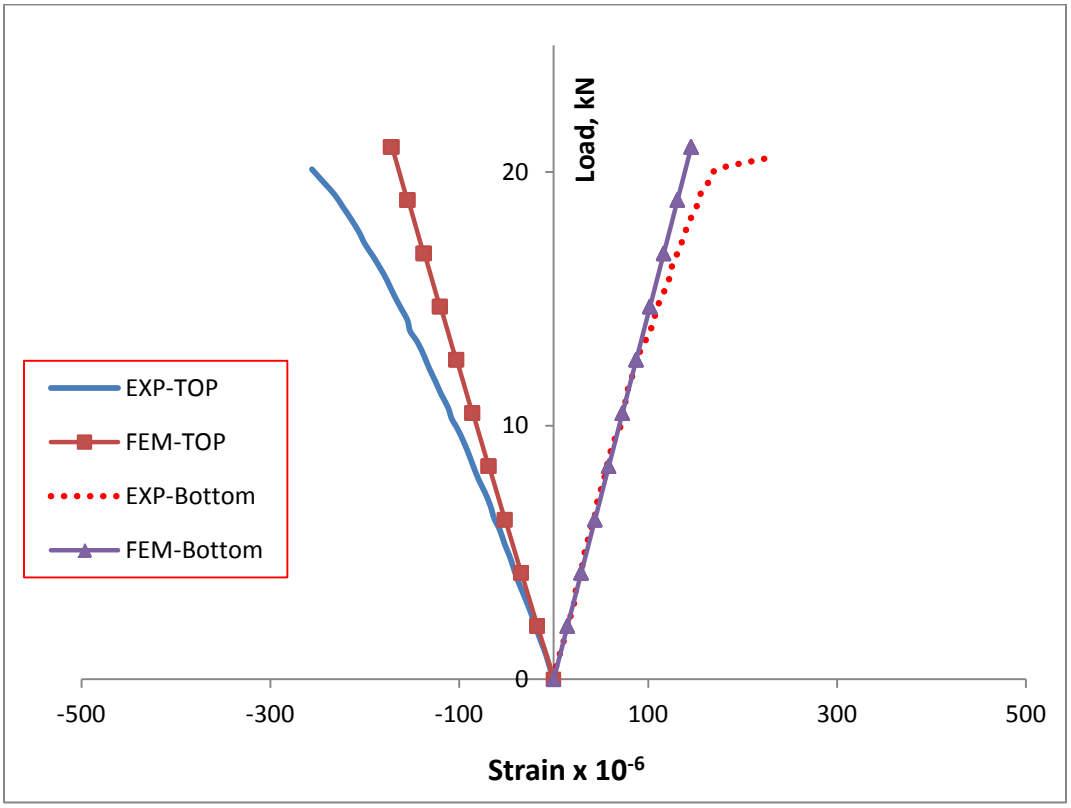

***FEM vs. experimentally observed longitudinal strain on top and bottom faces of hybrid beam of specimen* LS-C-C2**

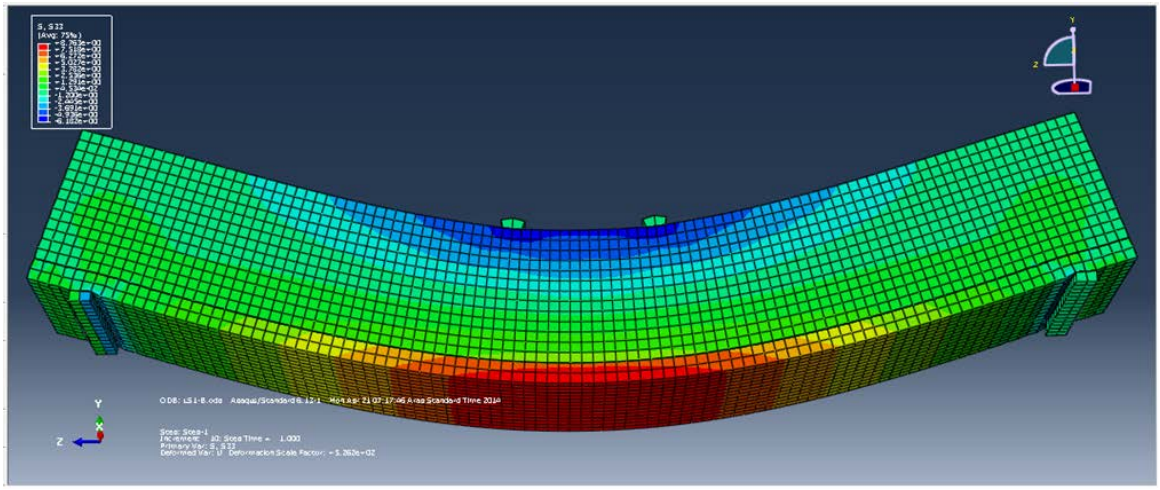

FEM longitudinal stress distribution of specimen **LS-C-C2**

(iii) Hybrid specimen LS-D-C2 of 40 mm thick UHPC layer of beam size 150x150x1000 mm (span=900)

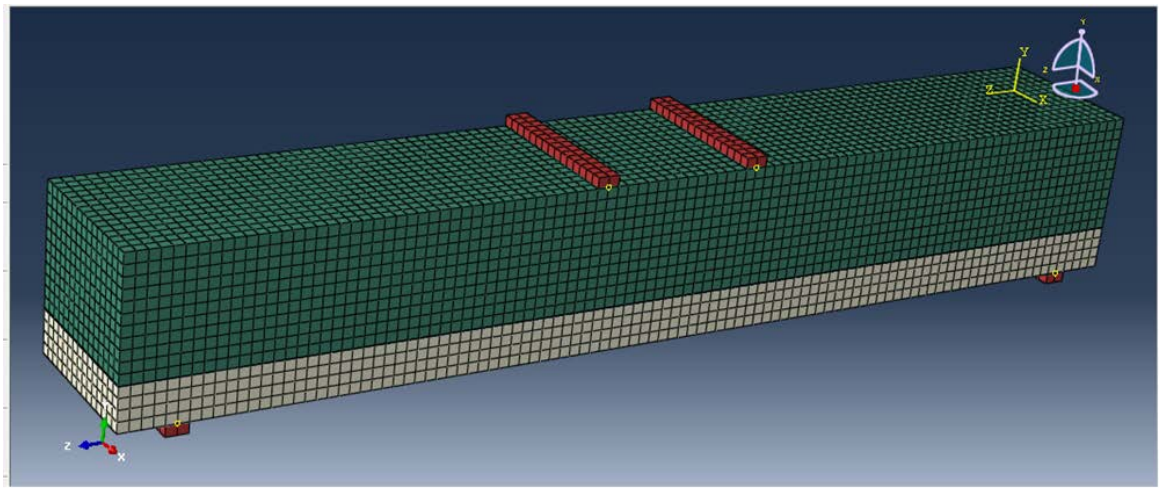

Meshing of layered hybrid specimen **LS-D-C2**

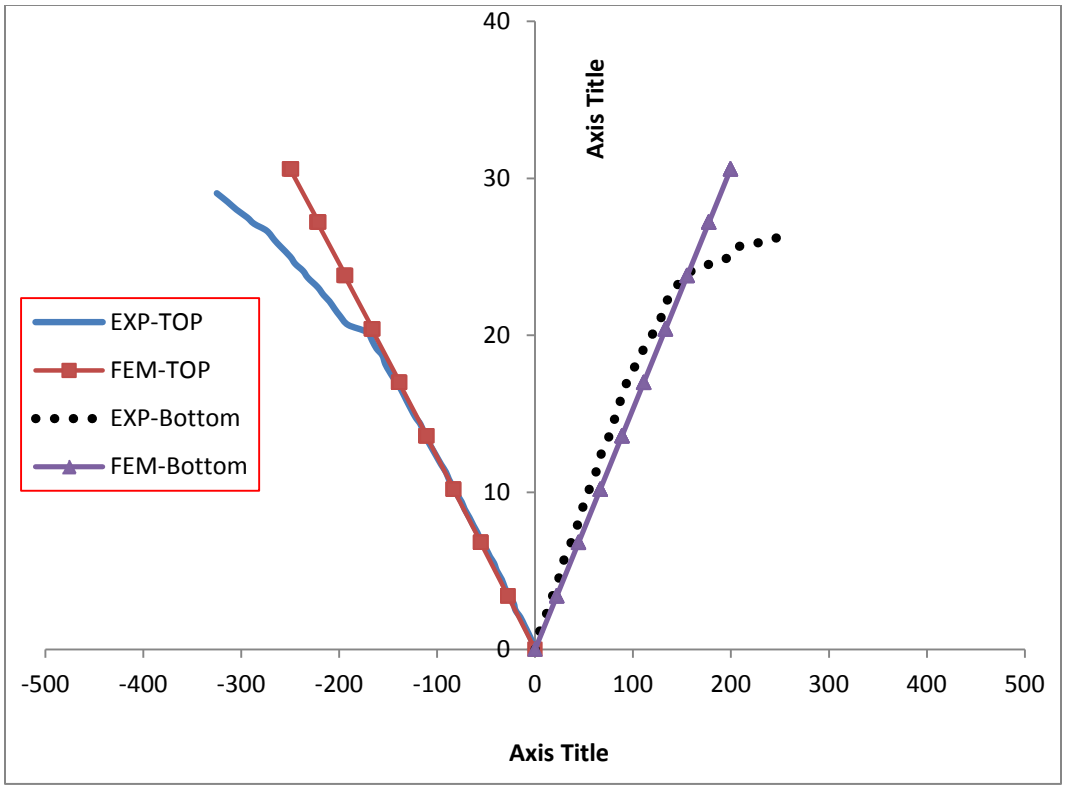

***FEM vs. experimentally observed longitudinal strain on top and bottom faces of hybrid beam of specimen* LS-D-C2**

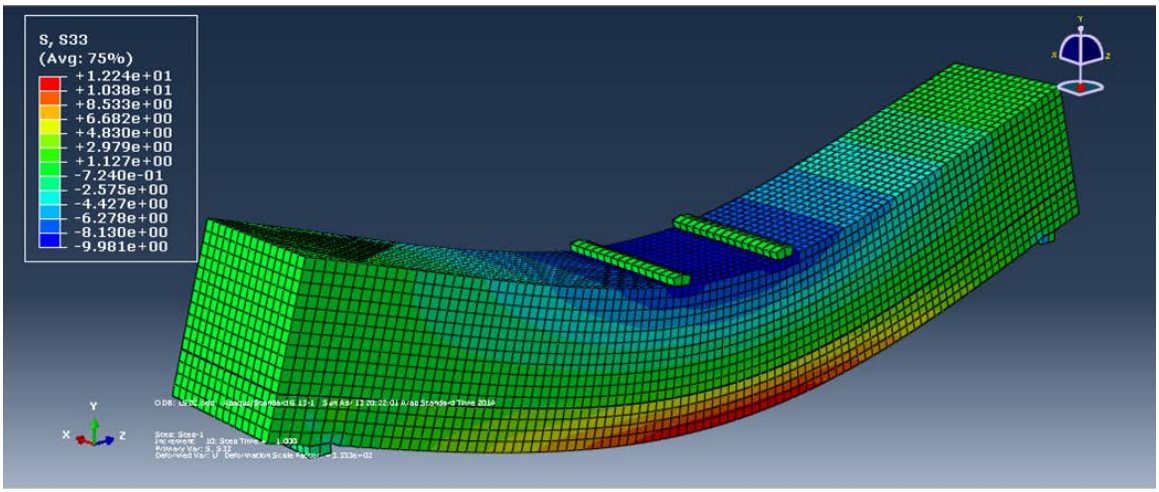

FEM longitudinal stress distribution of specimen **LS-D-C2**

(iv) Hybrid specimen LS-H-C2 of 50 mm thick UHPC layer of beam size 150x200x1000 mm (200 mm depth, span=900)

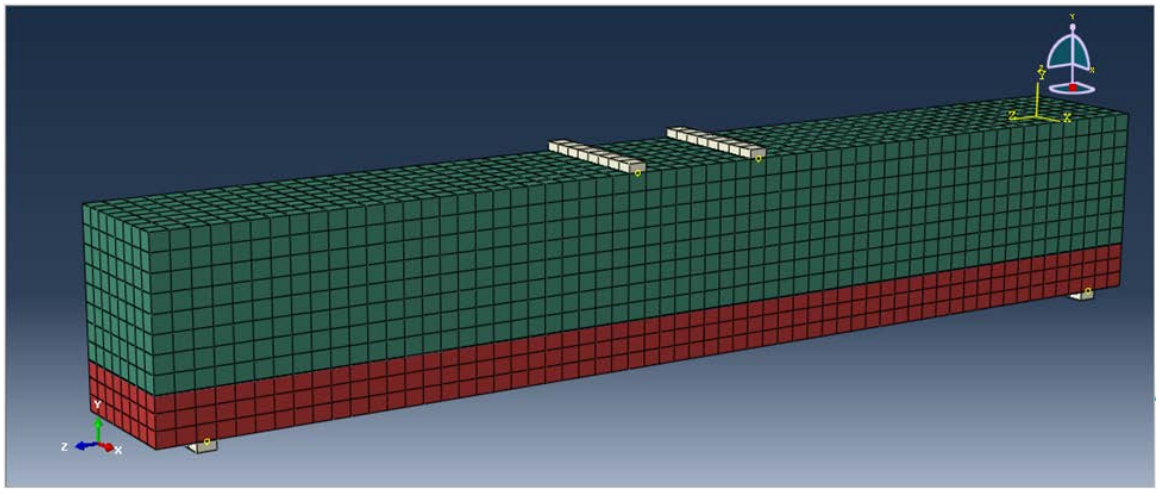

***Meshing of layered hybrid specimen* LS-H-C2**

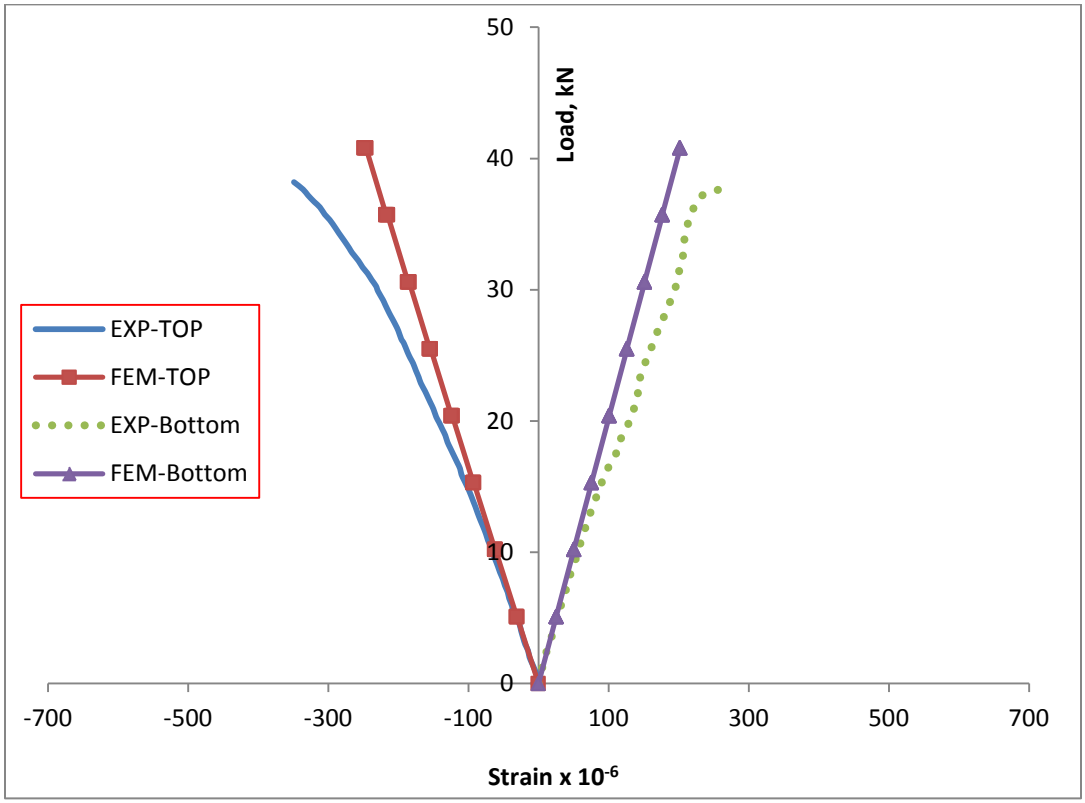

***FEM vs. experimentally observed longitudinal strain on top and bottom faces of hybrid beam of specimen* LS-H-C2**

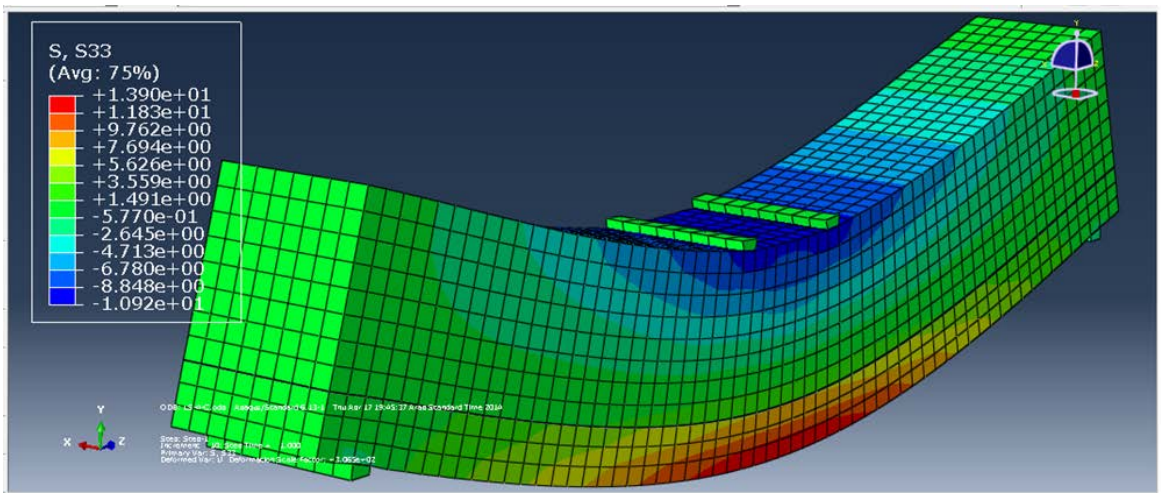

FEM longitudinal stress distribution of specimen **LS-H-C2**

E.2 HYBRID HOLLOW CORE SPECIMENS

(i) Hybrid specimen HC-A-L3 of Group (i) of beam size 260x140x1200 mm (span=1100)

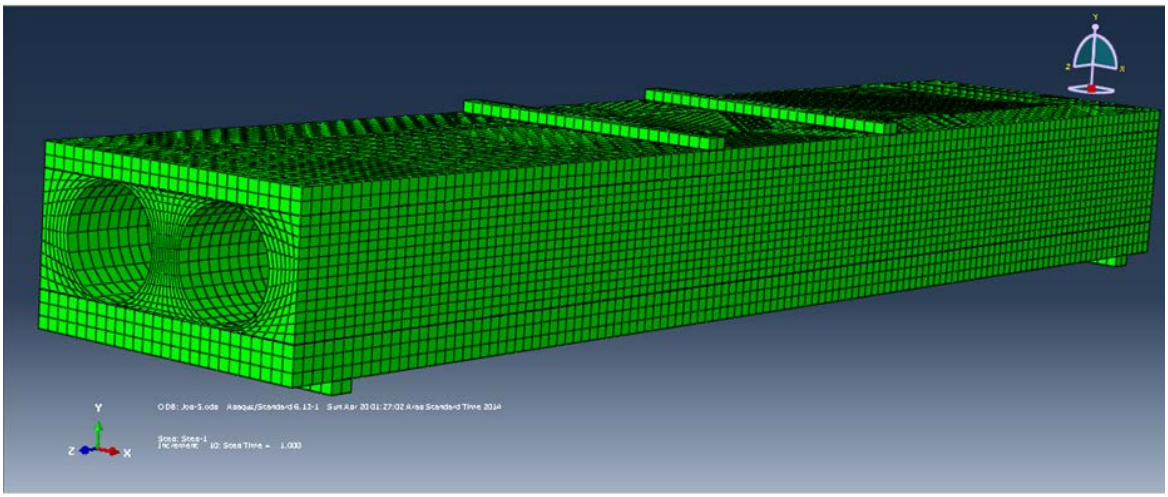

Meshing of hybrid specimen **HC-A-L3**

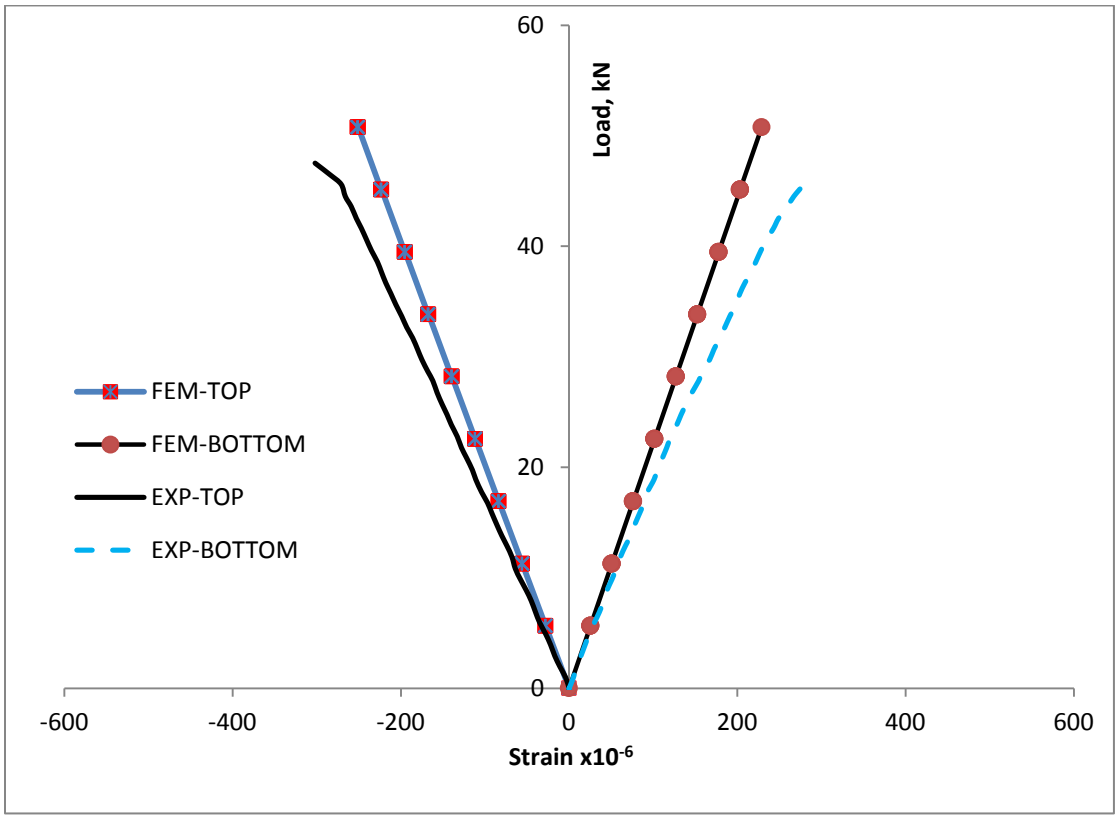

***FEM vs. experimentally observed longitudinal strain on top and bottom faces of hybrid beam of specimen* HC-A-L3**

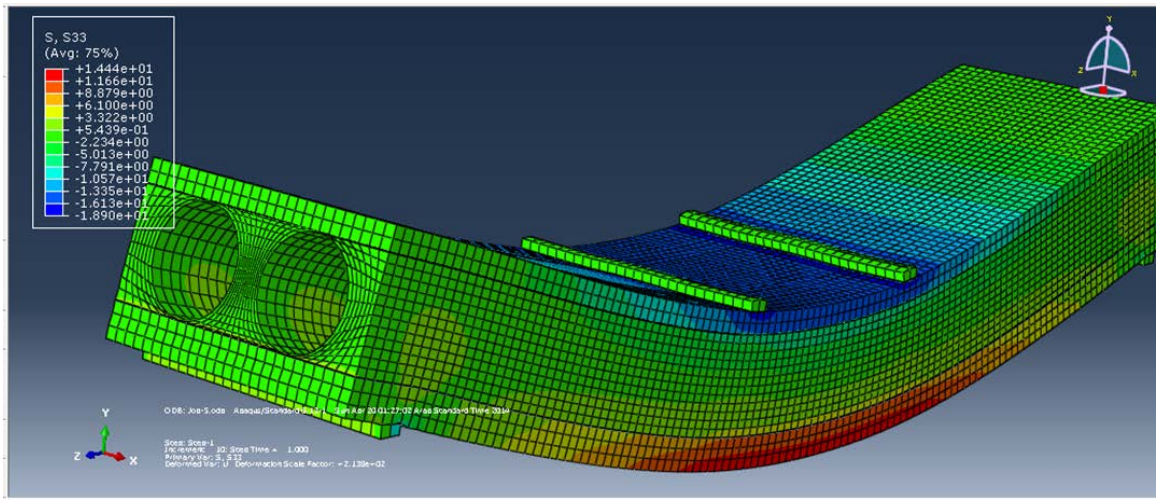

FEM longitudinal stress distribution of specimen **HC-A-L3**

(ii) Hybrid specimen HC-B-L3 of Group (ii) of beam size 330x175x1200 mm (span=1100)

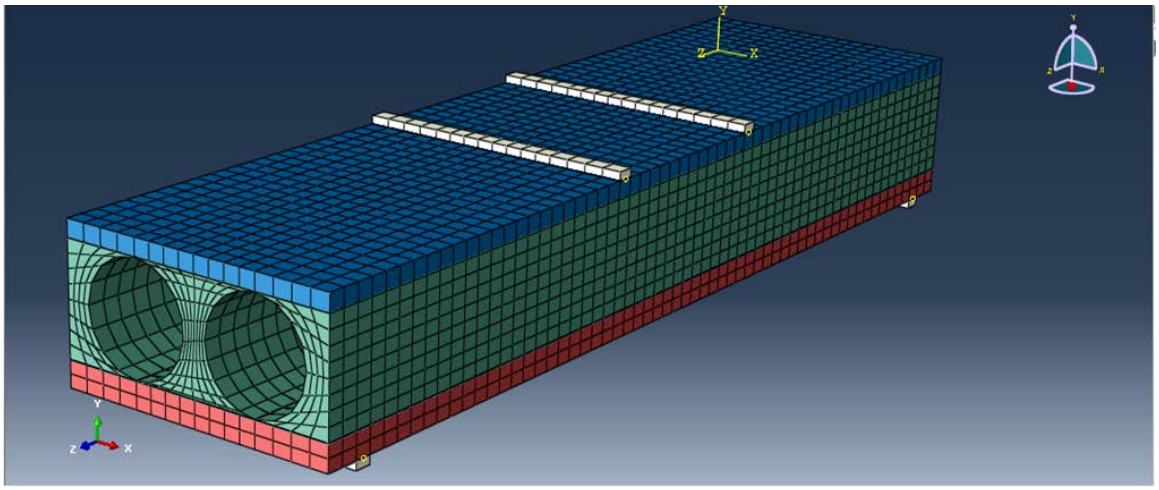

***Meshing of hybrid specimen* HC-B-L3**

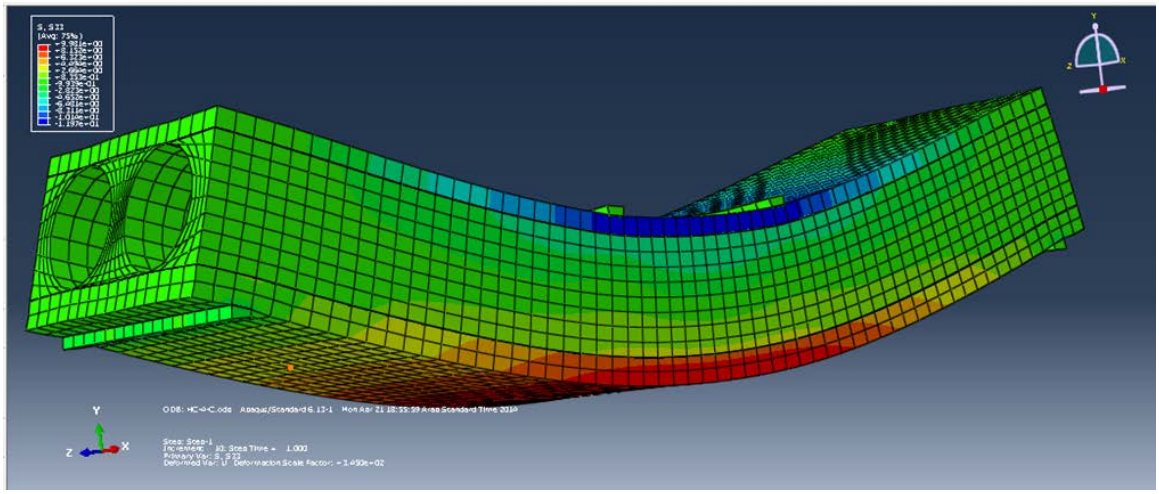

FEM longitudinal stress distribution of specimen **HC-B-L3**

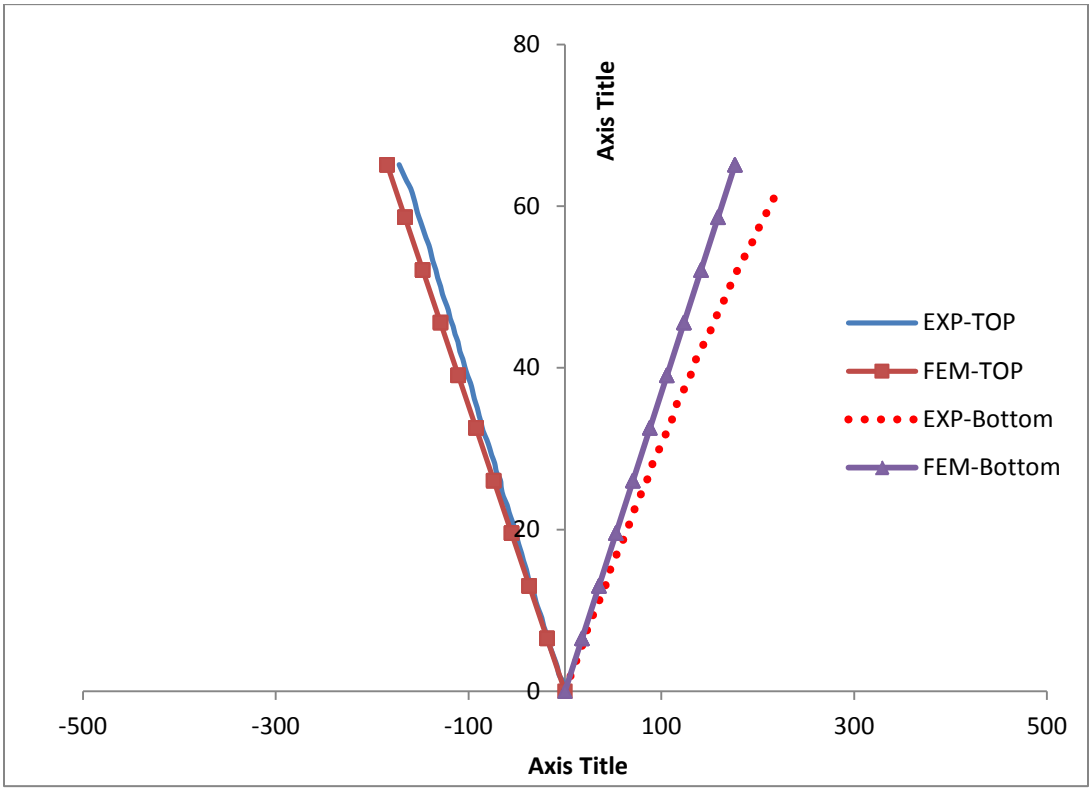

FEM vs. experimentally observed longitudinal strain on top and bottom faces of hybrid beam of specimen **HC-B-L3**

(iii) Hybrid specimen HC-C-S2 of Group (iii) of beam size 390x200x1000 mm (span=900)

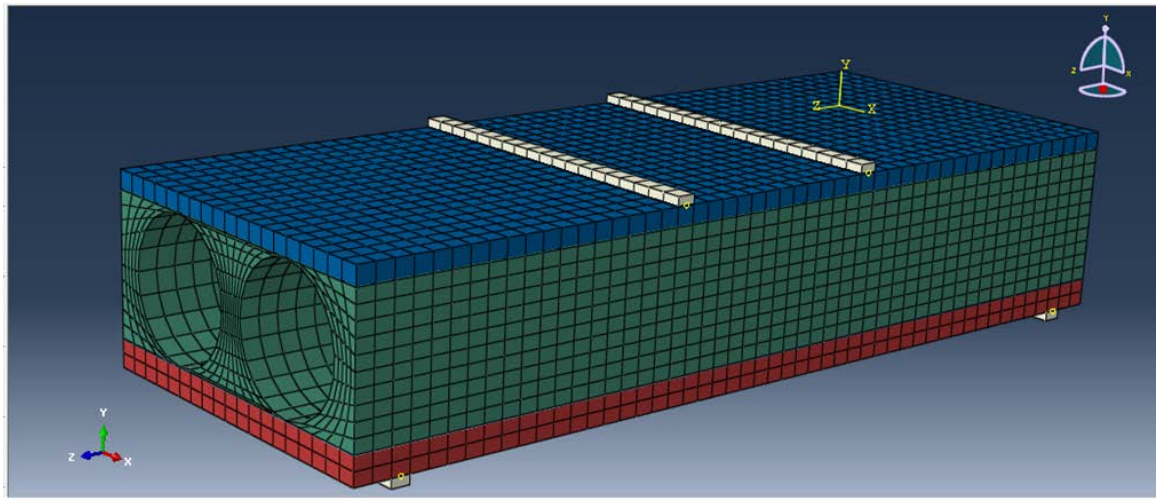

***Meshing of hybrid specimen* HC-C-S2**

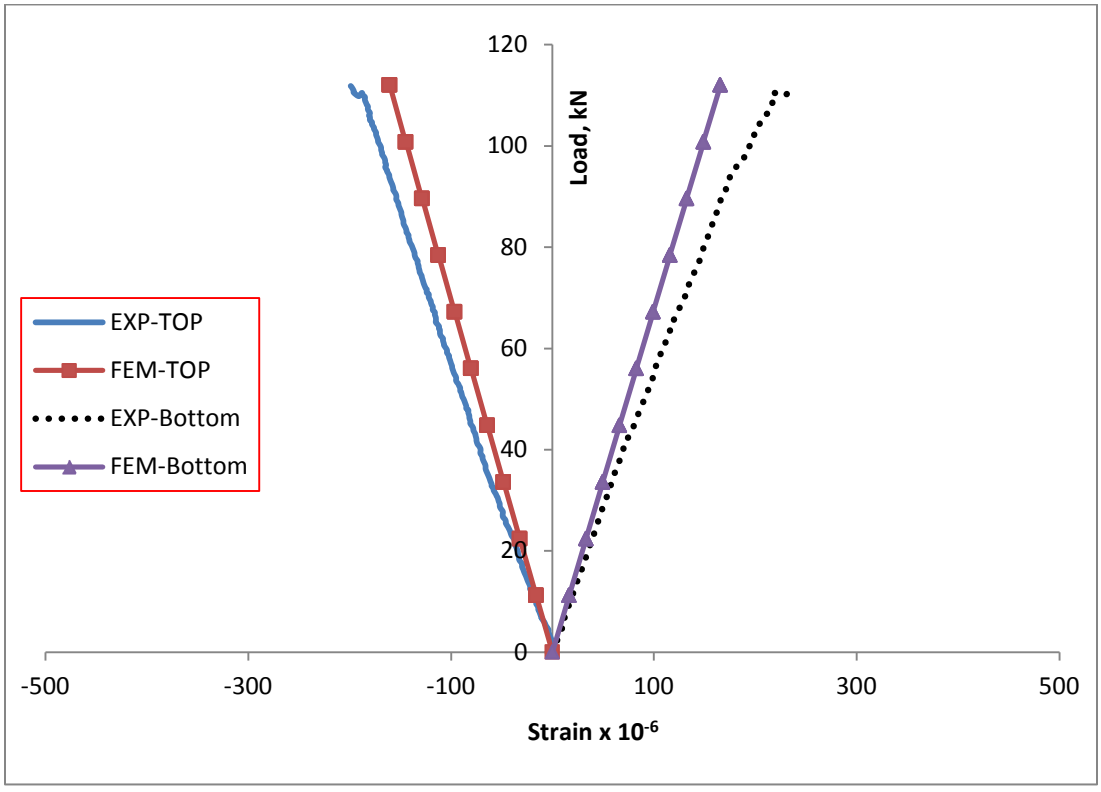

***FEM vs. experimentally observed longitudinal strain on top and bottom faces of hybrid beam of specimen* HC-C-S2**

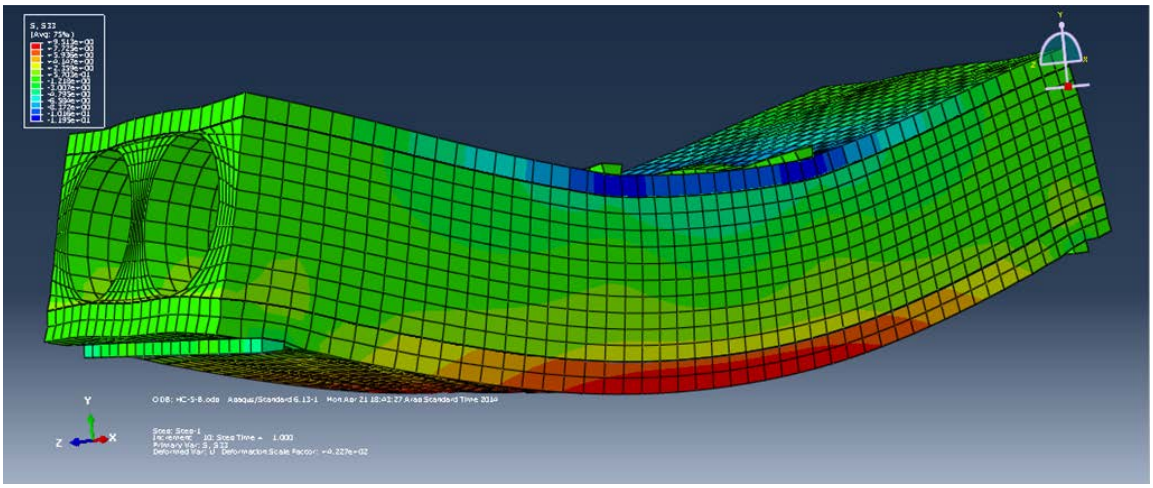

FEM longitudinal stress distribution of specimen **HC-C-S2**

(iv) Hybrid specimen HC-C-L2 of Group (iii) of beam size 390x200x1200 mm (span=1100)

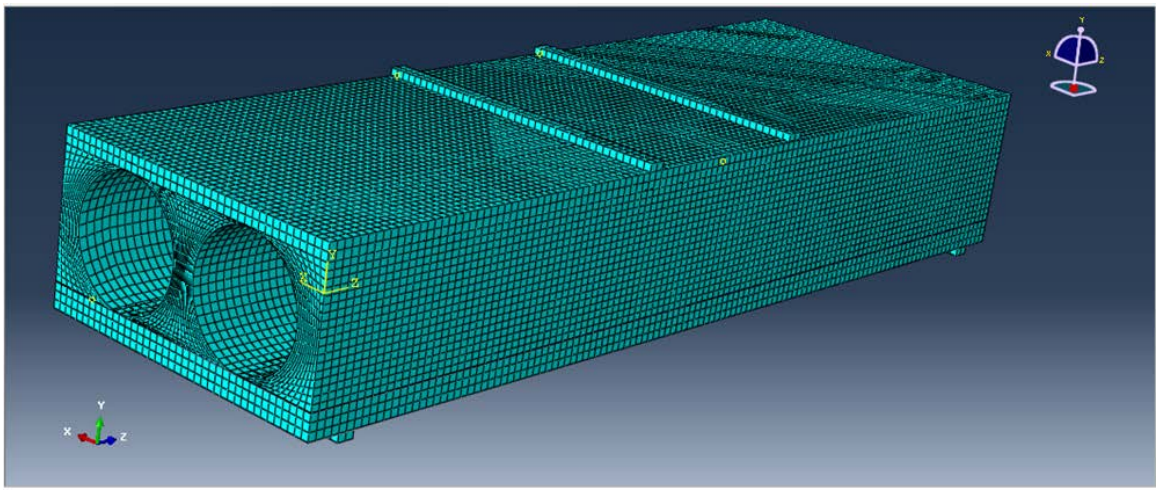

Meshing of hybrid specimen **HC-C-L2**

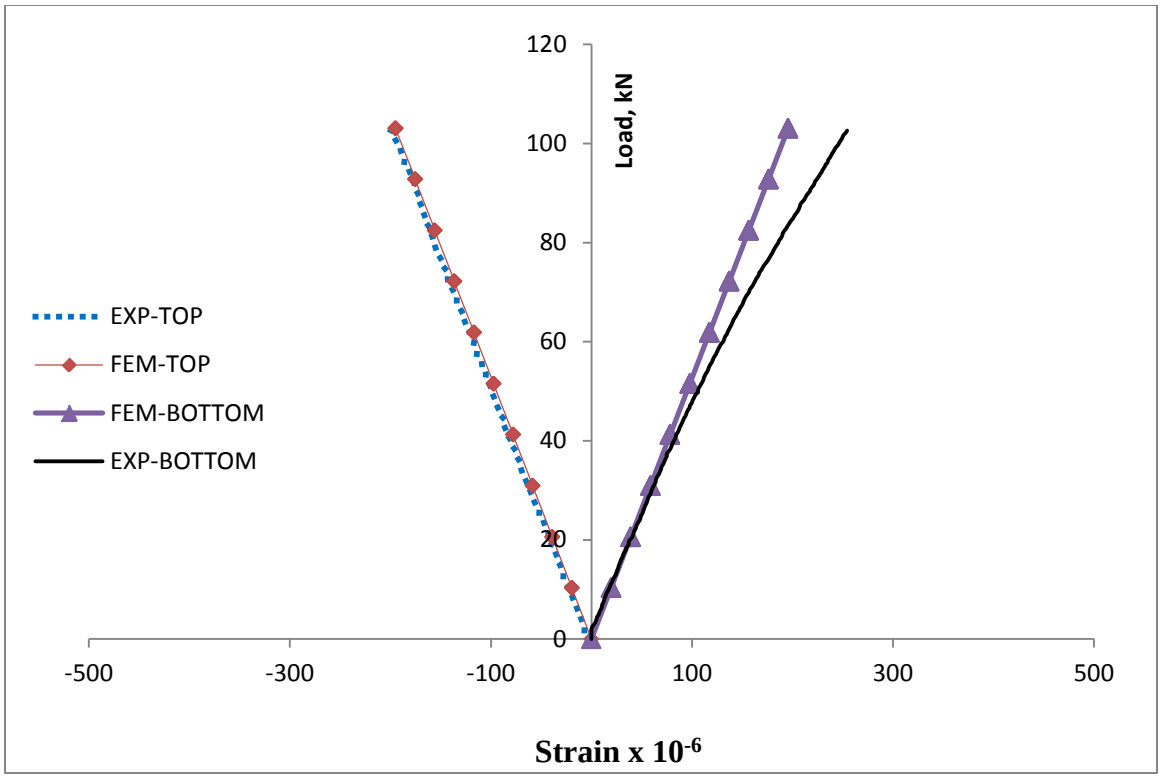

***FEM vs. experimentally observed longitudinal strain on top and bottom faces of hybrid beam of specimen* HC-C-L2**

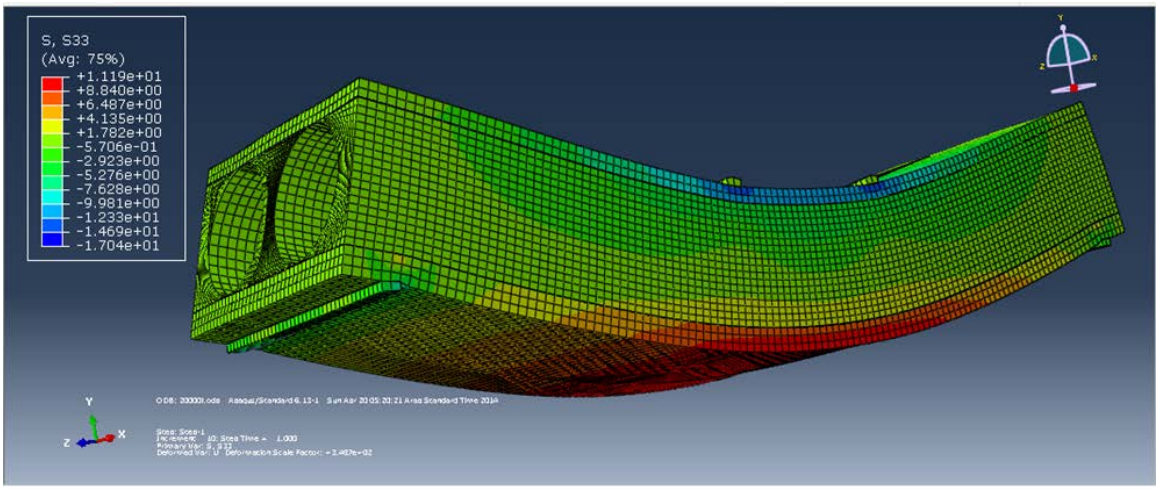

FEM longitudinal stress distribution of specimen **HC-C-L2**

(v) Hybrid specimen HC-D-L2 of Group (iv) of beam size 380x140x1200 mm (span=1100)

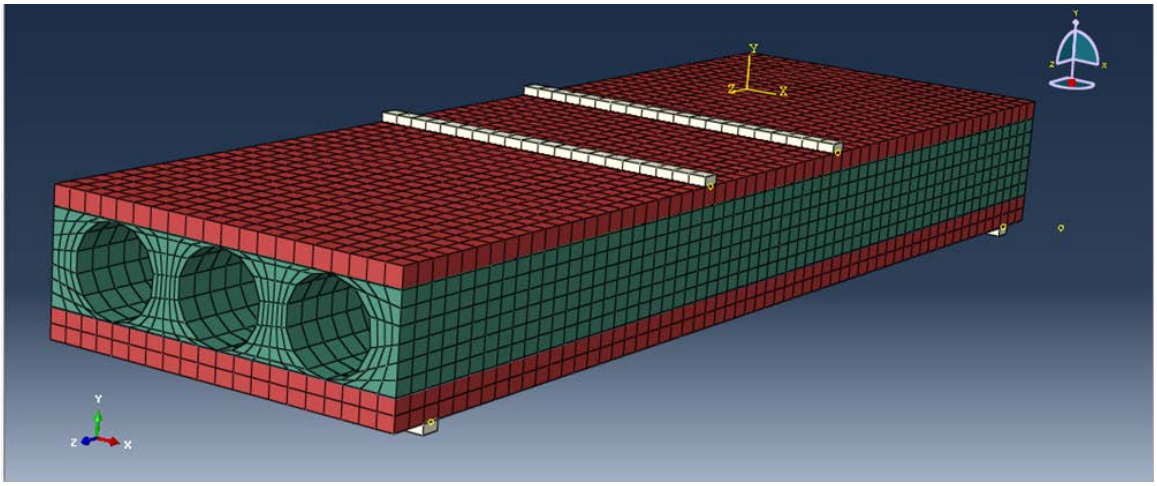

***Meshing of hybrid specimen* HC-D-L2**

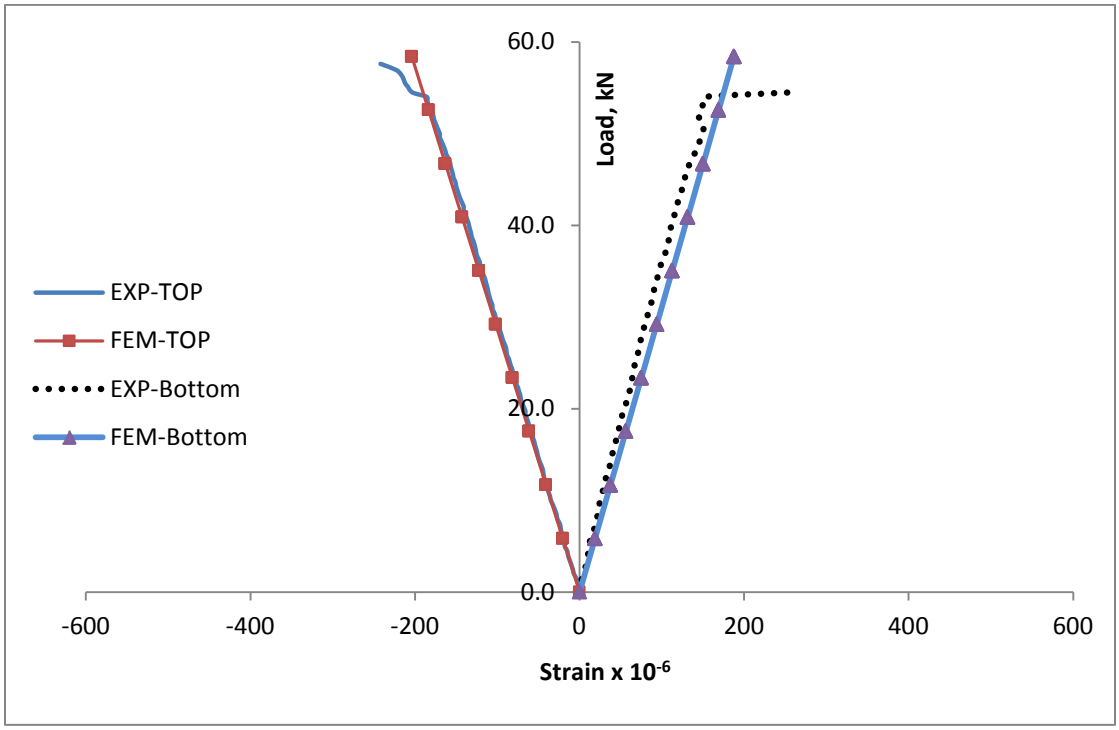

***FEM vs. experimentally observed longitudinal strain on top and bottom faces of hybrid beam of specimen* HC-D-L2**

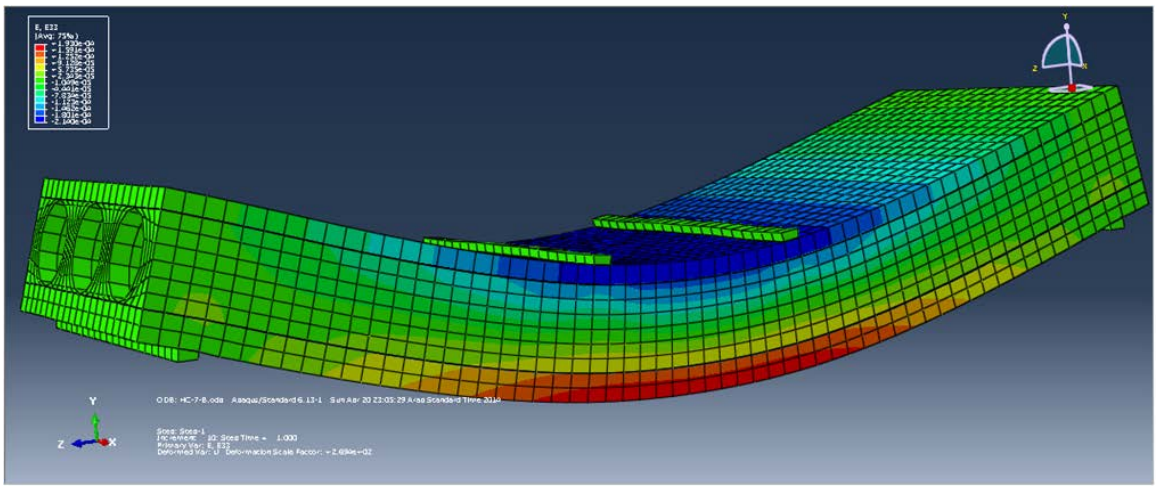

FEM longitudinal stress distribution of specimen **HC-D-L2**

VITAE

Name	:Ibrahim Yahya Ahmed Hakeem
Nationality	:Yemeni
Date of Birth	:1/23/1975
Email	:iyhakeem@kfupm.edu.sa; ibrahimhakeem75@yahoo.com
Address	:King Fahd University of Petroleum and Minerals (KFUPM), Dhahran, 31262, Saudi Arabia.
Academic Background	:Diploma Civil Engineering, Industrial Technical Institute, Aden, Yemen, 1995, (85/100), Received First rank with Honor Awards in all the semesters B.Sc. in Civil Engineering, Aden Univ., Aden, Yemen 2001. (Excellent degree of 4.62/5). First rank with honor). M.S., King Fahd University of Petroleum & Minerals, Dhahran, Saudi Arabia, May 2011. GPA (3.88/4.00). PhD, King Fahd University of Petroleum & Minerals 2014